

ISSN 1980-9743

# Soils and Rocks

An International Journal of Geotechnical  
and Geoenvironmental Engineering

$\frac{\Delta B}{MS}$



Volume 38, N. 3  
September-December 2015

**Soils and Rocks is an International Journal of Geotechnical and  
Geoenvironmental Engineering published by**

**ABMS - Brazilian Association for Soil Mechanics and Geotechnical Engineering  
Av. Queiroz Filho, 1700 - Torre A Sky, Sala 106 - Vila Hamburguesa  
05319-000, São Paulo, SP  
Brazil**

**SPG - Portuguese Geotechnical Society  
LNEC, Avenida do Brasil, 101  
1700-066 Lisboa  
Portugal**



*Issue Date: December 2015*

*Issue: 400 copies and 800 online-distributed copies*

*Manuscript Submission: For review criteria and manuscript submission information, see Instructions for Authors at the end.*

*Disclaimer: The opinions and statements published in this journal are solely the author's and not necessarily reflect the views or opinions of the publishers (ABMS and SPG). The publishers do not accept any liability arising in any way from the opinions, statements and use of the information presented.*

*Copyright: Authors and ABMS-Brazilian Society for Soil Mechanics and Geotechnical Engineering*

# **SOILS and ROCKS**

An International Journal of Geotechnical and Geoenvironmental Engineering

**Editor** Waldemar Coelho Hachich - University of São Paulo, Brazil

**Co-editor** Manuel Matos Fernandes - University of Porto, Portugal

## **Executive Board**

Alberto Sayão

*Pontifical Catholic University of Rio de Janeiro, Brazil*

Jorge Almeida e Sousa

*University of Coimbra, Portugal*

Ian Schumann Martins

*Federal University of Rio de Janeiro, Brazil*

João Maranhã

*LNEC, Portugal*

## **Associate Editors**

H. Einstein

*MIT, USA*

John A. Hudson

*Imperial College, UK*

Kenji Ishihara

*University of Tokyo, Japan*

Michele Jamiolkowski

*Studio Geotecnico Italiano, Italy*

Willy A. Lacerda

*COPPE/UFRRJ, Brazil*

E. Maranhã das Neves

*Lisbon Technical University, Portugal*

Nielen van der Merve

*University of Pretoria, South Africa*

Paul Marinou

*NTUA, Greece*

James K. Mitchell

*Virginia Tech., USA*

Lars Persson

*SGU, Sweden*

Harry G. Poulos

*University of Sidney, Australia*

Niek Rengers

*ITC, The Netherlands*

Fumio Tatsuoka

*Tokyo University of Science, Japan*

Luiz González de Vallejo

*UCM, Spain*

Roger Frank

*ENPC-Cermes, France*

## **Editorial Board Members**

Roberto F. Azevedo

*Federal University of Viçosa, Brazil*

Milton Kanji

*University of São Paulo, Brazil*

Antonio M.S. Oliveira

*University of Guarulhos, Brazil*

Omar Y. Bitar

*IPT, Brazil*

Lázaro V. Zuquette

*University of São Paulo, Brazil*

Fabio Taioli

*University of São Paulo, Brazil*

Tarcisio Celestino

*University of São Paulo-SC, Brazil*

Roberto Q. Coutinho

*Federal Univ. of Pernambuco, Brazil*

Nilo C. Consoli

*Federal Univ. Rio Grande do Sul, Brazil*

Sandro S. Sandroni

*Consultant, Brazil*

Sérgio A.B. Fontoura

*Pontifical Catholic University, Brazil*

Ennio M. Palmeira

*University of Brasília, Brazil*

Luciano Décourt

*Consultant, Brazil*

Faíçal Massad

*University of São Paulo, Brazil*

Marcus Pacheco

*University of the State of Rio de Janeiro, Brazil*

Paulo Maia

*University of Northern Rio de Janeiro, Brazil*

Renato Cunha

*University of Brasília, Brazil*

Orencio Monje Vilar

*University of São Paulo at São Carlos, Brazil*

Maria Eugenia Boscov

*University of São Paulo, Brazil*

Eda Freitas de Quadros

*BGTECH, Brazil*

Vinod Garga

*University of Ottawa, Canada*

Richard J. Bathurst

*Royal Military College of Canada*

Robert Mair

*University of Cambridge, UK*

Serge Leroueil

*University of Laval, Canada*

Mario Manassero

*Politécnico di Torino, Italy*

Luis Valenzuela

*Consultant, Chile*

Jorge G. Zornberg

*University of Texas/Austin, USA*

Andrew Whittle

*MIT, USA*

Pierre Bérest

*LCPC, France*

Peter Kaiser

*Laurentian University, Canada*

He Manchao

*CUMT, China*

Teruo Nakai

*Nagoya Inst. Technology, Japan*

Claudio Olalla

*CEDEX, Spain*

Frederick Baynes

*Baynes Geologic Ltd., Australia*

R. Kerry Rowe

*Queen's University, Canada*

R. Jonathan Fannin

*University of British Columbia, Canada*

Laura Caldeira

*LNEC, Portugal*

António S. Cardoso

*University of Porto, Portugal*

José D. Rodrigues

*Consultant, Portugal*

António G. Coelho

*Consultant, Portugal*

Luís R. Sousa

*University of Porto, Portugal*

Rui M. Correia

*LNEC, Portugal*

João Marcelino

*LNEC, Portugal*

António C. Mineiro

*University of Lisbon, Portugal*

António P. Cunha

*LNEC, Portugal New*

António G. Correia

*University of Minho, Portugal*

Carlos D. Gama

*Lisbon Technical University, Portugal*

José V. Lemos

*LNEC, Portugal*

Nuno Grossmann

*LNEC, Portugal*

Luís L. Lemos

*University of Coimbra, Portugal*

Ricardo Oliveira

*COBA, Portugal*

**“Ad hoc” Reviewers (2014-2015)**

Ana Cristina Sieira <i>UERJ, Brazil</i>	Edmundo Rogério Esquível <i>USP-S. Carlos, Brazil</i>	Luís Valenzuela <i>Arcadis, Chile</i>
André Luís Brasil Cavalcante <i>UnB, Brazil</i>	Eurípedes Vargas <i>PUC-RJ, Brazil</i>	Marc Vinches <i>Ecole des Mines d'Alès, France</i>
Antonio Airton Bortolucci <i>USP-S. Carlos, Brazil</i>	Fernando Antonio Medeiros Marinho <i>USP-Poli, Brazil</i>	Marcia Maria dos Anjos Mascarenhas <i>UFG, Brazil</i>
Arsenio Negro Jr. <i>Bureau, Brazil</i>	Fernando Olavo Franciss <i>Progeo, Brazil</i>	Maria Cláudia Barbosa <i>UFRJ, Brazil</i>
Bernadete Ragoni Danziger <i>UERJ, Brazil</i>	Francisco Chagas da Silva Filho <i>UFC, Brazil</i>	Maurício Ehrlich <i>UFRJ, Brazil</i>
Carlos Medeiros Silva <i>Embre, Brazil</i>	Francisco de Rezende Lopes <i>UFRJ, Brazil</i>	Nelson Aoki <i>USP-S. Carlos, Brazil</i>
Claudio Fernando Mahler <i>UFRJ, Brazil</i>	Frederico Falconi <i>ZF, Brazil</i>	Paulo Scarano Hemi <i>ITA, Brazil</i>
Claudio Michael Wolle <i>USP-Poli, Brazil</i>	Isabel Lopes <i>IST, Portugal</i>	Renato Pinto da Cunha <i>UnB, Brazil</i>
David Martins Geraldo Taborda <i>Imperial College, UK</i>	João Manuel Marcelino Mateus da Silva <i>LNEC, Portugal</i>	Sussumu Niyama <i>Tecnum, Brazil</i>
Denise Gerscovich <i>UERJ, Brazil</i>	José Camapum de Carvalho <i>UnB, Brazil</i>	Tácio Campos <i>PUC-RJ, Brazil</i>
Eda Quadros <i>BGTECH, Brazil</i>	José Renato Baptista de Lima <i>USP-Poli</i>	Tiago Miranda <i>Univ. do Minho, Portugal</i>
Edgar Odebrecht <i>Geoforma, Brazil</i>	Kátia Bicalho <i>UFES, Brazil</i>	Waldyr Lopes de Oliveira Filho <i>UFOP, Brazil</i>
Edgard Poiate <i>Petrobrás, Brazil</i>	Leonardo Becker <i>UFRJ, Brazil</i>	

*Soils and Rocks* publishes papers in English in the broad fields of Geotechnical Engineering, Engineering Geology and Geo-environmental Engineering. The Journal is published in April, August and December. Subscription price is US\$ 90.00 per year. The journal, with the name “Solos e Rochas”, was first published in 1978 by the Graduate School of Engineering, Federal University of Rio de Janeiro (COPPE-UFRJ). In 1980 it became the official magazine of the Brazilian Association for Soil Mechanics and Geotechnical Engineering (ABMS), acquiring the national character that had been the intention of its founders. In 1986 it also became the official Journal of the Brazilian Association for Engineering Geology and the Environment (ABGE) and in 1999 became the Latin American Geotechnical Journal, following the support of Latin-American representatives gathered for the Pan-American Conference of Guadalajara (1996). In 2007 the journal acquired the status of an international journal under the name of *Soils and Rocks*, published by the Brazilian Association for Soil Mechanics and Geotechnical Engineering (ABMS), Brazilian Association for Engineering Geology and the Environment (ABGE) and Portuguese Geotechnical Society (SPG). In 2010, ABGE decided to publish its own journal and left the partnership.

***Soils and Rocks***

1978,	1 (1, 2)
1979,	1 (3), 2 (1,2)
1980-1983,	3-6 (1, 2, 3)
1984,	7 (single number)
1985-1987,	8-10 (1, 2, 3)
1988-1990,	11-13 (single number)
1991-1992,	14-15 (1, 2)
1993,	16 (1, 2, 3, 4)
1994-2010,	17-33 (1, 2, 3)
2011,	34 (1, 2, 3, 4)
2012-2014,	35-37 (1, 2, 3)
<b>2015,</b>	<b>38 (1, 2, 3)</b>

ISSN 1980-9743

CDU 624.131.1

***SOILS and ROCKS***

An International Journal of Geotechnical and Geoenvironmental Engineering

**Publication of****ABMS - Brazilian Association for Soil Mechanics and Geotechnical Engineering****SPG - Portuguese Geotechnical Society****Volume 38, N. 3, September-December 2015****Table of Contents****PACHECO SILVA LECTURE***New Developments in the Control and Prediction of the Movements  
Induced by Deep Excavations in Soft Soils*

M.M. Fernandes

191

**ARTICLES***Use of Sugarcane Bagasse as Carbon Substrate in Permeable Reactive Barriers:  
Laboratory Batch Tests and Mathematical Modeling*

R.C. Mattos, P.S. Hemsí, E.Y. Kawachi, F.T. Silva

219

*Apparent Pressures on Multi-Propped Retaining Walls in Soils Under Drained Conditions  
with Shallow Water Table*

L. Andrade Viana, N.M. da Costa Guerra

231

*On the Interpretation of the Bidirectional Static Load Test*

F. Massad

249

**TECHNICAL NOTE***Revisiting Classical Methods to Identify Collapsible Soils*

O.M. Vilar, R.A. Rodrigues

265



## **Pacheco Silva Lecture**



**The Pacheco Silva Lecture** is delivered each two years by an important geotechnical professional from Brazil or abroad to honour the memory of the distinguished Brazilian geotechnical engineer Francisco Pacheco Silva (1918-1974). Pacheco Silva was a researcher of the Technological Research Institute (IPT/SP) for 33 years and consultant in geotechnical engineering in several occasions. In 1947 he obtained his MSc. degree from Harvard University, where he was a student of Karl Terzaghi and Arthur Casagrande. He worked in practically all fields of geotechnical engineering, but his main research interests were on soil behaviour, laboratory testing and geotechnical instrumentation. He was also one of the founders and past presidents of the Brazilian Association for Soil Mechanics and Geotechnical Engineering - ABMS.



### **Prof. Manuel de Matos Fernandes**

The 2014 Pacheco Silva Lecturer is Manuel de Matos Fernandes, 61 years, Full Professor at the Faculty of Engineering of University of Porto (FEUP), Portugal. He got his degree in Civil Engineering in 1976 at FEUP. The PhD thesis (1984), on flexible earth-retaining structures, was developed at LNEC, Lisbon. He was the main responsible for the development at FEUP of a team devoted to Geotechnics. His areas of interest have been focused on numerical modelling of geotechnical structures, deep excavations, Eurocodes and teaching Soil Mechanics (he is author of two text books). In the last 25 years he has had activity of design and consultancy, particularly in bridge foundations and urban excavations.

**Soils and Rocks**  
**v. 38, n. 3**



# New Developments in the Control and Prediction of the Movements Induced by Deep Excavations in Soft Soils

M. Matos Fernandes

**Abstract.** The paper corresponds to the Pacheco Silva Lecture delivered by the author in September 2014. In the first part of the text, a general perspective of the movements induced by deep excavations in soft soils is outlined. The general report presented by Ralph B. Peck to the 1969 ISSMFE México conference is taken as reference and the progress achieved since then in the control of the movements is emphasized. It is pointed out that such progress permits that in very demanding urban scenarios involving soft soils one should work towards a performance, with regard to induced movements, similar to (or even better than) that is achieved in comparable excavations in stiff soils. Starting from this general framework, some issues relevant to an effective control and to a reliable prediction of the movements are treated: the pre-stress of the strut system, the methodologies for providing support to the retaining wall before the removal of the soil, the surface settlements induced by the consolidation of the soil in the long-term and the influence of the non-linear behaviour of the reinforced concrete wall. Results of research on these topics are presented and discussed and general conclusions are extracted.

**Keywords:** deep excavations, soft soils, induced movements, soil improvement, consolidation, nonlinear reinforced concrete.

## 1. Introduction

Deep excavations in thick deposits of soft soils have been one of the major challenges that geotechnical engineers have faced in the last decades.

Literature contains a large number of references to such works in cities like Oslo (Karlsruud, 1983), Lisbon (Matos Fernandes, 1985, 2007), Chicago (Finno *et al.*, 1989), San Francisco (Clough & Reed, 1984; Koutsoftas *et al.*, 2000), Singapore (Wong *et al.*, 1997), Shanghai (Wang *et al.*, 2005; Lui *et al.*, 2011; Ng *et al.*, 2012) and Taipei (Ou *et al.*, 2006; Hwang *et al.*, 2007).

A major issue when dealing with excavations in thick deposits of soft clayey soils is the magnitude of the movements induced in the vicinity. This subject has known, for the first time, a consistent approach in the well-known General Report to the México ISSMFE conference by Peck (1969). Since then an auspicious progress in the understanding and the control of the movements was achieved as a result of the introduction of new construction technologies, new structural systems and new methods of analysis.

The fact that such excavations are becoming deeper and are being done under more daring and demanding conditions is the motive to reanalyse this topic in the light of the recent results published in the literature and of the new possibilities provided by the techniques currently available.

## 2. Moviments Induced by Excavations in Soft Clayey Soils. General Perspective

### 2.1. Introduction. Some previous matters

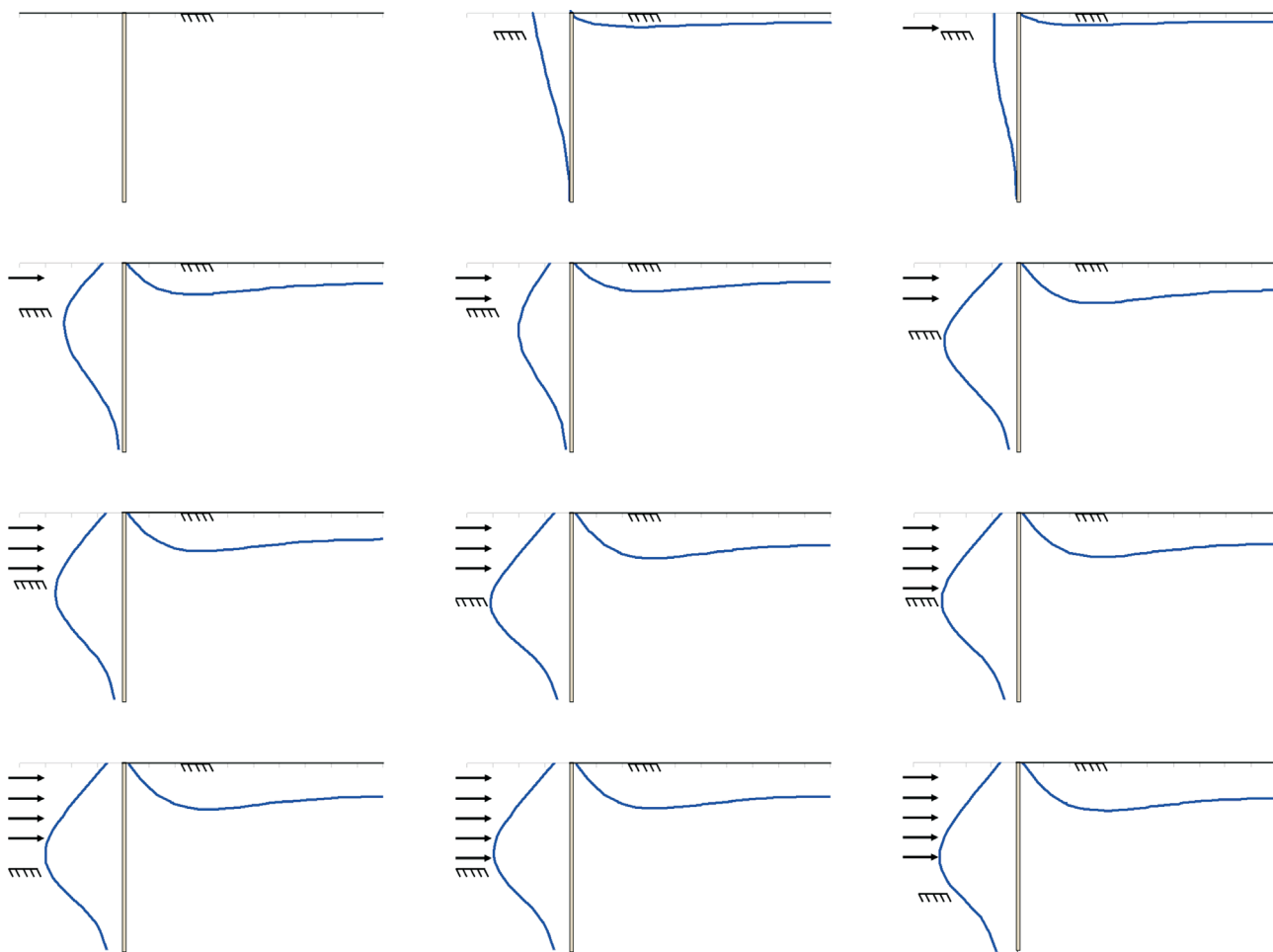
Figure 1 shows the typical sequence of movements of a strutted flexible retaining wall in a thick deposit of soft

clayey soils, with the wall tip embedded in a firm layer underlying the soft deposit. This sequence is selected from a finite element simulation but it could correspond to real observed results. In the finite element analysis the struts were pre-stressed.

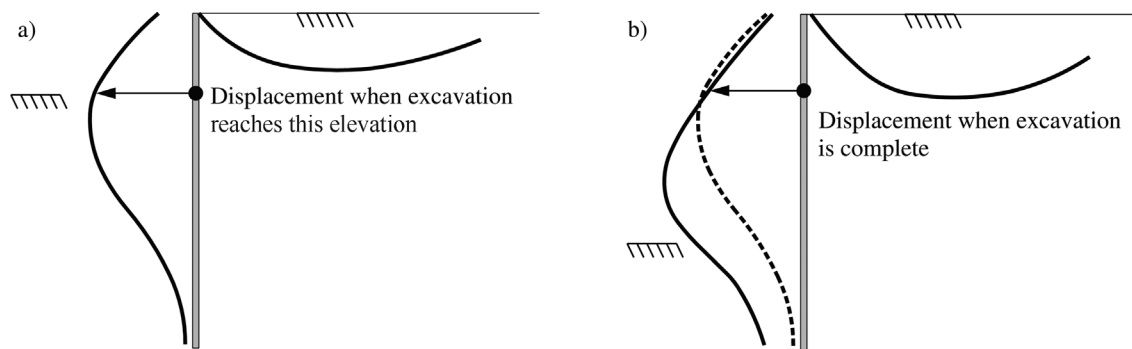
It is possible to observe that with the progress of the construction process the wall face at the excavated side exhibits an increasing convexity, with the point of maximum displacement at increasing depth. Simultaneously, the ground surface becomes concave, with the point of maximum settlement being situated at increasing distance in relation to the retaining wall. This concavity arises from the upward tangential stresses applied by the wall to the supported ground through its back face, therefore ensuring smaller settlements in the surface region adjacent to the excavation (Matos Fernandes, 2004).

Figure 2a is extracted from the sequence commented above, distinguishing the lateral displacement of a given point P of the wall face when the excavation platform reaches the elevation of that point. So, this displacement has occurred when P was *underneath the base of the excavation*. In Fig. 2b, the displacement of P at the completion of the excavation is shown. It can be observed that this displacement practically coincides with the one shown in Fig. 2a. So, it can be concluded that the displacement of P when this point was *above the current excavation platform* was practically null.

This result illustrates an important characteristic of this type of excavations with controlled construction (avoiding overexcavation and with pre-stressed struts having high axial effective stiffness). Basically, the observed lateral displacements at each point of the wall



**Figure 1** - Typical sequence of the movements of a strutted flexible retaining wall in a thick deposit of soft clayey soils.



**Figure 2** - Displacements underneath the current excavation base (a) and at the final excavation stage (b) of a generic point of the wall from the sequence illustrated in Fig. 1.

occur under the excavation base, that is, before an adequate structural support could be given to the wall at that point. This fact is the key of the major difficulty in controlling the movements induced by deep excavations in thick deposits of soft soils!

Obviously, the control of the lateral wall displacements is relevant because such displacements are the cause

of the ones of the ground surface during the excavation phase. Assuming undrained soil behaviour during the excavation, that is null volumetric strains, the two areas marked in Fig. 3, corresponding to the integral of the horizontal wall displacements and to the integral of surface settlements at the completion of the excavation will be practically equal.

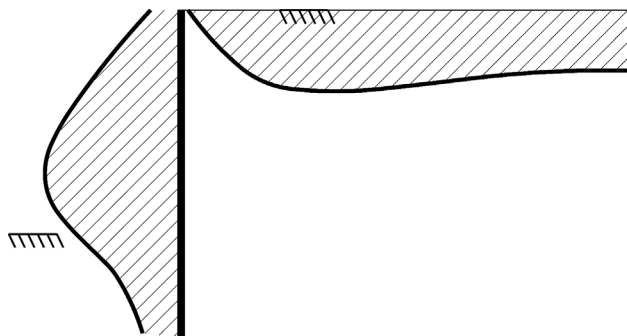


**Figure 3** - Integrals of the horizontal wall displacements and of surface settlements at the end of the excavation from the simulation shown in the preceding figures.

However, it must be taken into account that the surface movements are not restricted to the ones discussed above. As shown by Fig. 4, before the excavation, the wall installation (and other preparatory constructive operations, such as demolition of ancient foundations) will typically cause non negligible surface settlements (Clough & O’Rourke, 1990; Poh *et al.*, 2001; Finno *et al.*, 2002). In addition, the dissipation of excess pore pressures (mostly) after the excavation may originate further settlements by consolidation of the soil, which may achieve a considerable magnitude (Finno *et al.*, 1989; Alves Costa *et al.*, 2007; Matos Fernandes, 2010; Matos Fernandes *et al.*, 2012; Borges & Pinto, 2013; Borges & Guerra, 2014).

In the present state of our understanding about the phenomena involved in such works, and with the available constructive solutions, the component of surface movements concomitant with the excavation (among the three described above) seems easier to be minimized and, as well, it is the one that our analytical models (particularly, the finite element models) more faithfully capture. This explains the relevance of analysing and discussing all the issues that may contribute to minimize that component. That challenge will be a major goal of this work, although some attention will be focused on the third component, as well.

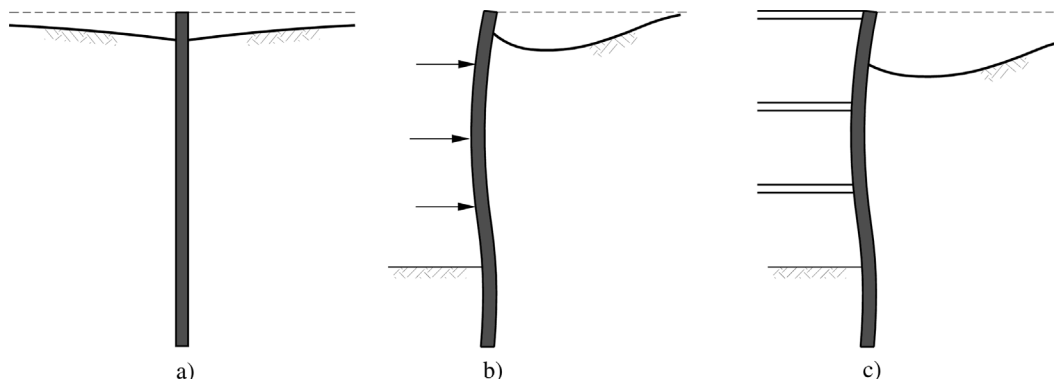


**Figure 4** - Movements (a) before, (b) during and (c) after of the excavation.

Before closing this section, it should be noticed that in most of the published case histories it is very difficult to separate the surface settlements into the three components referred above. In addition, the cases including observation of a time period after the conclusion of the excavation are relatively scarce. This turns difficult to interpret and to treat those observed results in a general way.

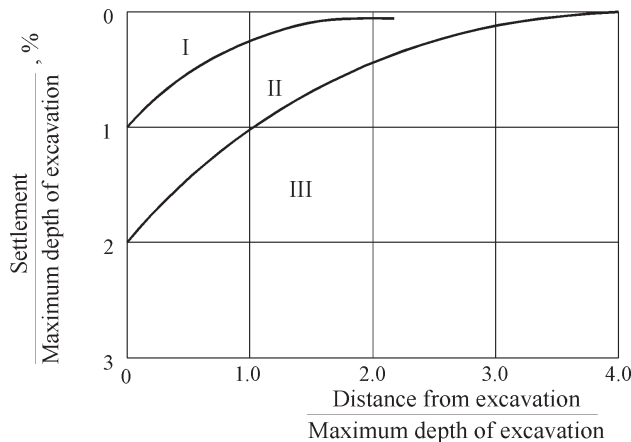
**2.2. General report of Peck (1969) - The founder document of the theme**

The first published work presenting a scientific analysis of the movements induced by deep excavations, and particularly by excavations in thick deposits of soft soils, is the general report presented by Ralph B. Peck to the VII<sup>th</sup> Conference of the ISSMFE, in México City (Peck, 1969). The report includes the famous settlement chart illustrated in Fig. 5.

That chart is organized according to the type of soil. In thick deposits of soft soils, the expected settlements may achieve very high values: over 1% to 2% of the excavation depth. This magnitude of the expected settlements mainly arose from the dramatic limitations of the type of retaining structures and construction employed until the sixties (and, to some extent, from the limitations of the methods of analysis, as well). This mainly consisted of very flexible sheet pile or soldier-pile walls with timber lagging associated with cross-bracing (generally non pre-stressed).

The ability of such retaining structures to control induced movements, particularly in soft soils, was in fact very modest. Then the statement of the author: “*The most important variable that determines the amount of movement is not the stiffness of the exterior wall or the vertical spacing of the bracing but the characteristics of the surrounding soils. (...)*”.

It is very stimulating to undertake a careful lecture of the report today and to check the solution suggested by Peck to control the movements induced by the excavations in soft clayey soils. This sequence of thoughts is particularly lucid:



Zone I – Sand and soft to hard clay. Average workmanship.

Zone II – a) Very soft to soft clay.

1 – Limited depth of clay below bottom of excavation.

2 – Significant depth of clay below bottom of excavation but  $N_b < N_{cb}$ .

b) Settlement affected by construction difficulties.

Zone III – Very soft to soft clay to a significant depth below bottom of excavation and with  $N_b \geq N_{cb}$ .

Note: All data shown are for excavations using standard soldier piles or sheet piles braced with cross-bracing or tiebacks.

**Figure 5** - Summary of settlements adjacent to open cuts in various soils, as function of distance from edge of excavation (Peck, 1969).

(...). While this excavation is going on, the walls move. Whatever portion of the movement takes place below the bottom of the excavation cannot be prevented irrespective of the capacity of the supports or the degree to which bracing is pre-stressed.

In principle, the movements could be prevented if the entire supporting structure (...) and even the base slab for the completed structure could be constructed in their final positions before the removal of the enclosed soil. (...) Such an idealized procedure can exist only in imagination. It may be approached in practice, however (...).

The approach suggested by the author is the so-called *trench method*, developed in Chicago in the very beginning of the XX<sup>th</sup> century - period of very rapid and profound transformation of the city - for the construction of the three basements of the new Chicago Tribune Building in the Madison Avenue (Fig. 6).

The three basements were required for housing the presses of the journal, in order that the vibration from them

did not affect the comfort in the rest of the building (Randall, 1999). The method adopted in the excavation, called the *trench method* by Peck, is depicted in Fig. 7 (drawings by Bárbara Rangel for the author of this paper), and is described as follows by Peck (1969):

According to this procedure, a trench was excavated by hand around the periphery of a building at the proposed locations of the permanent basement walls. The width of the trench was as small as practicable. The sides were supported by timber planks and large number of horizontal trench braces or jacks extending from one side to the other. The completely sheeted trenches were carried to the full depth of the outside walls of the structure. Reinforcement was then set in the trenches and the concrete placed directly against the sheeting which served as the form.

Simultaneously with the wall construction, cross-trenches were excavated, generally along the column lines, and were similarly timbered and braced to the same depth as the external walls. Concrete struts, later forming part of the lowest basement floor, were then cast in the bottoms of the trenches. The building columns were established at the intersections of these struts (...). In this manner, a complete system of cross-lot bracing was established while most of the soil within the future basement area was still in place. As the final step, the soil was excavated (...). Hence, the settlements were minimized.

This ingenious solution may be, to some extent, considered pioneer in relation to the diaphragm wall technology. On the other hand, it is fully understandable that its use had been relatively rare when urban excavations became much more common by the middle of the century, due to the high cost and execution time.

It is perhaps curious to observe that the best solution pointed out by Peck to control the induced movements is a procedure developed more than six decades before! And, that the method for predicting the magnitude of the movements is a chart organized by type of soil, so independent on the retaining structure. The same can be said about the well-known diagrams of apparent earth pressures, discussed in the same general report, dependent just on the type of soil, as well.

This permits to envisage the severe technological and analytical limitations at the time of this brilliant document. Fortunately, these limitations were about to be overcome!

### 2.3. The progress in the control of induced movements in the last decades

After the late sixties and in the following decades some remarkable new technologies were progressively introduced, such as reinforced concrete diaphragm walls and

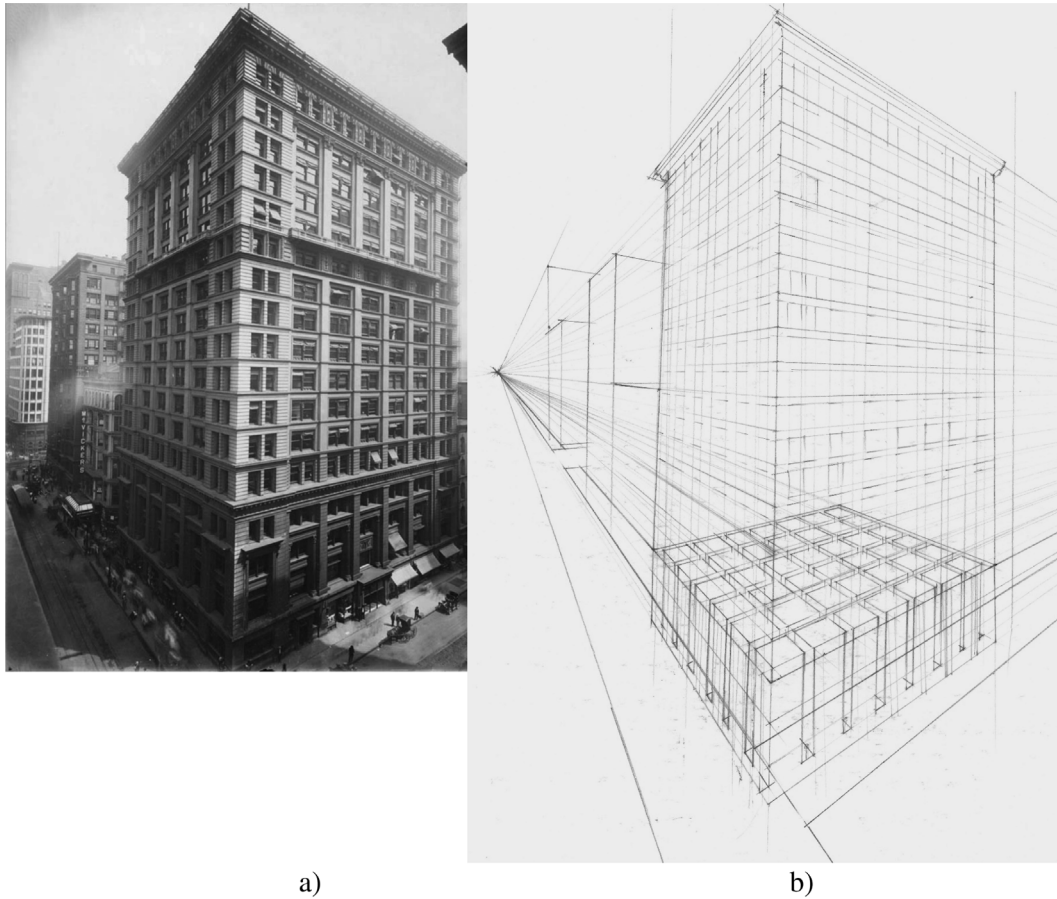


**Figure 6** - Tribune building, Madison Avenue, Chicago: a) photo in 1910; b) scheme of the Trench Method applied in the excavation for the three basements (drawing by Bárbara Rangel).

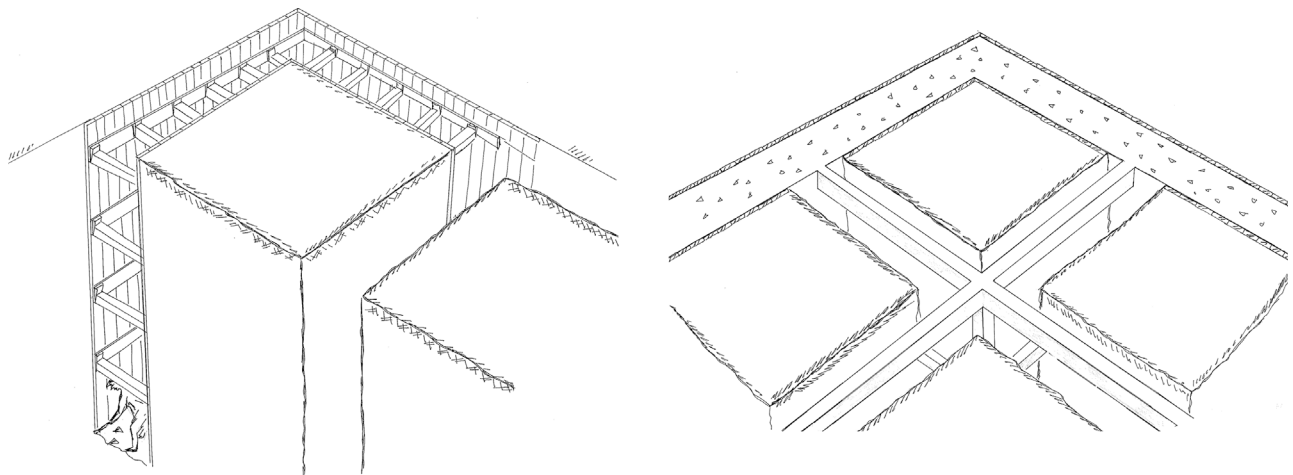


**Figure 7** - Two stages of the Trench Method used in the excavation for the three basements of Tribune building, Chicago, 1901 (drawings by Bárbara Rangel).

continuous pile walls, capable of better controlling induced movements.

These solutions and the understanding of the parameters affecting induced movements brought by the wide-

spread use of finite element analyses - whose first applications to deep excavations were published in the seventies (Bjerrum *et al.*, 1972; Egger, 1972; Palmer & Kenney, 1972; Clough & Tsui, 1974; Clough & Mana, 1976) - al-

lowed the execution of excavations in soft ground with much better results in comparison with Peck's chart.

This is well evidenced by the results presented two decades later by Clough and O'Rourke (1990), represented in Fig. 8. Additionally, the large scatter of the results collected proves that the specific parameters of the retaining structure and of the construction are extremely relevant with regard to the induced movements.

Clough & O'Rourke (1990) recognize this point, stating that: "Although the zones are helpful in delineating broad trends of performance, it is evident that the scatter in settlement magnitude places limitations on this type of empirical approach for making predictions about movement".

Figure 9 is extracted from a database collected by Moormann (2004) in which only a few case histories prior to 1980 were introduced. It illustrates the maximum lateral wall displacement, expressed as a percent of the excavation depth, with the factor of safety against basal heave. This factor is calculated by not considering the wall embedded length, according to the Terzaghi definition. It is interesting to observe that much better results appear in comparison with the trend identified by Mana & Clough (1981). Nevertheless, the data is highly scattered: for the same value of the safety factor, the displacements may vary more than ten times.

The results presented above confirm that the behaviour of excavations in thick deposits of soft clay is very complex, depending on a large set of features and parameters concerning the ground, the structure and the construction.

In spite of the enormous progress in the control of movements revealed by Figs. 8 and 9, it should be recognized that the actual displacement values shown by these figures are in many cases capable of inducing serious damage in the vicinity of the excavation. Many underground works in soft clay recently carried out in our cities (some involving excavation depth over 20 m), would be intolerable if the induced movements were in accordance with many of the results shown above.

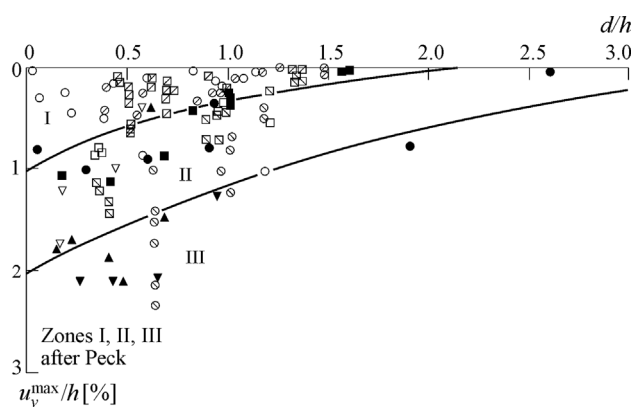


**Figure 8** - Summary of measured settlements adjacent to excavations in soft to medium clay collected by Clough and O'Rourke (1990) over Peck's chart.

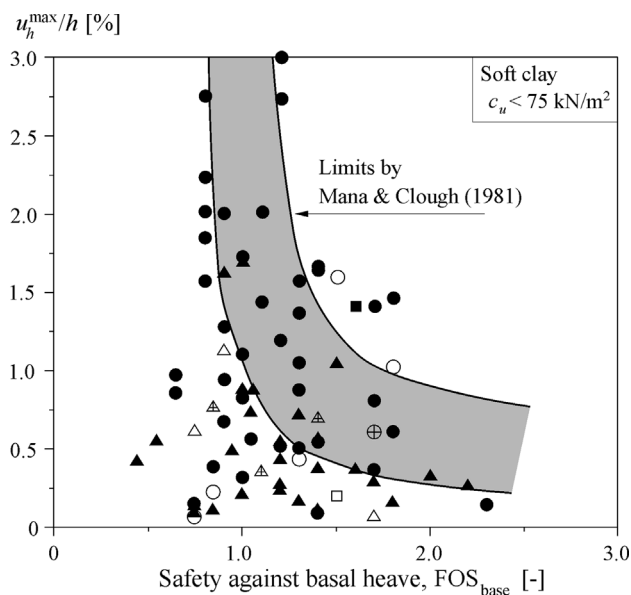


**Figure 9** - Maximum lateral wall displacement versus basal heave safety factor, for excavations in soft to medium clay (data collected by Moormann, 2004).

The author of this paper pointed out that if such results are relatively common even nowadays this is possibly related to the old idea - which is still widely accepted in practice - that the level of achievable performance with regard to movement control mainly depends on the ground conditions.

Due to this idea, the Profession has been, in fact, *more tolerant* with excavation induced movements in soft ground. However, ancient structures and services in soft ground may probably be *less tolerant* to further movements than similar constructions over stiff soils (Matos Fernandes, 2007).

#### 2.4. Eight golden rules for movement control

This reflection recommends, in fact, a complete inversion of the perspective commonly adopted when dealing with this critical matter. It should be pointed out that the experience of a number of works has shown that it is possible to achieve in soft soils levels of performance typical of more favourable geotechnical conditions, if appropriate structural solutions and construction sequences are employed. Namely, it is possible nowadays to deal with surface settlements one order of magnitude lower than the values considered in Peck's chart (Wang *et al.*, 2010).

Searching for case studies in the literature with small induced movements, while attempting to identify the features related with the structure and the construction which are more or less common to them, led to the formulation of the *eight golden rules* summarized in Fig. 10 (Matos Fernandes, 2007).

It is interesting to observe that the first letters of these eight rules form the word RELIABLE. In the thesaurus dic-

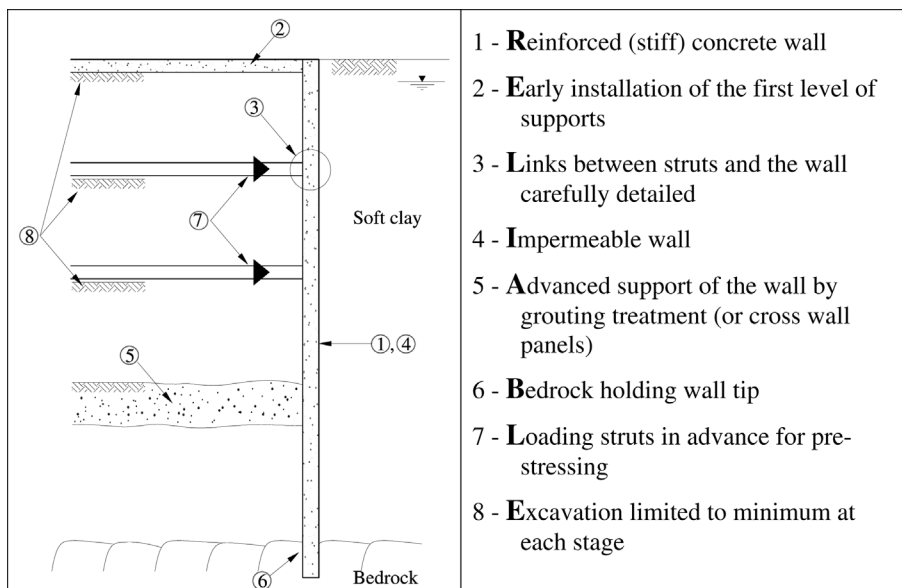


**Figure 10** - Golden rules for a reliable movement control induced by deep excavations in thick deposits of soft ground (Matos Fernandes, 2007).

tionary (Collins, 1984) it is possible to find the following synonymous for that word: safe, sound, stable and PREDICTABLE!

In fact, these rules may be further considered as conditions for obtaining *reliable predictions* of the induced movements: a retaining structure conceived and designed according to these rules is capable of maintaining the major part of the ground mass far from yielding. Thus, its performance shall be easier to predict because it will be mainly dependent on structural and construction features, exhibiting small sensitivity to those issues whose accurate characterization is more difficult. In short, it will be a *reliable* system.

In such cases, agreement between prediction and performance should be mainly credited to appropriate conception of the structure and to competent construction, and not so much assigned to the sophistication of the design prediction analyses.

Geotechnical engineers very often state that the analyses performed by our structural colleagues are more reliable because they deal with materials whose mechanical properties are carefully controlled. This is just one part (probably the smaller) of the truth! The other is that the safety factors and the design practice in Structural Engineering ensure that plastic yielding of structural elements is typically incipient, so linear elastic behaviour is, in general, a good approach. If a degree of plastic yielding similar to that achieved in many geotechnical problems with soft soils were allowed in conventional structures, the reliability of structural analyses would become very questionable.

In the following sections, four issues related with those golden rules will be discussed by reporting some recent research results. The key point is that in some very de-

manding urban scenarios involving soft soils one should work towards better or equal performance, with regard to induced movements, than in a similar excavation in stiff soils. This requires efforts and progresses in various fields, such as, new construction technologies, structural conception and methods of analysis.

### 3. The Pre-Stress of the Strut System

This part will be devoted to a brief note on the pre-stressing of the strut system, since the scope of this work corresponds to excavations in thick deposits of soft clayey soils. Traditionally, the pre-stress was looked as a mere expedient of adjusting the strut to the wall, therefore permitting that the effective axial stiffness could reach a high percentage of the theoretical axial stiffness (the one of the structural member materializing the strut), as expressed by Fig. 11.

In this context, the applied pre-stress was typically a small fraction of the design load of the strut. This was based on the following mental model: since the theoretical stiffness is very high, if the effective stiffness is not far from the theoretical one, the wall displacements at that point will be eradicated for the rest of the construction stages. This perspective neglects the very positive effect that a strong pre-stress may induce on the stress state of the ground mass, then, on the stiffness exhibited by the soil.

Figure 12 shows results from a finite element simulation of a multi-strutted excavation in soft soil, in terms of the total stress path of a given point of the supported soil mass. As shown in Fig. 12a, if struts are not pre-stressed the total stress path moves progressively and almost monotonically towards the failure envelop (the active state, in the context of classical Soil Mechanics). On the contrary, with

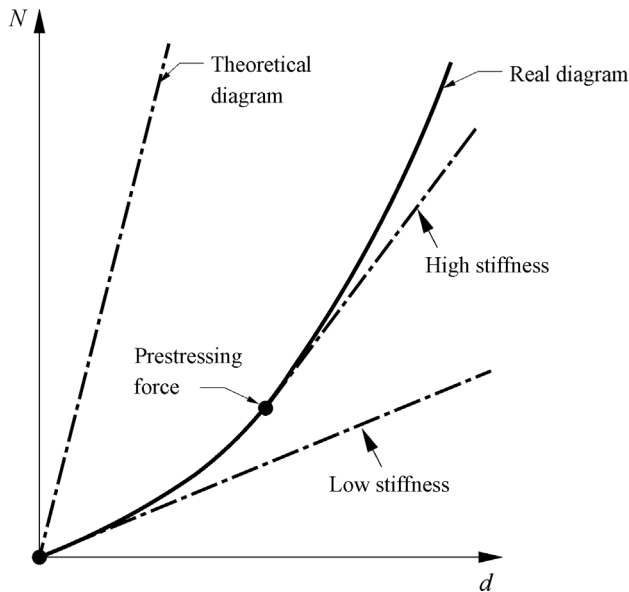


**Figure 11** - Axial load-displacement diagram of a strut and of its interface with the wall and effect of the pre-stress on the effective stiffness.

high pre-stressing applied on the struts, as shown by Fig. 12b, the stress path corresponds to a cyclic loading: the pre-stress applied on each level of supports compensates, in a high degree, the decompression associated with the previous excavation stage. If the stress state of each point of the ground is kept far from the failure envelop, that point will respond with higher stiffness in the sequent excavation stages.

Figures 13a and 13b represent, for the same analyses, the shear stress levels in the ground mass at the end of the excavation (the point whose stress path was mentioned above is marked in black). It may be observed that in the analysis with pre-stressed struts the stress levels are considerably smaller.

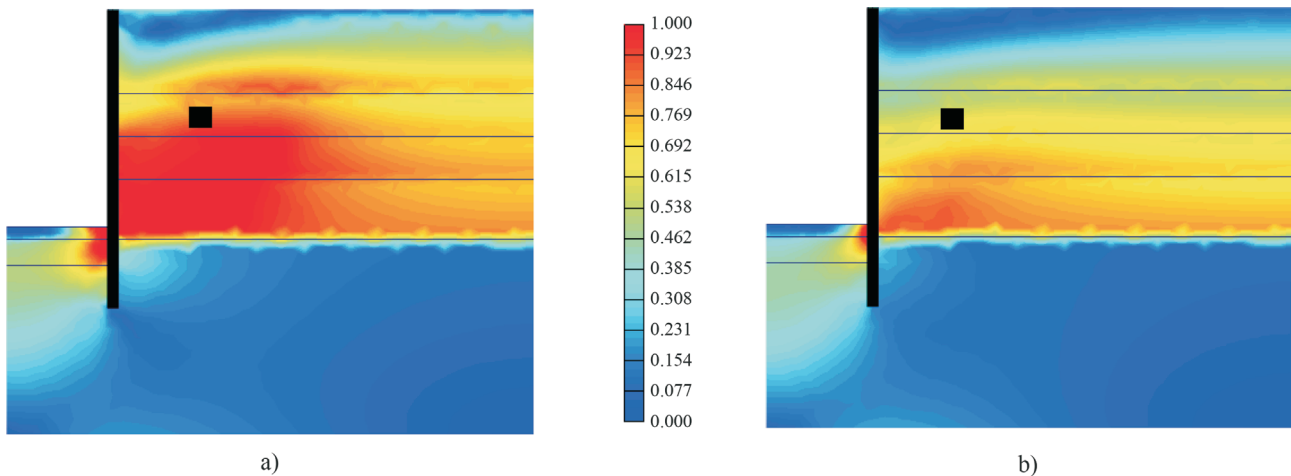


**Figure 13** - Shear stress levels in the ground mass at the end of the excavation: a) with no pre-stress of the strut system; b) with pre-stress of the strut system.

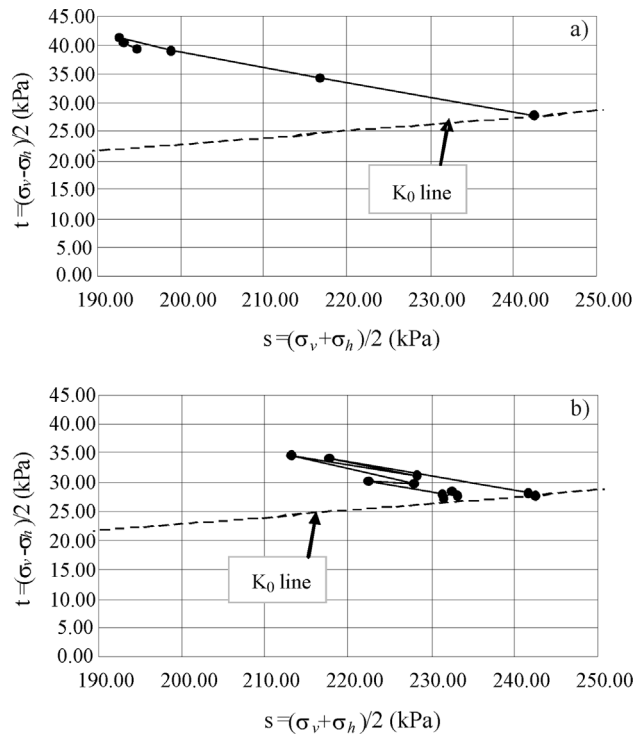


**Figure 12** - Total stress paths in a generic point of a soft clay mass supported by a multi-strutted wall: a) with no pre-stress of the strut system; b) with pre-stress of the strut system.

So, the pre-stress of the strut system is capable of: i) increasing effective axial strut stiffness; ii) recovering some displacements occurred in the preceding excavation stages; iii) *last but not least*, maintaining the state of stress of the soil far from failure, then, ensuring a stiffer response of the soil in the subsequent excavation stages.

It is therefore recommended to use high pre-stress to control the lateral wall displacements above and below the current excavation base. It should be noticed that this is fea-

sible just with a pre-stress system well-conceived and executed and with a reinforced concrete wall with adequate bending stiffness in order to get a reliable control of the forces effectively installed (Matos Fernandes, 2010).

#### 4. Ground Improvement. General Perspective and Proposal

##### 4.1. The “delay” in the installation of the retaining structure

The author begs the tolerance of the reader to remind this reflection of Peck (1969) on the question of the movements: *“In principle, the movements could be prevented if the entire supporting structure (...) and even the base slab for the completed structure could be constructed in their final positions before the removal of the enclosed soil”*.

This question about the *delay of the installation of the retention system* in relation to the execution of the excavation as the source of the inevitability of the movements, appears very clear, as well, in the first of the series of outstanding papers of Clough and co-workers with applications of finite element models to excavations (Clough & Tsui, 1974).

Evaluating the most appropriate distribution of anchor pre-stressing forces in a tied-back diaphragm wall, the authors find that the triangular at-rest diagram is not particularly effective (in comparison with trapezoidal diagrams) in reducing movements (see Fig. 14). They add the following comment: *“The results show that the old concept of restoring the initial soil pressure through pre-stress loads and eliminating movement does not work since wall movements occur during each excavation segment before the subsequent pre-stress load can “restore” the lost earth pressure”*.

By other words: due to the inelastic behaviour of soils, restoring the state of stress does not ensure the restoration of the state of strain!

As it was already emphasized, a real turn point in the field of deep urban excavations was the introduction of reinforced concrete diaphragm walls. With this technology, it was possible to install the entire retaining wall - stiff, resistant, impermeable, beyond the excavation bottom, with minor or modest impact on the ground - before performing the excavation. This fact was extremely relevant for the progress in the control of movements, as commented above.

The understanding of the deleterious effects of the mentioned *delay*, soon encouraged attempts to provide sup-

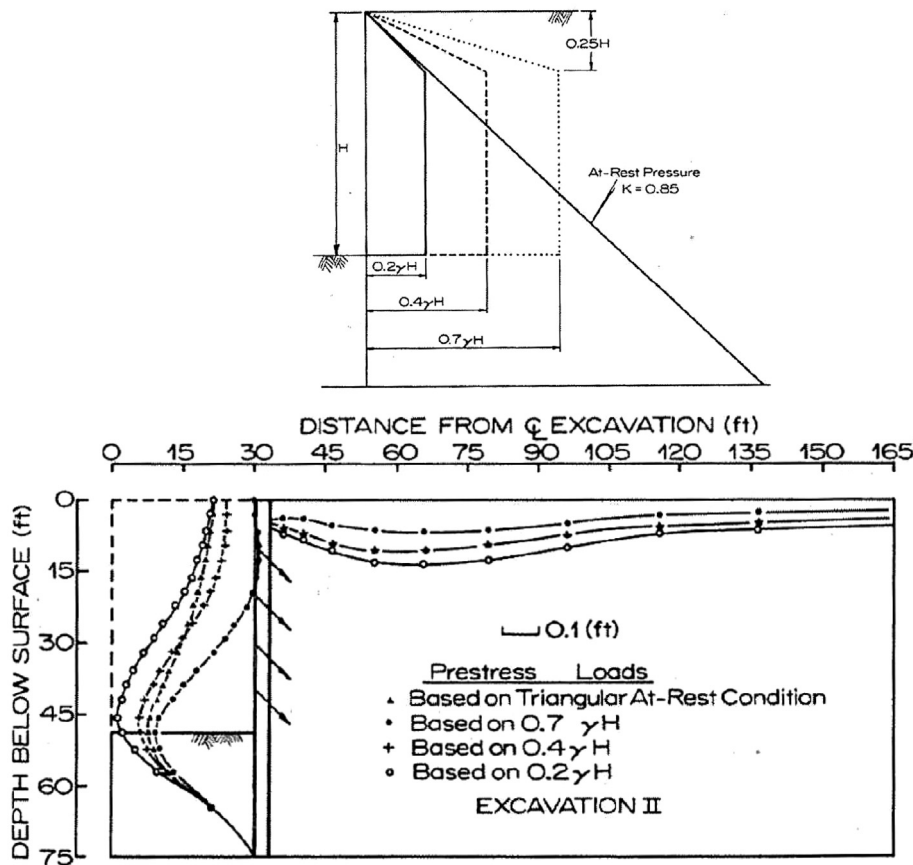


**Figure 14** - Parametric study on the effect of magnitude and distribution of anchor pre-stressing forces on soil and wall movements (Clough & Tsui, 1974).

port to the wall *before the excavation is made*, in complement with the previous installation of the concrete peripheral wall.

**4.2. Historical overview of the solutions providing support to the wall before the execution of the excavation**

The first solution, represented in Fig. 15, was applied in the Oslo Metro at the beginning of the 1970 decade. It consisted of cross diaphragm wall concrete panels, acting as buttresses, under the bottom of the excavation (Eide *et al.*, 1972).

In this solution: i) the cross wall panels remain underneath the excavation bottom due to the difficulty involved in their demolition; ii) difficulties arise due to imperfect cleaning of the interface between the longitudinal walls and the cross walls. This might explain why its application has been very rare and restricted to Scandinavian countries (Karlsrud & Andresen, 2007).

In the nineties, the application of various techniques of soil treatment became frequent as complement of conventional retaining structure solutions, particularly in deep excavations in soft soils (Karlsrud, 1997).

In most cases the treatment is applied in order to form a continuous “slab” of improved soil under the bottom of the excavation. This may be done by jet-grouting (Wang *et al.*, 2005; Matos Fernandes *et al.*, 2007; Ng *et al.*, 2012) or by compaction grouting (Liu *et al.*, 2011; Tan & Wei, 2012). Figure 16 illustrates the case of Cais do Sodré Station of the Lisbon Metro, concluded in 1994.

The use of isolated jet-grout columns in square mesh plan distribution under the base of the final excavation can also be found, as reported by Ou *et al.* (1996) and Hsieh *et al.* (2003).

When the excavation is very deep and its base is close to a firm layer, the slab of improved soil is placed above the final excavation platform, being demolished together with the excavated soil (Brito & Matos Fernandes, 2006; Matos Fernandes, 2007). Cases with two slabs of treated soil, above and below the final excavation level, can also be found in the bibliography, as the one illustrated in Fig. 17 (Lui *et al.*, 2005; Tan & Li, 2011).

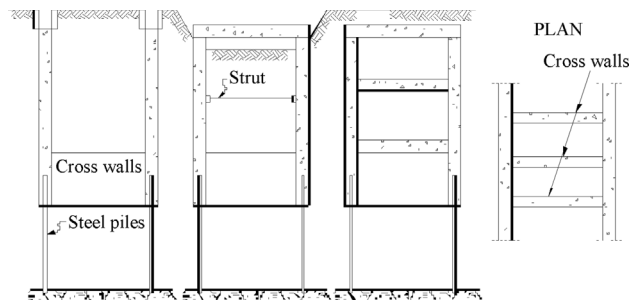


**Figure 15** - Cross diaphragm wall panels below the base of the excavation (Oslo Metro).

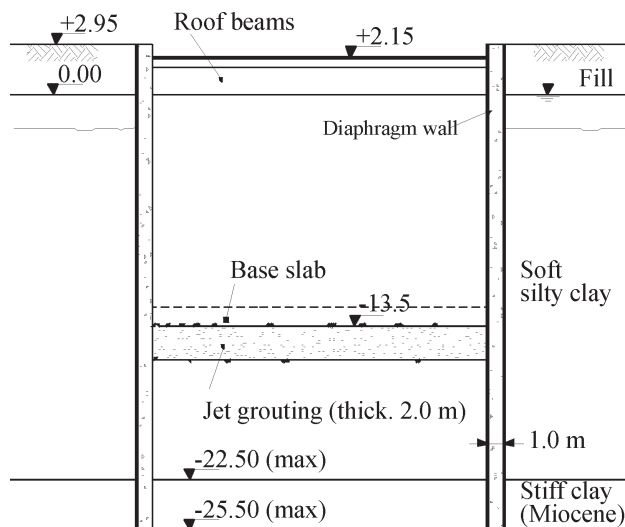


**Figure 16** - Cross section of the retaining structure of the excavation for the Cais do Sodré Station of Lisbon Metro, with a jet grout slab below the base of the excavation (Matos Fernandes, 2007).

One of the limitations of the treatment by jet grouting is that the control of the geometry of the columns is difficult, particularly in this context because they are executed at great depth. Bearing in mind that soft soil must not remain between columns, these are executed by adopting distance between column axes smaller than the expected diameter. This can lead to outward wall displacements even greater than the inward ones that are to be prevented with the treatment (Wong & Poh, 2000).

In this context, the application of the Deep Mixing Method (also known by Deep Soil Mixing) seems to present some advantages, with regard to the control of the geometry (diameter) of the treated soil columns, as well as with regard to the magnitude of the grouting pressures, far below jet-grouting ones. On the other hand, the strength of the treated material is not lower than the one provided by jet-grouting (Pinto, 2014).

O’Rourke & McGinn (2006) report the application of Deep Mixing Method forming vertical transversal elements working as buttresses in the large project of the Boston Central Artery, as shown by the example depicted in Fig. 18.

A very peculiar solution was conceived and constructed in London, in the nineties, in a very deep excavation (39 m) performed inside the old Westminster railway Station (XIX<sup>th</sup> century), as part of the construction of the new Jubilee Line of the London Metro (Glass & Stones, 1999; Mair & Harris, 2001). Even if the soil involved (London clay) is not a soft soil, the movement restrains were extremely severe, due to the presence of the Big Ben tower in the vicinity of the excavation.

As shown by Fig. 19, the toe of the 1.0 m thick diaphragm walls was supported by cylindrical “tunnelled struts” (1.8 m in diameter), built by hand-mining methods



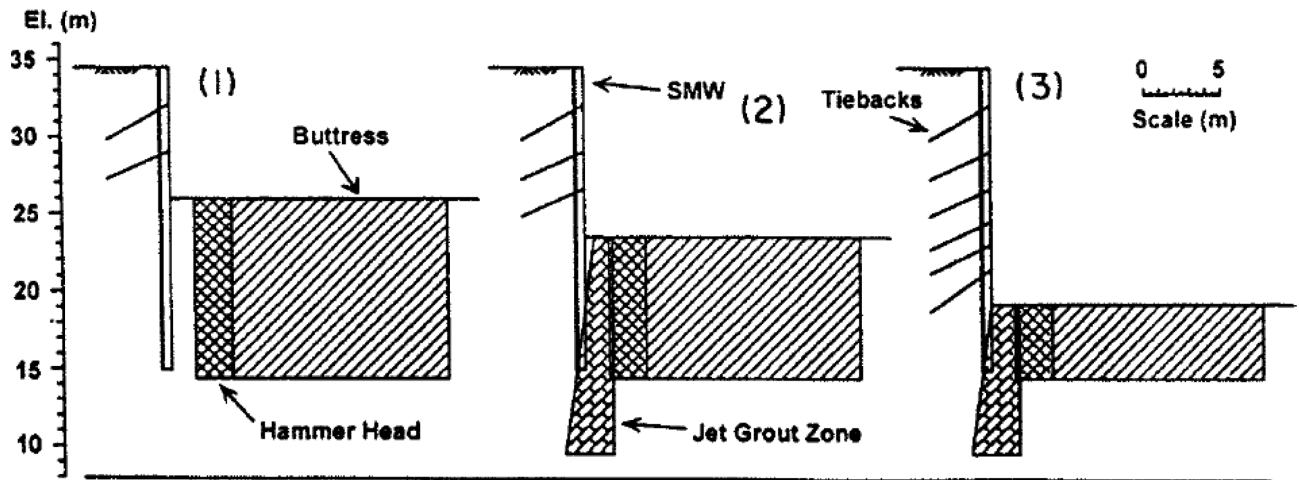


Figure 18 - Buttress of soil treated with Deep Mixing Method in the excavations for the Boston Central Artery and Tunnel Project (O'Rourke & McGinn, 2006).

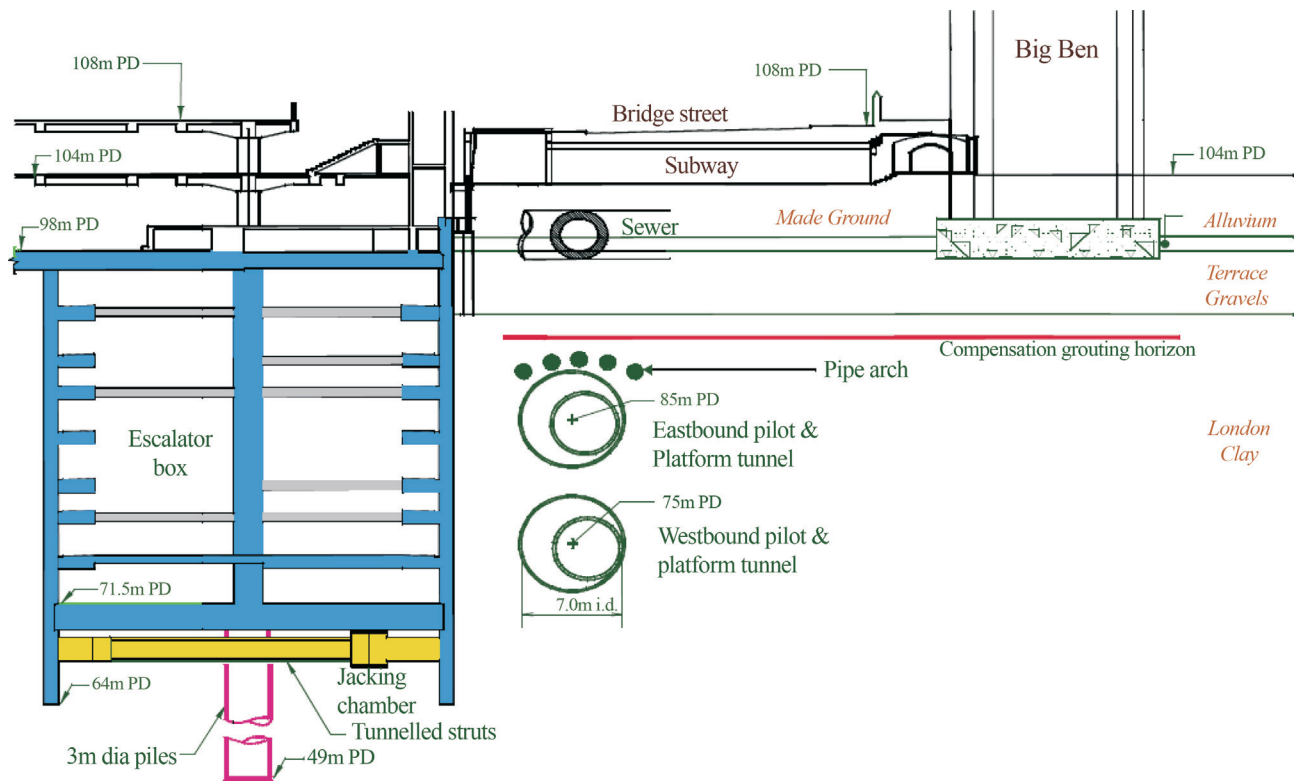
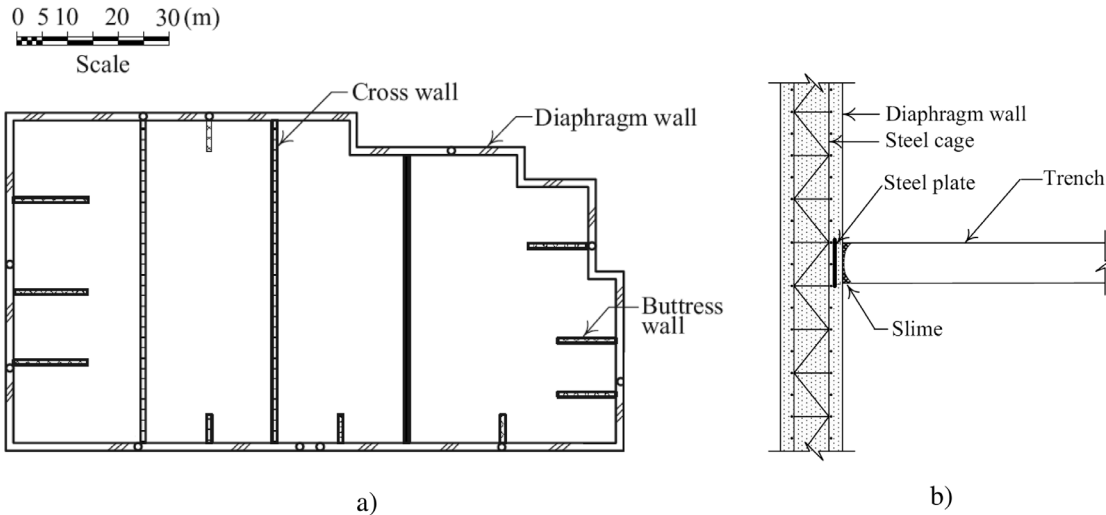


Figure 19 - Cross section of the solution applied in Westminster Station, London, showing the tunnelled struts underneath the excavation bottom (Mair & Harris, 2001).

corners of the excavation. Obviously, that effect will be potentiated if the excavation and the construction of the permanent buried structure are carried out, for each elemental area, in different phases over time. Some useful suggestions can be found in these works with regard to the execution of the joints between the peripheral wall and the cross wall in order to eliminate the lime (Hsieh *et al.*, 2008).

### 4.3. Application of buttresses of soil treated by cutter soil mixing

One recent and promising technology of ground treatment is the so-called cutter-soil-mixing (CSM). This method is similar to the deep mixing method/deep soil mixing (DMM/DSM) but the device that performs the mixture is inspired in diaphragm wall cutter wheels rotating around



**Figure 20** - Excavation with cross walls of concrete up to the ground surface: a) plan scheme; b) detail of a joint cross wall-peripheral wall (Ou *et al.*, 2006, Ou *et al.*, 2011).

a horizontal axis. This means that the geometry of treated mass corresponds to panels of rectangular section in plan. With this technique a continuous wall may be formed by the construction, in an alternating sequence, of overlapping primary and secondary panels. Secondary panels can be constructed immediately after completion of primary panels or by cutting into panels that have already hardened. Panels can be constructed in lengths ranging from 2.2 m to 2.8 m and wall thicknesses of 0.5 m to 1.0 m (Fiorotto *et al.*, 2003, 2005).

In the Manuel Rocha Lecture 2009, the author of this work pointed out this methodology as a very convenient solution to support the wall before the excavation (Matos Fernandes, 2010).

Figure 21 compares: i) the continuous horizontal support, obtained by jet-grouting, compaction grouting or by other method, which can already be considered a classic solution; ii) the proposed support by cross vertical (buttresses) elements, disposed at given intervals in the longitudinal direction, obtained by cutter-soil-mixing. The figure includes, for the two systems, the treatment ratio,  $TR_r$ , that is, the ratio of the volumes of the treated soil and the excavated soil. It should be noted that, in the case of buttresses, their top may rest at the elevation of the base of the first excavation stage, since above that elevation their effect is null.

As suggested by Fig. 21, it would be convenient to install the CSM panels coinciding with the joints of the pe-

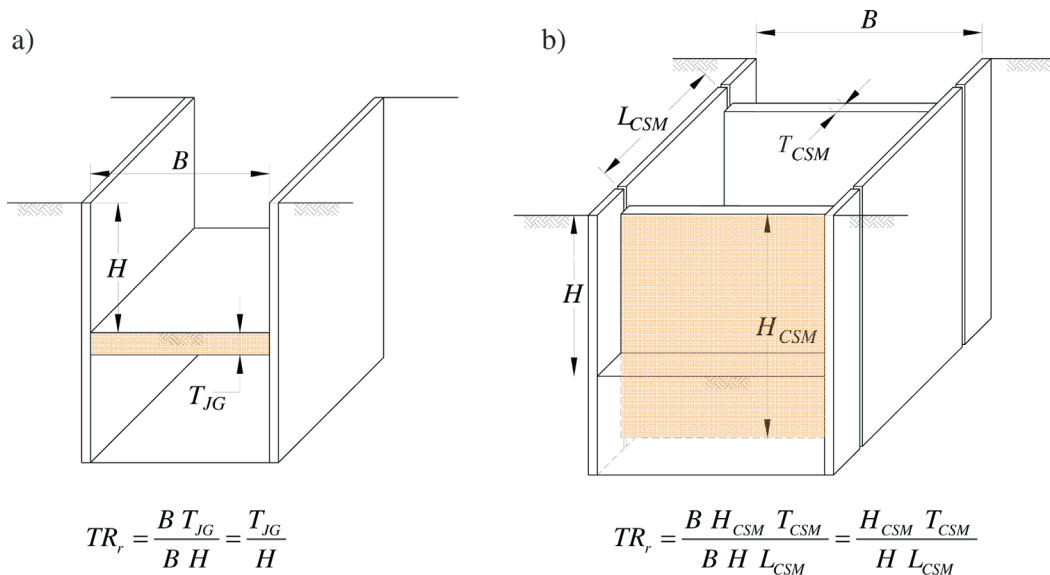


**Figure 21** - Comparative structural systems of the soil treatment and expressions of the treatment ratio: a) slab of jet-grout; b) buttresses of soil treated by CSM.

ripheral wall, whose interval is generally 5-6 m. For this range, and bearing in mind the diaphragm wall thickness commonly adopted in this type of excavations, it may be anticipated that the 3D effects (that is, the differences between the wall displacements and stresses in the supported sections and in the sections midway between supports) would be negligible.

Figure 22 illustrates the typical sequence of a deep excavation with the proposed treatment applied before excavation starts. The treated material is removed together with the soil, stage by stage, in conjugation with the installation and pre-stressing of the temporary struts.

The experience available suggests that this technique could fulfil the following five essential requirements in comparison with other treatment technologies:

- small impact associated with installation, avoiding over-compression or stress relief of the surrounding soil;
- constituent material easy to excavate but with good strength and stiffness, as well;
- very accurate installation position, namely with regard to verticality, position in plan and geometry of the treated soil;
- confidence regarding continuity in the transverse direction;
- confidence regarding the connection to the peripheral concrete wall.

Beyond these points, already confirmed by actual experience (Pinto *et al.*, 2012), there are other very important advantages, namely:

- the CSM panels remaining underneath the final excavation level may provide a foundation for the bottom slab of the permanent structure;
- the CSM treatment can seal a hole resulting from a serious defect at a wall joint;

- the CSM panels may be used, while they are fluid, to install vertical soldier piles for support of the bracing system;
- in comparison with the other solutions, full advantage of the constructive operations is taken, since practically all the penetration of the device is used to improve the ground mass.

There is already a substantial amount of data concerning the mechanical parameters of the treated soil achieved by CSM, as resumed by Fig. 23 (Denis *et al.*, 2012). For soft soils, the Portuguese experience, which is very significant, permits to indicate the following values:  $q_u = 2.5 - 3.0$  MPa and  $E_u / q_u = 400 - 500$  (Matos Fernandes *et al.*, 2010; Peixoto *et al.*, 2012; Pinto, 2014).

Numerical finite element simulations comparing the performance of the two systems illustrated by Fig. 21, as-

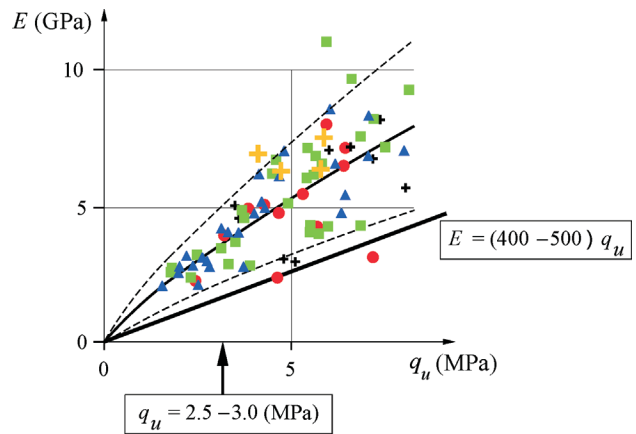


**Figure 23** - Values of the uniaxial compressive strength and of the deformation modulus of soil treated by Cutter Soil Mixing and values derived from the Portuguese experience (adapted from Denis *et al.*, 2012).

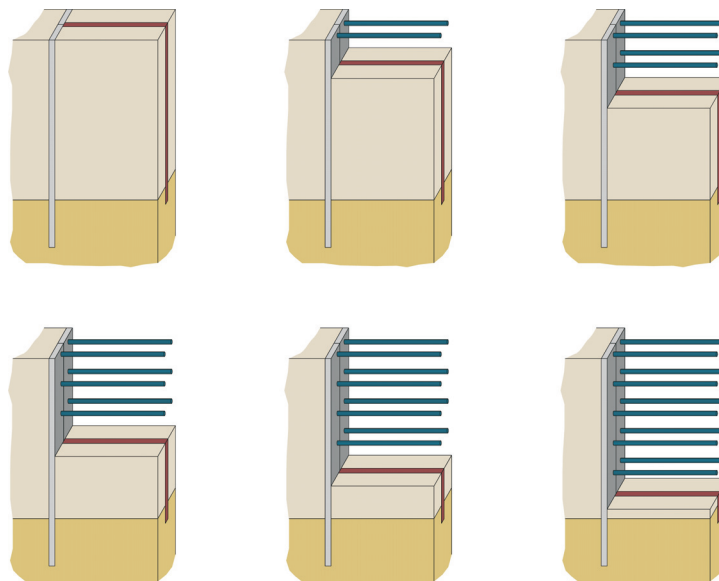


**Figure 22** - Simplified sequence of a multi-strutted deep excavation with buttress of soil treated by CSM (Matos Fernandes, 2010).

suming the same mechanical properties for the treated soil and similar treatment ratios, led to the following conclusions (Matos Fernandes, 2010):

- i) both solutions revealed similar efficacy with regard to the control of the soil and wall movements;
- ii) the solution employing CSM panels takes large advantage as far as the wall bending moments and shear forces are concerned; this is probably due to the fact that the vertical buttresses provide to the peripheral wall a more distributed support along the vertical direction, the one where the structural generalized forces are predominant.

A final comment on the effect of soil treatment in advance of the excavation may be presented with the help of Fig. 24, which collects results from a series of finite element simulations of a deep excavation in soft clay in order to evaluate: i) the effect of the level of the total pre-stress force applied by the struts without any soil treatment in advance; ii) the effect of strut pre-stressing combined with soil treatment by CSM cross panels. The total pre-stress force is expressed as a percentage of the integral of the at-rest total horizontal stresses computed from the surface to the base of the excavation.

The figure presents the soil displaced volume (that is, the integral of surface settlements) for all the analyses performed, at the completion of the excavation. As a reference, the figure also includes the volume from Peck’s chart for maximum settlement of 1% of the excavation depth.

The exam of the figure permits to observe that, for the analyses with no treated soil, the strut pre-stress is capable of reducing the displaced volume up to about 1/2 of that obtained when no pre-stress is applied, whereas a reduction to about 1/3 is obtained with similar pre-stress for the series of analyses with the soil treated by CSM. This result is very

inspiring: it suggests that there is a synergetic effect (that is, a virtuous combination) between pre-stressing and soil improvement in the control of the movements. This had been already identified by Matos Fernandes *et al.* (2008) with the soil improvement by a jet-grout slab.

## 5. The Long-Term Hydraulic Conditions and the Settlements by Consolidation

### 5.1. Introduction

As it was emphasized above, the consolidation induced by the excavation may originate surface settlements. Note that in many cases the soft soil consists of organic clayey silt, whose (not very small) permeability allows a consolidation process during a relatively short period after the conclusion of the excavation.

For very thick soft deposits, extending the wall in depth to the bedrock is a recommendable but expensive solution. An alternative solution consists of limiting the embedded wall length to the value required by a comfortable safety factor against bottom heave. In general, the bottom slab of the permanent buried structure incorporates a drain in order to avoid uplift pressures in the long-term.

When comparing the two solutions, depicted in Fig. 25, a relevant issue is related to the differences of the consolidation process during and, mostly, after the completion of the excavation, as will be highlighted below through finite element analyses (Matos Fernandes *et al.*, 2012).

### 5.2. Assumptions for the numerical study

The selected problem corresponds to an excavation with an infinite length, 10 m deep and 12 m wide, performed in soft clayey silt 30 m thick, overlying a hard and practically impermeable substratum (Fig. 25). The soft soil

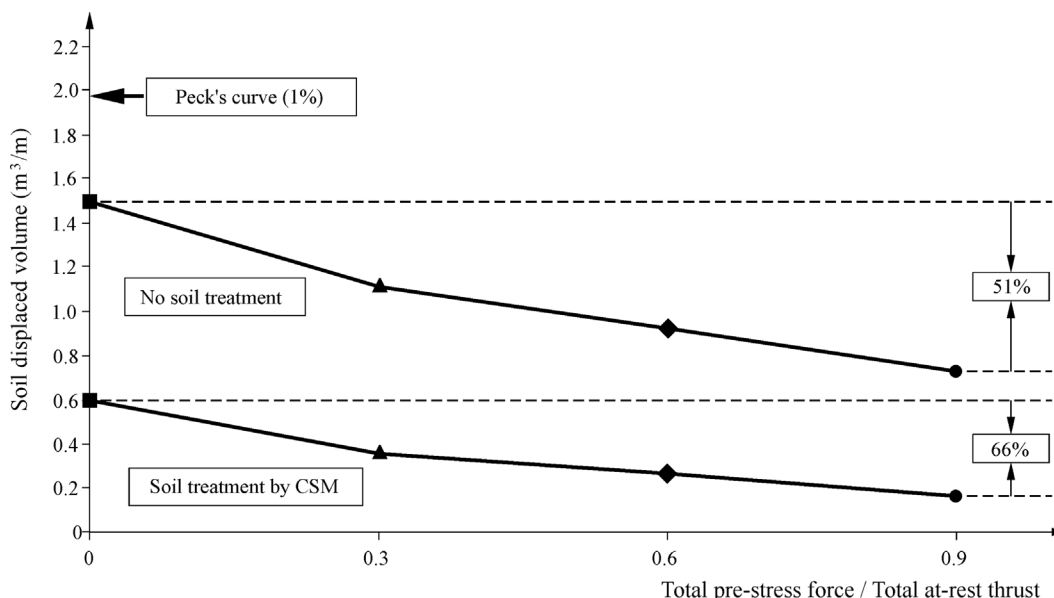
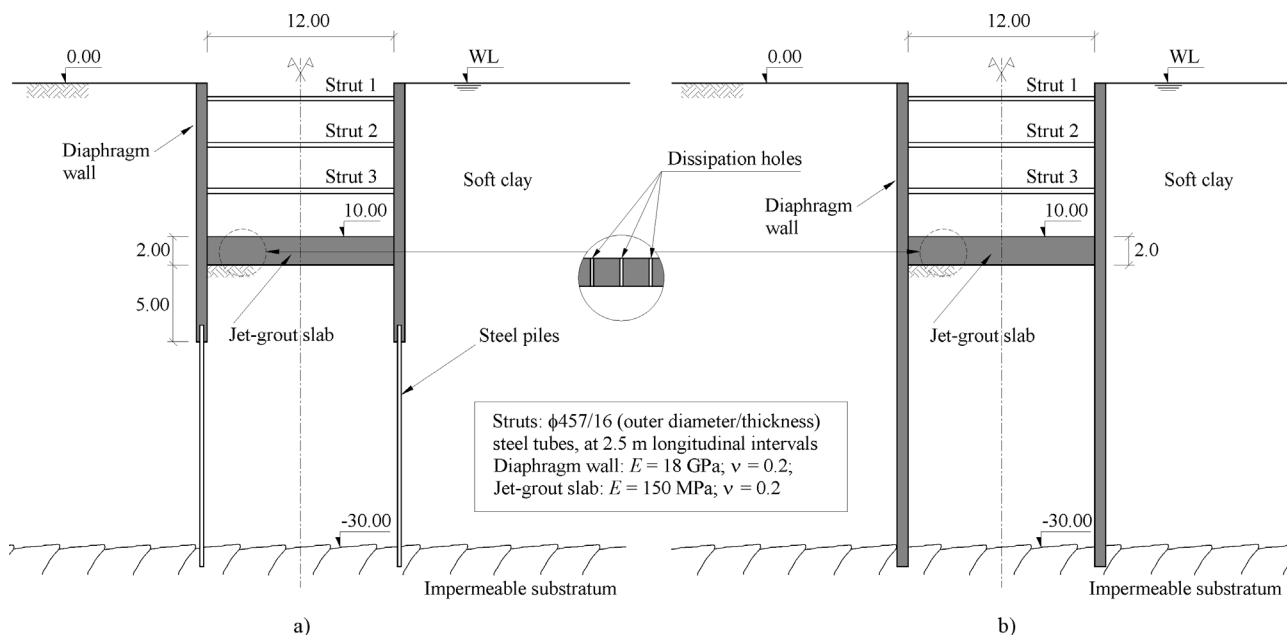


Figure 24 - Synergetic effect between pre-stressing and soil treatment in the control of the movements.



**Figure 25** - Cross section of the excavations considered for studying the influence of the long-term hydraulic conditions on the settlements by consolidation: a) case A; b) case B.

is lightly over-consolidated from the surface down to a depth of 4 m and normally consolidated for larger depths.

The retaining structure consists of a 1.0 m thick reinforced concrete diaphragm wall and three levels of cross-slot steel struts. Two solutions were considered for the retaining wall, as shown in Fig. 25: embedded length of 7.0 m (case A); embedded length of 20 m, which means that the wall is extended down to the substratum (case B). The safety factor against bottom heave for case A, calculated by the method of Bjerrum & Eide (1956), is 1.42.

In order that both retaining structures could ensure comparable control of the movements during the excavation phase, it was assumed a 2 m thick jet-grout slab, executed prior to the soil removal and placed immediately below the base of the excavation.

Basically, the finite element code uses a fully coupled formulation of the flow and equilibrium equations with soil constitutive relations in effective stresses, according to the Biot consolidation theory (Britto & Gunn, 1987; Borges, 1995) and the  $p - q - \theta$  critical state model (Lewis & Schrefler, 1987; Borges, 1995; Borges & Pinto, 2013; Borges & Guerra, 2014).

As for the hydraulic boundary conditions, it is assumed that: i) in the supported side, the water table remains at the ground surface (which is a conservative option, assuming that there is a flow providing water to the ground surface); ii) in the excavated side, the water level coincides with the current excavation base; iii) the diaphragm wall and the substratum are impermeable; iv) the long-term conditions correspond to null pore pressures at the top of the jet-grout slab.

The excavation is carried out in a total time of 25 days at a uniform rate. A fully coupled analysis is performed both during and after the excavation period.

### 5.3. Discussion of the results

#### 5.3.1. Excavation period

During the excavation period, because of the low permeability of the soft soil, the behaviour is approximately undrained.

Figure 26 illustrates the distribution of the excess pore pressure at the end of excavation for solutions A and

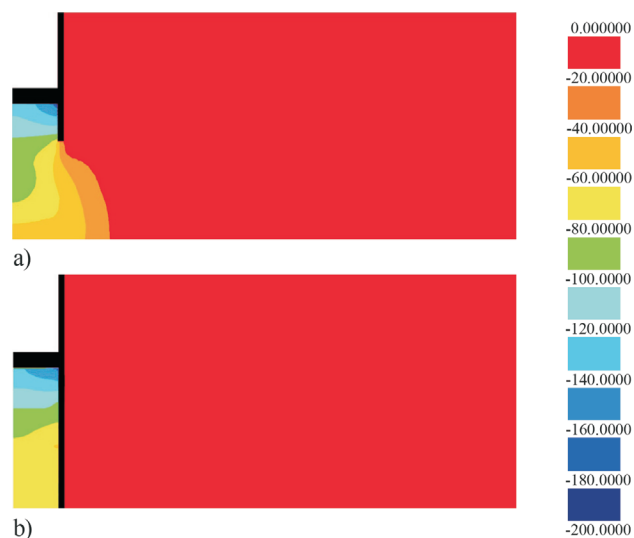


**Figure 26** - Excess pore pressure at the end of excavation: a) case A; b) case B.

B. Excess pore pressure is defined as the difference between pore pressure at a particular moment and its initial hydrostatic value.

The results reveal that negative values are generated by the excavation in both cases. As could be expected, highest negative values of excess pore pressure occur below the excavation base, in association with the very pronounced decrease of the total mean stress in that zone. On the supported side of the ground mass a tendency for generating negative excess pore pressures is also observed, although with much smaller values than at the opposite side. This is mainly explained by the effective restraint provided by the jet-grout slab, which decisively contributes to avoid a ground decompression with much larger magnitude. Maximum values of negative excess pore pressure on the supported side are around 55 kPa for case A (in a region below the wall tip) and 13 kPa for case B.

5.3.2. Post-excavation period

Figure 27 represents the distribution of pore pressure at the end of consolidation. It should be noted that, as said above, excess pore pressure is considered herein (as defined in the computer code) the difference between pore pressure at a particular moment and its initial hydrostatic value (before excavation), and not its final value (at the end of consolidation).

In case A long-term steady flow contouring the wall tip takes place, whereas in solution B hydrostatic states on both sides of the wall are obtained at end of consolidation.

Due to the distinct long-term pore pressure conditions, the most significant conclusion extracted from the comparison of results is that the consolidation process is qualitatively quite different in the two cases. As could be expected, the most significant variations of pore pressure are observed on the excavated side. However, on that side

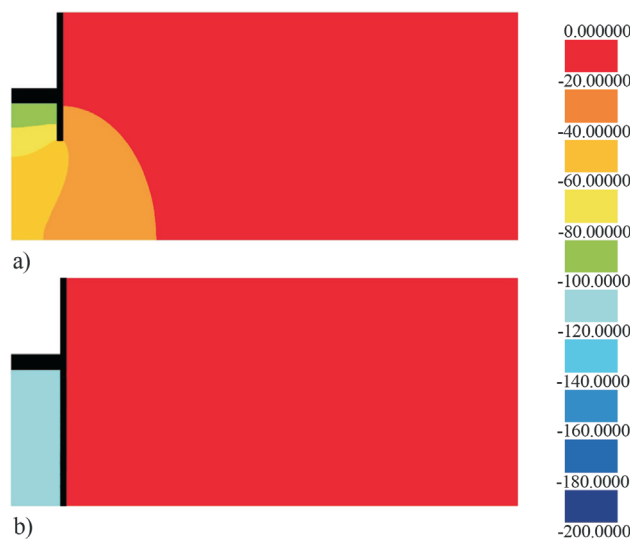


Figure 27 - Distribution of pore pressure at the end of consolidation: a) case A; b) case B.

water pressure increases in solution A whereas in solution B it decreases in a part of the ground (at larger depths) and increases in another (close to the excavation bottom). On the supported side, the evolution is contrary, although of lower magnitude: there is a decrease of pore pressure in case A, related with downward water flow, while an increase takes place in case B.

Horizontal displacements of the wall at the completion of the excavation and at the end of consolidation, for both cases, are shown in Fig. 28. As could be expected, the displacements are larger in case A. This is obviously due to the shorter embedded length, which allows a somewhat larger rotation of the wall around the contact with the jet-grout slab (between -10 m and -12 m in depth).

In overall terms, the wall displacements above the excavation base level do not significantly change with the consolidation. The most expressive variation is observed below that level, where displacements reduce in case A and increase in case B. For case A this evolution may be explained by the swelling effect of the soil underneath the excavation (associated to the decrease of mean effective stress, as seen above) as consolidation takes place in that zone. In case B the evolution is the opposite: since the mean effective stress increases (at larger depths) as the consolidation evolves, a shrinking on the soil underneath the excavation occurs, which permits a movement of the wall towards that side. The slight increase in the pore pressure on the

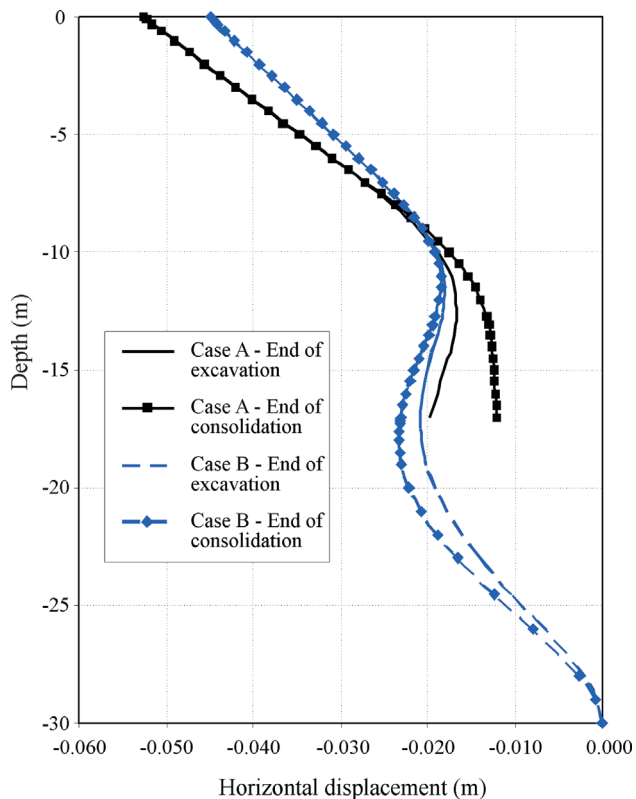


Figure 28 - Wall horizontal displacements at the completion of the excavation and at the end of the consolidation.

other side of the wall also contributes for the observed movement evolution.

The distribution of the surface settlements is illustrated in Fig. 29. In case A, there are pronounced downward displacements on the supported ground with the consolidation, while in case B upward displacements are observed, although with much less magnitude.

The evolution in case A is mainly justified by the reduction of volume on the supported soil, as discussed above. In case B there are two contrary effects: incremental horizontal displacements of the wall (below the excavation base) occur - which, by themselves, tend to increment surface settlements; however, the supported soil swells as the consolidation takes place - which tends to upraise the ground surface. This second effect is stronger, provoking upward displacements after the excavation period.

As a final comment, it is interesting to observe that the considered solutions provide similar lateral wall displacements, both at the completion of the excavation and at the end of the consolidation. As well, they ensure very resembling surface settlements at the end of the excavation. Nevertheless, the corresponding surface settlements at the end of the consolidation process are very discrepant (maximum settlement for case A is about six times greater than the one for case B).

This highlights the great convenience of preventing, for the long-term conditions, a steady flow of water towards the excavation. The settlements induced by the new distribution of effective stresses in the supported ground associated to this flow may cause serious damage in ancient constructions that in some urban areas are founded on the desiccated crust.

## 6. The Influence of the Nonlinear Behaviour of the Reinforced Concrete

### 6.1. Introduction

In flexible retaining structures the deformations by bending play a critical role in the distribution of earth pressures and of the structural stresses. The ability to experience deformation without stiffness reduction is quite

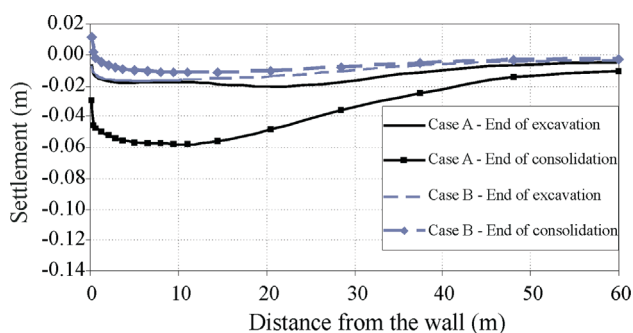


**Figure 29** - Surface settlement distribution at the completion of the excavation and at the end of the consolidation.

different in steel and in reinforced concrete walls. For the bending strain level commonly attained by concrete retaining walls, the behaviour is no longer linear elastic. In spite of this fact, the geotechnical finite element models commonly used in design practice assume a linear elastic behaviour for the structural components, while offering many non-linear constitutive laws for the soil, some of them highly sophisticated. It is interesting to observe that the opposite occurs with regard to the soil-structure interaction analyses performed by structural engineers: more or less complex non-linear constitutive laws are used for the reinforced concrete whereas the foundation soil is assumed to be linear elastic!

Figure 30 resumes this *analytical gap*, as this bizarre situation was classified by the author (Matos Fernandes, 2010). In that paper it was stated that to overcome this *gap* would probably be the most challenging and critical task for the near future in the field of the computational methods applied in design. Fortunately, some progress in this field may be presented in this occasion.

### 6.2. Numerical model

The solution found consists of an interaction between the geotechnical computational code (Code G) and the reinforced concrete (nonlinear) computational code (Code RC), as illustrated in Fig. 31.

For each stage of construction, the bending moment and axial stress diagrams in the wall, computed by Code G, are applied to the structure modelled by Code RC, which accounts for the actual steel reinforcement at each section. This code then calculates the strains and cracking in the reinforced concrete wall and the corresponding adjusted stiffness at each section, which is introduced in Code G for being used in the next construction stage.

This idea was implemented using as the geotechnical code FEMEP, developed at the Universities of Porto and Coimbra (Cardoso *et al.*, 2006; Almeida e Sousa *et al.*, 2011) and as the structural code EVOLUTION, developed at the University of Porto (Ferraz, 2010).

With the purpose of exemplifying the application of the procedure described it was taken the example illustrated in Fig. 32: an excavation 18 m deep and 24 m wide in a deposit of soft clay 27 m thick, supported by a diaphragm wall

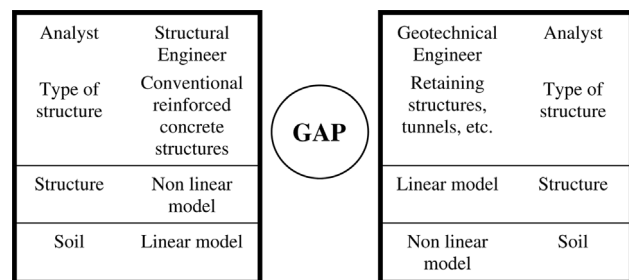


**Figure 30** - The “analytical gap” between structural and geotechnical analyses (Matos Fernandes, 2010).

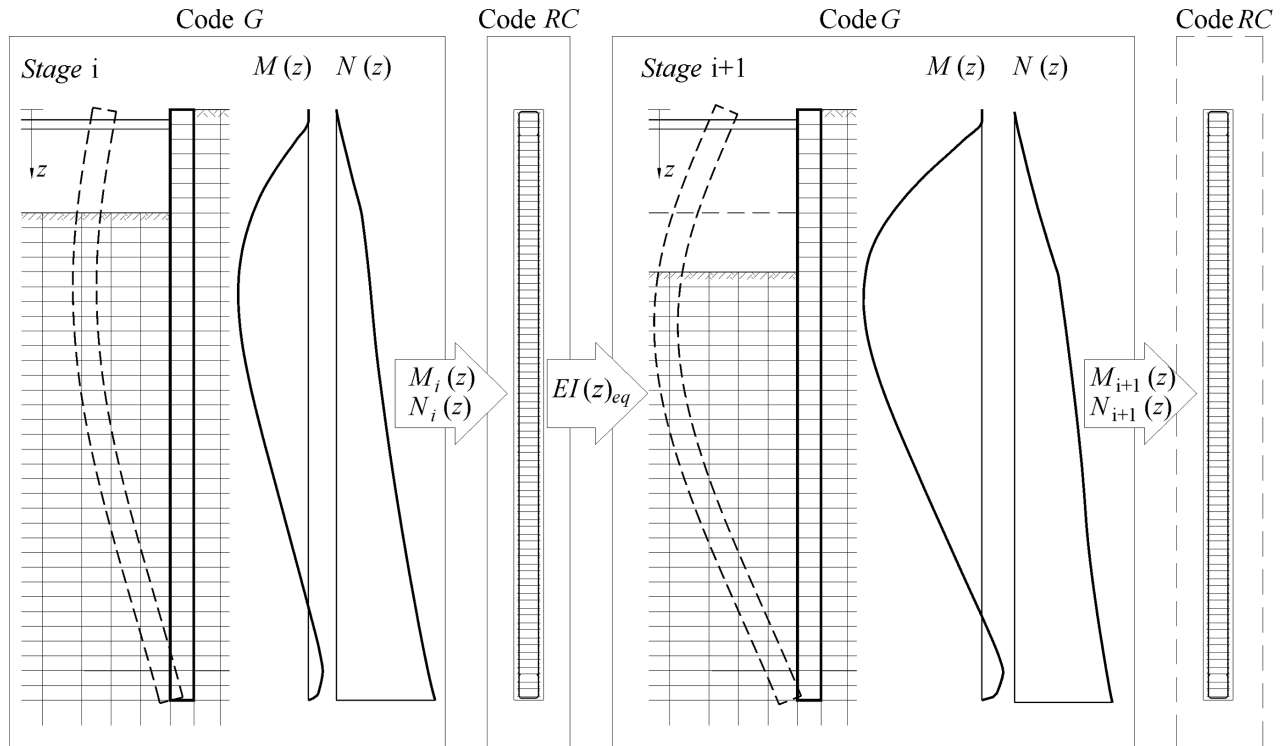


**Figure 31** - The interaction between the geotechnical code (code G) and the structural code (code RC) to account for the nonlinear behaviour of the reinforced concrete retaining wall.

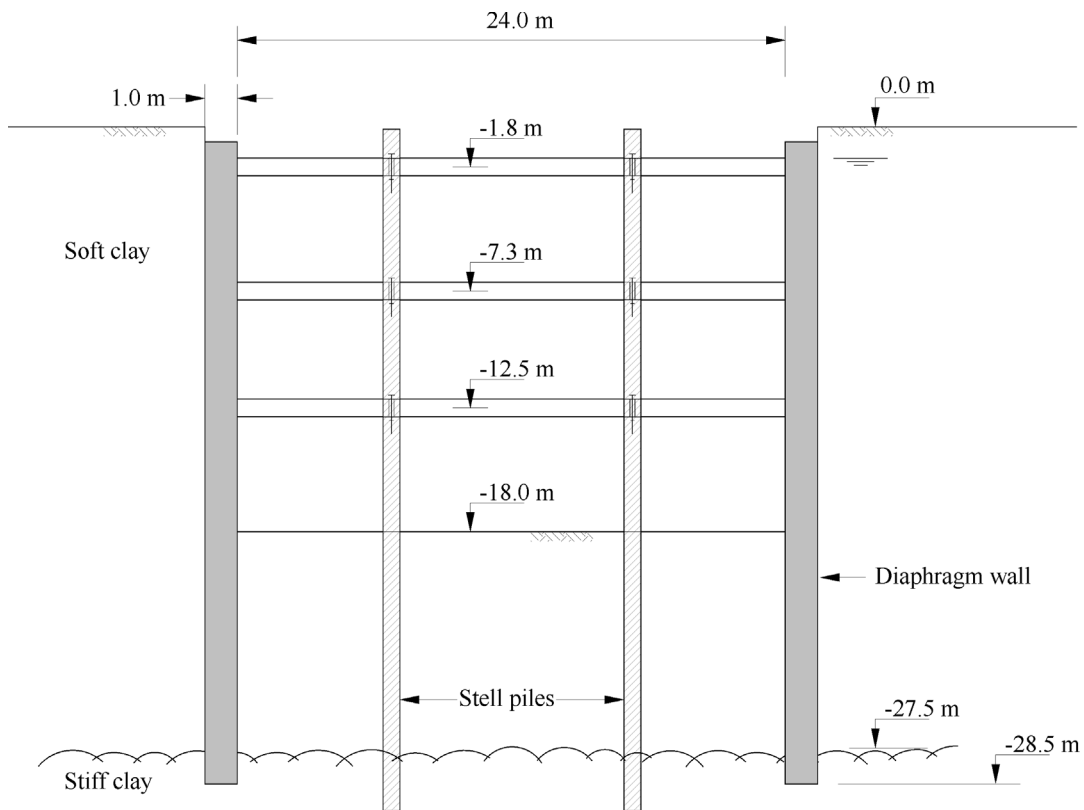


**Figure 32** - Cross section of the excavation considered for studying the influence of the non linear behaviour of the reinforced concrete wall.

(1.0 m thick and the toe sealed 1.0 m into the substratum) and by three levels of cross-lot non pre-stressed steel struts.

**6.3. Discussion of results**

Firstly, it was performed an analysis assuming the reinforced concrete wall as linear elastic. This analysis: i) served as comparison for the analysis in which the numerical model described above was applied; ii) on the other hand, its results concerning the structural stresses in the wall were the basis for calculating the steel reinforcement, using the conventional procedures of concrete structures. In particular, the bending moments obtained from the finite element analysis were multiplied by 1.35. This is illustrated in Fig. 33.

Figures 34 and 35 compare the results in terms of wall bending moments and lateral wall displacements provided by the analysis just mentioned above (linear elastic wall) and by the analysis which considers the nonlinear behaviour of reinforced concrete, with the steel reinforcement shown in Fig. 33b.

As expected, the nonlinear behaviour of reinforced concrete, implying a decrease of the wall bending stiffness, leads to a reduction of the maximum bending moments and to an increase of wall displacements. The influence regarding the bending moments is extremely relevant; as far as the wall movements are concerned, an increase of the order of

25% in the maximum displacement was obtained, which is rather expressive.

Figure 36 collects, for the final excavation stage, the results from the analysis with the nonlinear concrete behaviour, showing in its central part (Fig. 36b) the ratio, for each horizontal wall section, between the effective bending stiffness and the elastic bending stiffness. It can be observed that, in the region where bending moments and displacements are more pronounced, along more than 10 m, the effective stiffness ratio is about 1/3 of the elastic one.

These preliminary results seem to confirm the relevance of considering the nonlinear behaviour of reinforced concrete in the geotechnical finite element analyses for this type of excavations.

**7. Conclusions**

Deep excavations in thick deposits of soft soils have known, along the last decades, an outstanding evolution. We now accomplish, in that domain, works that a few decades ago were unimaginable or that would require cost, execution time and nearby impact of intolerable magnitude. Such evolution is hardly replicable in other fields of Civil and Geotechnical Engineering.

The interaction between a flexible retaining structure and the adjacent soil mass is what is called, in Structural Engineering, a highly hyper-static problem. Then, before

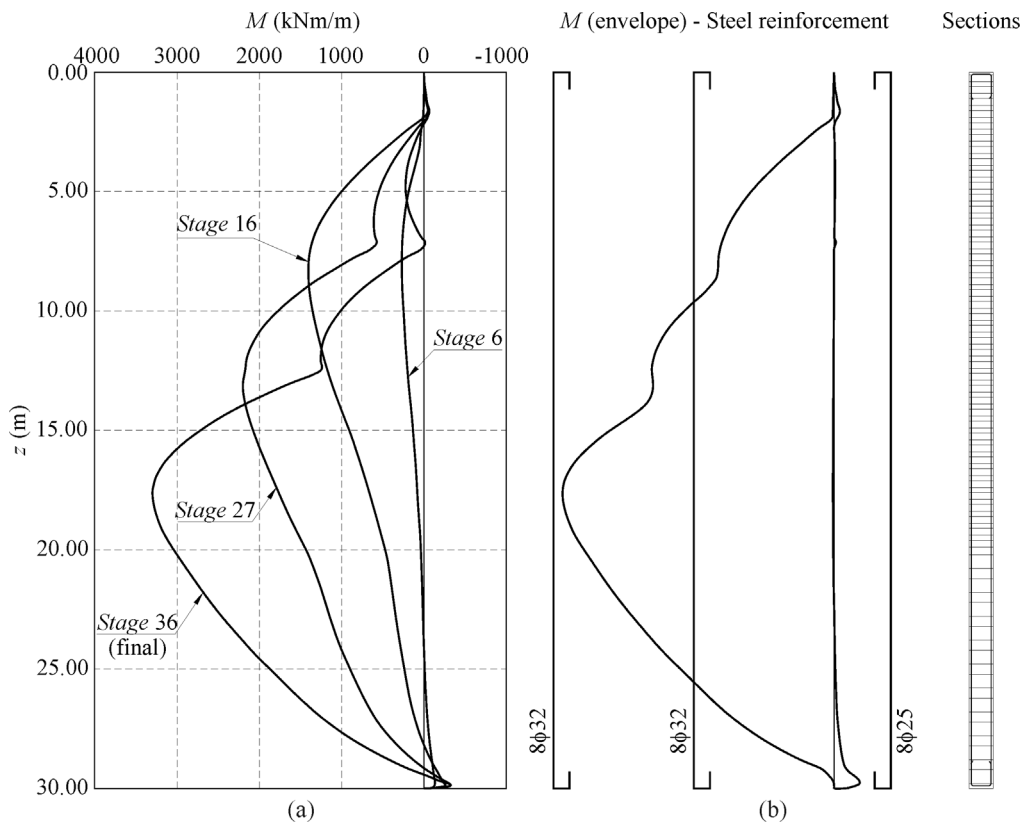


**Figure 33** - Design of the reinforced concrete wall: a) bending moment diagrams assuming linear elastic behaviour of the concrete; b) steel reinforcement.

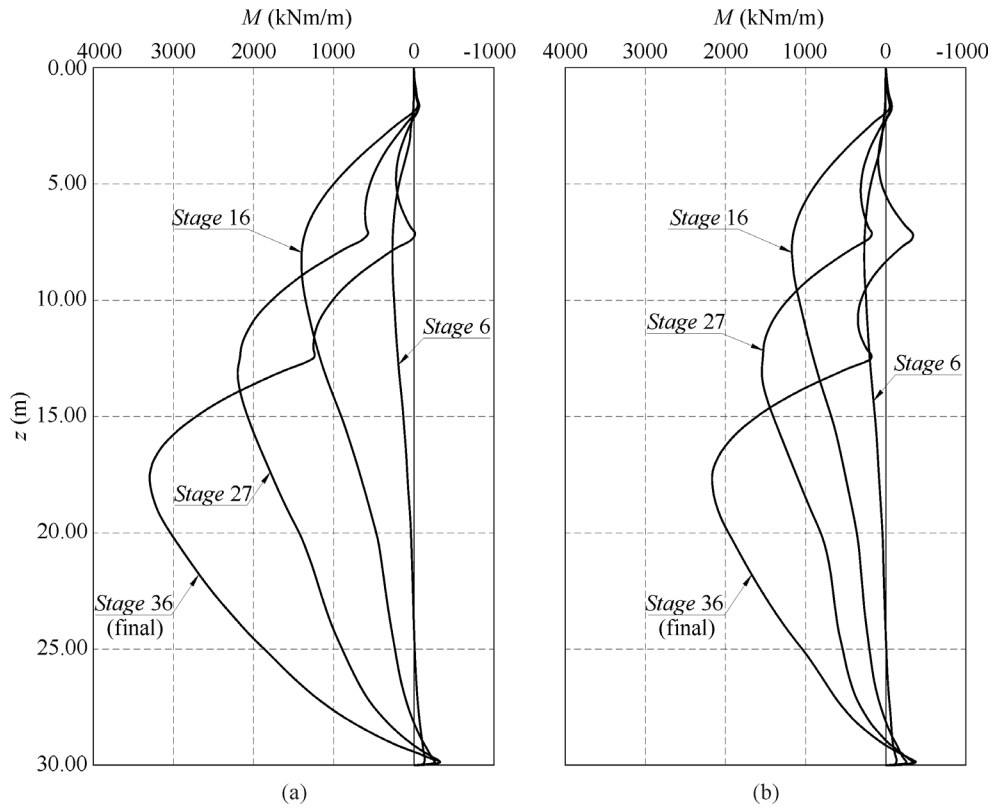


Figure 34 - Wall bending moments: a) linear elastic concrete wall; b) nonlinear concrete wall.

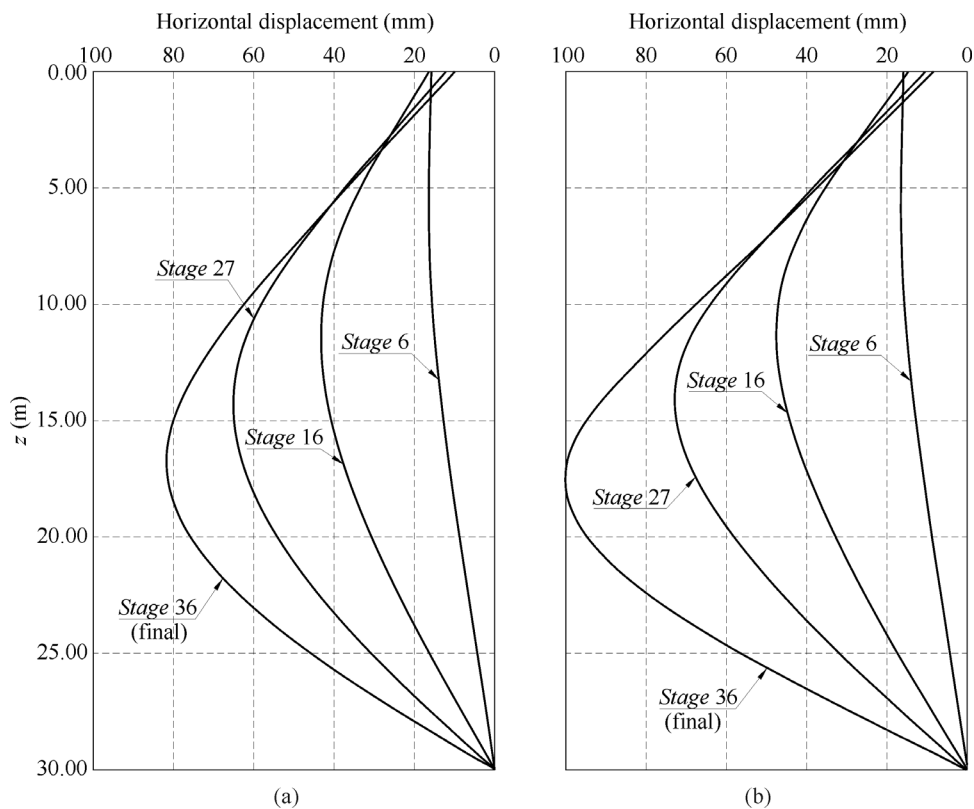


Figure 35 - Lateral wall displacements: a) linear elastic concrete wall; b) nonlinear concrete wall.



**Figure 36** - Results of the analysis considering the nonlinearity of the concrete wall at the completion of the excavation: a) wall bending moments; b) ratio between the effective and the elastic bending stiffness; c) lateral wall displacements.

the application of finite element models to these problems, the available design methods were very limited and of empirical or semi-empirical nature. Contrarily to various geotechnical fields - such as spread and deep foundations, natural slopes, etc. - modern deep excavations in soft soils would not be possible without the profit of an analytical tool as powerful as the finite element method.

In spite of such a brilliant progress, the Profession is tacitly *more tolerant* with excavation induced movements in soft ground. However, in soft ground ancient structures and services might probably be *less tolerant* with regard to further movements than similar constructions over stiff soils.

More *robust and reliable* solutions, exploiting the best the technology and the experience have convened, are highly recommendable. These solutions are not just a condition for minimizing the induced movements. They strongly increment the reliability of our prediction analyses!

Like in the sixties the introduction of diaphragm walls, permitting to install the entire reinforced concrete wall *before performing the excavation*, was a paramount technical advance, a number of solutions have been tested in order to provide support to the wall *before the removal of the soil*. The combination of these two expedients has permitted an auspicious progress in the control of the move-

ments induced by the excavations. Particularly in soft soils, it is possible today to achieve values of the surface settlements one order of magnitude below the most favourable results reported by Peck (1969) in his splendid general report.

The use of cutter-soil-mixing to construct vertical cross buttresses of treated soil at given intervals presents a remarkable set of advantages - concerning the conception, the execution and the structural performance - in comparison with other well-known solutions involving soil treatment.

The combination, in the retaining structure, of high level of strut pre-stressing with the treatment of the soft soil produces a synergetic effect for the minimization of the movements.

The settlements developed by consolidation of the soil after the conclusion of the excavation are a topic deserving more attention. The results presented show the great convenience of preventing, for the long-term conditions, a steady flow of water towards the bottom slab of the permanent buried structure. The settlements induced by the new distribution of effective stresses in the supported ground associated to this flow may achieve various times the ones prevailing at the conclusion of the excavation.

The consideration in finite element analyses of the nonlinear behaviour of reinforced concrete wall may have a

non negligible influence on the computed wall displacements and a strong influence on the values of the structural stresses in the wall.

The author would like to conclude by emphasizing that a sustainable progress in this area depends on an ingenious exploitation and combination of the advances in the three following fields: construction technologies, conception of the retaining structures and methods of analysis.

## Acknowledgments

The author expresses his deep gratitude to the Brazilian Association for Soil Mechanics for the kind and very prestigious invitation to present the 11<sup>th</sup> Pacheco Silva Lecture. He is indebted to the Colleagues that collaborated in the research presented, António Cardoso (Univ. Porto), António Pedro (Univ. Coimbra), Jorge Almeida e Sousa (Univ. Coimbra), José Cândido Freitas (Inst. Polit. Porto), José Leitão Borges (Univ. Porto), José Mateus de Brito (Cenorgeo, Lisbon), José Menezes (Univ. Porto), Miguel Ferraz (Univ. Porto), Pedro Alves Costa (Univ. Porto) and Pedro Pereira (Univ. Porto). Special appreciation is due to Alberto Sayão (PUC, Rio de Janeiro), Alexandre Pinto (JETSJ, Lisbon), Arsénio Negro Jr. (Bureau, São Paulo), Artur Peixoto (Georumo) and Nuno Cristelo (Univ. Trás-os-Montes e Alto Douro), that provided documents, technical advice and other data for the preparation of the lecture. Great esteem and recognition are due to Anna Laura Nunes (Federal Univ. Rio de Janeiro), Bárbara Rangel (Univ. Porto) and Manuel Carvalho (Univ. Porto) for their inestimable support in the presentation of the lecture. The careful review of the paper by Sara Rios is gratefully acknowledged.

## References

- Almeida e Sousa, J.; Negro, A.; Matos Fernandes, M. & Cardoso, A.S. (2010). Three-dimensional nonlinear analyses of a metro tunnel in Sao Paulo porous clay, Brazil. *Journal Geotechnical and Geoenvironmental Engineering*, ASCE, 137(4):376-384.
- Alves Costa, P.; Borges J.L. & Matos Fernandes, M. (2007). Analysis of a braced excavation in soft soils considering the consolidation effect. *Geotechnical and Geological Engineering*, 25(6):617-629.
- Bjerrum, L. & Eide, O. (1956). Stability of strutted excavations in clay. *Géotechnique*, 6(1):32-47.
- Bjerrum, L.; Clausen, C. & Duncan, J. (1972). Stability of flexible structures. Proc. V<sup>th</sup> European Conference on Soil Mechanics and Foundation Engineering, Madrid, General Report.
- Borges, J.L. (1995). Geosynthetic-Reinforced Embankments on Soft Soils. Analysis and Design. PhD Thesis in Civil Engineering, University of Porto, Portugal (in Portuguese).
- Borges, J.L. & Pinto, R.G. (2013). Strutted excavation in soft soil incorporating a jet-grout base slab: analysis considering the consolidation effect. *Geotechnical and Geological Engineering*, 31(2):593-615.
- Borges, J.L. & Guerra, G.T. (2014). Cylindrical excavations in clayey soils retained by jet grout walls: numerical analysis and parametric study considering the influence of consolidation. *Computers and Geotechnics*, 5(1):42-56.
- Britto, A.M. & Gunn, M.J. (1987). *Critical Soil Mechanics via Finite Elements*. Ellis Horwood Limited, England.
- Brito, J.M. & Matos Fernandes, M. (2006). Terreiro do Paço Station of Metropolitano de Lisboa: Conception, design predictions and performance (in Portuguese). Proc. 3<sup>rd</sup> Portuguese-Brazilian Congress, v. 1, pp. 21-42.
- Cardoso, A.S.; Guerra, N.C.; Antão, A. & Matos Fernandes, M. (2006). Limit analysis of anchored-concrete soldier-piles in clay under vertical loading. *Canadian Geotechnical Journal*, 43(5):516-530.
- Clough, G.W. & Tsui, Y. (1974). Performance of tied-back walls in clay. *Journal Geotechnical Engineering*, ASCE, 100(12):1259-1273.
- Clough, G.W. & Mana, A.I. (1976). Lessons learned in finite element analyses of temporary excavations in soft clay. Proc. 2<sup>nd</sup> Int. Conf. on Numerical Methods in Geomechanics, Blacksburg, Virginia, v. 1, pp. 496-510.
- Clough, G.W. & Reed, M.W. (1984). Measured behavior of braced walls in very soft clay. *Journal Geotechnical Engineering*, ASCE, 110(1):1-18.
- Clough, G.W.; Smith, E.M. & Sweeney, B.P. (1989). Movement control of excavation support systems by iterative design. Proc. ASCE Conf. on Foundation Engineering: Current Principles and Practices, v. 2, pp. 869-884.
- Clough, G.W. & O'Rourke, T.D. (1990). Construction induced movements of insitu walls. Proc. ASCE Conf. on Design and Performance of Earth Retaining Structures, Cornell University, Ithaca, New York, pp. 439-470.
- Collins (1984). *The Collins Thesaurus in A-Z Form*. HarperCollins Publishers, Glasgow, 432 p.
- Denies, N.; Huybrechts, N.; De Cock, F.; Lameire, B.; Vervoot, A.; Van Lysebetten, G. & Maertens, J. (2012). Soil mix walls as retaining structures - mechanical characterization. International Symposium of ISSMGE - TC211 on Recent Research, Advances and Execution Aspects of Ground Improvement Works. Brussels, Belgium.
- Egger, P. (1972). Influence of wall stiffness and anchor prestressing on earth pressure distribution. Proc. V<sup>th</sup> European Conference on Soil Mechanics and Foundation Engineering, Madrid, v. 1, pp. 259-264.
- Eide, O.; Aas, G. & Josang, T. (1972). Special application of cast-in-place walls for tunnels in soft clay in Oslo. Proc. V<sup>th</sup> European Conference on Soil Mechanics and Foundation Engineering, Madrid, v. 1, pp. 485-498.

- Ferraz, M. (2010). Model for structural behavioural assessment of bridges. PhD thesis, University of Porto.
- Finno, R.J.; Atmatzidis, D.K. & Perkins, S. B. (1989). Observed performance of a deep excavation in clay. *Journal Geotechnical Engineering, ASCE*, 115(8):1045-1064.
- Finno, R.J.; Bryson, S. & Calvello, M. (2002). Performance of a stiff support system in soft clay. *Journal Geotechnical and Geoenvironmental Engineering, ASCE*, 128(8):660-671.
- Fiorotto R.; Stoetzer E. & Schoepf, M. (2003). CSM Cutter Soil Mixing An innovation in Soil Mixing for Cut-off and Retaining Walls. BAUER Maschinen, Germany.
- Fiorotto, R.; Stötzer, E.; Schöpf, M. & Brunner, W. (2005). Cutter Soil Mixing (CSM). Proc. Int. Conf. on Deep Mixing'05, 6 p (CD-Rom).
- Glass, P. & Stones, C. (1999). Construction of Westminster Station, London. Proc. of the Institution of Civil Engineers, Structures & Buildings, 146(3):237-252.
- Hsieh, H.S.; Wang, C.C. & Ou, C.Y. (2003). Use of jet grouting to limit diaphragm wall displacement of a deep excavation. *Journal Geotechnical and Geoenvironmental Engineering, ASCE*, 129(2):146-157.
- Hsieh, H.S.; Lu, Y.C. & Lin, T.M. (2008). Effects of joint detail on the behavior of cross walls. *Journal of Geo-Engineering*, 3(2):55-60.
- Hwang, R.N.; Moh, Z. & Wang, C.H. (2007). Performance of wall systems during excavation for Core Pacific City. *Journal of Geoengineering*, 2(2):53-60.
- Karlsrud, K. (1983). Performance and design of slurry walls in soft clay. NGI, Publication N° 149, Oslo.
- Karlsrud, K. (1997). Some aspects of design and construction of deep supported excavations. Proc. XIV<sup>th</sup> Int. Conf. Soil Mechanics and Foundation Engineering, Hamburg, v. 4, pp. 2315-2320.
- Karlsrud, K. & Andresen, L. (2007). Design of deep excavations in soft clays. Proc. XIV<sup>th</sup> ECSMGE, Madrid, v. 1, pp. 75-99.
- Koutsoftas, D.C.; Frobenius, P.; Wu, C.L.; Meyersohn, D. & Kulesza, R. (2000). Deformations during cut-and-cover construction of MUNI Metro Turnback Project. *Journal Geotechnical and Geoenvironmental Engineering, ASCE*, 126(4):344-359.
- Lewis, R.W. & Schrefler, B.A. (1987). The Finite Element Method in the Deformation and Consolidation of Porous Media. John Wiley and Sons, Inc., New York.
- Lui, G.B.; Ng, W.W. & Wang, Z.W. (2005). Observed performance of a deep multi-strutted excavation in Shanghai soft clays. *Journal Geotechnical and Geoenvironmental Engineering, ASCE*, 131(8):1004-1013.
- Liu, G.B.; Jiang, R.J.; Ng, C.W. & Hong, Y. (2011). Deformation characteristics of a 38 m deep excavation in soft clay. *Canadian Geotechnical Journal*, 48(12):1817-1828.
- Mair, R. & Harris, D. (2001). Innovative engineering to control Big Ben's tilt. *Ingenia, Royal Academy of Engineering*, Issue 9, pp. 23-27.
- Mana, A.I. & Clough, G.W. (1981). Prediction of movements for braced cuts in clay. *Journal Geotechnical Engineering, ASCE*, 107(6):759-777.
- Matos Fernandes, M. (1985). Performance and analysis of a deep excavation in Lisbon. Proc. XI<sup>th</sup> ICSMFE, San Francisco, v. 4, pp. 2073-2078.
- Matos Fernandes, M. (2004). Supported excavations. Soil-structure interaction analysed through tangential stress at the interface (in Portuguese). *Soils & Rocks*, 27(1):3-14.
- Matos Fernandes, M.; Maranhã das Neves, E.; Salgado, F.; Caldeira, L.; Pina, R.; Flor, A.; Brito, J.M. & Tavares, A. (2007). Jet grouting solutions for cut-and-cover subway metro stations in Lisbon downtown. Proc. XIV<sup>th</sup> ECSMGE, Madrid, v. 2, pp. 895-900.
- Matos Fernandes, M. (2007). An overview on induced movements by deep excavations in soft ground and eight golden rules for their control. Proc. XIV<sup>th</sup> ECSMGE, Madrid, v. 5, pp. 379-384.
- Matos Fernandes, M.; Pereira, C.D. & Guerra, N. (2008). Search for null displacement of walls supporting deep excavations in soft clay - A numerical experiment on a real case. Proc. Int. Conf. Development Urban Areas and Geotechnical Engineering, S. Petersburg, v. 2, pp. 587-592.
- Matos Fernandes, M.; Peixoto, A., Pinto, A., Pita, X.; Topa Gomes, A. & Pedro, A. (2010). The technology of cutter soil mixing applied in urban excavations (in Portuguese). Proc. 5<sup>th</sup> Portuguese-Brazilian Congress, Gramado, Rio Grande do Sul, CD-Rom.
- Matos Fernandes, M. (2010). Deep urban excavations in Portugal: practice, design, research and perspectives. *Soils & Rocks* 33(3):115-142.
- Matos Fernandes, M.; Cardoso, A.S.; Topa Gomes, A.; Borges, J.L.; Guerra, N.C. & Antão, A. N. (2012). Deep excavations in urban areas - Finite element modelling for three geotechnical scenarios and retaining solutions. Ribeiro e Sousa *et al.* (eds). *Innovative Numerical Modelling in Geomechanics*. Taylors & Francis, Oxford, chapter 3, pp. 51-76.
- Moormann, C. (2004). Analysis of wall and ground movements due to deep excavations in soft soil based on a new worldwide database. *Soils and Foundations*, 44(1):87-98.
- Ng, C.W., Hong, Y., Liu, G.B. & Liu, T. (2012). Ground deformations and soil-structure interaction of a multi-propped excavation in Shanghai. *Géotechnique*, 62(10):907-921.
- O'Rourke, T.D. & McGinn, J. (2006). Lessons learned for ground movements and soil stabilization from Boston Central Artery. *Journal Geotechnical and Geoenvironmental Engineering, ASCE*, 132(8):966-989.

- Ou, C.Y.; Wu, T.S. & Hsieh, H.S. (1996). Analysis of deep excavation with column type of ground improvement in soft clay. *Journal Geotechnical Engineering, ASCE*, 122(9):709-716.
- Ou, C.Y.; Lin, Y.L. & Hsieh, P.G. (2006). Case record of an excavation with cross walls and buttress walls. *Journal of GeoEngineering*, 1(2):79-86.
- Ou, C.Y.; Hsieh, P.G. & Lin, Y.L. (2011). Performance of excavations with cross walls. *Journal Geotechnical and Geoenvironmental Engineering, ASCE*, 137(1):94-104.
- Palmer, J.H. & Kenney, T.C. (1972). Analytical study of a braced excavation in weak clay. *Canadian Geotechnical Journal*, 9(2):145-164.
- Peck, R.B. (1969). Deep excavations and tunnelling in soft ground. Proc. VII<sup>th</sup> ICSMFE, Mexico City, General Report, State-of-the-Art Volume, pp. 225-290.
- Peixoto, A.; Matos Fernandes, M.; Sousa, E. & Gomes, P. (2012). The application of Cutter Soil Mixing to an urban excavation at the riverside of Lagos, Portugal. Proc. International Symposium of ISSMGE - TC211 on Recent Research, Advances and Execution Aspects of Ground Improvement Works. Brussels, Belgium.
- Pinto, A.; Tomásio, R.; Pita, X.; Godinho, P. & Peixoto, A. (2012). Ground improvement solutions using CSM technology. Proc. International Symposium of ISSMGE - TC211 on Recent Research, Advances and Execution Aspects of Ground Improvement Works. Brussels, Belgium.
- Pinto, A. (2014). Personal communication.
- Poh, T.Y.; Goh, A.T. & Wong, I. H. (2001). Ground movements associated with wall construction: case histories. *Journal Geotechnical and Geoenvironmental Engineering, ASCE*, 127(12):1061-1069.
- Randall, F.A. (1999). *History of the Development of Building Construction in Chicago*. 2<sup>nd</sup> edition, University of Illinois Press, Champaign.
- Tan, Y. & Li, M. (2011). Measured performance of 26 m deep top-down excavation in downtown Shanghai. *Canadian Geotechnical Journal*, 48(5):704-719.
- Tan, Y. & Wei, B. (2012). Observed behaviors of a long and deep excavation constructed by cut-and-cover technique in Shanghai soft clay. *Journal Geotechnical and Geoenvironmental Engineering, ASCE*, 138(1):69-88.
- Wang, Z.W.; Ng, C.W. & Liu, G.B. (2005). Characteristics of wall deflections and ground surface settlements in Shanghai. *Canadian Geotechnical Journal*, 42(5):1243-1254.
- Wang, J.H.; Xu, Z.H. & Wang, W.D. (2010). Wall and ground movements due to deep excavations in Shanghai soft soils. *Journal of Geotechnical and Geoenvironmental Engineering, ASCE*, 136(7):985-994.
- Wong, I.H.; Poh, T.Y. & Chuah, H.L. (1997). Performance of excavations for depressed expressway in Singapore. *Journal Geotechnical and Geoenvironmental Engineering, ASCE*, 123(7):617-625.
- Wong, I.H. & Poh, T.Y. (2000). Effects of jet grouting on adjacent ground and Structures. *Journal Geotechnical and Geoenvironmental Engineering, ASCE*, 126(3):247-256.
- Wu, S. H.; Ching, J. & Ou, C.Y. (2013). Predicting wall displacements for excavations with cross walls in soft clay. *Journal Geotechnical and Geoenvironmental Engineering, ASCE*, 139(6):914-927.



## ***Articles***

***Soils and Rocks***  
**v. 38, n. 3**



# Use of Sugarcane Bagasse as Carbon Substrate in Permeable Reactive Barriers: Laboratory Batch Tests and Mathematical Modeling

R.C. Mattos, P.S. Hems, E.Y. Kawachi, F.T. Silva

**Abstract.** The combination of the lignocellulosic residue sugarcane bagasse and poultry litter as carbon and nutrients sources, respectively, in organic permeable reactive barriers for remediation of metal laden acid mine drainage has not yet been extensively tested and may be promising based on chemical composition. This system is being tested in the laboratory by means of microcosm batch experiments using sugarcane bagasse with and without poultry-litter as nitrogen and phosphorous source. As expected based on the compositions of sugarcane bagasse and poultry litter, the experiments (duplicate) combining both residues achieved the highest rates of sulfate reduction, between ~ 30 to 45 mg sulfate/L-day, and better sustained these rates throughout the duration of the experiment (78 days). Also, pH values increased from ~ 6 to 8, and the oxidation-reduction potential achieved < -100 mV, indicating anaerobic sulfate-reducing conditions. Mathematical modeling performed on these experiments, with a previously-tested model, resulted in simulated results that approached the experimental data when the sugarcane bagasse was modeled as comprising a cellulose fraction with a Contois specific degradation rate similar to that for wood chips and leaf mulch, plus an additional easily-degradable fraction to account for the occurrence of soluble sugars in sugarcane bagasse.

**Keywords:** acid mine drainage, batch tests, permeable reactive barrier, remediation, sugarcane bagasse, sulfate reduction.

## 1. Introduction

Detrimental environmental impacts result from ground and surface water contamination from acid mine drainage (AMD). In Brazil, examples include metalliferous-mining sites in Minas Gerais (iron, gold, nickel, copper, zinc, among others) and coal-mining sites in Santa Catarina, among others. According to FEAM (2011), in 2010, the state of Minas Gerais alone produced more than  $3.2 \times 10^6$  tons of fine residues with high AMD-releasing potential. Inadequate disposal may result in environmental contamination and a threat to groundwater, soil and surface water. In the carboniferous regions of Santa Catarina, currently approximately 5,000 ha of land are contaminated by mining residues including contamination of water bodies (Rubio *et al.*, 2008). In this state, 809 abandoned mines have been listed up to 2010 with 192 generating AMD (Krebs, 2010). Internationally, AMD contamination is very significant. For example, in the USA, thousands of areas are reported as contaminated with AMD in the western region alone (WGA, 1998).

Groundwater remediation in areas affected by AMD effluents, infiltrating or emanating from surface and underground mines, or leaching from tailings pits, may be accomplished using *in-situ* passive remediation systems that

are advantageous in comparison to operation-intensive and energy-demanding pump-and-treat remediation (Wilde-man *et al.*, 1997, Benner *et al.*, 1999, Voudrias, 2001, Whitehead *et al.*, 2005, Hallberg and Johnson, 2005). Among other possibilities, such as constructed wetlands, open limestone channels, anoxic limestone drains, or vertical flow systems, *in-situ* passive remediation may be accomplished using permeable reactive barriers (PRBs) (U.S. EPA, 1998, Blowes *et al.*, 2000, Benner *et al.*, 2002, Groudev *et al.*, 2003).

The concept of a PRB is illustrated in Fig. 1. Permeable reactive barriers are an *in-situ* passive-remediation technology in which reactive materials are emplaced in a subsurface trench in order to intercept the path of a contamination plume and allow the occurrence of reactions based on the contact between contaminants in the plume and the materials emplaced in the PRB, retaining or transforming pollutants into environmentally acceptable forms to meet remediation goals down gradient from the barrier.

The majority of PRBs worldwide are filled with metallic zero-valent iron ( $\text{Fe}^0$ ) to promote abiotic reductive dehalogenation of chlorinated solvents (Gillham and O'Hannesin, 1994) or Cr (VI) reduction, among others, generally in industrial sites. The first field application of an organic PRB occurred in 1995 at the Nickel Rim mine site

---

Renata Cotrim de Mattos, MSc., Instituto Tecnológico de Aeronáutica, Praça Mal. Eduardo Gomes 50, São José dos Campos, SP, Brazil. e-mail: renatacm04@hotmail.com.  
Paulo Scarano Hems, Ph.D., Instituto Tecnológico de Aeronáutica, Praça Mal. Eduardo Gomes 50, São José dos Campos, SP, Brazil. e-mail: paulosh@ita.br.  
Elizabeth Yoshie Kawachi, DSc., Instituto Tecnológico de Aeronáutica, Praça Mal. Eduardo Gomes 50, São José dos Campos, SP, Brazil. e-mail: bete@ita.br.  
Flávio Teixeira da Silva, DSc., Escola de Engenharia de Lorena, Universidade de São Paulo, Estrada Municipal do Campinho s/n, Lorena, SP, Brazil. e-mail: flavio@debiq.eel.usp.br.

Submitted on June 25, 2015; Final Acceptance on November 4, 2015; Discussion open until April 30, 2016.

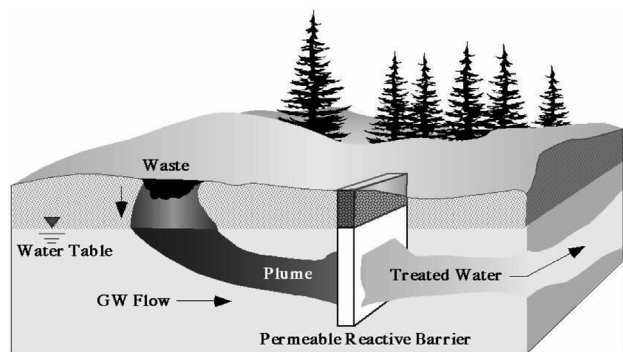


**Figure 1** - Conceptual illustration of a permeable reactive barrier for groundwater remediation (from U.S. EPA, 1998).

in Sudbury, Ontario, Canada (Benner *et al.*, 1999). More recently, mulch biowalls have been studied and implemented at several contaminated sites in the USA, aimed at degrading plumes of organic contaminants such as chlorinated solvents, perchlorate, and explosives (U.S. AFCEE, 2008). Thus far, the PRB application has been limited in Brazil. For example, in the state of São Paulo, only nine field installations have been reported out of ~ 400 industrial, commercial, or land-disposal sites currently under remediation (CETESB, 2013).

Organic PRBs are based on a mixture of filling solid materials, comprising (a) liable-carbon sources, (b) sources of nutrients, (c) pH buffering materials, such as calcite, (d) microbial inocula, and (e) porous media as support materials, such as gravel, sand, etc. The liable-carbon sources include agricultural by-products and are aimed at providing carbon and energy (electrons) for sulfate-reducing bacteria (SRB).

The results of laboratory studies involving sulfate-reducing systems for metal precipitation have demonstrated the potential use of these systems for AMD remediation, coupled to the decomposition of carbon sources in the form of solid organic low-cost lignocellulosic residues (Gibert *et al.*, 2004). Examples of the solid substrates tested include sawdust (Tuttle *et al.*, 1969, Wakao *et al.*, 1979), spent mushroom compost (Dvorak *et al.*, 1992, Hammack and Edenborn, 1992), fresh alfalfa (Bechard *et al.*, 1994), leaf mulch and wood chips (Waybrant *et al.*, 1998, Chang *et al.*, 2000), and corn stover (Figueroa *et al.*, 2007, Hemsí *et al.*, 2010), among others.

This paper describes the experimental results from laboratory batch tests aimed at testing the ability of reactors using sugarcane bagasse as the liable-carbon source, complemented by poultry litter as nutrient source, to remediate a synthetic AMD solution. In addition, simulation results obtained with a mathematical model previously calibrated for this type of remediation system are presented.

## 2. Theoretical Background

The organic PRB relies on the activity of a bacterial consortium with functions of hydrolysis and decomposition of lignocellulosic (polymer) tissues in the solid organic materials placed in the PRB, that are hydrolyzed to form monomers (*e.g.*, sugars), and fermented to produce soluble shorter-chain organic compounds such as lactate, acetate, propionate, butyrate, as well as hydrogen, which are, in turn, utilizable as carbon and energy (electrons) sources by sulfate-reducing bacteria (Fig. 2).

Microbial sulfate reduction promotes the consumption of sulfate ( $\text{SO}_4^{2-}$ ) from the plume, production of hydrogen sulfide in solution ( $\text{H}_2\text{S}$ ), and promotion of alkalinity, as illustrated by the following reaction mechanism at pH ~ 6 to 7:

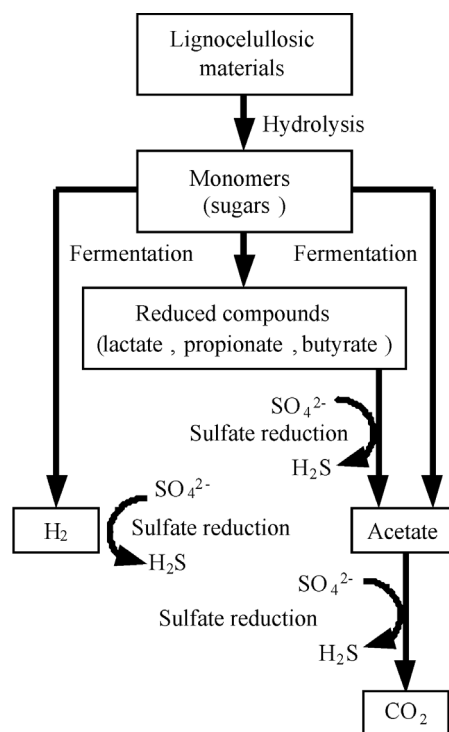
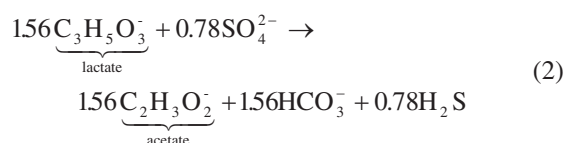
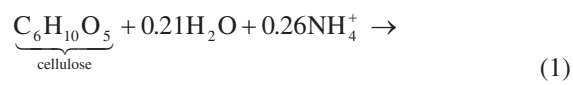
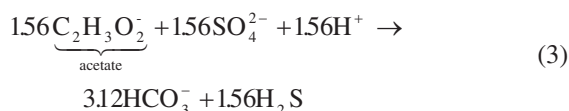


**Figure 2** - Sequence of anaerobic transformations of solid organic matter with emphasis on sulfate reduction (modified from Logan *et al.*, 2005).

where Eq. 1 is a simplified heterogeneous reaction for cellulose degradation releasing soluble lactate, and Eq. 2 is the incomplete oxidation of lactate coupled with sulfate reduction and releasing acetate, alkalinity, and hydrogen sulfide. In Eq. 1, cellulose is in fact the polymer of  $C_6H_{10}O_5$ , i. e.,  $n(C_6H_{10}O_5)$ . The release of acetate and bicarbonate in Eq. 2 provides a buffer capacity to neutralize  $H^+$  released in Eq. 1. In addition, further sulfate reduction coupled to acetate oxidation promotes more alkalinity, as follows:



Hydrogen sulfide released in solution ( $H_2S$ ), in turn, promotes the precipitation of metals (e.g., Fe, Cd, Cu, Ni, Pb, Zn) in the form of stable metal monosulfides:



Although two moles of  $H^+$  are released per mole of metals precipitated, the impact of Eq. 4 on pH is alleviated by the fact that the number of moles of metals is generally significantly lower than the number of moles of lactate, acetate and sulfate.

In Eq. 2, lactate is representative of the range of reduced organic compounds utilizable by SRB. Fermentation and sulfate reduction require negative oxidation-reduction potential,  $E_h < -100$  mV (Szogi *et al.*, 2004), and pH between 6 and 9. The pH optimum for anaerobic digestion is within the similar range of pH between 6.5 and 8.2.

The kinetic rate-limiting step in these systems (Fig. 2) is the hydrolysis of lignocellulosic materials releasing soluble organic molecules (Logan *et al.*, 2005, Hemsli *et al.*, 2005, Neculita *et al.*, 2007). Thus, the rates of fermentation, sulfate reduction and metals precipitation are critically dependent on the rates of solids hydrolysis. For this reason, emphasis must be placed on the selection of the lignocellulosic residues to be employed in the organic PRB.

Sugarcane bagasse, an abundant agro-industrial residue in central-southern Brazil, has not yet been extensively tested as a solid-carbon source for environmental bioremediation. As discussed in de Mattos and Hemsli (2012), sugarcane bagasse is rich in liable to moderately recalcitrant carbon (sugars and cellulose/polyose), but poor in the nutrients nitrogen and phosphorous. A review by de Mattos (2013) indicates that sugarcane bagasse has a composition (dry-mass basis) of ~ 40-50% cellulose, ~ 10-25% polyose, and ~ 20 to 35% lignin, carbon/nitrogen ratio (C/N) ranging from ~ 65-130 and lignin/nitrogen ratio (L/N) ranging from ~ 15-25. The high values of C/N and L/N denote nitrogen-to-carbon deficiency for bacterial degradation and recalcitrance (Gibert *et al.*, 2004).

The desirable ranges for the parameters C/N and L/N for bacterial decomposition are from 10-20 (Neculita *et al.*, 2007, Khalid *et al.*, 2011) and  $< \sim 20$  (Duryea *et al.*, 1999),

respectively. For example, urea was added (as N source) to wood chips and leaf mulch in batch tests in order to lower the C/N ratio to ~ 16 (Cocos *et al.*, 2002).

Grubb *et al.* (2000) tested a sugarcane bagasse from Peru for immobilizing metals and buffering pH of a synthetic AMD solution in batch laboratory experiments. Pure bagasse was not capable of significant pH or metals (Al, As, Cu, Fe, Mn, Zn) amelioration after 180 days. Digester sludge then was amended to sugarcane bagasse, producing near neutral pH and achieving very high metals removal (Cu, Pb and Zn) after a similar period. Grubb *et al.* (2000) concluded that an exogenous labile-carbon source (glucose) was not necessary, but that the addition of digester sludge was required for remediation. The digester sludge requirement is likely to reflect the need for nutrients N and P addition to sugarcane bagasse.

The high C/N and L/N ratios of sugarcane bagasse require nutrients N and P from a different source. Another solid residue, poultry litter, is reported, on the other hand, to be rich in N (C/N ~10-18, L/N ~2-5) and P (%P = 1.2) (de Mattos, 2013). The comparison indicates that mixtures of sugarcane bagasse and poultry litter, with bagasse providing both liable and durable carbon and poultry litter nutrients N and P, may be a promising composition for a low-cost sulfate-reducing reactor for AMD amelioration.

## 3. Materials and Methods

### 3.1 Sulfate-reducing batch experiments

The batch tests involved placing the contaminant solution in contact with the organic solid materials and SRB, under closed, anaerobic conditions and ambient temperature of  $24 \pm 2$  °C in the dark. Each reactor was prepared with a solid-to-liquid ratio of 1:20 in terms of total mass. Thus, in each reactor, 1 L of the synthetic AMD solution was added to 50 g dry mass of total solids. The selected solid-to-liquid ratio was lower than used by Zagury *et al.* (2006), which performed sulfate-reducing batch tests with a 1:4 solid-to-liquid ratio. The ratio used in this study (1:20) was aimed at testing the possibility and extent of remediation of the synthetic solution at a low solid-substrate content.

Table 1 presents the proportions of solid materials employed in each of the three types of batch reactors used in this study. Each reactor type was prepared in duplicate. These proportions were based on those used by Zagury *et al.* (2006), but sugarcane bagasse and poultry litter were used in this study. Cow manure was included as a bacterial inoculum for SRB (Choudhary and Sheoran, 2011).

The sugarcane bagasse used in this research was obtained from the University of São Paulo, and consisted of a fresh sample taken from the discarded bagasse generated at an ethanol and sugar refinery in Piracicaba/São Paulo (Brazil).

**Table 1** - Dry mass percentage of solid materials used in reactor types 1 to 3.

Reactor type	1	2	3
% (dry mass)			
Reactive materials			
Sugarcane bagasse	50	30	0
Poultry litter	0	20	50
Base materials			
Sand	30	30	30
Limestone	2	2	2
Inoculum			
Cow manure	18	18	18
Total	100	100	100

The chemical composition of the synthetic AMD solution prepared for this study is shown in Table 2. Sulfate salts were used, avoiding the toxic threshold concentrations for Zn and Ni (Zagury *et al.*, 2006), and adding the bacterial nutrient potassium (K). The initial sulfate concentration was chosen as approximately 5000 mg/L. For example, Zagury *et al.* (2006) used an initial sulfate concentration of 4244 mg/L. Type I deionized water (inorganics < 18.2 MΩ cm at 25 °C, total organic carbon < 10 ppb, bacteria < 1 CFU/mL) (Purelab Option Q-7, Elga) and scientific-grade reagents and salts were used. Calcium carbonate (CaCO<sub>3</sub>) was added when preparing the solution at 487.5 mg/L. A volume of ~ 0.37 mL 98-% sulfuric acid (H<sub>2</sub>SO<sub>4</sub>) was added per liter of solution to correct the initial pH to ~ 6.0. This pH of the synthetic solution may be considered too high to represent AMD, but may be representative of a solution reaching the up-gradient side of a PRB after passing through a layer of sand with limestone, which would have increased pH. Also, Waybrant *et al.* (1998) per-

**Table 2** - Ion concentrations and resulting pH of the synthetic AMD solution used for the batch tests.

Ion	Concentration (mg/L)
Ca <sup>2+</sup>	390.5
CO <sub>3</sub> <sup>2-</sup>	584.5
Mg <sup>2+</sup>	98.9
Ni <sup>2+</sup>	8.64
Zn <sup>2+</sup>	8.41
Na <sup>2+</sup>	472.8
K <sup>+</sup>	2400
Mn <sup>2+</sup>	12.46
SO <sub>4</sub> <sup>2-</sup>	5036
pH	6

formed batch tests for evaluating the sulfate-reducing remediation of a simulated mine drainage with an initial pH ranging from 5.5 to 6.5.

After preparation of the solution, the solution was analyzed in an ion chromatographer (Dionex, DX-600 IC) with an anions column IonPac AS-14A and guard column IonPac AG-14A. The initial sulfate concentration in solution was determined as 5281 mg/L, which was considered similar to the expected initial concentration (Table 2).

The three types of batch reactors were prepared in duplicate, totalizing six sulfate-reduction reactors (1A, 1B, 2A, 2B, 3A and 3B). As shown in Fig. 3, low-cost reactors were assembled using 2-L polyethylene (PET) discarded bottles, previously washed with a 2-% nitric acid (HNO<sub>3</sub>) solution and rinsed with water.

Periodically, liquid samples were collected from each reactor (2 mL for pH/ORP and 8 mL for chromatography), using a disposable 10-mL syringe, and pH and oxidation-reduction potential, corrected to  $E_h$ , were determined immediately, and sulfate ion (SO<sub>4</sub><sup>2-</sup>) concentration was determined using ion chromatography (Dionex, DX-600 IC). Samples for chromatography were pre-treated by filtering using simple coffee filter papers to remove sugarcane-bagasse solids from the liquid followed by two consecutive separations using 98-% hexane in a separation funnel, in order to separate the organic fraction of the sample (which aggregated to hexane forming a gel) from the inorganic fraction of the sample, in which sulfate was determined. Finally, the inorganic fraction was filtered with syringe filters of acetate-cellulose (0.45 μm and 0.2 μm) mounted in series, diluted by a factor of 50 with deionized water, and analyzed by chromatography.

### 3.2 Mathematical modeling

The mathematical model for the sulfate-reducing system based on solid hydrolysis has been formulated as a sim-

**Figure 3** - Batch reactors mounted on a shaking wood support, also showing valves used for periodic gas venting.

plification of the sequence shown in Fig. 2 (Hemsi *et al.*, 2010), including: (i) solid-substrate hydrolysis, (ii) sulfate reduction, release of hydrogen sulfide, and (iii) consumption of metals based on precipitation of metal sulfides.

### 3.2.1. Solid substrate hydrolysis

Hydrolysis of solid organic substrates (S) and bacterial (X) growth due to fermentation are coupled, with first-order or Contois kinetics. Considering Contois kinetics as previously recommended by Hemsi *et al.* (2010):

$$\begin{cases} \frac{d[S]}{dt} = -k_c [X] \frac{[S]/[X]}{K_A + ([S]/[X])} \\ \frac{d[X]}{dt} = -Y_1 \frac{d[S]}{dt} - r_d [X] \end{cases} \quad (5)$$

where [X] is the equivalent biomass concentration for degrading bacteria (mg/L),  $k_c = k_c(t)$  is a specific rate of decomposition for Contois kinetics ( $d^{-1}$ ),  $K_A$  is an affinity coefficient (mg/mg),  $Y_1$  is a biomass mass yield coefficient,  $r_d$  is a decay rate for degrading bacteria ( $d^{-1}$ ), and  $t$  is time. Sulfate-reducing bacteria are capable of utilizing only simple soluble organic substrates, such as acetate, lactate, propionate, or  $H_2$ . Of all these possibilities, lactate is selected as the model utilizable soluble organic substrate for SRB (Neculita *et al.*, 2007).

Based directly on Eq. 5, the kinetics for the production of lactate in solution is given by:

$$\frac{d[LA]}{dt} = -Y_2 \sum_{i=1}^N \frac{d[S_i]}{dt} \quad (6)$$

where [LA] is the concentration of lactate in solution (mg/L),  $N$  is the number of solid decomposable organic substrates considered and  $Y_2$  is a mass yield coefficient obtained from the chemical reaction. For low values of [S], the Contois kinetic model approaches first-order kinetics with respect to [S]. Also in this case, the specific rate coefficient may be considered to decline with time as a result of the composition change undergone by the solid organic material:

$$\frac{d[S]}{dt} = -k(t)[S] \quad (7)$$

where  $k(t)$  is a time-declining first-order specific rate coefficient.

### 3.2.2. Bacterial sulfate reduction

Dual-substrate Monod kinetics limited by sulfate and lactate could be used to model the growth of SRB and the production of sulfide from sulfate reduction. However, after the onset of the experiments, the release of lactate in solution due to solid-substrate hydrolysis and fermentation becomes the rate-limiting step to sulfate reduction (Logan *et al.*, 2005, Neculita *et al.*, 2007). Thus, sulfate reduction

was modeled using an instantaneous-reaction algorithm, based on the presence of lactate (Hemsi *et al.*, 2010):

$$\begin{aligned} &\text{If } [LA] > 0 \text{ and } ([SO] - Y_3 [LA]) \geq 0 \\ &[SO] = [SO] - Y_3 [LA] \\ &[HS] = [HS] + Y_4 [LA] \\ &[LA] = 0 \\ &\text{If } [LA] > 0 \text{ and } ([SO] - Y_3 [LA]) < 0 \quad (8) \\ &[LA] = [LA] - \frac{1}{Y_3} [SO] \\ &[HS] = [HS] + \frac{Y_4}{Y_3} [SO] \\ &[SO] = 0 \end{aligned}$$

where [SO] is the concentration (mg/L) of sulfate ( $SO_4^{2-}$ ), [HS] is the concentration (mg/L) of hydrogen sulfide in solution ( $H_2S$ ), and  $Y_3$  and  $Y_4$  are mass yield coefficients based on the reaction.

### 3.2.3. Metal sulfide precipitation

Second-order kinetics could be used to model metal precipitation with hydrogen sulfide in solution. However, similarly, the rate-limiting step to metal-sulfide precipitation is the release of hydrogen sulfide based on sulfate reduction. Thus, for the precipitation of metal-sulfide, an instantaneous process formulation also was employed (Hemsi *et al.*, 2010), as follows:

$$\begin{aligned} &\text{If } [HS] > 0 \text{ and } ([M] - Y_5 [HS]) \geq 0 \\ &[M] = [M] - Y_5 [HS] \\ &[MS] = [MS] + Y_6 [HS] \\ &[HS] = 0 \\ &\text{If } [HS] > 0 \text{ and } ([M] - Y_5 [HS]) < 0 \quad (9) \\ &[HS] = [HS] - \frac{1}{Y_5} [M] \\ &[MS] = [MS] + \frac{Y_6}{Y_5} [M] \\ &[M] = 0 \end{aligned}$$

where [M] is the metal concentration (mg/L), [MS] is the equivalent metal-sulfide precipitate concentration (mg/L), and  $Y_5$  and  $Y_6$  are mass yield coefficients obtained from the precipitation reactions. When considering solution  $H_2S$ , volatilization to the gas phase may be an important process to consider if contact with the atmosphere is significant (Hemsi *et al.*, 2005).

### 3.2.4. Model parameters and solution

Previous model calibrations using published experimental data from batch and column tests without sugarcane bagasse provided values for the Contois decomposition parameters ( $k_c$  and  $K_A$ ) for specific organic residues as summa-

rized in Table 3. The  $k_c$  and  $K_A$  values depend on chemical composition, structure (cellulose/lignin) and grain sizes of the residues, as well as temperature, pH,  $E_h$ , nutrient availability, and other environmental characteristics.

The mathematical model for cellulose degradation includes a set of three adjustable parameters, which are  $k_c$ ,  $K_A$ , and  $r_d$ , and an unknown initial condition, the initial ratio  $[S]/[X]$ . For the parameter calibrations shown in Table 3, the affinity coefficient,  $K_A$ , was maintained at 30 mg/mg, whereas the specific rate of decomposition,  $k_c$ , was varied reflecting higher or lower material degradability. In these simulations (Table 3), the initial equivalent biomass concentration of degrading bacteria ( $X$ ) was assumed as 0.5% of the initial equivalent concentration of the solid cellulosic substrate being degraded, and the decay rate for degrading bacteria,  $r_d$ , was assumed as 10% of the specific rate of decomposition for Contois kinetics. Maintaining  $K_A$  at 30 mg/mg allows for the comparison of  $k_c$  adjusted for different materials, as shown in Table 3.

Initial parameter values for sugarcane bagasse were based on parameters shown in Table 3, and adjusted on the basis of the comparisons between simulated results and experimental data.

In terms of the model simulations, the ordinary differential equations of the kinetic model (Eqs. 5 and 6) were numerically integrated in time using the Runge-Kutta-Fehlberg method coupled to the algorithms for the instantaneous reactions of Eqs. 8 and 9.

## 4. Results and Discussion

### 4.1 Sulfate-reducing batch experiments

The six batch reactors used in this study consisted of three reactor types (1, 2 and 3), as described in Table 1, prepared in duplicate (for each type, duplicates were designated as A and B). Liquid samples from the solution in each batch reactor were collected every 7 to 15 days during the total testing period of 78 days.

#### 4.1.1. pH

Figure 4a presents the pH results in each reactor versus time. After 30 days, pH values had increased from 6 to ~ 7.5 to 8 in reactors 1A and 1B, and 2A and 2B, respec-

tively. However, in reactors 3A and 3B, pH values remained near the initial value of 6. Between 30 and 78 days, the pH values started to decrease. However, the pH values remained around 7 in reactors of types 1 and 2, reaching values below 6 only for reactors of type 3. The behavior of pH versus time in these reactors depends on solid-substrate decomposition, which releases  $H^+$  (Eq. 1), decreasing pH, and sulfate reduction, which releases acetate and alkalinity (Eq. 2) and tends to increase pH. In general, the sequential processes are expected to result in overall pH increase (Blowes *et al.*, 2000), as observed in batch tests of types 1 and 2 of this study.

#### 4.1.2. Sulfate concentrations and rates of sulfate reduction

Figures 4b to d present the results in terms of sulfate concentrations versus time for each reactor type. The comparison between these results shows that the most significant decline in sulfate ( $SO_4^{2-}$ ) occurred in reactors 2A and 2B between 0 and 40 days. In contrast, reactors of type 3 showed a very slight variation in sulfate concentrations over time. Decreasing sulfate concentrations over time in reactors of types 1 and 2 were corroborated by two aspects, intense sulfidric gas ( $H_2S$ ) odor in these reactors and a change in color of the solid mixture in these reactors, which went from greenish brown to black. Reactors of type 3 did not exhibit these changes in odor and color to a similar extent. Neculita *et al.* (2007) and Waybrant *et al.* (1998) tested poultry and sheep manures, respectively, as carbon and nitrogen sources for sulfate-reducing batch tests, and concluded that the residues were poor substrates for sulfate reduction based on the lack of total organic carbon (TOC).

After the total testing period of 78 days, the sulfate concentrations in solution decreased, on average, by 1170, 1600, and 1060 mg sulfate/L in reactors of types 1, 2 and 3, respectively.

The average rates of sulfate reduction over time were calculated for each interval between measured data, and are shown in Fig. 5 for each reactor, with rate values (bars) plotted at the center of each time interval (*e.g.*, plotted at time 67.5 days, for interval between 58 and 77 days).

**Table 3** - Contois kinetic decomposition parameters based on model calibrations using experimental data (temperature = 25 °C).

Material	$k_c$ (d <sup>-1</sup> )	$K_A$ (-)	References	
			Experiment	Modeling
Wood chips	0.4	30	Waybrant <i>et al.</i> (1998), batch tests	Hemsi <i>et al.</i> (2005)
Leaf mulch	0.6	30		
Sawdust	0.8	30		
Corn stover	0.5	30	Figueroa <i>et al.</i> (2007), column tests	Hemsi <i>et al.</i> (2010)
Walnut shells	0.05	30		

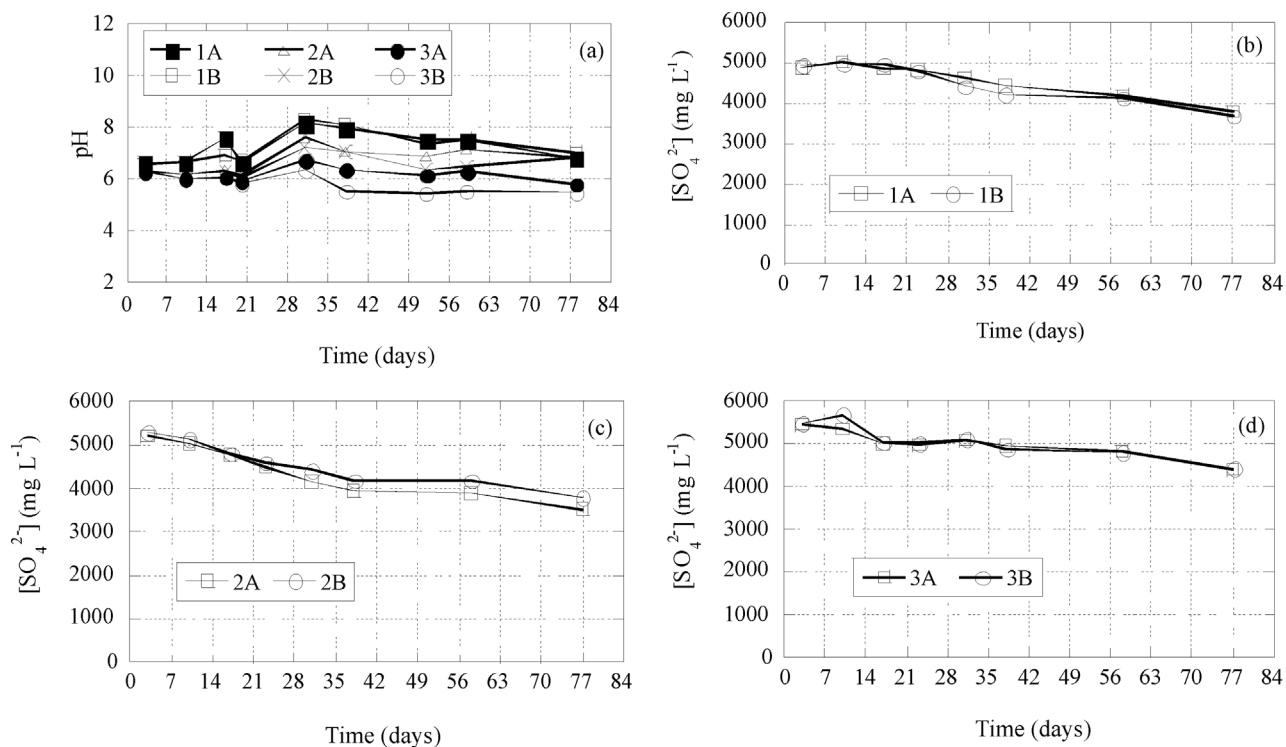


**Figure 4** - Batch tests results: (a) pH in all reactors, (b) sulfate concentrations in reactors of type 1, (c) sulfate concentrations in reactors of type 2, and (d) sulfate concentrations in reactors of type 3.

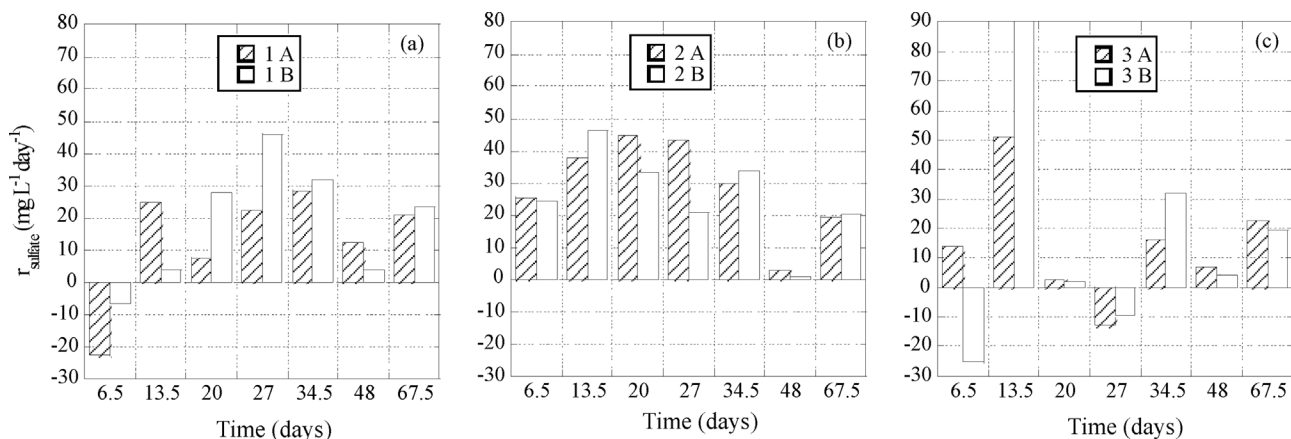


**Figure 5** - Average sulfate-reduction rates ( $r_{\text{sulfate}}$ ) over time for batch reactors: (a) type 1, (b) type 2, and (c) type 3 reactors.

A comparison among the results in Fig. 5 reveals that the calculated rates of sulfate reduction over time are in closer agreement for the duplicate reactors of type 2 (2A and 2B) than for either one of the other two types of reactors. Also, average rates of sulfate reduction for reactors of type 2 were > 30 mg sulfate/L-day, peaking at ~40-50 mg sulfate/L-day for times up to 38 days, which are greater than the values achieved in reactors of types 1 and 3 during the entire testing period. Greater variability is observed for reactors of types 1 and 3. Negative values of rates of sulfate reduction, indicating increase in sulfate concentrations,

may be explained as analytical measurement imprecision, or actual release of sulfate by the solid materials.

#### 4.1.3. $E_h$

Figure 6 presents values of  $E_h$  plotted against testing time for different batch reactors. For all reactors, the  $E_h$  value was measured at 78 days. The data for these reactors indicate reactors of types 1 and 2 with 78-day  $E_h$  values less than -100 mV, whereas reactors of type 3 with 78-day  $E_h$  values of ~ 0.

The  $E_h$  in Fig. 6 is the corrected value, *i.e.*, relative to the standard hydrogen electrode. Such values were calcu-

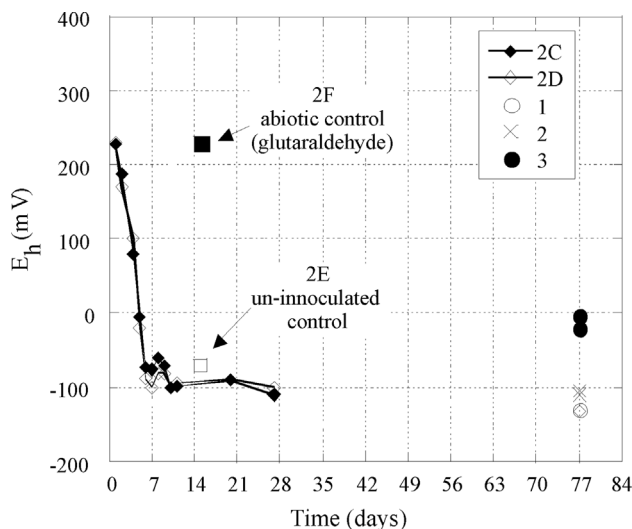


**Figure 6** - Oxidation-reduction potential values relative to the standard hydrogen electrode in reactors 1A, 1B, 2A, 2B, 3A and 3B at 78 days, in reactors 2C and 2D from zero to 28 days, and in reactors 2E and 2F at 15 days.

lated from the direct ORP measurements obtained with a Ag/AgCl half-cell electrode (Hanna HI-3131B), according to (Stumm and Morgan, 1996, Szogi *et al.*, 2004):

$$E_h = ORP + 200 \text{ (mV)} \quad (10)$$

Values of  $E_h$  less than -100 mV are indicative of sulfate-reducing conditions in solution, whereas values  $\sim 0$  are not (Szogi *et al.*, 2004).

In order to follow the evolution of  $E_h$  with time from the onset of the batch experiments, two additional reactors, 2C and 2D, were assembled identically to reactors 2A and 2B. The values of  $E_h$  in these reactors were measured from 0 to 28 days, as shown in Fig. 6.

The results for reactors 2C and 2D (Fig. 6) indicate  $E_h$  values declining from  $> 200$  mV (aerobic conditions) to  $\sim -100$  mV within 7 days, *i.e.*, denoting oxygen depletion followed by establishment of sulfate-reducing conditions after 7 days. Also, the results for the duplicate reactors 2C and 2D were similar.

From 7 to 28 days, the values of  $E_h$  remained at -100 mV, indicating sustained sulfate reduction during this period. The final values were in agreement with the values of  $E_h$  measured at 78 days for reactors 2A and 2B, which also were -100 mV.

Finally, two additional batch reactors were assembled to further study  $E_h$ . These reactors were control reactors, designated 2E and 2F, prepared almost identically to reactors of type 2, with the following differences: reactors 2E and 2F did not contain cow manure and reactor 2F contained 50 mL of a 2-% (by volume) Glutaraldehyde solution. Thus, reactor 2E was intended to be an un-inoculated control, whereas reactor 2F was intended to be an abiotic control.

The bacterial activity of organic decomposition/fermentation and sulfate reduction was annulated in reactor 2F, since the value of  $E_h$ , measured at 15 days from the onset of this reactor, was equal to +230 mV (Fig. 6), indicating aerobic conditions and the absence of sulfate reduction that lowered  $E_h$  in reactors of type 2. Thus, the concentration of glutaraldehyde utilized was adequate to promote the biocide effect in this abiotic control.

In contrast, the un-inoculated reactor 2E displayed a 15-day value of  $E_h$  similar to the values for reactors 2C and 2D (at 15 days), indicating that the addition of cow manure in reactors 2C and 2D as inoculum material for SRB may not be required, and that sulfate reducing bacteria may be present in this system via the sugarcane bagasse and poultry litter. In addition, as shown in Fig. 7, reactor 2E displayed a black to dark grey color, whereas the abiotic reactor 2F remained of a light brown color, basically the same color of the reactors right after assemblage. Also, reactor 2E emitted a strong hydrogen sulfide-gas odor, whereas reactor 2F did not exhibit hydrogen sulfide-gas odor.

## 4.2 Mathematical modeling

The mathematical model was used in batch mode (hydrostatic conditions) in order to simulate sulfate dynamics in batch reactors 2A and 2B, which were the reactors that better sustained bacterial sulfate reduction in this study. Sulfate reduction was modeled as an instantaneous process limited by lactate from hydrolysis/decomposition of cellulose based on Contois kinetics.

### 4.2.1. Initial conditions

The multi-species model is a set of ordinary differential equations that require a set of initial conditions to evolve in time. The initial concentrations for sulfate ( $[SO] = 5200$  mg/L), nickel and zinc ( $[M] = 17$  mg/L), lactate ( $[LA] = 0$ ), and dissolved hydrogen sulfide ( $[HS] = 0$ ) were assigned. The initial equivalent concentration of cel-

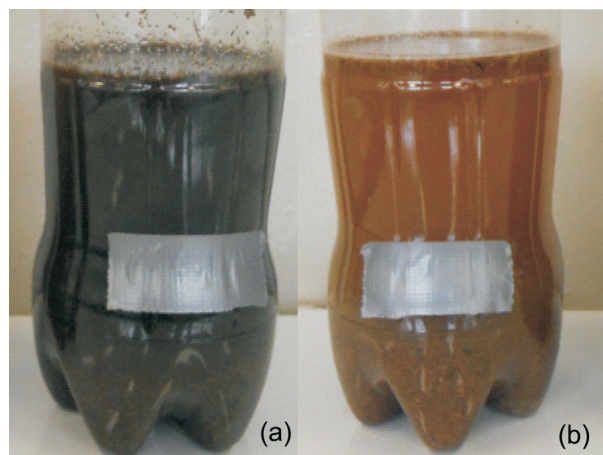


**Figure 7** - Visual aspect at 15 days for batch reactors: (a) 2E, and (b) 2F.

lulose, [S], in a reactor, coming from the packed sugarcane bagasse was unknown. The total dry mass of sugarcane bagasse in type-2 reactors was 30% (by mass) of 50 g/L, *i.e.*, 15 g/L per reactor. Based on the compositions reviewed by de Mattos (2013), cellulose and polyose contents may be 50-75% by dry mass in sugarcane bagasse. Discounting cellulose that may be protected by lignin, a 50-% degradable polysaccharide fraction, on a dry-mass basis, was considered in this study, corresponding to initial [S] = 7500 mg/L. The initial equivalent concentration [X] was thus assumed = 37.5 mg/L, as per Hemsí *et al.* (2010).

#### 4.2.2. Modeling results

The modeling results depend critically on the parameter values assumed for degradation of cellulose in sugarcane bagasse. The Contois specific degradation rate (Eq. 5),  $k_c$ , was chosen from 0.5 to 1.0 d<sup>-1</sup> with affinity coefficient,  $K_A$ , of 30 mg/mg (Table 3).

Simulation case 1, with  $k_c = 0.5$  d<sup>-1</sup>, considering cellulose in sugarcane bagasse to degrade similarly to that in wood chips or leaf mulch, resulted in significant under-prediction of the rates of sulfate reduction for time 0-78 days. Then, simulation case 2, with  $k_c = 1.0$  d<sup>-1</sup>, considering a degradability close to that of very fine-graded sawdust (Table 3) resulted in slight over-prediction of the rates of sulfate reduction from 50-70 days (Figs. 8a, b).

Better modeled results were obtained for simulation case 3, in which cellulose in sugarcane bagasse was considered to be as degradable as that in wood chips or leaf mulch, but highly-degradable sugars were included, *i.e.*, 7500 mg/L of cellulose with  $k_c = 0.5$  d<sup>-1</sup> (= Case 1) plus an additional 1500 mg/L of a degradable material with  $k_c = 5.0$  d<sup>-1</sup>. This highly-degradable material may be thought of as being soluble sugars observable in sugarcane bagasse.

The results in Fig. 8 indicate that the two-substrate model ( $N = 2$  in Eq. 6) with an easily-degradable fraction ( $k_c = 5.0$  d<sup>-1</sup>) allowed simulating the initial high rates of sulfate reduction that were verified in the experiments. These results indicate that, when trying to simulate the performance of a system using sugarcane bagasse, considering an easily-degradable substrate in addition to cellulose may be important.

## 5. Conclusions

The use of the lignocellulosic residue sugarcane bagasse as carbon source in organic permeable reactive barriers for the environmental remediation of mining effluents was tested at the laboratory bench scale. Microcosm batch experiments using sugarcane bagasse with and without poultry-litter amendments for nutrients N and P were performed. The experiments combining sugarcane bagasse and poultry litter (reactors type 2) achieved rates of sulfate reduction between ~ 30 to 45 mg sulfate/L-day, outperforming experiments based on single substrates. The rates

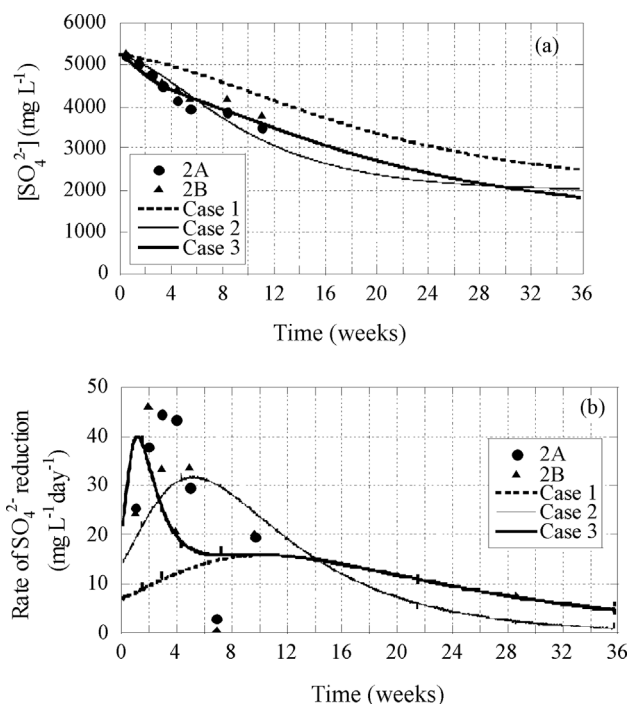


**Figure 8** - Modeling results for simulation cases 1, 2 and 3: (a) sulfate concentrations over time; (b) rates of sulfate reduction over time.

of sulfate reduction in type-2 reactors were maintained throughout the 78-day duration of the duplicate tests. Also, pH values increased from ~ 6 to 8, and  $E_h$  achieved < -100 mV, indicating anaerobic sulfate-reducing conditions. Mathematical modeling performed on these experiments with a previously-tested model resulted in better results when the sugarcane bagasse was modeled as comprising cellulose with a Contois specific degradation rate similar to that of wood chips and leaf mulch added to a fraction of easily-degradable substrate, to account for the presence of soluble sugars in sugarcane bagasse. The results from the batch experiments performed in this study provide an indication for assessing the performance of sugarcane bagasse as a carbon source for sustained sulfate-reduction in reactors treating AMD, and the modeling results may be useful for trying to estimate the performance of these systems. However, the limited time scales in this study relative to the actual field application must be considered.

## Acknowledgments

The authors acknowledge the financial support from FAPESP, Project number 2012/08797-2. Thanks to Prof. Dr. Cláudio Aguiar (Esalq/USP) for providing bagasse samples.

## References

Bechard, G.; Yamazaki, H.; Gould, W.D. & Bedard, P. (1994). Use of cellulosic substrates for the microbial

- treatment of acid mine drainage. *Journal of Environmental Quality*, 23(1):111-116.
- Benner, S.G.; Blowes, D.W.; Gould, W.D.; Herbert, R.B. & Ptacek, C.J. (1999). Geochemistry of a permeable reactive barrier for metals and acid mine drainage. *Environmental Science and Technology*, 33(16):2793-2799.
- Benner, S.G.; Blowes, D.W.; Ptacek, C.J. & Mayer, K.U. (2002). Rates of sulfate reduction and metal sulfide precipitation in a permeable reactive barrier. *Applied Geochemistry*, 17:301-320.
- Blowes, D.W.; Ptacek, C.J.; Benner, S.G.; McRae, C.W. & Puls, R.W. (2000). Treatment of dissolved metals and nutrients using permeable reactive barriers. *Journal of Contaminant Hydrology*, 45(1):123-137.
- CETESB (2013). Companhia Ambiental do Estado de São Paulo. Relação de Áreas Contaminadas e Realibiladas no Estado de São Paulo. <http://areascontaminadas.cetesb.sp.gov.br/wp-content/uploads/sites/45/2013/11/texto-explicativo.pdf>.
- Chang, I.S.; Shin, P.K. & Kim, B.H. (2000). Biological treatment of acid mine drainage under sulphate-reducing conditions with solid waste materials as substrates. *Water Research*, 34(4):1269-1277.
- Choudhary, R.P & Sheoran, A.S. (2011). Comparative study of cellulose waste versus organic waste as substrate in a sulfate reducing bioreactor. *Bioresource Technology*, 102:4319-4324.
- Cocos, I.A.; Zagury, G.J.; Clément, B. & Samson, R. (2002). Multiple factor design for reactive mixture selection for use in reactive walls in mine drainage treatment. *Water Research*, 32:167-177.
- de Mattos, R.C. (2013). Utilização dos Resíduos Ligno-lulósicos Bagaço de Cana-de-Açúcar e “Cama de Aviário” como Substratos Orgânicos em Ensaio de Laboratório de Redução Bacteriana de Sulfato. MSc. Thesis (in portuguese), Instituto Tecnológico de Aeronáutica, São José dos Campos, Brazil.
- de Mattos, R.C. & Hems, P.S. (2012). Estimativa do potencial de utilização de resíduos agrícolas em barreiras reativas permeáveis com base em sua composição e degradabilidade. In: XVI Brazilian Congress on Soil Mechanics and Geotechnical Engineering, COBRAMSEG 2012, Porto de Galinhas, Brazil.
- Duryea, M.L.; English, R.J. & Hermanesen, L.A. (1999). A comparison of landscape mulches: Chemical, allelopathic, and decomposition properties. *Journal of Arboriculture*, 25:88-97.
- Dvorak, D.H.; Hedin, R.S.; Edenborn, H.M. & McIntire, P.E. (1992). Treatment of metal-contaminated water using bacterial sulfate reduction: Results from pilot-scale reactors. *Biotechnology and Bioengineering*, 40(5):609-616.
- FEAM (2011). Fundação Estadual do Meio Ambiente. Inventário de Áreas Impactadas pela Mineração do Estado de Minas Gerais, 2011. FEAM-GESAD-RT-3-2011.
- Figuerola, L.; Miller, A.; Zaluski, M. & Bless, D. (2007). Evaluation of a two-stage passive treatment approach for mining influenced waters. In: 2007 National Meeting of the American Society of Mining and Reclamation, R.I. Barnhisel (ed), Gillette, WY.
- Gibert, O.; de Pablo, J.; Cortina, J.L. & Ayora, C. (2004). Chemical characterization of natural organic substrates for biological mitigation of acid mine drainage. *Water Research*, 38(19):4186-4196.
- Gillham, R.W. & O'Hannesin, S.F. (1994). Enhanced degradation of halogenated aliphatics by zero-valent iron. *Groundwater*, 32(6):958-967.
- Groudev, S.; Nicolova, M.; Spasova, I. & Schutte, R. (2003). Treatment of waters from a copper mine by means of a permeable reactive barrier. Fifty Years of the University of Mining and Geology “St. Ivan Rilski”, University of Mining and Geology, Sofia, 46(II):229-231.
- Grubb, D.G.; Landers, D.G. & Hernandez, M. (2000). Utilization of sugarcane bagasse to treat acid mine drainage. Proc. GeoEng 2000, Melbourne, Australia.
- Hallberg, K. & Johnson, D. (2005). Microbiology of a wetland ecosystem constructed to remediate mine drainage from a heavy metal mine. *Science of the Total Environment*, 338(1-2):53-66.
- Hammack, R.W. & Edenborn, H.M. (1992). The removal of nickel from mine waters using bacterial sulfate reduction. *Applied Microbiology and Biotechnology*, 37(5):674-678.
- Hemsi, P.S.; Shackelford, C.D. & Figuerola, L.A. (2005). Modeling the influence of decomposing organic solids on sulfate reduction rates for iron precipitation. *Environmental Science and Technology*, 39(9):3215-3225.
- Hemsi, P.S.; Shackelford, C.D. & Figuerola, L.A. (2010). Calibration of reactive transport models for remediation of mine drainage in solid substrate bio-columns. *Journal of Environmental Engineering*, 136(9):914-925.
- Khalid, A.; Arshad, M.; Anjum, M.; Mahmood, T. & Dawson, L. (2011). The anaerobic digestion of solid organic waste. *Waste Management*, 31:1737-1744.
- Krebs, A.J. (2010). Monitoramento de bocas de minas abandonadas com drenagens ácidas na área correspondente à Bacia Carbonífera de Santa Catarina. In: Brazilian Groundwater Congress, 2010, São Luiz, Brazil.
- Logan, M.V.; Reardon, K.F.; Figuerola, L.A.; McLain, J. & Ahmann, D.M. (2005). Microbial community activities during establishment, performance, and decline of bench-scale passive treatment systems for mine drainage. *Water Research*, 39(18):4537-4551.
- Neculita, C.M.; Zagury, G.J. & Bussière, B. (2007). Passive treatment of acid mine drainage in bioreactors using sulfate-reducing bacteria: Critical review and research needs. *Journal of Environmental Quality*, 36(1):1-16.

- Rubio, J.; Silva, R. & Silveira, A. (2008). Técnicas para tratamento e alternativas de reuso de águas ácidas de minas de carvão. In: Proc. VI Internacional Symposium on Environmental Quality, ABES-RS & PUCRS, Porto Alegre, Brazil.
- Stumm, W. & Morgan, J.J. (1996). Aquatic Chemistry: Chemical Equilibria and Rates in Natural Waters. John Wiley & Sons, NY.
- Szogi, A.A.; Hunt, P.G.; Sadler, E.J. & Evans, D.E. (2004). Characterization of oxidation- reduction processes in constructed wetlands for swine wastewater treatment. *Applied Engineering in Agriculture*, 20(2):189-200.
- Tuttle, J.H.; Dugan, P.R. & Randles, C.I. (1969). Microbial sulfate reduction and its potential utility as an acid mine water pollution abatement procedure. *Applied Microbiology*, 17(2):297-302.
- U.S. Air Force Center for Engineering and the Environment (2008). Final technical protocol for enhanced anaerobic bioremediation using permeable mulch biowalls and bioreactors. Washington (DC), <http://www.cluin.org/download/techfocus/prb/Final-Biowall-Protocol-05-08.pdf>.
- U.S. Environmental Protection Agency (1998). Permeable Reactive Barrier Technologies for Contaminant Remediation. Report EPA/600/R-98/125.
- Voudrias, E.A. (2001). Pump-and-treat remediation of groundwater contaminated with hazardous waste: Can it really be achieved? *Global Nest Journal*, 3(1):1-10.
- Wakao, N.; Takahashi, T.; Sakurai, Y. & Shiota, H. (1979). A treatment of acid mine water using sulfate-reducing bacteria. *Journal of Fermentation Technology*, 57(5):445-452.
- Waybrant, K.R.; Blowes, D.W. & Ptacek, C.J. (1998). Selection of reactive mixtures for use in permeable reactive walls for treatment of mine drainage. *Environmental Science & Technology*, 32(13):1972-1979.
- Western Governors' Association, WGA (1998). Cleaning up Abandon Mines: A Western Partnership. Electronic document. <http://www.westgov.org/wga/publicat>.
- Whitehead, P.G.; Cosby, B.J. & Prior, H. (2005). The Wheal Jane wetlands model for bioremediation of acid mine drainage. *Science of the Total Environment*, 338(1-2):125-135.
- Wildeman, T.R.; Gusek, J.J.; Miller, A. & Fricke, J. (1997). Metals, sulfur, and carbon balance in a pilot reactor treating lead in water. In: *In Situ and On-Site Bioremediation*, Battelle Press, Columbus.
- Zagury, G.J.; Kulnieks, V. & Neculita, C.M. (2006). Characterization and reactivity assessment of organic substrates for sulphate-reducing bacteria in acid mine drainage treatment. *Chemosphere*, 64:944-954.



# Apparent Pressures on Multi-Propped Retaining Walls in Soils Under Drained Conditions with Shallow Water Table

L. Andrade Viana, N.M. da Costa Guerra

**Abstract.** In the design of flexible retaining walls supported by several levels of struts, apparent design diagrams are frequently used, particularly to predict the loads on the struts. In the case of sandy soils, the traditional design diagrams do not consider water table. The present work deals with apparent design diagrams for cases considering water table. A brief analysis of the problem based on published information is presented. Stress-strain finite element analyses are applied to a case study, comparing situations without water table with others where the water table is assumed. For the cases where water table is assumed two types of conditions are considered: those where seepage is allowed and those where it is not. A parametric analysis is performed to study the effects on soil pressures and on apparent pressures of geometrical and mechanical parameters of the soil and structure. From the analysis of the results a proposal for the apparent diagrams for the design of retaining walls performed in soils under drained conditions with water table above the bottom of the excavation is presented.

**Keywords:** multi-propped retaining walls, apparent earth pressures, water pressures, seepage.

## 1. Introduction

Numerical methods are commonly used in the design of multi-propped retaining walls. They allow the stress-strain step-by-step analysis of the construction procedure and therefore the prediction of the displacements induced in the supported soil, the forces and bending moments on the wall and the loads on the struts. However, its use needs the pre-definition of several geometrical and structural characteristics. In the case of the wall and struts, such pre-definition needs the prediction of the loads installed, which is frequently done using apparent design diagrams.

The most known and used apparent design diagrams are those proposed by Terzaghi & Peck (1967). In case of sandy soils, the diagram is rectangular, with horizontal stress given by:

$$\sigma_H = 0.65K_a \gamma H \quad (1)$$

in which  $K_a$  is the Rankine active earth pressure coefficient,  $\gamma$  is the unit weight of the soil and  $H$  is the depth of the excavation.

These diagrams were the result of monitoring the loads on the struts of several multi-propped flexible retaining walls throughout a few decades of the twentieth century. In most cases, for drained situations, the adopted construction procedure allowed lowering the water table in cases where it was above the bottom of the excavation and therefore no water pressures existed on the retaining walls.

There is no generally accepted way to take into account in the apparent diagrams the existence of water table above the bottom of the excavation in flexible retaining

walls supported by several levels of struts. When the excavation is carried out below the water table, without lowering it, and the wall is impermeable, a substantial part of pressures on the wall will be due to water. When seepage is not allowed (because the wall was extended to an impermeable stratum) the structure has to be designed to withstand the hydrostatic pressures. Strom & Ebeling (2001) proposed an apparent diagram considering both soil and water pressures (see Fig. 1).

This diagram is based on Terzaghi and Peck's, using an average effective unit weight to which the pore-water pressure is added. The average effective unit weight,  $\gamma_e$ , can be calculated by either of two methods, in which the soil above the water table is considered with the moist unit weight,  $\gamma$ , and the soil below the water table is considered with the buoyant unit weight,  $\gamma'$ .

In method 1 (Strom & Ebeling, 2001),  $\gamma_e$  is the weighted average using depths  $H - z_w$  and  $z_w$  shown in Fig. 2:

$$\gamma_e = \frac{\gamma'(H - z_w) + \gamma z_w}{H} \quad (2)$$

In method 2 (Ebeling & Morrison, 1992),  $\gamma_e$  is the weighted average using  $A_1$  and  $A_2$  also shown in Fig. 2:

$$\gamma_e = \frac{\gamma' A_1 + \gamma A_2}{A_1 + A_2} = \frac{\gamma'(H - z_w)^2 + \gamma z_w^2}{H^2} \quad (3)$$

In the particular case of water table on the ground surface the application of methods 1 and 2 results in the same

Laís Andrade Viana, MSc, Departamento de Engenharia Civil, Faculdade de Ciências e Tecnologia, Universidade Nova de Lisboa, Lisboa, Portugal. e-mail: l.viana@campus.fct.unl.pt.

Nuno M. da Costa Guerra, Associate Professor, UNIC, Departamento de Engenharia Civil, Faculdade de Ciências e Tecnologia, Universidade Nova de Lisboa, Lisboa, Portugal. e-mail: nguerra@fct.unl.pt.

Submitted on July 16, 2015; Final Acceptance on November 2, 2015; Discussion open until April 30, 2016.

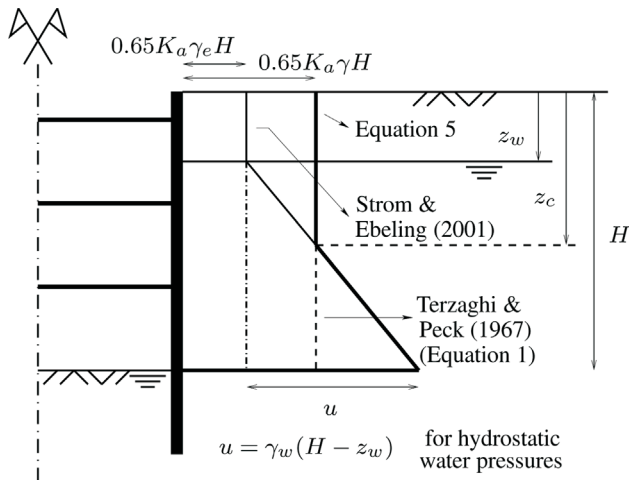


**Figure 1** - Apparent diagrams for sandy soils for no water table (Terzaghi & Peck, 1967) and for water table above the bottom of the excavation (Strom & Ebeling, 2001) and proposed correction of this method, given by Eq. 5.

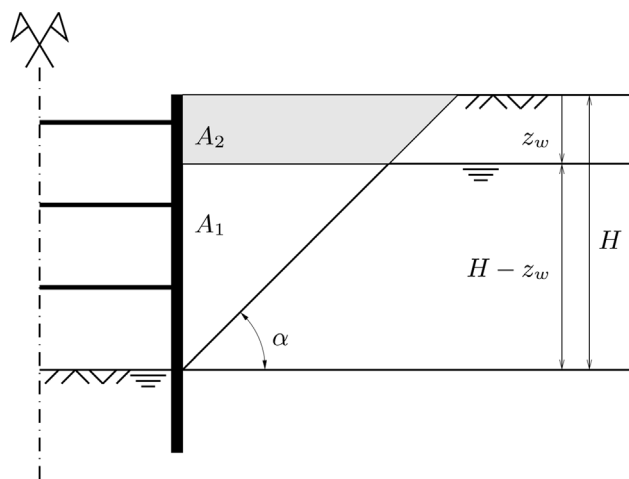


**Figure 2** - Geometric parameters for determining the effective unit weight for partially submerged soils. Angle  $\alpha$  is the angle defining the failure wedge.

solution and the average effective unit weight is equal to the buoyant unit weight.

The resulting diagram implies the consideration up to a certain depth,  $z_c$ , given by:

$$z_c = 0.65K_a H \frac{\gamma - \gamma_e}{\gamma_w} + z_w \quad (4)$$

of a total pressure that is lower than the one that would be considered if there were no water table, which does not seem to make much sense. Therefore, a proposal that seeks to rectify this aspect is also shown in Fig. 1 and the horizontal pressures take the following values (see Andrade Viana, 2014):

$$\sigma_H = \begin{cases} 0.65K_a \gamma H & , z \leq z_c \\ 0.65K_a \gamma_e H + \gamma_w (z - z_w), & z > z_c \end{cases} \quad (5)$$

In cases where seepage is allowed around the wall into the excavation, with steady-state seepage conditions, there are seepage forces on the ground. The diagrams, adapted from the previous, consider, instead of the buoyant unit weight  $\gamma'$ , this unit weight plus the seepage forces. In addition, the water pressures will no longer be hydrostatic and  $u$  (see Fig. 1) will therefore not be  $\gamma_w(H - z_w)$  and the linear distribution will be a simplification. It is possible to verify that this proposal leads to lower total pressures on the wall when compared to the ones from the hydrostatic case, and therefore only the hydrostatic ones will be shown in the paper, for comparison with the results obtained from the numerical analyses.

The diagrams described above have not been confirmed either by monitoring or numerical analyses. Therefore, the present work intends to numerically obtain apparent diagrams, for cases considering the presence of the water table in the soil. It is somehow interesting that a numerical procedure is felt useful to obtain diagrams of the same type as others that were probably only developed because of the lack of such advanced techniques, at the time.

## 2. Modelling

Stress-strain finite element analyses were performed for this study, using the finite element program Plaxis (2014). The problem consists of a symmetrical excavation supported by a multi-propped retaining wall and plane strain conditions are assumed.

Five scenarios were analyzed and they are schematically shown in Fig. 3:

- Scenario A: no water table, the wall does not reach the rigid impermeable stratum.
- Scenario B: water table at depth  $z_w$ ; the wall does not reach the rigid impermeable stratum and the water level is lowered inside the excavation by continuous pumping. Seepage modelling is performed.
- Scenario C: no water table, the wall reaches the rigid impermeable stratum and it can not rotate at the toe.
- Scenario D: water table at depth  $z_w$ ; the wall reaches the rigid impermeable stratum and it can not rotate at the toe. No seepage is allowed.
- Scenario E: water table at depth  $z_w$ ; the wall reaches an almost impermeable stratum and the water level is lowered inside the excavation by continuous pumping. Seepage modelling is performed, even though seepage occurs mainly in the stratum with very low permeability.

The excavation was modelled in alternating stages of excavation and installation of strut levels. The excavation stages also consider that the water level is lowered inside the excavation (scenarios B, D and E) and the calculation of the associated seepage (scenarios B and E). It should also be mentioned that the soil was assumed homogeneous and

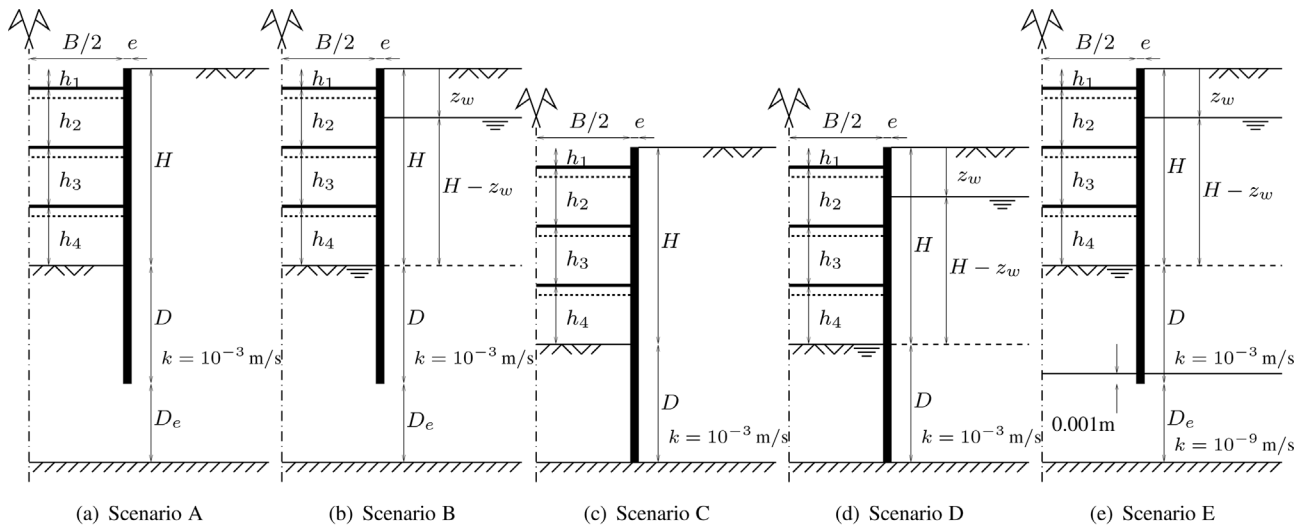


Figure 3 - Schematic representation of scenarios A, B, C, D and E.

isotropic. If real conditions of the soil involved heterogeneity and (or) anisotropy, the groundwater flow could have a significant effect on the pressures on the wall (Kaiser & Hewitt, 1982).

The wall and the struts were admitted linear elastic. The soil was modelled by the "Hardening Soil Model" (Schanz *et al.*, 1999). The HSM is an elastoplastic type of hyperbolic model, formulated in the framework of shear hardening plasticity. The model also involves compression hardening to simulate irreversible compaction of soil under primary compression (Plaxis, 2014).

Limiting states of stress are described by means of the shear strength angle,  $\phi'$ , the effective cohesion,  $c'$ , and the dilatancy angle,  $\psi$ . Soil stiffness is described by using three different input stiffnesses: the secant triaxial loading stiffness to half of the tensile strength,  $E_{50}$ , the triaxial unloading and reloading stiffness,  $E_{ur}$ , and the oedometer loading stiffness,  $E_{oed}$ . These stiffnesses depend on stress-state according to the relations:

$$E_{50} = E_{50,ref} \left( \frac{\sigma'_3 + c'_{ref} \cot \phi'}{p'_{ref} + c'_{ref} \cot \phi'} \right)^m \quad (6)$$

$$E_{ur} = E_{ur,ref} \left( \frac{\sigma'_3 + c'_{ref} \cot \phi'}{p'_{ref} + c'_{ref} \cot \phi'} \right)^m \quad (7)$$

$$E_{oed} = E_{oed,ref} \left( \frac{\sigma'_1 + c'_{ref} \cot \phi'}{p'_{ref} + c'_{ref} \cot \phi'} \right)^m \quad (8)$$

in which  $m$  is a power that expresses the dependence of the soil stiffness with the stress state in the soil,  $p'_{ref}$  is a reference stress, usually taken equal to 100 kPa,  $\sigma'_1$  is the major principal stress and  $\sigma'_3$  is the minor principal stress. In order to characterize the soil stiffness the following reference

stiffnesses are required:  $E_{50,ref}$ ,  $E_{ur,ref}$  and  $E_{oed,ref}$ . As average values for various soil types,  $E_{ur,ref} = 3E_{50,ref}$  and  $E_{oed,ref} = E_{50,ref}$  are suggested as default settings (Plaxis, 2014).

### 3. Case Study

The case study has the following values for the geometrical parameters:  $B/2 = 5$  m;  $e = 0.4$  m;  $H = 10$  m;  $D = 6$  m;  $D_e = 4$  m;  $h_1 = 1$  m;  $h_2 = h_3 = h_4 = 3$  m;  $z_w = 0$  m. The excavation was modelled in stages, for a total of nine stages. It was performed in four levels of excavations and the wall is supported by three levels of struts.

The soil was considered as a sandy soil with drained behaviour. In scenarios A and C the moist unit weight was set as 20 kN/m<sup>3</sup>. In scenarios B, D and E the water table was considered on the ground surface and the saturated unit weight was also taken equal to 20 kN/m<sup>3</sup>.

The chosen stiffness parameters intend to portray the behaviour of a medium sand:  $E_{50,ref} = 25000$  kPa,  $E_{ur,ref} = 75000$  kPa,  $E_{oed,ref} = 25000$  kPa and  $m = 0.5$ . It was assumed a shear strength angle,  $\phi'$ , of 30°, a reference effective cohesion,  $c'_{ref}$ , of 1 kPa and a dilatancy angle,  $\psi$ , of 1°. The at rest earth pressure coefficient,  $K_0$ , was taken equal to 0.5. The soil was considered with homogeneous hydraulic characteristics (permeability coefficient in the horizontal direction equal to the permeability coefficient in the vertical direction,  $k_x = k_y$ ). This coefficient was taken equal to 10<sup>-3</sup> m/s. In scenario E the soil below the wall was considered with a very low permeability coefficient, in both directions, of 10<sup>-9</sup> m/s. All other parameters were considered equal to the ones of the soil above.

Interfaces were modelled by joint elements and its strength and stiffness properties are defined by the strength reduction factor,  $R_{inter}$  (Plaxis, 2014), which was set as 0.67.

The wall was considered built before the excavation, with elastic characteristics of a reinforced concrete wall with a bending stiffness,  $EI$ , of 160000 kNm<sup>2</sup>/m. Given that

it is an "infinite" wall, since the analysis is in plane strain conditions, a null Poisson's ratio,  $\nu$ , was adopted.

The wall weight per unit area was considered equal to 10 kN/m/m.

The stiffness of the struts was chosen by performing preliminary calculations using scenarios A and C, so that pressures on the wall and apparent pressures inferred from the maximum loads on the struts roughly correspond to the apparent diagrams of Terzaghi and Peck with horizontal stresses given by Eq. 1. The same characteristics were adopted in scenarios B, D and E. Thus, the struts were assumed as linear elastic with axial stiffness,  $EA$ , of 120000 kN/m.

Figure 4 shows the distribution of hydraulic head in the soil mass after the last excavation stage in scenarios B and E. The distributions of hydraulic head correspond to the expected and it is possible to note that the lines defined by color changes correspond to equipotential lines.

Figure 5 shows the displacements obtained for the wall and for the surface of the supported soil mass after the last stage of excavation. It can be observed that the displacement values corresponding to scenarios with water (B, D and E) are substantially higher than those associated to scenarios without water (A and C). In particular, in scenario B, wherein the wall is not based on rigid impermeable stratum and seepage is allowed, the displacements of the wall

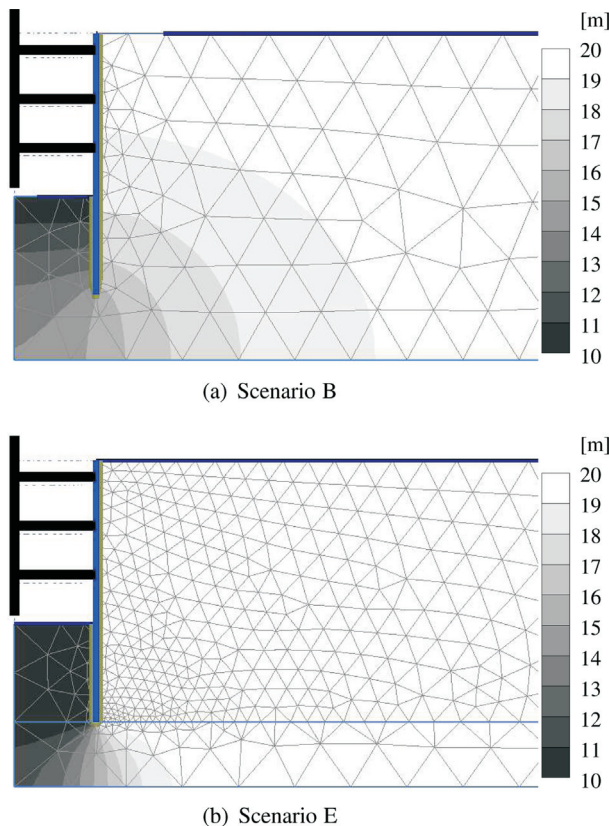


**Figure 4** - Distribution of water head after the last excavation stage.

and, thus, of the surface of the supported soil, are particularly high. It is interesting to notice that the displacements for this scenario (B) are greater than the ones for scenario E, where the wall toe can move and water pressures on the right side are hydrostatic and larger than in scenario B.

Figure 6 shows the plastic points obtained after the last excavation stage for all scenarios that were analysed. It is possible to observe that in scenarios A and C there are few failure points which occur specially in the soil-structure interface. In scenario B failure points occur mainly in the soil mass, showing the beginning of a sliding surface; it should be noted that this occurs even though the global safety factor against the hydraulic uplift is, in this case, relatively high ( $FS = 1.43$ ). In scenario D failure points occur especially in the soil-structure interface and in a band of soil inside the excavation, without any hint of a sliding surface. In scenario E there is, again, an intermediate situation between scenarios B and D, with failure points in soil-structure interface and also the beginning of a potential sliding surface in the soil on the right side of the wall.

Figure 7 shows the results obtained after the last stage of excavation for total, effective and pore water pressures on the wall. It also shows the apparent pressures inferred from the maximum loads on the struts. The apparent diagram of Terzaghi and Peck (Eq. 1) and the apparent diagram given by Eq. 5 are also shown in Figs. 7(a) and 7(b), for comparison with the results obtained.

Scenarios A and C have equal total and effective pressures as there are no pore water pressures. In scenario B pore water pressures deviate progressively from hydrostatic pressures, while in scenarios D and E they are equal to hydrostatic pressures. In fact, in scenario E, the seepage is negligible and therefore the pore water pressures are very similar to hydrostatic pressures.

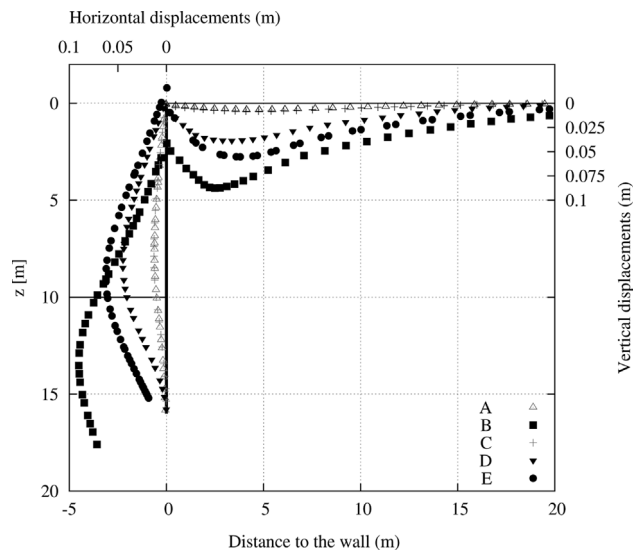


**Figure 5** - Displacements of the wall and of the surface of the supported soil mass after the last excavation stage.

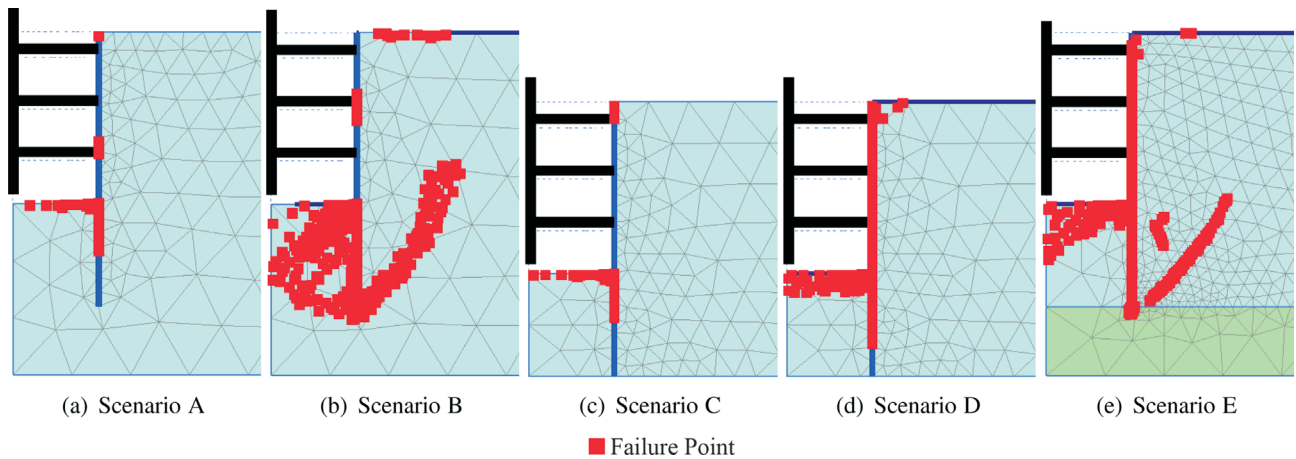


Figure 6 - Failure points after the last excavation stage.

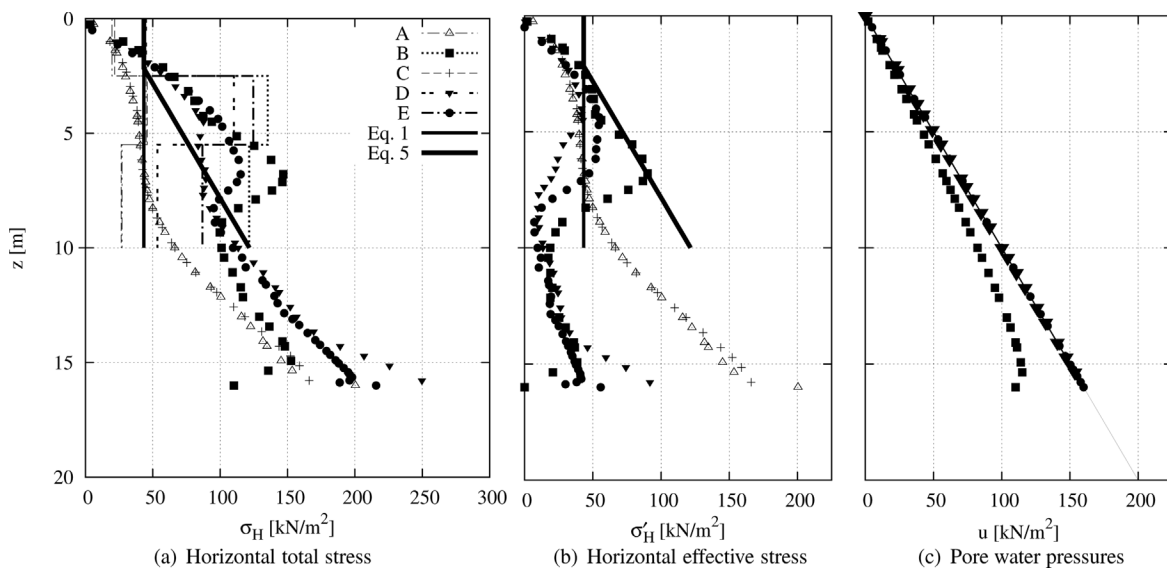


Figure 7 - Pressures on the flexible retaining wall after the last excavation stage (symbols) and apparent pressures inferred from the maximum loads on the struts (lines; Fig. 7(a)).

In scenarios A and C the distribution of total stresses on the wall approaches the apparent diagrams of Terzaghi and Peck. Indeed, as referred, the axial stiffness adopted for struts was chosen so that the distribution of pressures on the wall for these scenarios would be approximately constant in depth and equal to the value obtained from Eq. 1.

In scenario B total stresses on the wall are greater than those corresponding to the apparent diagram given by Eq. 5. This diagram is, up to a certain depth, similar to the obtained distribution of effective stresses, despite this apparent diagram being established in terms of total stresses. It can be seen that the apparent pressures corresponding to the last level of struts are very close to the ones corresponding to the second level of struts. In fact, the apparent pressures corresponding to the last level of struts are, up to a certain depth, lower than the distribution of total stresses on

the wall at the same depth, while, from that same depth, the apparent pressures become greater than the distribution of total stresses on the wall.

In scenario D total stresses on the wall are also greater than the apparent diagram given by Eq. 5. However, it can be noted that in this scenario the distribution of total stresses on the wall is closer to this apparent diagram than in scenario B. Thus, contrary to what is verified in the situation in which the existence of water level is not considered, the existence of a rigid impermeable stratum shows considerable influence on the distribution of total pressures on the wall. It can be seen that in this scenario the apparent pressures corresponding to the last level of struts are much lower than the distribution of total stresses on the wall at the same depth. This is probably due to the fact that the wall is embedded in a more competent stra-

tum, which is responsible to absorb a significant percentage of the pressures.

In scenario E there is an intermediate situation between scenarios B and D, with total stresses on the wall that remain greater than the apparent diagram given by Eq. 5. It is interesting to note that, when compared with scenario D, in scenario E the apparent pressures corresponding to the last level of struts are much closer to the distribution of total stresses on the wall. It is also interesting to notice that effective stresses are greater at the upper part of the wall and much lower at the bottom than in cases where soil is considered dry.

Figure 7 shows that the diagrams proposed in the literature are not suitable approximations for the distribution of pressures on the wall or the apparent pressures for the cases where water table was considered. Therefore, this justifies further research and, in particular, the parametric analysis presented below.

## 4. Parametric Analysis

### 4.1. Cases

Based on the case study, parametric analyses of several geometrical and mechanical aspects were performed. A brief overview of all the analyses performed is presented in Table 1.

Those analyses were performed in two stages. In the first stage (left part of Table 1) the parametric analyses consisted in the variation of one parameter at a time. In these analyses scenarios A, B, C and D were studied. For example, when the analysis of the variation of the embedded length of the wall was performed, only this parameter took different values: the one corresponding to the case study itself (in bold in the Table 1), a value above and another below it. A similar procedure was performed for the axial stiffness of the struts, the wall bending stiffness, the width of the excavation, the scale of the problem and the unit weight of the soil. In the parametric analysis of the scale of the problem, two additional calculations were performed:

one where all dimensions of the problem were halved and one other where they were doubled. For the analysis of the variation of the mechanical characteristics of the soil, only two soils were studied: the soil that was considered in the case study (soil 1, in bold in the Table 1), and a soil with better mechanical characteristics (soil 2):  $\phi' = 40^\circ$ ,  $\psi = 8^\circ$ ,  $E_{50,ref} = 90000$  kPa,  $E_{ur,ref} = 270000$  kPa and  $E_{oed,ref} = 90000$  kPa. For soil 2, the at rest earth pressure coefficient was taken equal to 0.8, assuming an overconsolidated material.

In the second stage of the parametric analyses (right part of Table 1), different depths of the water table,  $z_w$ , and different embedded lengths of the wall, for both soils – 1 and 2 – were considered. In these analyses scenarios B, D and E were studied.

As previously presented, the main objective of this paper is to propose apparent diagrams that can be used in the design of flexible retaining walls with water table above the bottom of the excavation. For such purpose, an overall analysis of all calculations is needed. The procedure followed is next presented as an example, and the same steps were taken for all the other analyses.

### 4.2. Example: analysis of the variation of the embedded length of the wall, $D$

As an example of the adopted procedure, the analysis of the variation of the embedded length of the wall is presented for all scenarios A to E. The pressures on the flexible retaining wall after the last excavation stage and apparent pressures inferred from the maximum loads on the struts are, for these cases, shown in Fig. 8.

In scenarios A and C the total stress distributions on the wall do not show major differences between the results obtained for each adopted value for the embedded length of the wall. However, for very small values of  $D$ , in scenario C it is possible to observe a change of the pressure distributions that show greater values for lower values of length  $D$  for greater depths and the reverse more superficially. In scenario B the distribution of total stress on the wall does not have a continuous evolution. Also, for  $D = 8$  m, apparent pressures are lower than the ones for  $D = 6$  m; however, for  $D = 3$  m, apparent pressures at the lowest level significantly increase. This is due to the fact that in this case, the hydraulic uplift safety factor is very low. Also, it can be seen that for the lowest value of  $D$ , apparent pressures inferred from the strut loads are very large for scenario B. It should however be noticed that these correspond to unusual situations with very low hydraulic uplift safety factors. In scenario D, in the middle of the excavation height, the greater the embedded length of the wall, the greater the stress. In the last meters of the excavation height there is an inversion of this relationship. The apparent pressures show greater difference between the results corresponding to each embedded length of the wall the greater the depth. In scenario E the pressure distributions do not show major dif-

**Table 1** - Cases analysed in the parametric analyses.

Case	A	B	C	D	B	D	E
$D$ [m]		<b>3/6/8</b>		<b>2/6/8</b>	<b>3/6/8</b>		<b>2/6/8</b>
$EA$ [kN/m]		$0.2 EA_{cs} / EA_{cs} / 5EA_{cs}$					<b><math>EA_{cs}</math></b>
$EI$ [kNm <sup>2</sup> /m]		$EI_{cs} / 8 / EI_{cs} / 8EI_{cs}$					<b><math>EI_{cs}</math></b>
$B$ [m]		<b>6/10/20</b>					<b>10</b>
Scale		$\times 0.5 / \times 1 / \times 2$					$\times 1$
Soil - S		<b>1/2</b>					<b>1/2</b>
$\gamma$ [kN/m <sup>3</sup> ]		<b>17.5/20/25</b>					<b>20</b>
$z_w$ [m]	-	<b>0</b>	-	<b>0</b>	<b>0/2.5/5/7.5/10</b>		

$EA_{cs}$  and  $EI_{cs}$  are the values adopted in the case study.

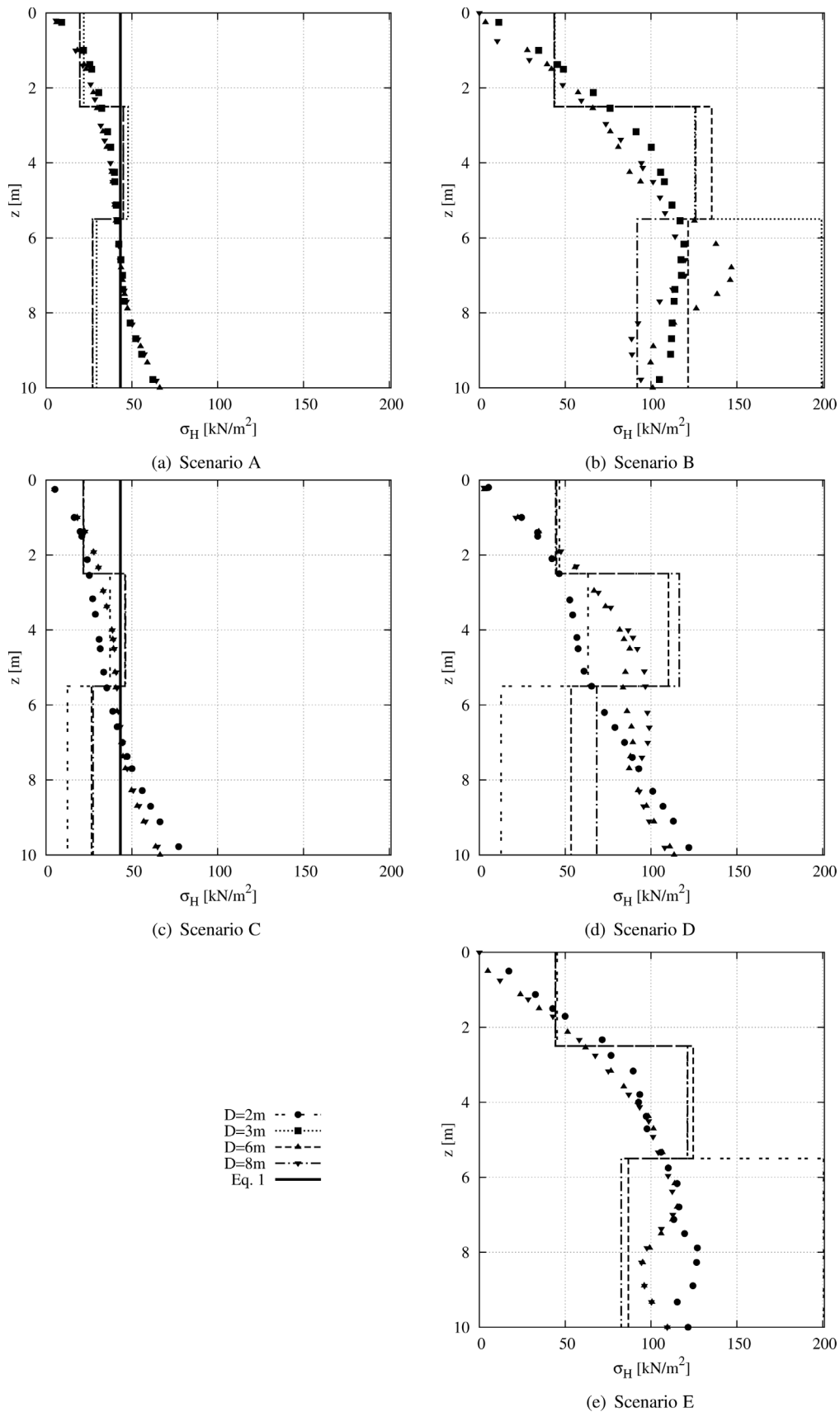


**Figure 8** - Analysis of the variation of the embedded length of the wall: pressures on the flexible retaining wall after the last excavation stage (symbols) and apparent pressures inferred from the maximum loads on the struts (lines).

ferences between the results obtained for each adopted value for the embedded length of the wall, except, however, for the results corresponding to the embedded length of the wall with very small value (2 m). It is possible to note that in this case the pressures are globally higher than those corresponding to other cases. In this case this is caused by the large water pressures on one side of the wall and the considerably lower ones at the other side.

The results obtained after the last excavation stage for the pressures on the wall and for the apparent pressures (inferred from the maximum loads on the struts) were converted into dimensionless quantities by determining the ratio between the obtained pressures and the ones from Terzaghi and Peck's diagram (without water table):

$$\beta = \frac{\sigma_H}{0.65K_a \gamma H} \quad (9)$$

and are shown in Fig. 9. This figure includes a proposed diagram that will be presented in section 5.

Figure 9 shows that the results can be reasonably normalized using Eq. 9, resulting in values of  $\beta$  approximately constant for each set of calculations. The same representation will be used for the other results obtained in the parametric analysis.

#### 4.3. Analysis of the variation of other geometric and mechanical aspects

The same procedure followed in subsection 4.2 was adopted for the different parameters shown in Table 1 and the results for the dimensionless pressures are shown in Appendix A in Figs. A.1 to A.4. Scenarios B and D are the subject of the analysis; however, scenarios A and C are also studied for comparison.

It can be briefly mentioned that in the case where high water table with steady-state seepage is considered (Scenario B), the parameters that show greater influence on pressures on the retaining wall and on apparent pressures using the loads on the struts are: embedded length of the wall, width of excavation, mechanical characteristics of the soil and unit weight of the soil (which is more relevant in Soil 1); the parameters that have less influence than the previous ones are: axial stiffness of the struts, bending stiffness of the wall and scale of the problem.

In the case where high water table with hydrostatic pressures is considered (Scenario D), the parameters that show greater influence on pressures on the retaining wall and on apparent pressures using the loads on the struts are: embedded length of the wall, bending stiffness of the wall (in contrast to what is verified for Scenario B), mechanical characteristics of the soil and unit weight of the soil (which, as for Scenario B, is more relevant in Soil 1); the parameters that have less influence than the previous ones are: axial stiffness of the struts, scale of the problem (which have greater influence on the apparent pressures using the loads on the struts), but mostly the width of excavation (which

does not have great influence, the opposite of what is verified in Scenario B).

Results represented in the dimensionless way shown by Eq. 9, as performed in Figs. A.1 to A.4, show approximately constant values of  $\beta$ , which means that this is an adequate way of presenting the results. These figures, as in Fig. 9, include the same proposed diagram that will be presented in Section 5.

#### 4.4. Analysis of the variation of the depth of the water table ( $z_w$ )

Parametric analyses to study the influence of the variation of the depth of the water table were also performed and the results of the dimensionless pressures in scenario B are shown in Fig. 10 as an example.

As expected, the more shallow the water table, the greater the pressures. The lower the  $z_w$ , the greater the difference between the distribution of total pressures on the wall and the apparent pressures inferred from the strut loads, specially at the depth corresponding to the last strut level. For  $z_w/H = 1$  soil 1 leads to greater normalized pressure on the wall than the soil 2. However, for water table closer to the ground surface, there is a reversal of this relation.

Scenarios D and E were also studied in order to analyse the influence of the depth of the water table variation and the results of the dimensionless pressures are shown in Appendix B in Figs. B.1 and B.2, respectively. As expected, it can be seen that shallower water tables result in greater pressures on the wall and greater apparent pressures. As in previous figures, Figs. 10, B.1 and B.2 include proposed diagrams (now depending on the water table depth) that will be presented next.

### 5. Proposal for Apparent Pressures

For cases without water table, scenarios A and C (Figs. A.1 and A.3), the dimensionless horizontal stresses,  $\beta$ , are reasonably approximated by 1.00, corresponding to the diagram of Terzaghi & Peck (1967) (Eq. 1). Moreover, this value remained globally adequate in most of the analyses (see Figs. 9(a), 9(c), 10(a), A.1, A.3, B.1(a) and B.2(a)), showing the suitability of the traditional diagram of Terzaghi and Peck as a conservative diagram for the results of the pressures.

For cases where water table is taken into account, scenarios B, D and E, the results obtained for the total pressures on the wall and apparent pressures inferred from maximum loads on the struts allow to propose apparent diagrams. These diagrams are also shown in Figs. 9, 10, A.2, A.4, B.1 and B.2 and are detailed in Fig. 11. Such diagrams admit that apparent pressures should not be less than the ones from the diagram of Terzaghi and Peck. They consider Terzaghi and Peck's value at the ground level and increase linearly down to a depth of  $0.4H$ , after which a constant dia-

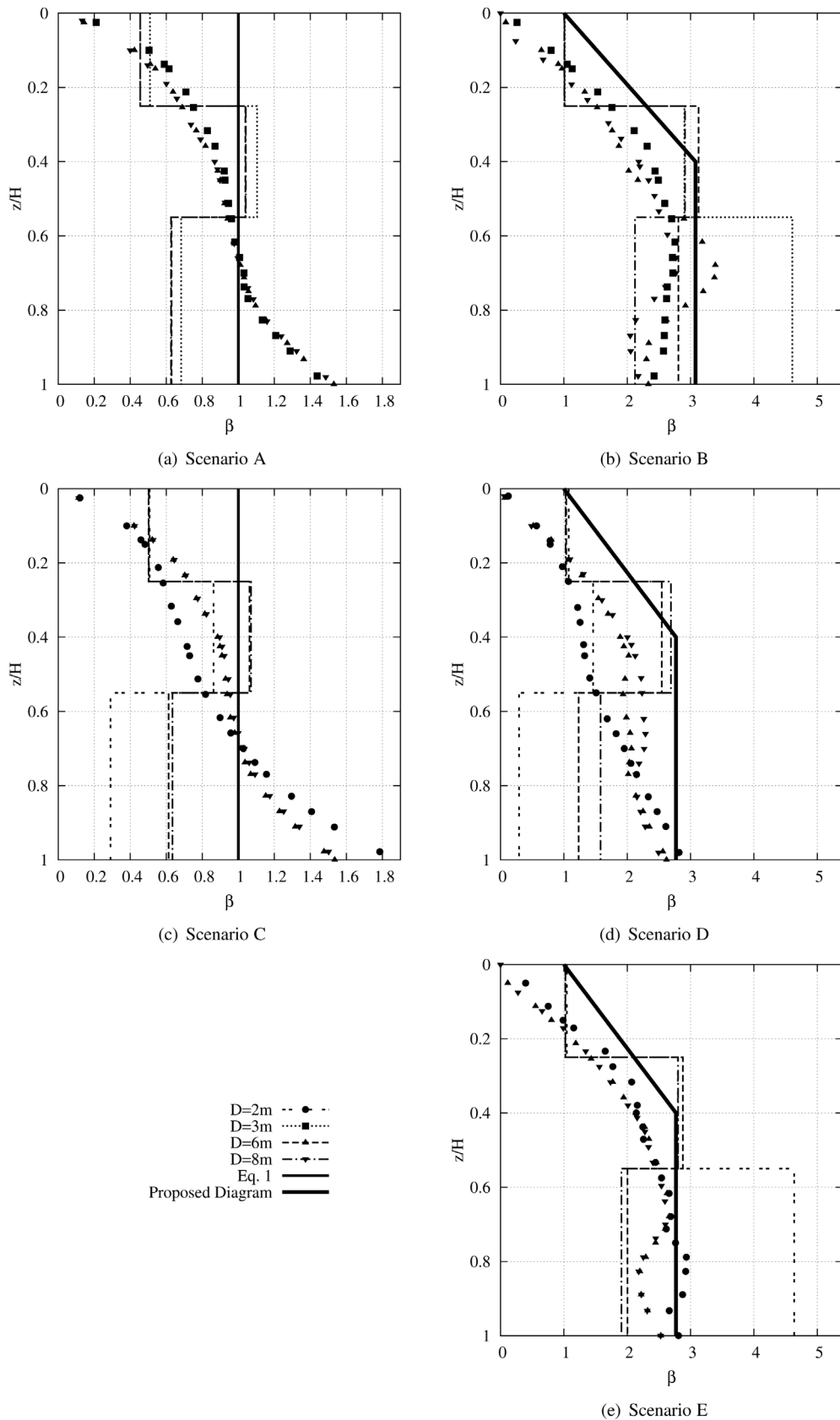


**Figure 9** - Analysis of the variation of the embedded length of the wall: Dimensionless pressures on the flexible retaining wall after the last excavation stage (symbols) and apparent pressures inferred from the maximum loads on the struts (lines). Note the difference between the horizontal scales of the graphics on the left and on the right.

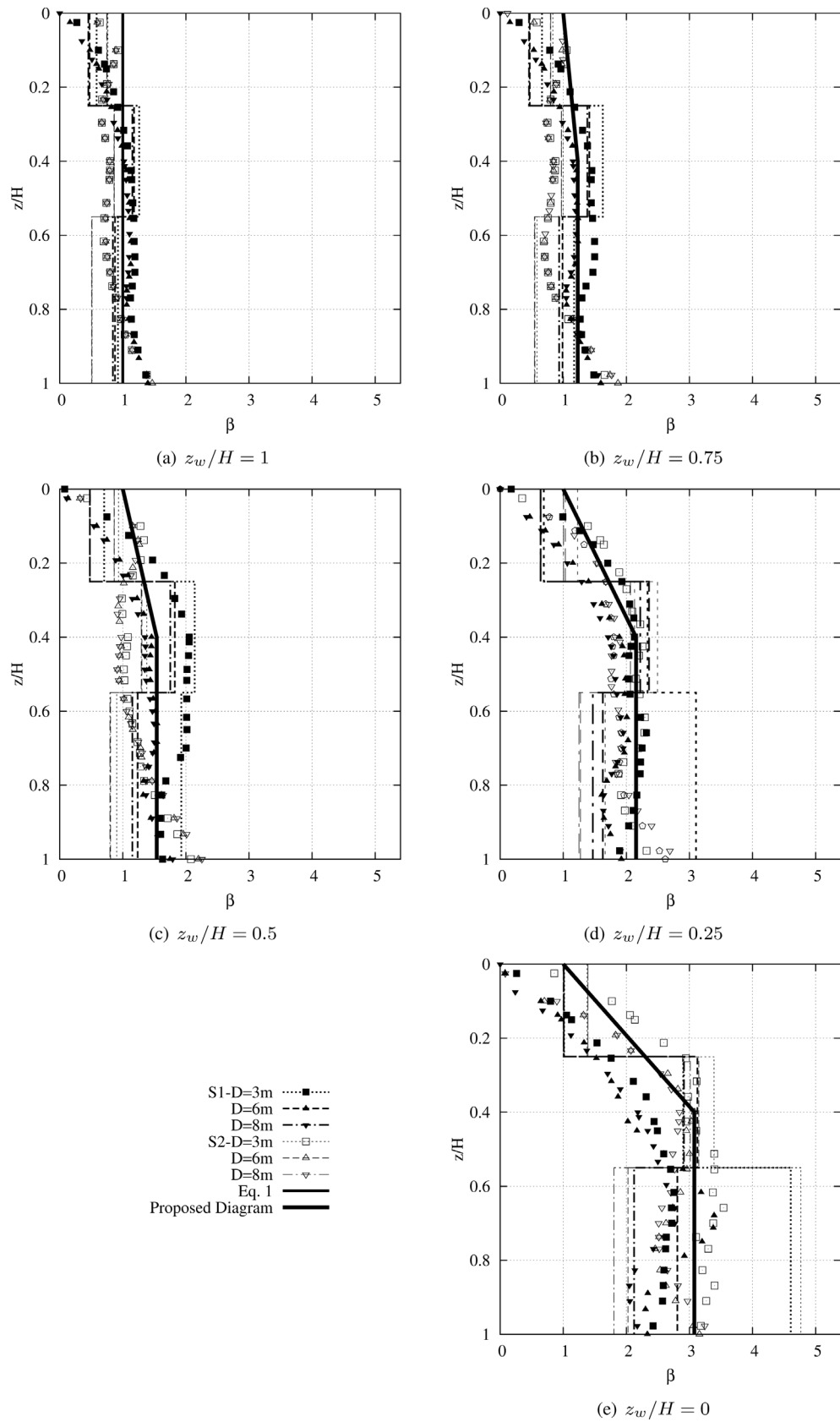


**Figure 10** - Scenario B - analysis of the variation of the embedded length of the wall to different depths of the water table: dimensionless pressures on the flexible retaining wall after the last excavation stage (symbols) and apparent pressures inferred from the maximum loads on the struts (lines).

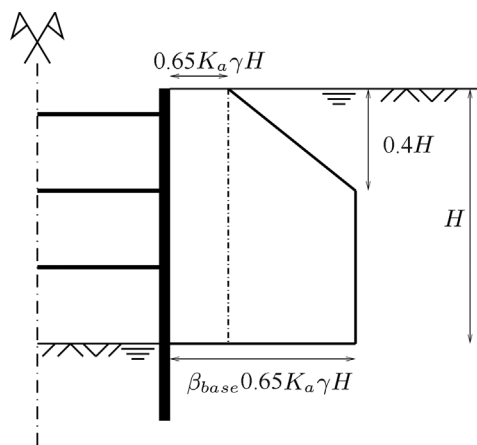


Figure 11 - Proposal for apparent design diagrams.

gram given by a horizontal pressure of  $\beta_{base} 0.65 K_a \gamma H$  is proposed.

In the particular case of water table on the ground surface, it appears from Figs. 9, A.2 and A.4 that the results of the dimensionless pressures can be approximated by  $\beta_{base} = 3.1$  for scenario B and 2.75 for scenarios D and E. These values show a considerable influence of the water table on total pressures and on the loads on the struts. It should be noted that in the course of the parametric analysis performed, a few cases of very large apparent pressures corresponding to the last strut level were obtained. These few cases mainly correspond to situations where hydraulic uplift safety factors are very low and beyond the scope of usual design. Such cases involve the same type of phenomena also present in undrained situations with poor basal stability conditions (Terzaghi & Peck, 1967; Bjerrum *et al.*, 1972; Peck *et al.*, 1974). Therefore, these situations were ignored for the proposal of the apparent pressure distribution diagrams presented.

Based on the parametric analysis of the variation of the depth of the water table that was performed for scenarios B, D and E (Figs. 10, B.1 and B.2) a chart with the corresponding values of  $\beta_{base}$  (Fig. 12) for different values of  $z_w/H$  is further proposed. The resulting diagrams are shown in Figs. 10, B.1 and B.2.

## 6. Conclusions

From the developed study it can be concluded that the existing proposals in the literature for the apparent diagrams corresponding to situations in which the water level is considered and seepage is allowed, as well as the situations in which the water level is considered with hydrostatic pressures, are not suitable approximations for the distribution of pressures on the wall or the apparent pressures. Indeed, in all calculations the results achieved were greater than the values corresponding to these diagrams.

The calculations were performed for a relatively wide range of situations, assuming homogeneous and isotropic

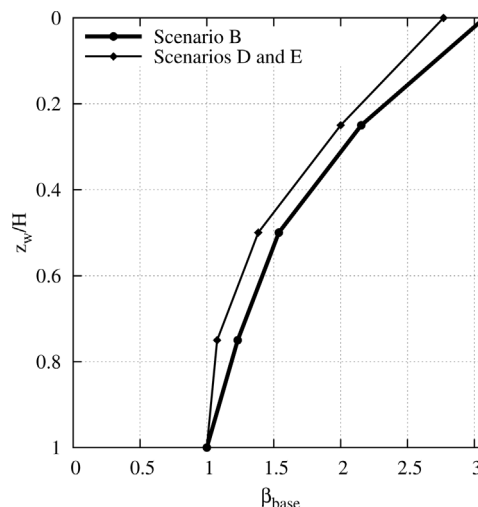


Figure 12 - Proposed values of  $\beta_{base}$  as a function of the depth of the water table.

behaviour of the soil, for two soil conditions, for different geometries (embedded length of the wall, width of the excavation, scale of the problem), different soil unit weights and different stiffnesses of the wall and of the struts. Also, several positions of the water table was considered.

The obtained pressures were normalized using the stress of Terzaghi and Peck's apparent diagram for sands and the normalized results could be reasonably represented by a proposed apparent design diagram for cases in which the water level is assumed, either when seepage is allowed and when hydrostatic pressures are considered. The exceptions correspond to cases with low hydraulic uplift safety factors. The proposed apparent design diagram shows a very large influence of the water table on the pressures on the wall, increasing them significantly.

## References

- Andrade Viana, L. (2014). Pressões Sobre Cortinas de Contenção em Solos com Nível Freático Elevado. Master's Thesis, UNL, Faculdade de Ciências e Tecnologia, Universidade Nova de Lisboa, Lisboa.
- Bjerrum, L., Frimann Clausen, C. & Duncan, J. (1972). Earth pressure on flexible structures - A state of the art report. In: Proc. 5th European Conference on Soil Mechanics and Foundation Engineering, Madrid, volume 2, p. 169-196.
- Ebeling, R.M. & Morrison, E.E. (1992). The seismic design of waterfront retaining structures. Technical Report ITL-92-11, U.S. Army Engineer Waterways Experiment Station.
- Kaiser, P.K. & Hewitt, K.J. (1982). The effect of groundwater flow on the stability and design of retained excavations. Canadian Geotechnical Journal, 19:139-153.
- Peck, R.B., Hanson, W.E. & Thornburn, T.H. (1974). Foundation Engineering. John Wiley and Sons, New York, 2nd edition.

- Plaxis (2014). Plaxis 2D Manual. Brinkgreve *et al.*, eds. Delft.
- Schanz, T., Vermeer, P.A. & Bonnier, P.G. (1999). The hardening-soil model: Formulation and verification. In: Proc. Beyond 2000 in Computational Geotechnics, Balkema, Rotterdam, p. 281-290.
- Strom, R.M. & Ebeling, R.M. (2001). State of the practice in the design of tall, stiff, and flexible tieback retaining walls. Technical Report ITL TR-01-1, US Army Corps of Engineers. Engineer Research and Development Center.
- Terzaghi, K. & Peck, R.B. (1967). Soil Mechanics in Engineering Practice. John Wiley & Sons, Inc., 2nd edition.

## Appendix A

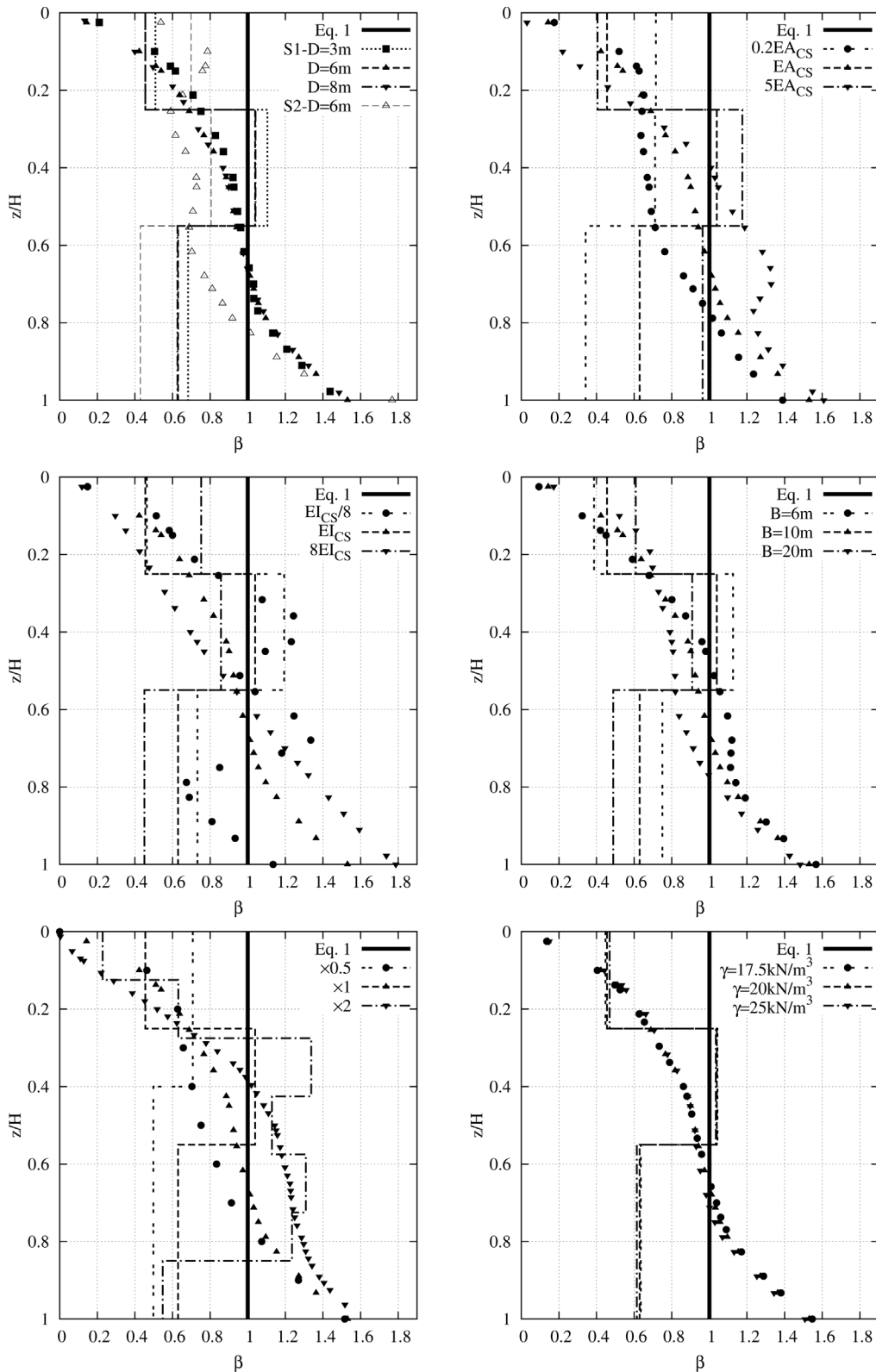


**Figure A.1** - Scenario A - analysis of the variation of the: embedded length of the wall; stiffness of the struts; stiffness of the wall; width of excavation; scale and unit weight of the soil. Dimensionless pressures: total stresses on the flexible retaining wall after the last excavation stage (symbols) and apparent pressures inferred from the maximum loads on the struts (lines).

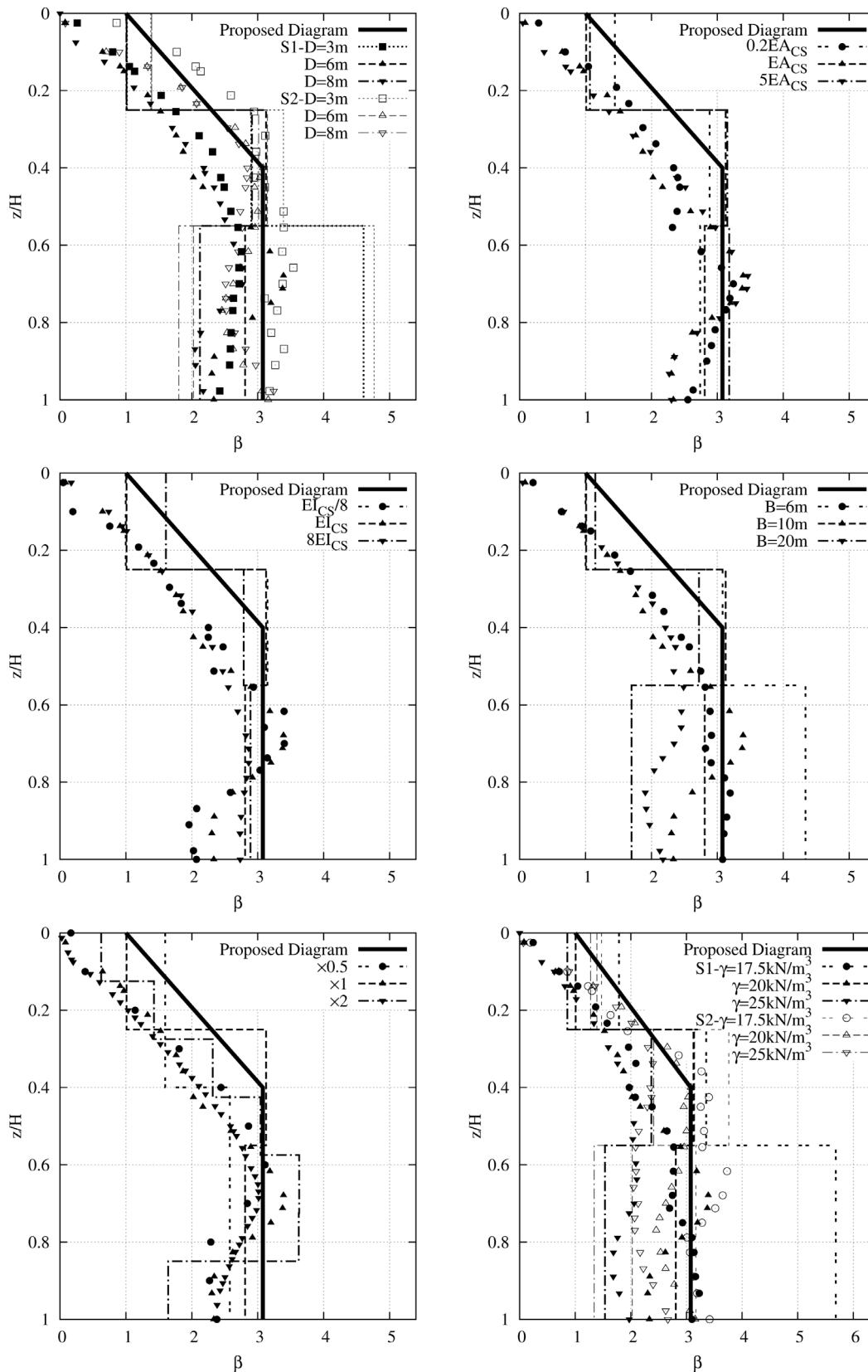


**Figure A.2** - Scenario B - analysis of the variation of the: embedded length of the wall; stiffness of the struts; stiffness of the wall; width of excavation; scale and unit weight of the soil. Dimensionless pressures: total stresses on the flexible retaining wall after the last excavation stage (symbols) and apparent pressures inferred from the maximum loads on the struts (lines). Note the difference in the horizontal scale in the bottom right graphic.

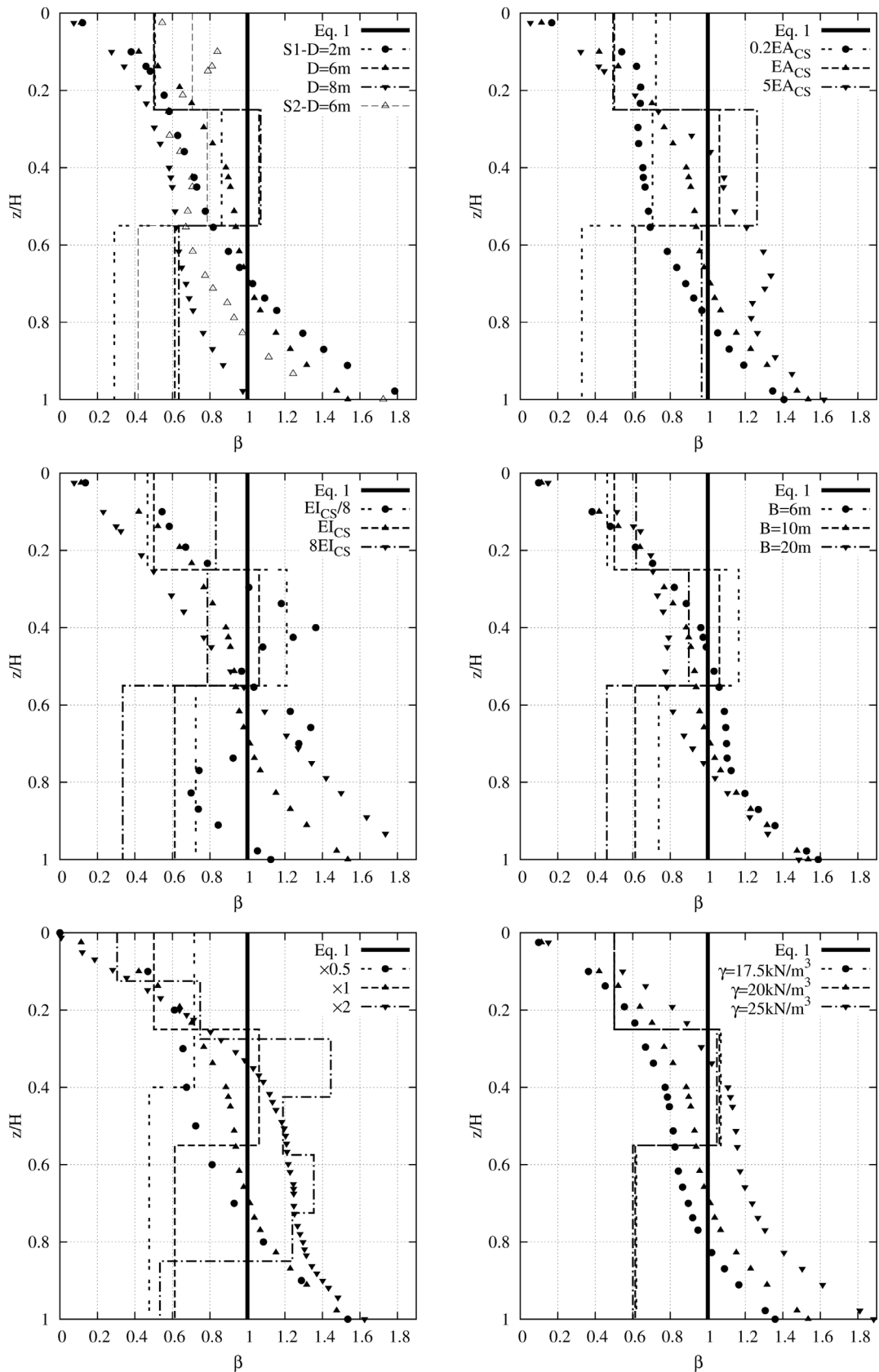


**Figure A.3** - Scenario C - analysis of the variation of the: embedded length of the wall; stiffness of the struts; stiffness of the wall; width of excavation; scale and unit weight of the soil. Dimensionless pressures: total stresses on the flexible retaining wall after the last excavation stage (symbols) and apparent pressures inferred from the maximum loads on the struts (lines).

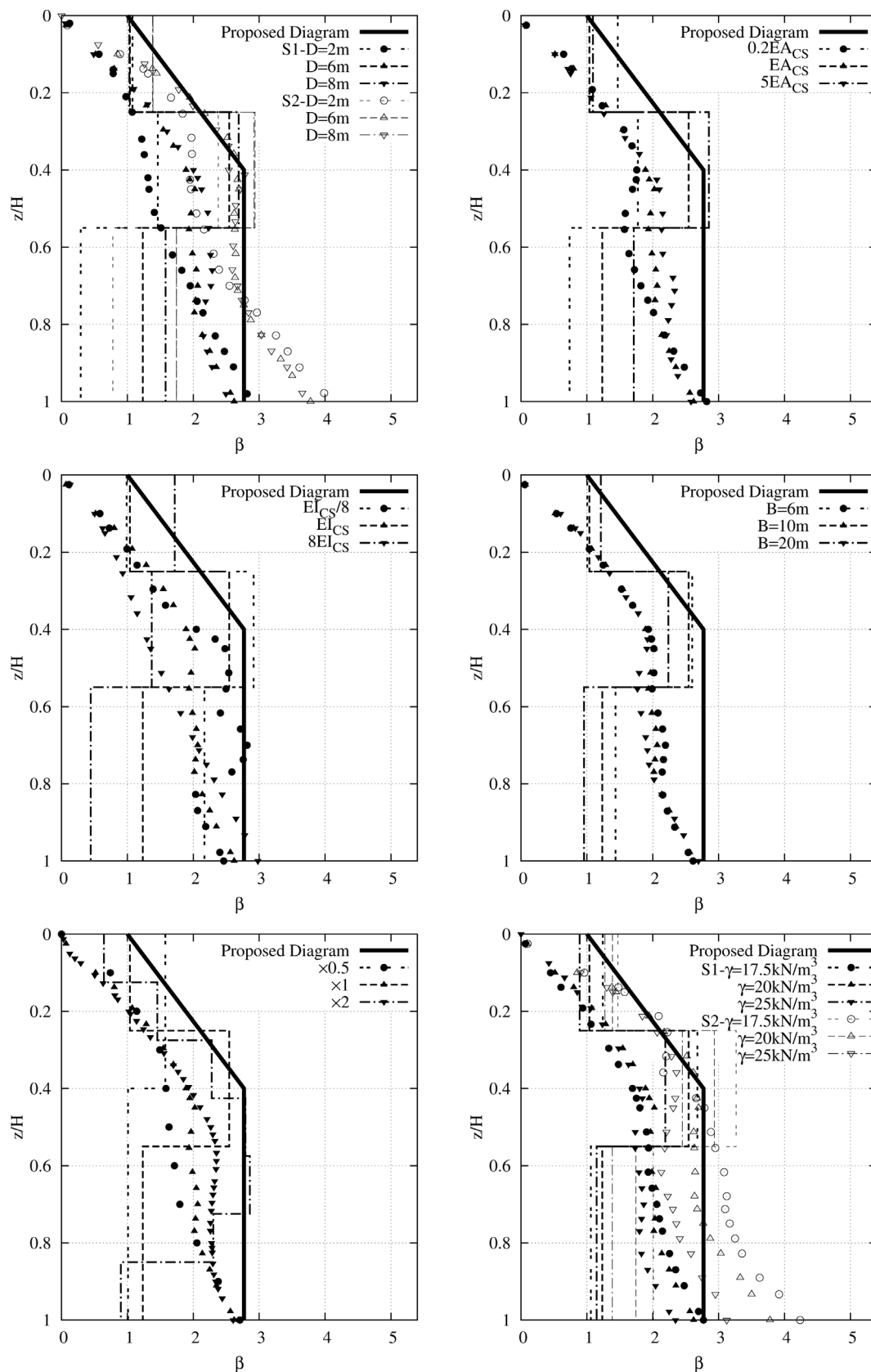


**Figure A.4** - Scenario D - analysis of the variation of the: embedded length of the wall; stiffness of the struts; stiffness of the wall; width of excavation; scale and unit weight of the soil. Dimensionless pressures: total stresses on the flexible retaining wall after the last excavation stage (symbols) and apparent pressures inferred from the maximum loads on the struts (lines).

### Appendix B

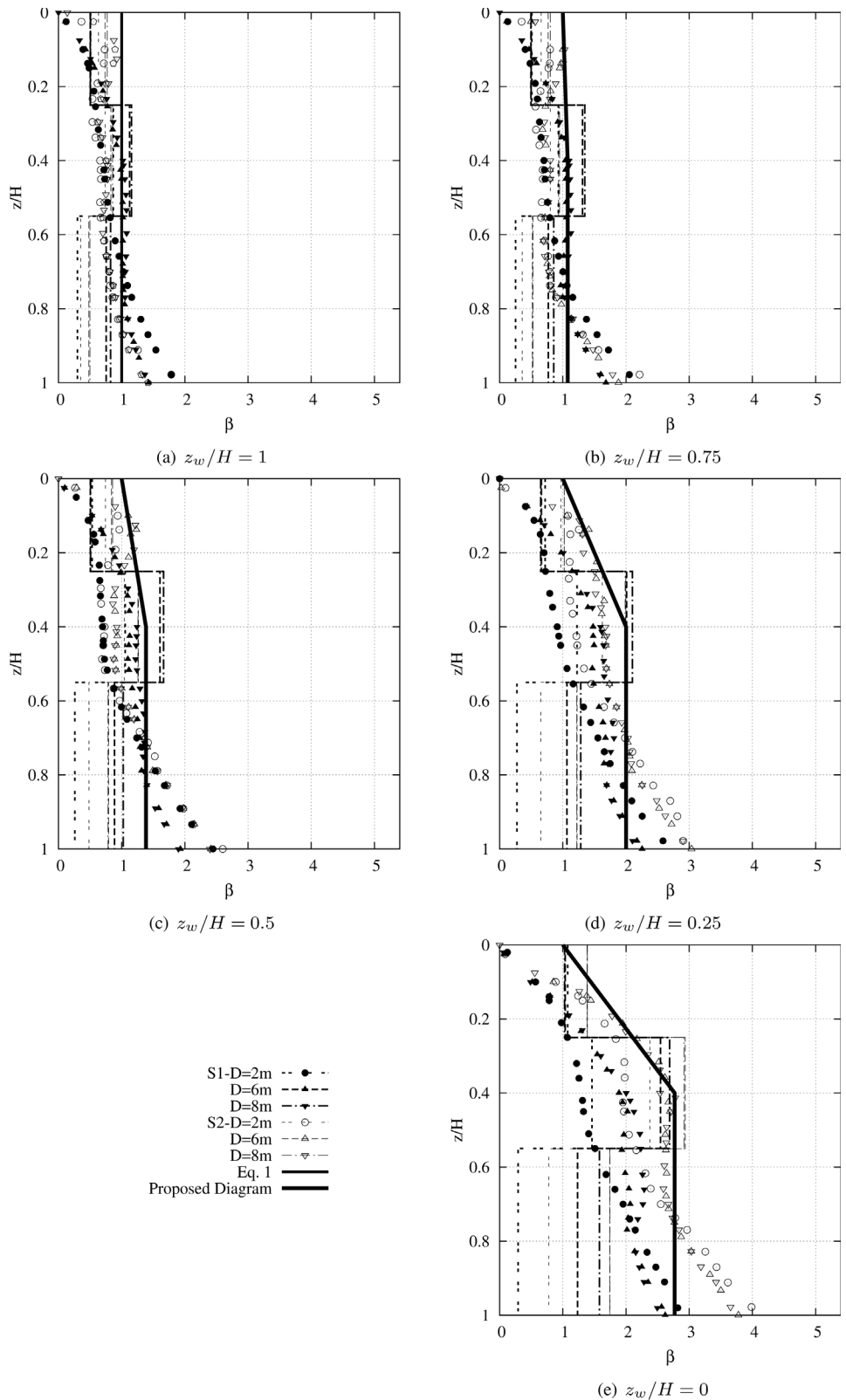


**Figure B.1** - Scenario D - analysis of the variation of the embedded length of the wall to different depths of the water table. Dimensionless pressures: pressures on the flexible retaining wall after the last excavation stage (symbols) and apparent pressures inferred from the maximum loads on the struts (lines).

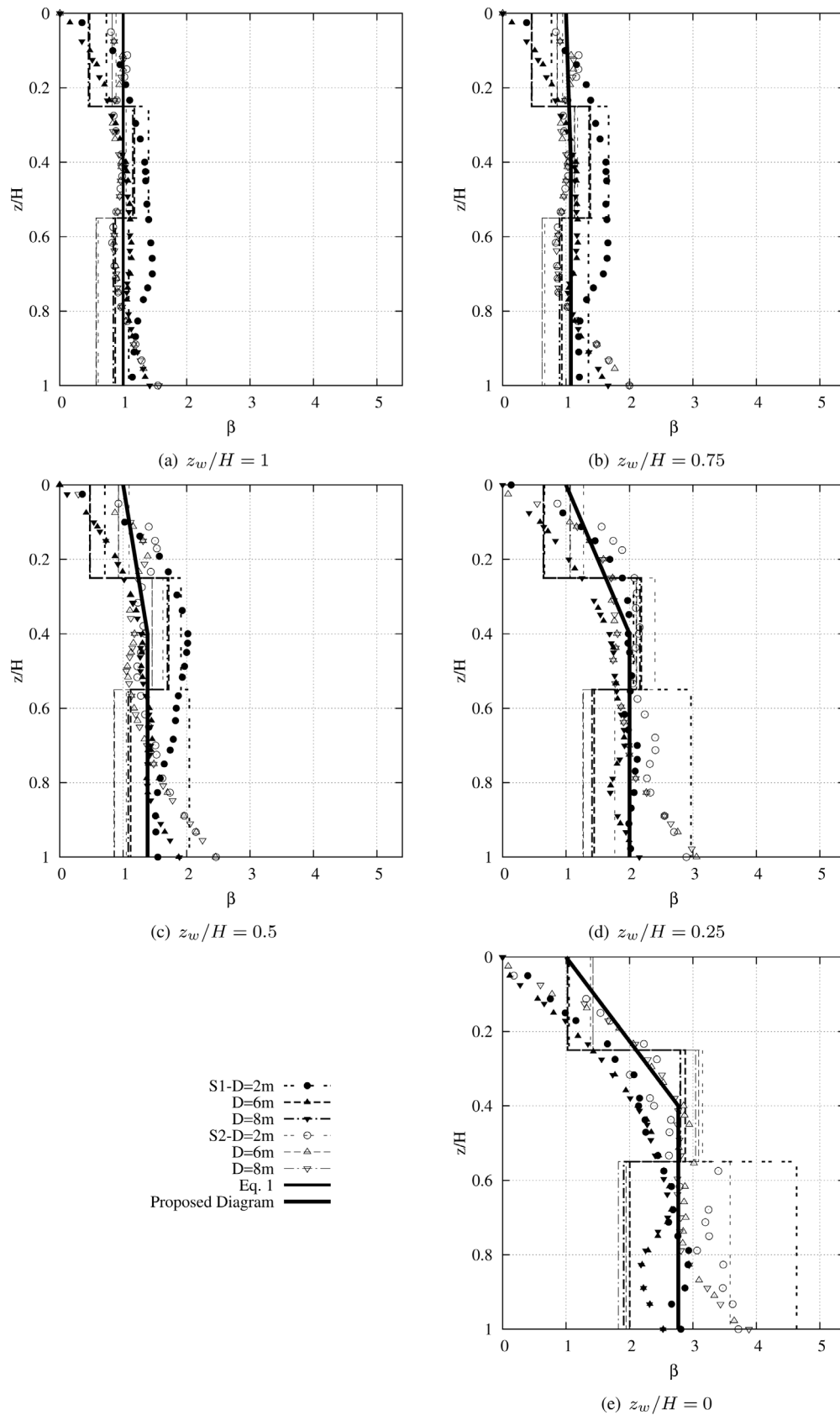


**Figure B.2** - Scenario E - analysis of the variation of the embedded length of the wall to different depths of the water table. Dimensionless pressures: pressures on the flexible retaining wall after the last excavation stage (symbols) and apparent pressures inferred from the maximum loads on the struts (lines).

# On the Interpretation of the Bidirectional Static Load Test

F. Massad

**Abstract.** The paper deals with the bidirectional test, aiming at interpreting its results, showing the factor that governs the upward movement and presenting approximate formulas to find the equivalent load-settlement curve of a conventional compressive test. The factor is the product  $c' \cdot k = (1 - c) \cdot k$ , where  $c'$  and  $c$  are the Leonards-Lovell coefficients, related to the elastic shortening of the shaft under bidirectional and conventional static loading tests, respectively, and  $k$  is the relative stiffness of the pile-soil (shaft) system. The paper shows that when this product is constant the properly normalized upward curve is invariant, independently on shaft resistance distribution. Nomograms are presented to quickly determine  $c'$  for two patterns of shaft friction associated to weak upper layers over deep more resistant soils. Under this condition, it is shown that  $c > c'$ , *i.e.*, the load causing the downward movement in the conventional test induces greater elastic shortening than in the bidirectional test. Therefore, additional movement must be added to the measured displacement in the bidirectional test, which constitutes the basis of the proposed approximate formulas to find the equivalent curve of the conventional test. To validate these findings a mathematical model is used together with five case histories, comprising short to long piles. In one case a conventional compressive loading test was also available.

**Keywords:** bidirectional test, elastic shortening, equivalent curve, compressive loading test.

## 1. Introduction

The Brazilian hydrodynamic expansive cell was developed by Silva (1983 and 1986) and since the 1980's has been used in static load tests chiefly in bored piles. Its use spread worldwide after Osterberg (1989) and is known as "O-Cell Test" or the bidirectional test. One or more expansive interconnected cells are placed on the tip of a metal frame and introduced into the shaft, generally near the pile toe, and concreted together with the pile. The activation of the cells takes place hydraulically causing its expansion, pushing the shaft upward and the toe downward. The upward and downward movements can be measured at the level of the cells (bottom and top) with "tell tales" and at the top of the pile with dial gauges or displacement transducers.

The reaction system is provided by the pile shaft and the test is limited to the exhaustion of one of the pile capacity, tip or friction. Its execution is rapid and very high loads may be applied when associated with several cells.

The issue has been the subject of analysis by Alonso & Silva (2000), trying to simulate the equivalent conventional static load test. The usual procedure to obtain an equivalent conventional test curve consists in adding the shaft and toe applied loads which cause the same measured displacement, up and down. As the load causing the downward movement in the equivalent test induces greater elastic shortening than in the bidirectional test, additional movement must be added to the measured displacement. Many procedures were proposed accounting for pile compression to construct the equivalent download curve, like those presented by Alonso & Silva (2000), Loadtest (2001); Kwon *et al.* (2005); and Kim *et al.* (2012). The relevance of

this curve is in the evaluation of pile bearing capacity, using, for instance, the Davisson Offset Limit (Davisson, 1972 cited by Fellenius, 2015).

The objectives of this paper are: a) to show that the product  $c' \cdot k = (1 - c) \cdot k$ , where  $c$  is the Leonards-Lovell coefficient, related to the elastic shortening of the shaft under conventional test, and  $k$  the relative stiffness of the pile-soil (shaft) system, governs the normalized upward movement of a bidirectional test; and b) to present approximate formulae to determine the equivalent load-settlement curve of a conventional test in a simpler and more rational way.

## 2. Shortening of Piles Under Compressive Loadings

The analysis will be initiated evaluating the shortening of piles subjected to both download conventional test and bidirectional test.

### 2.1. Shortening of piles during a download conventional test

To estimate the shortening of vertical piles, under axial compressive loading at the pile head ( $P_o$ ), not necessarily at failure, the following expression may be used (see the list of symbols):

$$\Delta e = \frac{Q_p}{K_r} + c \cdot \frac{A_l}{K_r} \quad (1)$$

where  $Q_p$  and  $A_l$  are toe and shaft loads, respectively, so that:

$$P_o = Q_p + A_l \quad (2)$$

Faiçal Massad, Dr. Eng., Full Professor and Geotechnical Consultant, Escola Politécnica of the São Paulo University, Av. Prof. Almeida Prado 271, trav. 2, São Paulo, SP, Brazil. e-mail: faissal@usp.br.

Submitted on October 7, 2015; Final Acceptance on November 11, 2015; Discussion open until April 30, 2016.

$K_r$  is the pile stiffness, with height  $h$ , cross sectional area  $S$  and modulus of elasticity  $E$ , given by:

$$K_r = \frac{E \cdot S}{h} \quad (3)$$

In Eq. 1  $c$  is the Leonards & Lovell (1979) coefficient, *i.e.*, the ratio of the average value of the transferred lateral load (the hatched area of Fig. 1-a over pile height) and the total shaft load ( $A_l$ ), *i.e.*:

$$c = \frac{A_l - \bar{A}_l}{A_l} \quad (4)$$

The coefficient  $c$  depends on the distribution of the unit shaft friction ( $f$ ). If the shaft load is fully mobilized ( $A_l = A_{lr}$ ), then  $c = 0.5$  for  $f_u = \text{const}$  along depth and  $c = 2/3$  for  $f_u$  increasing linearly with depth. Values of  $c$  for other

simple forms of distribution of  $f_u$  can be obtained rapidly using the nomograms prepared by Leonards & Lovell (1979) or the equations proposed by Fellenius (1980), shown in Fig. 2. Note that  $h_1$  and  $h_2$  are the thicknesses of the softer and stiffer layers, respectively, and  $f_{u1}$  and  $f_{u2}$  are the corresponding shaft frictions.

### 2.2. Shortening of piles during a bidirectional test

For upward loads in the bidirectional test Eq. 1 changes to:

$$\Delta e = c' \cdot \frac{A_l}{K_r} \quad (5)$$

where  $c'$  is given by Eq. 4 but related to Fig. 1-b. A similar nomogram may be constructed for  $c'$ , as shown in Fig. 3 with the associated equations. Note that now  $h_1$  and  $h_2$  are

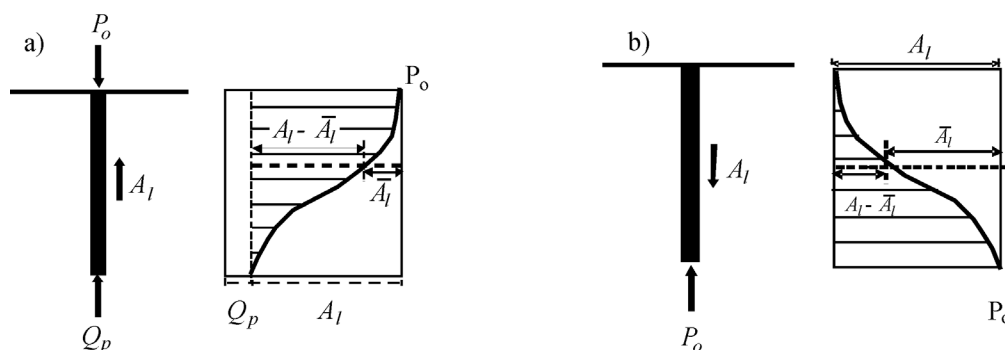


Figure 1 - Load distribution -a) Conventional test; and b) - Bidirectional test.

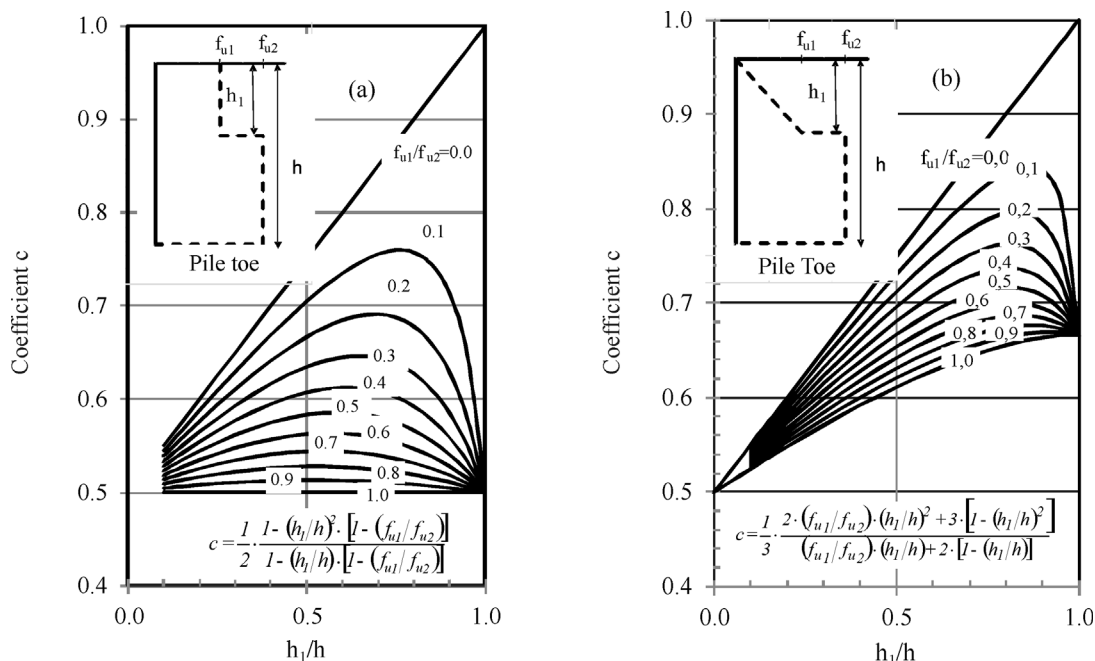


Figure 2 - Nomograms for head-down loads (conventional loading test).

the thicknesses of the stiffer and softer layers, respectively, and  $f_{u1}$  and  $f_{u2}$  are the corresponding shaft frictions. Comparing Figs. 1-a and 1-b, on one hand, and Figs. 2 and 3, on the other hand, it can be seen that:

$$c + c' = 1 \tag{6}$$

Note also that in general  $c' < c$ , that is, the elastic compression of piles under O-Cell upward loads is smaller than the corresponding value for the download test. This is due to the fact that the O-Cell upward loads mobilize first the deeper and more resistant soils and later the upper softer layers.

### 3. Mathematical Simulation of Bidirectional Tests. The Upward Curve Invariance with $c' \cdot k$

#### 3.1. The mathematical model

For the simulation of bidirectional tests a mathematical model developed by the author (Massad, 1995) for

download conventional test is used. It is based on Modified Cambeft Relations (Fig. 4) and consideration is made of many aspects of load transfer phenomena, like the progressive failure, due to pile compressibility, and the residual stresses due to driving or subsequent loadings. As the piles in this paper are supposed to be cast in place and submitted to a single loading, residual stresses will be ignored.

A coefficient that measures the relative stiffness of the pile-soil (shaft) system was introduced and is defined as follows:

$$k = \frac{A_{lr}}{K_r \cdot y_1} \tag{7}$$

where  $A_{lr}$  is the ultimate shaft load;  $y_1$ , the pile displacement, of the order of a few millimeters, required to mobilize full shaft resistance. The coefficient  $k$  may be associated to the term  $(\mu h)^2$  of Randolph & Wroth (1978). The model gave a further insight on pile behavior and led to a pile classification, with respect to the  $k$  values: "short" or rigid

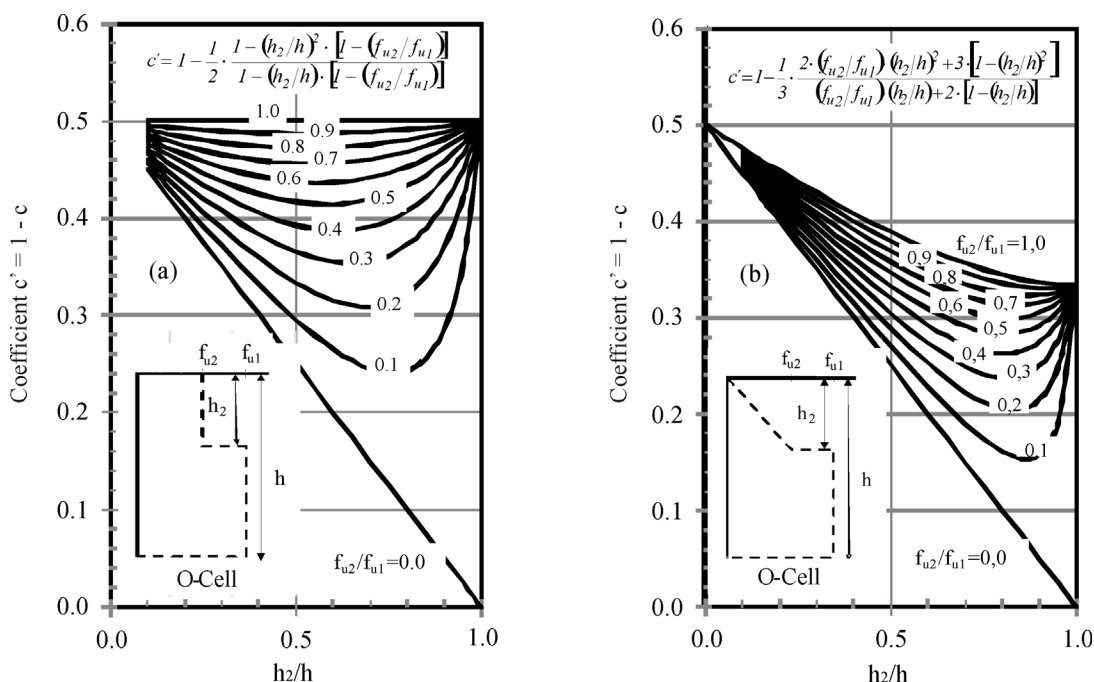


Figure 3 - Nomograms for upward loads (bidirectional test).

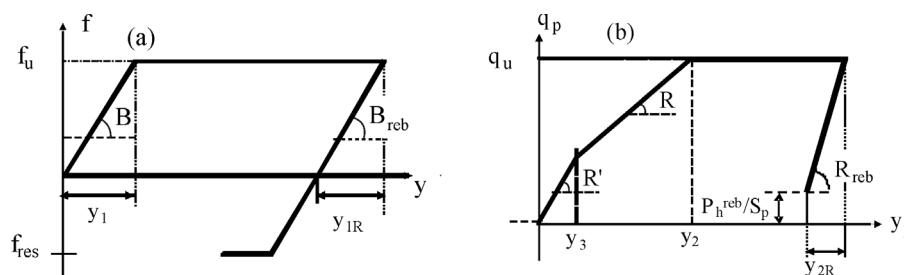


Figure 4 - Modified Cambeft Relations: a) shaft and b) toe.

( $k \leq 2$ ); intermediate ( $2 \leq k \leq 8$ ); and “long” or compressible ( $k \geq 8$ ).

### 3.2. Simulation of the Bidirectional test: invariance of the upward curves with $c' \cdot k$

To simulate the bidirectional test this model was changed to incorporate a soft upper layer ( $f_{u2}$ ) over a deep more resistant soil ( $f_{u1}$ ). For each layer along the shaft a relation as shown Fig. 4-a holds. Using subscripts 1 and 2 to distinguish them, it follows that:

$$f_{u1} \geq f_{u2} \quad \text{and} \quad A_{lr} = A_{lr1} + A_{lr2} \quad (8)$$

For both layers the value of  $y_1$  (see Fig. 4-a) was assumed to be the same, so that the  $k$  value (Eq. 7) may be associated to the whole subsoil along the pile shaft. Note that  $K_r$  in Eq. 7 refers to the pile height above the O-Cell.

Ten cases of the bidirectional tests were simulated, varying the relations  $f_{u2}/f_{u1}$  and  $h_2/h$ , as displayed on Fig. 5. For each case the soil below the O-Cell was the same, obeying the relation of Fig. 4-b, with the following parameters:

$$y_3 = y_1 \quad \text{besides} \quad \frac{R' \cdot S_p}{K_r \cdot k} = 0.80 \quad \text{and} \quad \frac{R'}{R} = 5 \quad (9)$$

where  $S_p$  is the cross sectional area of the pile toe.

Figures 6-a, 7-a and 8-a show, respectively, results for a rigid pile ( $k = 1$  and Case 5), an intermediate pile ( $k = 5$  and Case 3) and a long pile ( $k = 10$  and Case 10). Note that the loads and movements are normalized with respect to  $A_{lr}$  and  $y_1$ , respectively. The range 0-3 corresponds to the initial pseudo elastic line of Fig. 4-a, with inclination  $B$ ; the range 3-4 refers to the progressive mobilization of shaft resistance, from bottom to top, up to  $y_h = y_1$  ( $y_h$  is the pile top movement); point  $M$  corresponds to the fully mobilization of  $f_{u1}$  of the deep stiffer layer. For the unloading the analogous ranges are indicated through the points 3' and M'.

At the O-Cell level, the following relations hold for point 4:

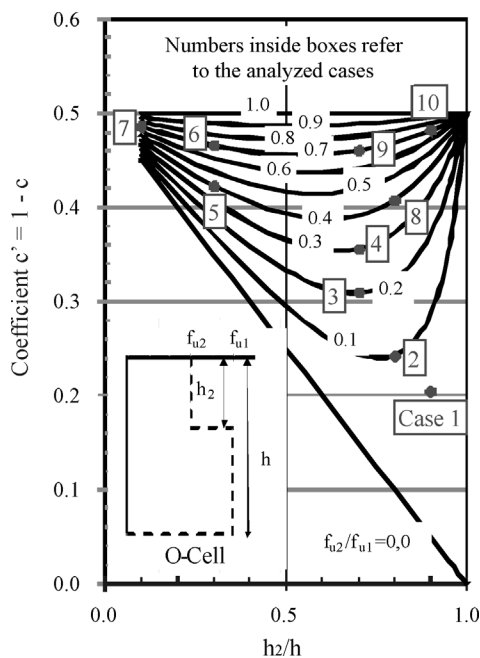


Figure 5 - Analyzed cases.

$$P_{o4} = A_{lr} \quad \text{and} \quad y_4 = y_1 + \frac{c' \cdot A_{lr}}{K_r} = y_1 \cdot (1 + c' \cdot k) \quad (10)$$

$$\text{then} \quad \frac{y_4}{y_1} = 1 + c' \cdot k$$

Eqs. 10 still holds for cases of linearly increasing maximum unit skin friction with depth: in this case,  $c' = 1/3$  (see Fig. 3-b).

The full mobilization of  $f_{u1}$  of the deep stiffer layer initiates at points 3 of Figs. 6-a, 7-a and 8-a. The following relation holds:

$$\frac{y_3}{y_1} = 1 \quad (11)$$

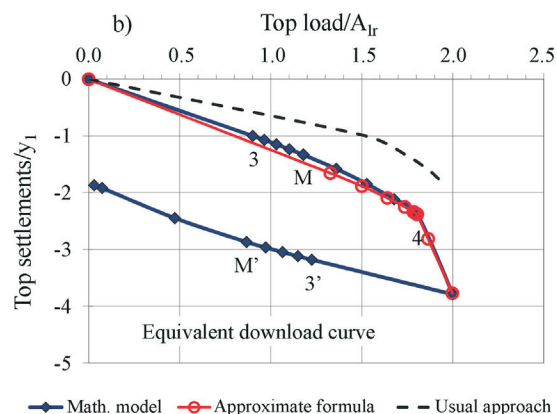
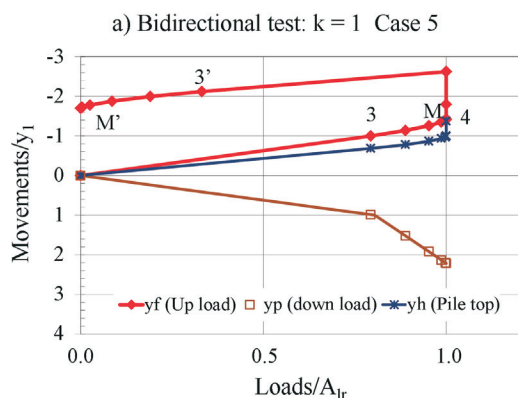


Figure 6 - Bidirectional test simulation for a rigid pile ( $k = 1$ , Case 5).

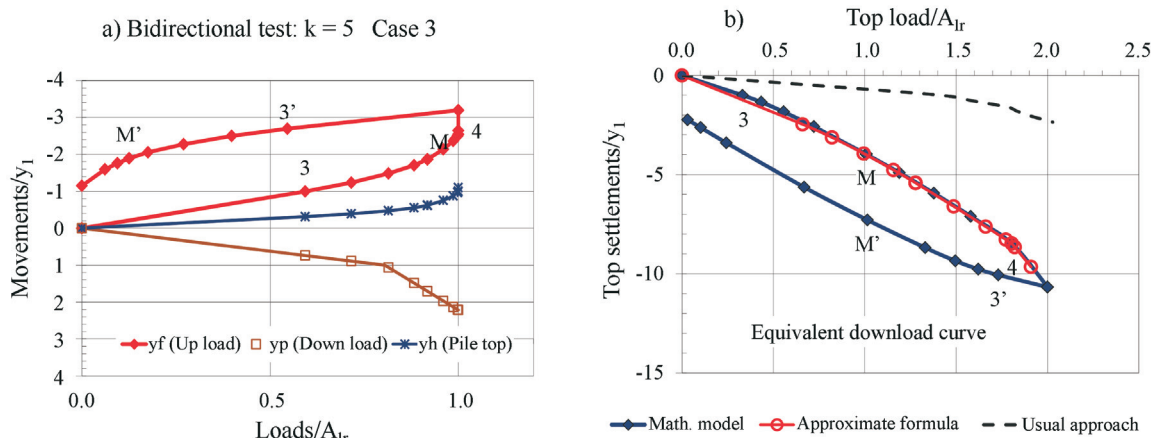


Figure 7 - Bidirectional test simulation for an intermediate pile ( $k = 5$ , Case 3).

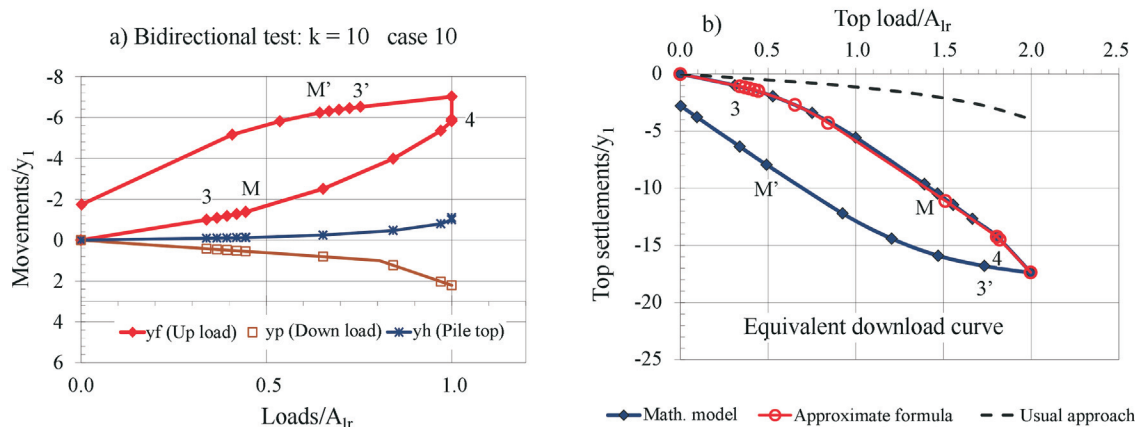


Figure 8 - Bidirectional test simulation for a long pile ( $k = 10$ , Case 10).

Moreover, the ratio  $P_{o3}/A_{lr}$  depends only on  $c'.k$ , as shown in Figs. 9 and 10. Note that the case of linearly increasing maximum unit skin friction with depth ( $c' = 1/3$ ) is included in Fig. 9.

Taking also into account the last equation of Eq. 10, it follows that the normalized upward curves of the bidirectional tests are approximately invariant with respect to  $c'.k$ , independently on the distribution of shaft resistances. This conclusion is confirmed by the plots of Figs. 11-a ( $c'.k \cong 0.5$ ), 12-a ( $c'.k \cong 2.3$ ) and 13-a ( $c'.k \cong 4.7$ ). Note that the Arabic numbers associated to the curves refer to the cases of Fig. 5. To stress this point, Fig. 14 was prepared showing different distribution of shaft resistances for cases 7 and 10 of Fig. 13, but with almost the same  $c'.k$ , i.e., 4.9 and 4.8, respectively.

The conclusion about the invariance of the normalized upward movements related to  $c'.k$  is maintained even when one compares the cases of Fig. 15, with different values of  $k$ , and also the cases of Fig. 16, whose skin friction distribution is presented in Fig. 17. Note that in the latter cases the product  $c'.k$  is close together.

In the attached Appendix more cases are presented showing that the mentioned invariance with respect to  $c'.k$  still holds, even for other transfer function besides the Cambofort Relation for the shaft friction.

It is worth mentioning that the movement at pile top ( $y_h$ ) reaches the value  $y_h = y_1$  at shaft failure load ( $A_l = A_{lr}$ ), as can be seen in Figs. 6-a, 7-a and 8-a. Moreover, taking into account Eqs. 5 and 7, it follows:

$$c'.k = c' \cdot \frac{A_{lr}}{K_r \cdot y_1} = \frac{\Delta e_{\max}^s}{y_1} \tag{12}$$

that is, the ratio between the maximum elastic shortening of the pile shaft and the value of  $y_1$  governs the upward curve of a bidirectional test.

#### 4. Mathematical Simulation of the Equivalent Curve of the Conventional Test

The same mathematical model was also applied to simulate an equivalent download conventional test. Figs. 6-b, 7-b and 8-b show the equivalent curves for the cases of a rigid pile ( $k = 1$ ), an intermediate pile ( $k = 5$ ) and a

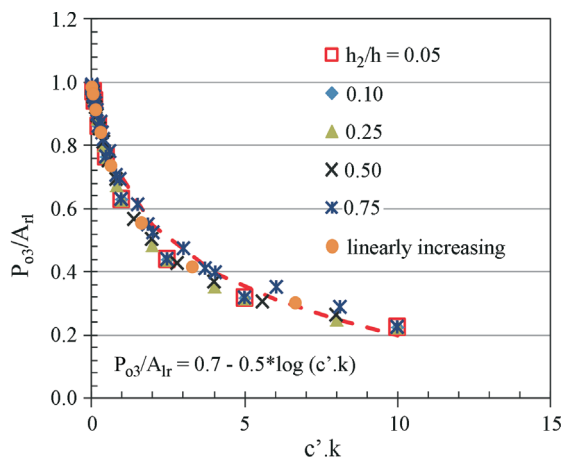


Figure 9 -  $P_{o3}/A_{lr}$  versus  $c'.k$  for  $h_2/h \leq 0.75$ .

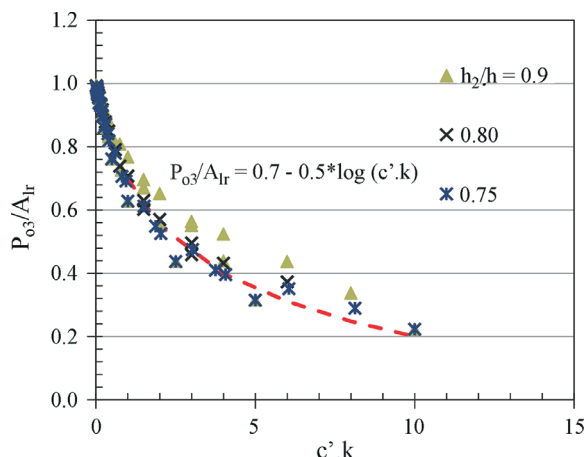


Figure 10 -  $P_{o3}/A_{lr}$  versus  $c'.k$  for  $h_2/h \geq 0.75$ .

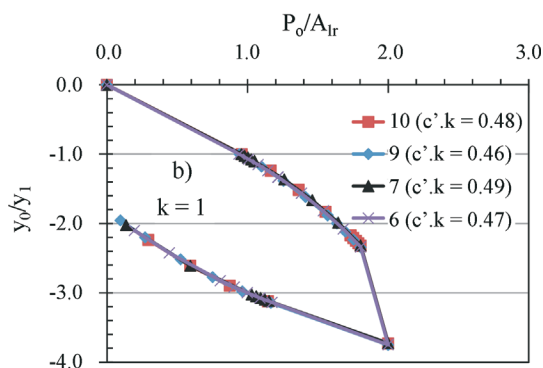
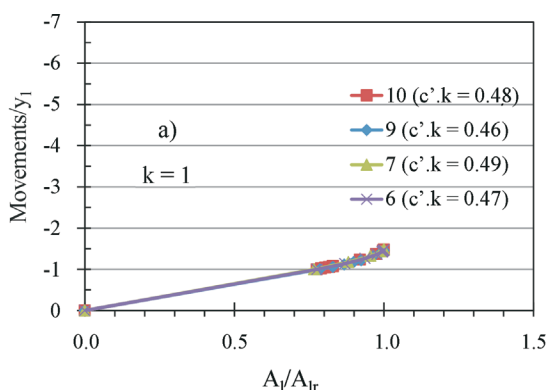


Figure 11 - Bidirectional test simulations on short piles. Arabic numbers refer to the cases of Fig. 5.

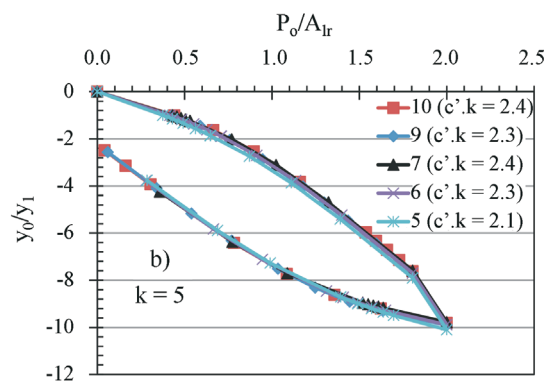
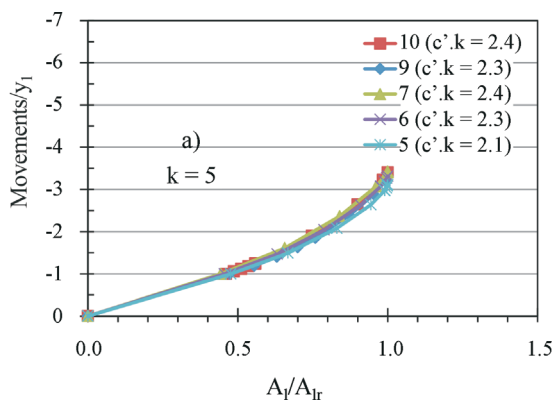


Figure 12 - Bidirectional test simulation for intermediate piles. Arabic numbers refer to the cases of Fig. 5.

long pile ( $k = 10$ ), respectively. The notable points 3, M and 4 (for loading) and 3' and M' (for unloading) are indicated in these plots. They have the same meaning as in the bidirectional tests, but with the progressive mobilization of shaft resistance going from top to bottom.

For point 4, the following relationships hold:

$$y_4 = y_1 + \frac{c \cdot A_{lr}}{K_r} + \frac{R' \cdot S_p}{K_r} \cdot y_1 \tag{13}$$

then  $\frac{y_4}{y_1} = 1 + c \cdot k + \frac{R' \cdot S_p}{K_r}$

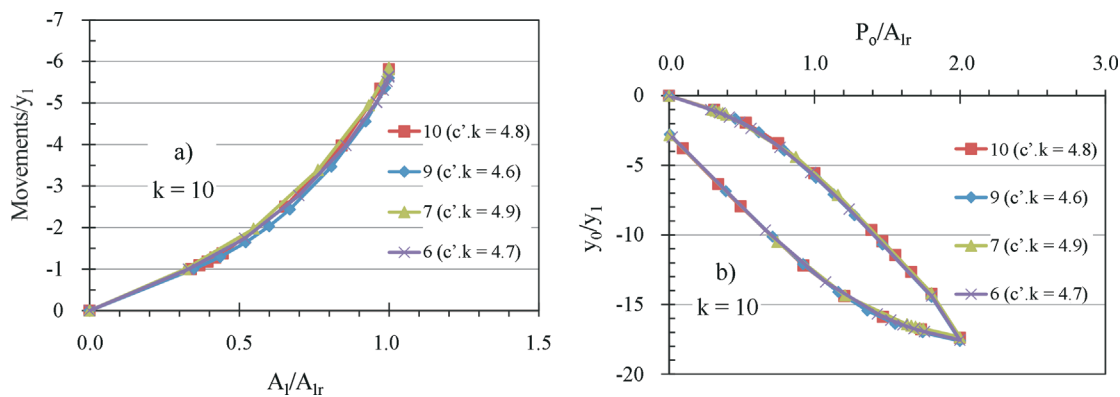


Figure 13 - Bidirectional test simulations for long piles. Arabic numbers refer to the cases of Fig. 5.

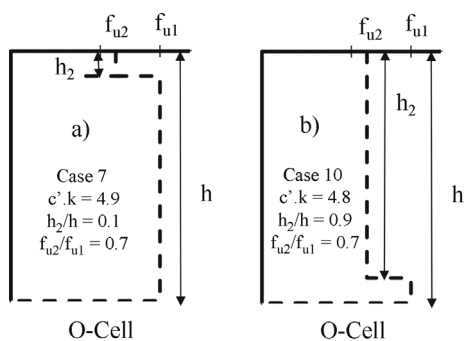


Figure 14 - Distribution of unit skin friction with depth: a) case 7 and b) case 10 of Fig. 13-a.

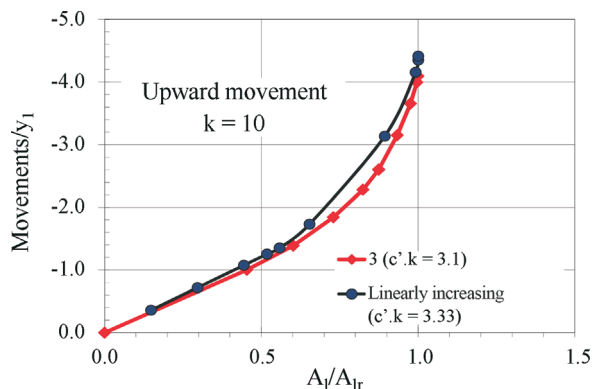


Figure 16 - Bidirectional tests with different skin friction distribution (see Fig. 17).

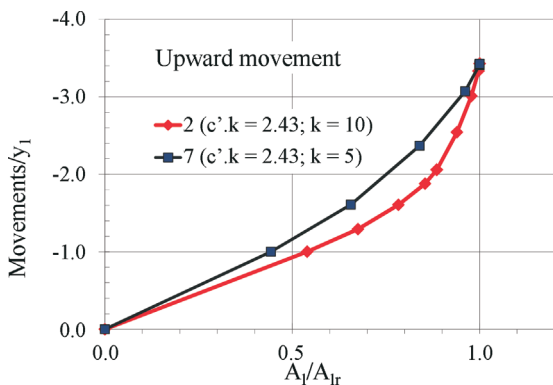


Figure 15 - Bidirectional tests with different values of  $k$ , but with the same product  $c \cdot k$ .

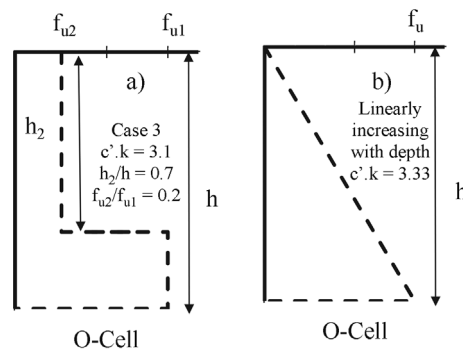


Figure 17 - Distribution of unit skin friction with depth of cases of Fig. 16.

$$P_{o4} = A_{lr} + R' \cdot S_p \cdot y_1$$

$$\text{then } \frac{P_{o4}}{A_{lr}} = 1 + \frac{R' \cdot S_p}{K_r \cdot k} \quad (14)$$

From Eqs. 13 and 14 it follows that if  $k$  and  $c$  are constants, then  $c \cdot k$  is also a constant and the coordinates of point 4 coincide, regardless the values of  $f_{u2}/f_{u1}$  and  $h_2/h$  associated to  $c$  or to  $c' = 1 - c$  (Eq. 6). Additionally, as the soil

below the O-Cell was supposed to be the same (Eqs. 9), the downward curves of the conventional tests are invariant with  $c \cdot k$ , as shown in the plots of Figs. 11-b, 12-b and 13-b, taken separately.

Finally, as  $P_{o4}$  is a function of  $k$  (Eq. 14), different values of  $k$  lead to distinct curves  $P_o - y_o$ . This fact can be confirmed by comparing together Figs. 11-b, 12-b and 13-b.

### 5. Approximate Formulas to Determine the Equivalent Curve of the Conventional Test

To derive approximate formulas for the equivalent curve, considerations will be made using Fig. 18, supposing that the upward movement was measured at the top of the O-Cell and the load reached  $A_{lr}$ . Let  $P$  be a point of the upward curve with the coordinates  $y_f$  and  $A_l$ .

Next, the elastic shortening of the shaft and  $y'_p$ , an approximate measure of the pile head displacement, are computed as follows:

$$\Delta e = \frac{c' \cdot A_l}{K_r} \tag{15}$$

$$y'_p = y'_f - \Delta e \geq 0 \tag{16}$$

Equation 16 is an approximate value of  $y'_p$  because  $c$  and  $c'$  depend on the amount of shaft friction mobilized during the loading. In a similar problem involving unloading in a conventional test, Massad (2001) showed that, for practical purposes,  $c$  may be approximated to the value corresponding to the maximum unit skin friction. It will be validated later on.

To simulate the download conventional test,  $y'_p$  is settled as the toe movement; it is associated to  $Q'_p$ , as indicated in Fig. 18.

Finally, a pair  $y_o - P_o$  of the equivalent curve is determined by the equations:

$$y_o = y'_p + \Delta e \cdot \frac{c}{c'} + \frac{Q'_p}{K_r} \tag{17}$$

$$P_o = A_l + Q'_p \tag{18}$$

A first validation of Eqs. 17 and 18 is shown in Figs. 6-b, 7-b and 8-b: the curves of the approximate formulas and the mathematical model are in excellent agreement.

The usual procedure to construct the equivalent curve, also shown in Figs. 6-b, 7-b and 8-b, consists in adding the cell loads ( $A_l + Q'_p$ ) for equal measured movements up and down; no consideration is made to the correction of the measured movements due to elastic shortening of the pile.

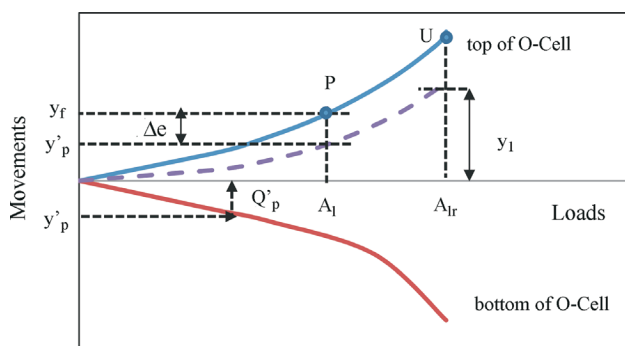


**Figure 18** - Schematic curves of a bidirectional test-upward movements measured at the top of the O-Cell.

The differences are greater for long piles as compared to short piles. As a matter of fact, for very rigid or very short piles,  $K_r$  is very large and both,  $\Delta e$  and  $Q'_p/K_r$  approach to zero and Eqs. 17 and 18 reduce to  $y_o = y'_p = y_f$  and  $P_o = A_l + Q'_p$ ; the usual procedure is valid.

If the movement of the pile head is available, instead of that of the top of the O-Cell, the procedure is analogous, as displayed in Fig. 19. And finally, if the movements at the pile head and on top of O-Cell are available, the measured  $\Delta e$  is used instead the value of Eq. (15).

It is worth highlighting that cases like those of Figs. 14 and 17 conduct to the same values of  $c$  and  $c'$ . In fact, for the pair  $h_z/h = 0.1$  and  $f_{uz}/f_{ul} = 0.7$  (Case 7 Fig. 14-a) it follows from Fig. 3-a  $c' = 0.49$  than  $c = 0.51$ , and for  $h_z/h = 0.9$  and  $f_{uz}/f_{ul} = 0.7$  (Case 10 Fig. 14-b),  $c' = 0.48$  than  $c = 0.52$ . The same conclusion arises from Fig. 17: for Case 3  $c' = 0.31$  than  $c = 0.69$  (see Fig. 3-a), very close to  $c' = 0.33$  and  $c = 0.67$  for the case of linearly increasing shaft resistance with depth (see Fig. 3-b). The conclusion is that different distribution of shaft resistance may lead to the same elastic shortening and so the same equivalent curve: the key factor is the elastic shortening of the shaft.

### 6. Practical Applications

Applications will be made to five case histories, comprising short to long piles, with heights and diameters varying from 11.5 to 41.0 m and 0.60 to 2.40 m, respectively. In one place a conventional compressive test was also available (see Table 1).

#### 6.1. Continuous Flight Auger (CFA) piles in Belo Horizonte (Brazil)

Two CFA piles E 46 and E 46A, 0.60 m in diameter, were installed in Belo Horizonte, Brazil, 2.5 m apart. One of them was submitted to a conventional loading test and the other to a bidirectional test as shown in Table 1. The subsoil consisted of 1.8 m earth fill, on top of soft silty clay and clayey silt layers (SPT = 3 to 5), up to 10 m depth, and below a sandy silt residual soil (SPT = 17 to 30). The water table was at 8 m depth.

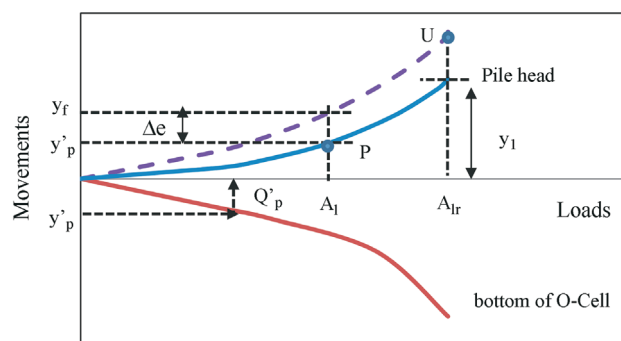


**Figure 19** - Schematic curves of a bidirectional test-upward movements measured at the pile head.

**Table 1** - Case Histories -general information of the piles.

Type of test	Pile	Diameter (m)	Height (m)	Place	Source
Conventional	CFA (E-46)	0.60	16.0	Belo Horizonte (BR)	Alonso & Silva (2000)
Bidirectional	CFA (E-46A)	0.60	14.0 + 1.5 = 15.5		
Bidirectional	Omega (PC-02)	0.70	8.5 + 3.0 = 11.5	São Paulo (BR)	Fellenius (2014-a)
Bidirectional	Omega (PC-07)	0.70	7.2 + 4.3 = 11.5		
Bidirectional	Bored (1)	0.90	16.0	Puerto Rico (USA)	Fellenius (2015)
Bidirectional	Bored (2)	1.25	40.0	Mississippi River (USA)	Fellenius (2014-b)
Bidirectional	Bored (3)	2.40	41.0	Tucson Arizona (USA)	Loadtest (2014)

Figure 20 presents the results the bidirectional test on E 46A pile, performed by Arcos. The O-Cell was placed at 14.0 m depth and the upward and downward movements were measured at pile head and at the base of the O-Cell, respectively.

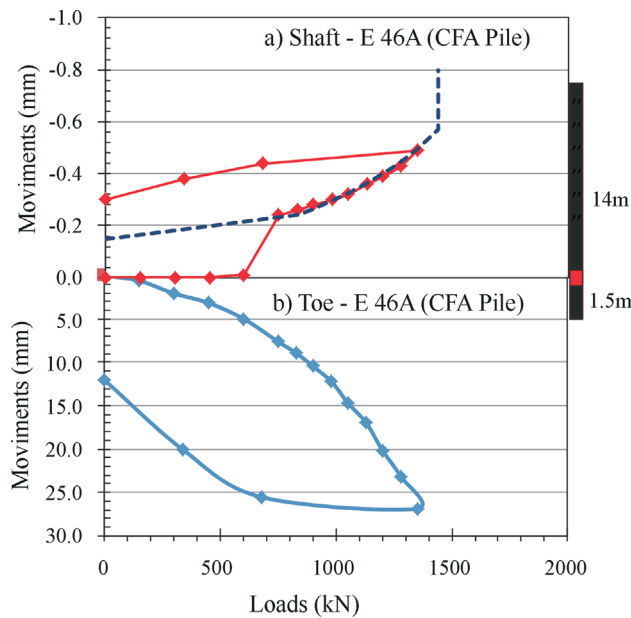


**Figure 20** - Bidirectional test on a CFA pile in Belo Horizonte.

Table 2 shows other relevant data. The value of  $c$  was estimated using SPT data and the Décourt-Quaresma Method (1978) to determine the  $f_u$  and the load distribution along depth, like shown in Fig. 1-b.

For the conventional loading test on Pile E 46, presented in Fig. 21, the Two Lines Method (Massad & Lazo, 1998 and Fonseca *et al.*, 2007) was applied leading to an ultimate side friction ( $A_{fr}$ ) of 1,900 kN,  $y_1$  equals to 0.35 mm and a toe stiffness of 3,000 kN/mm; some strain hardening was observed at the toe, probably due to the compression of a partially remolded soil, an outcome of pile installation.

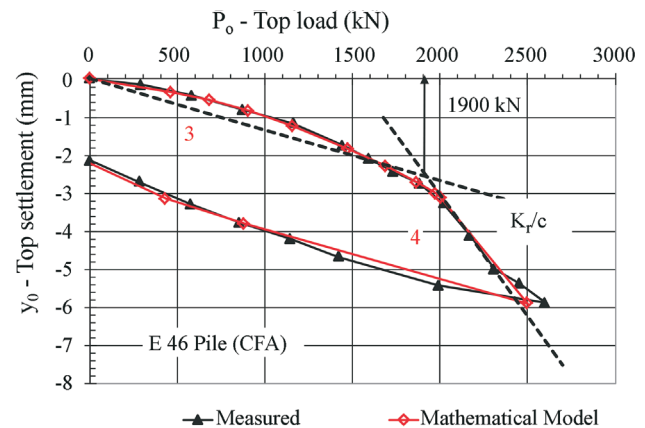


**Figure 21** - Conventional test on a CFA Pile in Belo Horizonte.

**Table 2** - Results of the analysis.

Type of test	Pile	$K_r$ (kN/mm)	$c$	$c'$	$k$	$c'.k$	Pile behavior
Conventional	CFA (E-46)	442	0.59	0.41	12.3	5.0	Long or Compressible
Bidirectional	CFA (E-46A)	505	0.57	0.43	7.6	3.3	Long or Compressible
Bidirectional	Omega (PC-02)	906	0.58	0.42	0.2	0.1	Short or rigid
Bidirectional	Omega (PC-07)	1069	0.58	0.42	0.2	0.1	Short or rigid
Bidirectional	Bored (Puerto Rico)	795	0.50	0.50	1.6	0.8	Short or rigid
Bidirectional	Bored (Mississippi)	614	var.	var.	0.9	var.	Short or rigid
Bidirectional	Bored (Tucson)	4414	0.80	0.20	4.4	0.9	Intermediate

Legend: see appended list of symbols.

The toe did not reach failure. These values were confirmed by applying the Mathematical Model based on Cambeftor Relations: the fitting between the measured and calculated curves is remarkable. The pile behaved as a long pile, with  $k \sim 8$  (Table 2). It is worth pointing out that Décourt-Quaresma Method (1978) led to  $A_{fr} = 1,860$  kN.

As far as the Pile E 46A is concerned, submitted to the bidirectional test, the maximum side friction ( $A_{fr}$ ) up to 14 m was estimated to be 1,440 kN by the Décourt-Quaresma Method (1978), above the maximum upward load of 1,350 kN (see Fig. 20-a). Adjustments were made in the upward curve, as displayed in Fig. 20-a, eliminating the “jump” in the beginning and extrapolating at the end assuming a failure load of 1,440 kN. Table 3 was prepared using Eqs. 17 and 18 that led to the equivalent curve for the E 46A pile, as shown in Fig. 22. The segment of pile below 14 m, with a length of 1.5 m, was taken as a fictitious toe, with a transfer function given by Fig. 20-b. It includes the real toe and the side friction of the 1.5 m pile segment.

Next the same Mathematical Model (Cambeftor) was applied to the bidirectional test on E 46A pile, using the ultimate side friction ( $A_{fr}$ ) of 1,440 kN,  $y_1$  equals to 0.35 mm and toe stiffness of 150 kN/mm, this last figure gotten from the initial part of the “downward” curve (Fig. 20-b). The result is also shown in Fig. 22 together with the measured curve of the conventional test (Pile E 46). Again, the fitting is remarkable amongst the three curves up to the full mobilization of the shaft resistance in Pile E 46A. This is a second validation of the approximate formulas, Eqs. 17 and 18. Figure 22 shows moreover that the fictitious toe resistance of Pile E 46A, given by Fig. 20-b, is much smaller than the toe resistance of Pile E 46, submitted to the conventional

**Table 3** - Application of the approximate formulae to E 46A CFA pile.

$y'_p$ (mm)	$Q_p$ (kN)	$A_{fr}$ (kN)	$P_o$ (kN)	$y_o$ (mm)
0.00	0	0	0	0.00
0.09	50	836	886	1.13
0.11	55	892	947	1.23
0.13	65	945	1010	1.33
0.15	70	995	1065	1.41
0.17	75	1042	1117	1.50
0.21	80	1128	1208	1.64
0.24	93	1185	1278	1.76
0.28	96	1255	1351	1.89
0.34	100	1345	1445	2.06
0.42	140	1442	1582	2.33
0.85	200	1442	1642	2.88
3.85	500	1442	1942	6.47

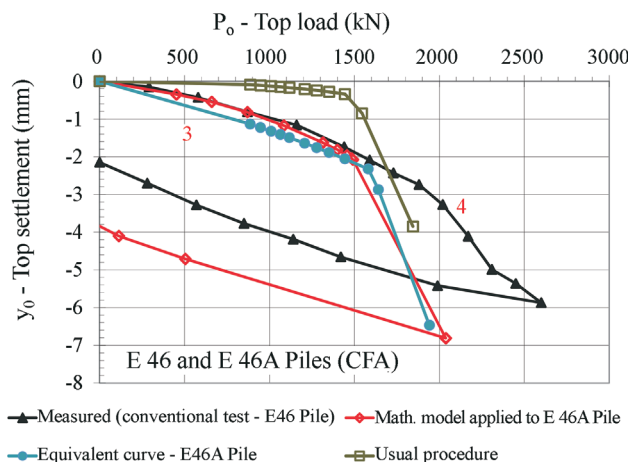


**Figure 22** - Comparison of the download curves - CFA Piles in Belo Horizonte.

test, due to an unknown reason. This fact is supported by the result presented in Fig. 20-b. Finally, the application of the usual procedure as defined above led to unrealistic values of settlements.

### 6.2. Omega piles in São Paulo City (Brazil)

Fellenius (2014-a) presented the results (see Fig. 23) of bidirectional tests performed by Arcos at a site in São Paulo, Brazil, on two Omega Piles both with diameter 700 mm and embedment 11.5 m (see Table 1). Pile PC-02 was provided with a bidirectional cell at 8.5 m depth and Pile PC-07 at 7.2 m depth. The upward and downward movements were measured at pile head and at the base of the O-Cell, respectively. These and other information are presented in Table 2. The subsoil consisted of 2.5 m earth fill on top of layers of silty clay and sandy silt, SPT varying erratically from 5 to 15, and a very dense silty sand below 9 m depth. The water table was at 2 m depth. The value of  $c' = 0.42$  was estimated using SPT data and the Décourt-Quaresma Method (1978) to determine the  $f_u$  and the load distribution along depth.

The use of Eqs. 17 and 18 led to the results shown in Fig. 24. The agreement with the curves obtained by Fellenius with a software algorithm (UniPile) is remarkable. This is a third validation of the approximate formulas, Eqs. 17 and 18. Note that it was assumed fictitious toes below the O-Cells. As the pile is short or rigid, the usual procedure gave reasonable results.

### 6.3. Bored pile in Puerto Rico

Results of a bidirectional test on a 900 mm diameter bored pile, 16 m height (see Table I), are shown in Fig. 25. The pile was drilled in clayey saprolite and socketed a short distance into weathered bedrock. The O-Cell was placed near the pile toe and the movements were taken at its base and top. The head down equivalent curves, obtained by Fellenius (2015) and with the application of Eqs. 17 and 18,

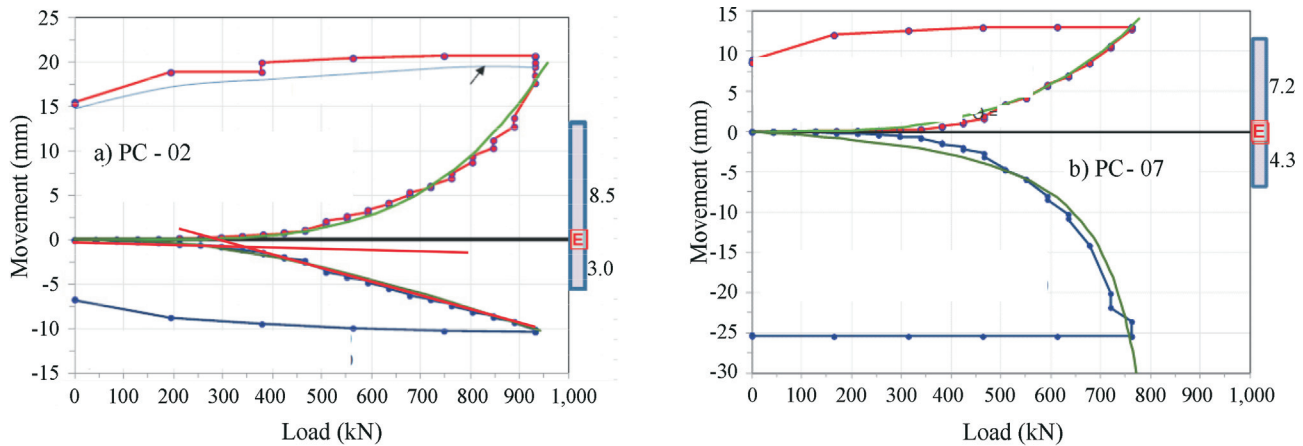


Figure 23 - Bidirectional tests on omega piles in São Paulo. Adapted from Fellenius (2014-a).

are again in quite a good agreement. This is a fourth validation of the approximate formulas. A value of  $E = 20$  GPa was assumed for the pile and  $c'$  was taken equals to 0.5 (Table 2).

#### 6.4. Bored pile US82 Bridge across Mississippi River (USA)

A bidirectional test on a 1.25 m diameter 40 m deep bored pile (see Table 1) was performed at US82 Bridge across Mississippi River installed into dense sand. The O-Cell was placed near the pile toe and the movements were taken at its base and top. The results are shown in Fig. 26. Figure 27 displays the equivalent head-down curve for 3 hypotheses with respect to the parameter  $c'$ . Also shown is the curve obtained by the usual procedure. The differences are relatively small, because the pile behaved like a rigid or short pile: the value of  $y_1$  was large and  $k$  assumed a value close to 1 (see Table 2).

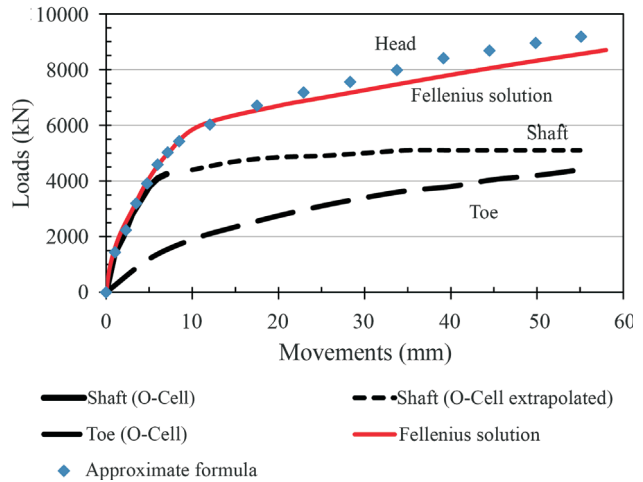


Figure 25 - Bidirectional test - Bored pile of Puerto Rico.

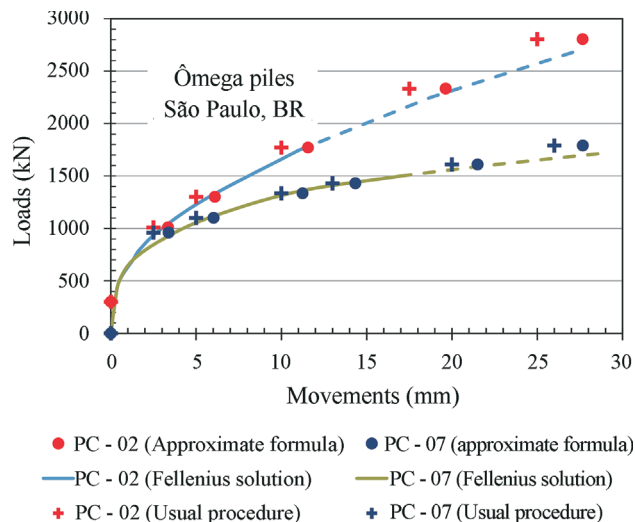


Figure 24 - Equivalent curves for Piles PC-02 and PC-07.

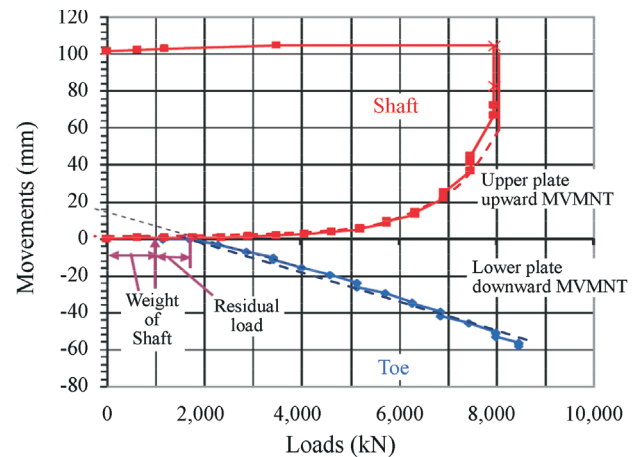


Figure 26 - Bidirectional Test: Bored pile US82 Bridge-Mississippi River (From Fellenius, 2014-b).

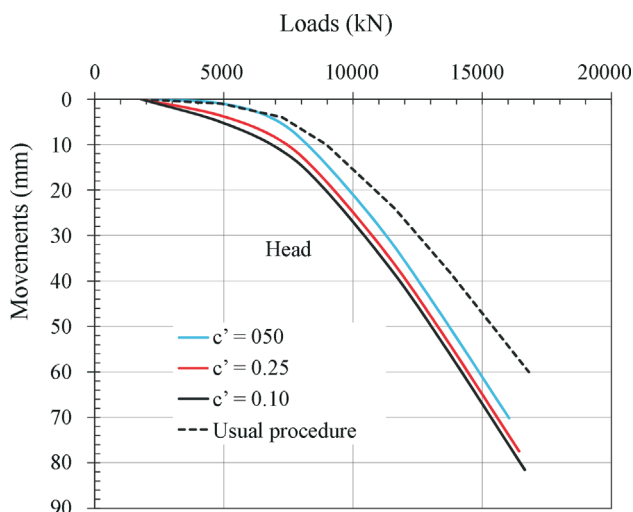


Figure 27 - Equivalent head-down test: Bored pile US82 Bridge across Mississippi River.

### 6.5. Bored pile - Tucson, Arizona (USA)

A bidirectional test was carried out in an instrumented bored pile, 2.4 m diameter and 41 m deep in Tucson, Arizona (USA) (See Tables 1 and 2). The O-Cell was placed near the pile toe and the movements were taken at its base and at pile head. Figure 28 shows the results. Based on the distribution of shear stresses given by the strain gages it was possible to estimate  $c' = 0.20$ . The value of  $y_1$  was assumed to be 3.8 mm,  $y_3 = y_1$ ,  $R^*S_f/(K_r.k) = 0.56$  and  $R^*/R = 10$ .

The application of the Mathematical Model led to a good agreement with the measured up and downward load-movement curves (Figs. 28-a and b).

A good fitting (Fig. 29) was also obtained amongst the three equivalent curves: a) one computed with the Mathematical Model; b) the other with the approximate formulas (Eqs. 17 and 18), being this its fifth validation, and c) the curve referred by Loadtest Procedure (2001), mentioned before and shown in Loadtest (2014). The same

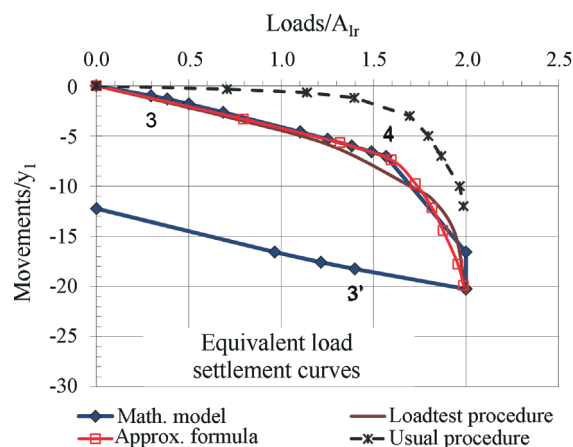
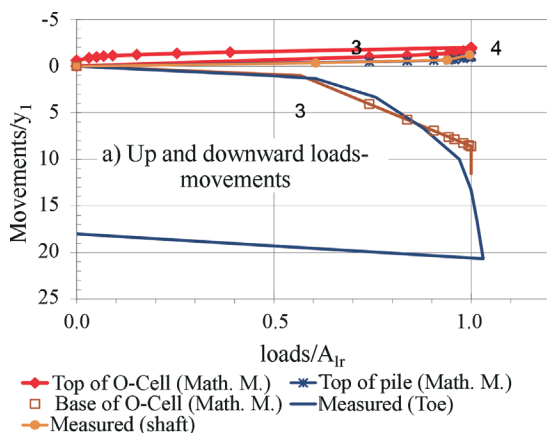


Figure 29 - Head-down test: Bored Pile- Tucson (AZ).

cannot be said about the usual procedure: the  $k$  value was relatively large, of the order of 4.4 (Table 2). Moreover, it is noticeable that: a)  $c'.k \cong 0.9$  and  $P_{os}/A_{lr} \cong 0.74$ , in agreement with the data of Fig. 9; b)  $y_{os}/y_1 \cong 1.9$ , in accordance with Eq. 10; and c)  $y_h = y_1$ , as mentioned before.

### 7. Conclusions

The elastic compression of piles under O-Cell upward loads is generally smaller than the corresponding value for the download test or conventional loading test. Its estimation may be done using de coefficient  $c' = 1 - c$ , where  $c$  is the Leonards-Lovell Coefficient for axial compressive loading applied at the pile head. Nomograms of  $c'$  were presented for two patterns of shaft resistance distribution. The value of  $c'$  may be estimated through the shaft resistance prediction by means of empirical methods based on SPT data. A reasonable estimation of the pile elasticity modulus ( $E$ ) and its stiffness  $K_r$  is also needed. Both parameter  $c'$  and  $K_r$  can be better determined by means of instrumentation.

The simulation of the bidirectional test using a mathematical model showed that the coefficient  $c'$  plays an important role. The normalized upward curve is invariant

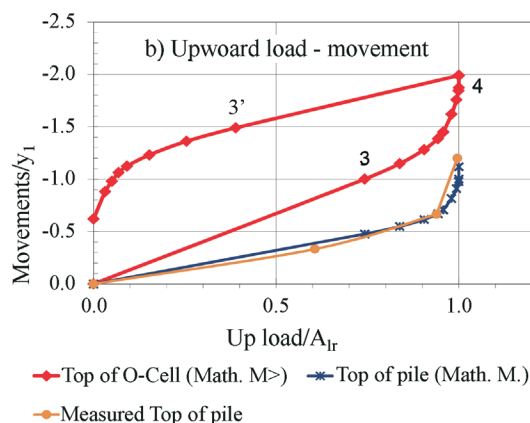


Figure 28 - Bidirectional test, Bored Pile - Tucson, Arizona.

when the product  $c'.k$  is constant, regardless may be the shaft resistance distribution and the separate value of  $k$ , the relative pile-soil (shaft) stiffness.

Approximate formulas to determine the equivalent curve were proposed, correcting the shaft elastic shortening induced by the upward loads in the bidirectional test. The measured or estimated displacement at pile top ( $y'_p$ ) in the bidirectional test is set as the toe movement in the down-load conventional test. The load ( $Q'_p$ ) at the base of the O-Cell associated to  $y'_p$  is taken as the toe load. The shaft elastic shortening, measured or estimated in the bidirectional test, is corrected by the factor  $c/c'$  and added to the pile compression due to  $Q'_p$  and to  $y'_p$  to get the pile head movement of the equivalent curve. The head load is obtained adding the O-Cell shaft load ( $A_l$ ) to the O-Cell base load ( $Q'_p$ ), both values associated do  $y'_p$ . Application was made to five case histories, revealing the potentiality and easiness of the proposed procedure. It is shown that, when the pile is very rigid, the usual procedure gives good results, but, for compressible piles, the differences are relevant.

**Appendix**

The conclusion about the invariance with the term  $c'.k$  still holds even when one compares the cases of Fig. A-1, with different transfer functions, namely, Ratio Function (RF) and Cambefort (C) Relation, as displayed in Fig. A-2, and different resistance distribution along depth (Fig. A-3). In this figure RR and TR mean, respectively, rectangular-rectangular and triangular-rectangular shapes. The Ratio Function has been used by Fellenius (2014-a) to analyze the results of bidirectional tests and its general form is included in Fig. A-2.

Note that:

- a) while the Mathematical Model presented in this paper was applied to the cases related to the Cambefort Relation, the Coyle-Reese (1966) Method was used to deal with the Ratio Function; and

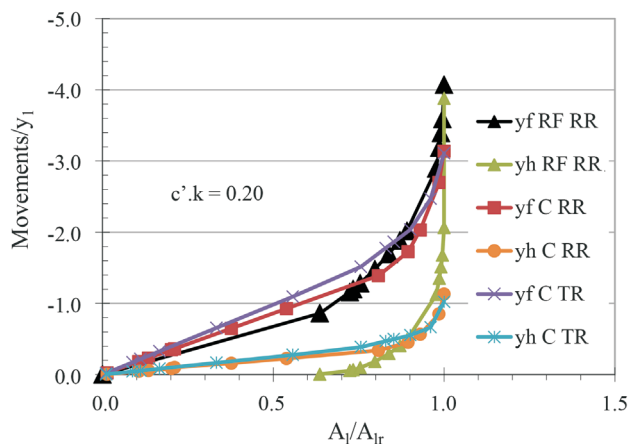


Figure A1 - Bidirectional tests for

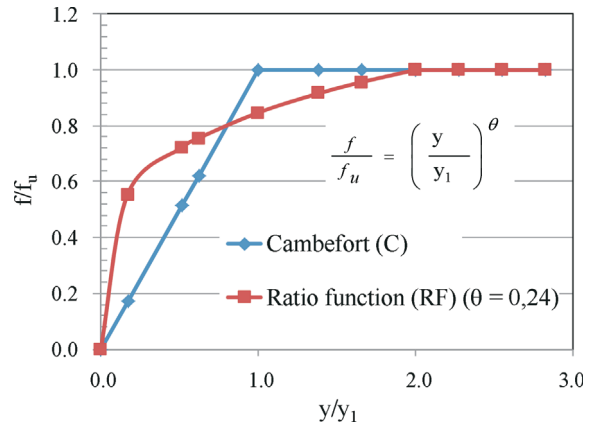


Figure A2 - Transfer functions.

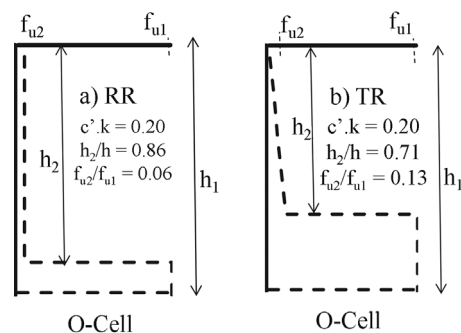


Figure A3 - Distribution of unit skin friction with depth of cases of Fig. A-1.

- b) the value of  $k$  associated to the Ratio Function cases was taken as:

$$k = \frac{A_{lr}}{K_r \cdot (y_1 / 2)} \tag{A-1}$$

in substitution of Eq. 7. The invariance of the upward curves at the top of the O-Cell ( $y_j$  of fig. A1) is remarkable.

**Acknowledgments**

The author acknowledges the support given by EPUSP - Escola Polit cnica of S o Paulo University.

**References**

Alonso, U. & Silva, P.E.C.A.F. (2000). Equivalent curve of a continuous flight auger pile submitted to a test with the hydrodynamic expansive cell (EXPANCELL). 4th Seminar on Special Foundations Engineering and Geotechnics, v. 1, p. 416-425, S o Paulo (In Portuguese).  
 Coyle, H.M. & Reese, L.C. (1966). Load transfer for axially loaded piles in clay. Journal of Soil Mechanics and Foundation Division. Proc. of the ASCE, v. 92:2, p.1-26, March.  
 D cort, L. & Quaresma, A.R. (1978). Load capacity of piles from SPT. In: Proc. VI Brazilian Conference on

- Soil Mechanics and Foundation Engineering, Rio de Janeiro, ABMS, p. 45-53 (In Portuguese).
- Fellenius, B.F. (1980). The analysis of results from routine pile load tests. *Ground Engineering*, v. 13, September, p. 19-31.
- Fellenius, B.F. (2014-a). Analysis of results from routines static loading tests with emphasis on the bidirectional test. XVII Brazilian Conference on Soil Mechanics and Geotechnical Engineering, Goiânia, Brasil.
- Fellenius, B.F. (2014-b). Basic of design of piled foundations: the static loading test - Performance, instrumentation and interpretation. Lecture given on September 8, 2014, in Belo Horizonte, Brazil.
- Fellenius, B.F. (2015). The red book basic foundation design. Eletronic edition, Jan/2014 (<http://www.fellenius.net/papers.html>).
- Fonseca, A.V.; Santos, J.A.; Esteves, E.C. & Massad, F. (2007). Analysis of piles in residual soil from granite considering residual loads. *Soils and Rocks*, v. 30, p.63 - 80.
- Kim, S.R. & Chung, S.G. (2012); Equivalent head-down load vs. movement relationships evaluated from bidirectional pile load tests. *Journal of Civil Engineering of KSCE* 16(7):1170-1177.
- Kwon, O.S.; Choi, Y.K.; Kwon, O.K. & Kim, M.M. (2005). "Comparison of the bidirectional load test with the top-down load test." *Transportation Research Record*. 1936, Transportation Research Board, Washington, D.C., pp. 108-116.
- Leonards, G.A. & Lovell, D. (1979). Interpretation of load tests in high capacity driven piles. Behavior of deep foundations, ASTM STP 670, Raymond Lundgren, Ed., ASTM, p. 388-415.
- Loadtest (2001). Construction of the equivalent top-loaded load settlement curve from the results of an O-cell test, Loadtest Appendix to Reports.
- Loadtest (2014). Retrieved on January, 04th, 2014, from [www.loadtest.com](http://www.loadtest.com).
- Massad, F. (1995). Pile analysis taking into account soil rigidity and residual stresses. X Pan-American Conference on Soil Mechanics and Foundation Engineering, México, v. 2. p: 1199-1210.
- Massad, F. & Lazo G. (1998). Graphical method for the interpretation of the load-settlement curve from vertical load tests on rigid and short piles. XI Brazilian Conference on Soil Mechanics and Geotechnical Engineering. v. 3, p. 1407-1414, Brasília, Brazil (In Portuguese).
- Massad, F. (2001). On the use of the elastic rebound to predict pile capacity. In: 15th International Conference of Soil Mechanics and Geotechnical Engineering, 2001, Istanbul. London: Balkema, v. 2: 1100-1104.
- Osterberg, J. (1989). New load cell testing device. *Proceedings - 14th Annual Conference* p. 17-28. Deep Foundations Institute.
- Randolph, M.F., & Wroth, C.P. (1978). Analysis of deformation of vertically loaded piles. *Journal of the Geotechnical Engineering Division*, v. 10:12, p.: 1465-1488, December.
- Silva, P.E.C.A.F. (1983). Hydrodynamic expansive cell. A new way to perform loading tests. Independent publisher, Belo Horizonte, Minas Gerais State, Brazil, 106 p. (In Portuguese).
- Silva, P.E.C.A.F. (1986). Hydrodynamic expansive cell. A new way to perform loading tests.. VIII Brazilian Conference on Soil Mechanics and Foundation Engineering, p. 223-241. Porto Alegre (In Portuguese).

## List of Symbols

- $A_l$ : Total lateral (shaft) load  
 $A_{lr}$ : Total lateral (shaft) load at failure  
 $B$ ;  $B_{reb}$ : Cambefort Parameters (see Fig. 4-a)  
 $c$ : Leonards & Lovell Coefficient (see Eq. 4)  
 $c'$ : Correlate of  $c$  for bidirectional tests  
 $D$ : Diameter of solid pile  
 $E$ : Modulus of elasticity of the pile  
 $f$ : Unit skin friction  
 $f_u$ : Maximum (ultimate) unit skin friction  
 $f_{u1}$ ;  $f_{u2}$ :  $f_u$  of layers 1 and 2  
 $f_u$ : Residual unit skin friction  
 $h$ : Pile length embedded in soil  
 $h_1$ ;  $h_2$ : Thickness of the layers of the subsoil  
 $k$ : Relative stiffness of the pile-soil (shaft)  
 $K_p$ : Pile stiffness, as a structural piece  
 $P_h$ : Residual toe load  
 $P_h^{reb}$ : Residual toe load at the end of rebound  
 $P_o$ : Vertical load at the pile head  
 $P_{o3}$ :  $P_o$  associated to the initial shaft friction mobilization  
 $P_{o4}$ :  $P_o$  associated to the full shaft friction mobilization  
 $P_o^{max}$ : Maximum value of  $P_o$   
 $q_p$ : Toe pressure  
 $q_u$ : Ultimate toe pressure  
 $Q_p$ : Toe load  
 $Q_{pmax}$ : Maximum value of  $Q_p$   
 $R$ ;  $R'$ ;  $R_{reb}$ : Soil stiffness at the pile toe (see Fig. 4-b)  
 $S$ : Cross sectional area of the pile shaft  
 $S_p$ : Cross sectional area of the pile toe  
 $SPT$ : Standard Penetration Test blow count  
 $y$ : Pile movement  
 $y_o$ ;  $y_p$ : Movements of the pile at head and bottom  
 $y_h$ ;  $y'_p$ : Movements of the pile top (Bidirectional test)  
 $y_r$ : Upward movement at the top of O-Cell  
 $y_1$ ;  $y_{1R}$ : See Figs. 4-a  
 $y_3$ ;  $y_2$ ;  $y_{2R}$ : See Figs. 4-b  
 $z$ : Square root of  $k$   
 $\Delta e$ : Elastic pile shortening  
 $\Delta e_{max}^s$ : Maximum elastic shortening of the pile shaft  
 $\rho$ : Elastic rebound measured at the pile head  
 $\theta$ : See Fig. A-2 of the Appendix

## ***Technical Notes***

***Soils and Rocks***  
**v. 38, n. 3**



# Revisiting Classical Methods to Identify Collapsible Soils

O.M. Vilar, R.A. Rodrigues

**Abstract.** The paper revisits and updates two expedite methods used to identify the occurrence of collapsible soils. The methods were proposed by Gibbs (1961) and de Mello (1973) and have in common the assumption that collapsible soils are usually low density soils characterized through the relative compaction at natural condition, ratio between *in situ* dry-density and maximum dry density from Standard Proctor compaction test. The method by Gibbs (1961) considers in addition the soils moisture deviation, the difference between *in situ* moisture content and optimum moisture content. Data from different origin soils of all over the world were used and analyzed and equations were proposed to separate collapsible and non-collapsible soils. The updated procedures, as the original ones, were intended for use during preliminary investigation to identify potentially collapsible soil and to serve as a basis for planning more precise methods of investigation.

**Keywords:** collapsible soils; identification; unsaturated soil.

## 1. Introduction

Some soils under constant stress show volume decrease related to an increase of moisture content. This wetting-induced or soil collapse deformation characterizes the so called collapsible soils. Collapse deformation is a typical behavior of non-saturated low dry density soils and has been reported as occurring in many places all over the world in soils of different genesis such as aeolian, alluvial, colluvium and residual soils and even in poorly compacted embankments (Dudley 1970, Clemence & Finbar 1981, Vilar *et al.*, 1981, Vilar and Gaioto 1994).

Soil collapse can take place upon wetting for a wide range of applied stress. As the applied stress is increased, the amount of collapse deformation experienced by an unsaturated soil reaches a maximum and then decreases to a negligible value. The maximum value attained depends on the soil type, density and moisture content. Larger collapse deformations are associated to low densities and low degrees of saturation. (Alonso *et al.*, 1990).

The classical oedometer test with some variation has been extensively used to characterize and to quantify the soil collapse. In one option, the unsaturated specimen is loaded until a load of interest and, after equilibrium of load deformation, is wetted, thus allowing measuring the wetting induced deformation. The other option is the double oedometer test (Jennings & Knight 1957), performed with two similar samples, one unsaturated and the other soaked since the beginning of load application.

Figure 1 illustrates typical results of soil collapse using both options of test. The soil tested is from the North-west Region of Sao Paulo State, Brazil and has experienced collapse strains after the filling of a reservoir (Vilar & Rodrigues, 2011). This region is covered by sandy soils that

are of colluvial nature and reach depths of about 10 m. Their characteristics are: specific gravity,  $G_s = 2.63$ , dry density,  $\rho_d = 1.44 \text{ g/cm}^3$ , moisture content,  $w = 7.2\%$ , void ratio,  $e = 0.85$ , porosity,  $n = 46\%$ , liquid limit,  $w_L = 18\%$ , plastic limit,  $w_p = 11\%$ , clay = 15%, silt = 6% and sand = 79% and they typically classifies as SC in the Unified Soil Classification System. Standard Proctor maximum dry density,  $\rho_{dmax}$  is  $2.04 \text{ g/cm}^3$ , which is associated to optimum moisture content,  $w_{opt}$ , of 8.6%. From Fig. 1(a) one can observe the influence of stress on the magnitude of soil collapse and in Fig. 1(b) the differences in unsaturated and soaked sample, attributed to soil collapse.

Field tests also have been performed with procedures similar to the ones used in laboratory tests. The tests used were plate and pile load tests (Cintra 1998), cone penetration tests (Ferreira *et al.*, 1989), and load tests especially designed to measure the phenomenon (Ferreira 1993, Houston *et al.*, 1988).

Suction has long been recognized as a fundamental variable in the understanding of the mechanical behavior of unsaturated soils (Escario & Saez 1973, Fredlund & Morgentern 1977, Alonso *et al.*, 1990). Thus modern options of oedometer tests with controlled suction are currently available, allowing a detailed description of the collapse phenomenon. For instance, Fig. 2 shows compression curves from oedometer tests with controlled suction using the axis translating technique obtained in the same collapsible soil presented in Fig. 1. The tests were performed on samples with initial suction,  $s$ , of 200 kPa. After equilibrium of suction, each specimen was loaded under net normal stress of 50, 100, 200 and 400 kPa allowing for the equilibrium of deformation under load. Then the suction was gradually reduced to 0 kPa and the corresponding col-

Orencio Monje Vilar, Professor, Escola de Engenharia de São Carlos, Universidade de São Paulo, São Carlos, SP, Brazil. e-mail: orencio@sc.usp.br.

Roger Augusto Rodrigues, Assistant Professor, Faculdade de Engenharia de Bauru, Universidade Estadual Paulista "Júlio de Mesquita Filho", Bauru, SP, Brazil. e-mail: roger\_ar@feb.unesp.br.

Submitted on April 4, 2015; Final Acceptance on November 11, 2015; Discussion open until April 30, 2016.

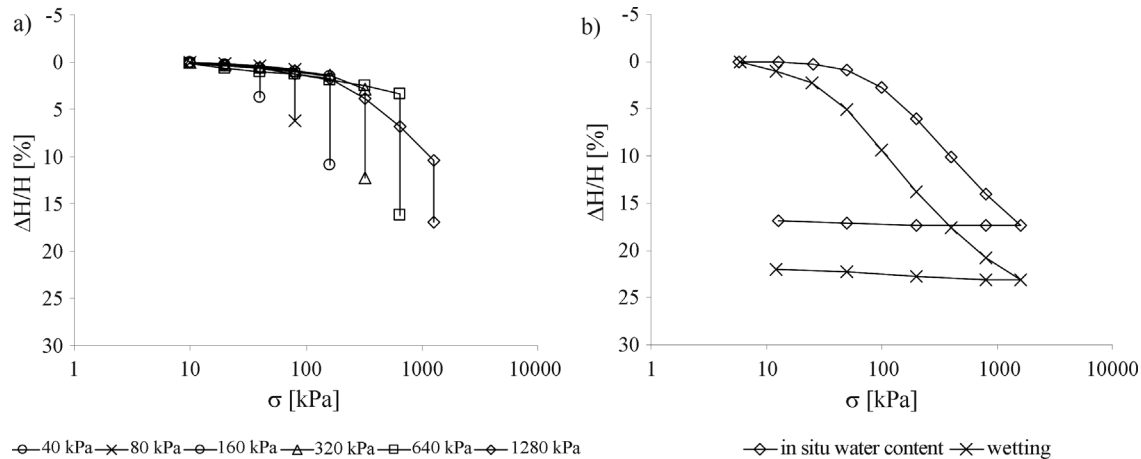


**Figure 1** - Conventional oedometer test results from Pereira Barreto-SP, Brazil: (a) single oedometer tests; (b) double oedometer tests.

lapse strains were measured. In Fig. 2 (a) the variation of collapse deformation with net vertical stress, the difference between total stress and pore air pressure,  $\sigma - u_a$ , can be appreciated, indicating the influence of stress on collapse strain. These are small for lower stress, tend to increase with load and then decrease and negligible values of strain can be attained if larger loads are applied.

Figure 2 (b) shows collapse strain ( $\Delta H_c/H$ ) that arises as suction is reduced, where  $\Delta H_c$  is the height variation of the sample after a stage of suction reduction and  $H$  is the specimen height. As can be seen in Fig. 2 (b), in the initial stages of suction reduction, the collapse potential is negligible and it tends to increase for the lower values of suction, reaching its maximum as suction approaches zero. Wetting-drying cycles such as those that seasonally takes place in natural soil did not introduce additional deformation, as expected.

Figure 2(c) shows the influence of suction on confined compression curves. Each pair of curves of saturated specimen ( $s = 0$  kPa) and at a known suction can be considered as a double oedometer test and allows observing the influence of suction (or moisture content) on collapse strain, calculated from the difference in void ratio at a known load.

The improvement of collapsible soil testing, both in laboratory and in the field, has been accompanied by the development of analytical models, such as the Barcelona Basic Model (Alonso *et al.*, 1990), which allows to reproduce the unsaturated soil behavior, including soil collapse, in a more comprehensive way. However, it is necessary to recognize that the use of more elaborated testing techniques and sophisticated constitutive models demand expertise, are time consuming and expensive. In many applications, the geotechnical engineer needs simple and straightforward methods to deal with some particular problem, especially in the preliminary parts of the project. This is the case of identification or detection of the occurrence of collapsible soils in a particular site or large areas, as those traversed by lin-

ear works such as canals and roads. In this context, this paper revisits and updates former criteria proposed by Gibbs (Gibbs, 1961; USBR, 1998) and by de Mello (1973), analyzing the density characteristics of soils and data from soil collapse occurrences registered in many parts of the world.

## 2. Some Features of Methods to Identify Collapsible Soils

The existing methods for identifying collapsible soils generally rest on some basic principles: a) regional methods developed from empirical concepts and expedite tests, such as the methods based on consistency limits and physical indexes (Denisov 1951, Feda 1966, Sultan 1971, Gibbs & Bara 1967); b) methods based on oedometer tests with wetting (Denisov 1951, Jennings & Knight 1957, Reginatto & Ferrero 1973) and c) methods based on field test, as the cone penetration test (Ferreira *et al.*, 1989) or specially designed plate load tests (Houston *et al.*, 1988, Ferreira 1993).

Many of the empirical criteria incorporate the idea of a low density soil, expressed in different direct and indirect ways. Gibbs (1961) has used a criterion based on the relationship between in-place dry density and laboratory maximum dry density and the moisture content deficiency, as shown on Fig. 3(a). If the relative compaction and moisture content difference plot below and to the right of the limit line, significant wetting induced deformation must be expected even under low pressures, and treatment of in-place materials may be required. This criterion was developed on the basis of the Bureau of Reclamation experience, considering soils classified as ML, CL, ML-CL, SM and MH and the loads within the range applicable for small dams (USBR 1998). This option comes to the heart of the problem since it encompasses soil looseness and moisture deficiency, however it has not, apparently, gained acceptance of geotechnical community and it is hardly referenced in the literature issued after 1970.

In the same report Gibbs (1961) has proposed an alternative method for fine grained soils that was based on in

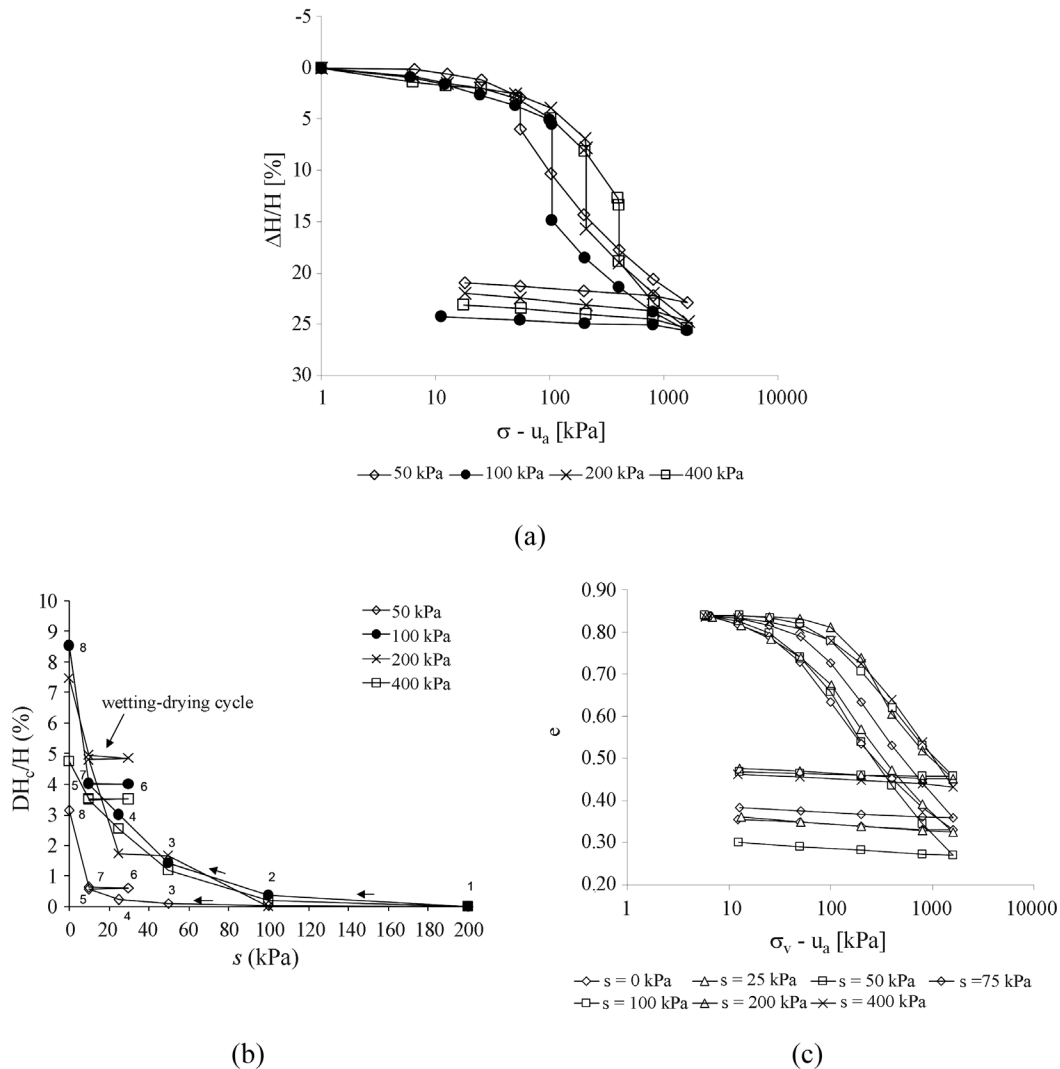


**Figure 2** - Suction controlled oedometer test results from Pereira Barreto-SP, Brazil: (a) tests with initial suction of 200 kPa; (b) collapse potential during suction decrease and wetting-drying cycle; (c) compression curves for different suction (Rodrigues & Vilar 2006; Vilar & Rodrigues 2011).

situ dry unit weight and liquid limit, as sketched in Fig. 3(b) taken from Gibbs & Bara (1967). This method, from now on called the Gibbs and Bara method, rests on the soil void ratio expressed through in-situ dry density and liquid limit. Case I shows a soil whose volume of voids is larger than that required to hold the volume of water needed to reach the liquid limit. Saturation will result in moisture content in excess of the liquid limit, consistency will be low and the potential for collapse would be high. In this case, if collapse did not occur, the soil would be in a very sensitive condition (Knodel 1981). If voids volume is less than that required to hold the moisture content at the liquid limit, as shown by Case III, the soil at saturation will remain in the plastic state and have greater resistance against particle shifting and only settle as a normal result of loading. The extensive and successful use of this method is shown in Gibbs & Bara (1967) and Knodel (1981). Similar concepts are usually

embodied in other proposal, usually incorporating some local correction factors trying to better match field observation and criteria result (Denisov 1951, Feda 1966).

De Mello (1973) has considered for colluvium soils similar to those illustrated in Fig. 1, that the condition for collapse deformation to occur is that the relationship between in-place dry density and laboratory maximum dry density should be lower than 80%. In fact, Gibbs & Bara (1967) method applied to the soil of Fig. 1 lead to a collapsible soil as the void ratio capable of retaining the moisture content associated to the liquid limit is 0.48, which is lower than natural void ratio (0.85). In addition, the relationship between in-place dry density and laboratory maximum dry density (Standard Proctor) is 76%, which is lower than the value proposed by de Mello (1973), thus also, classifying this as a collapsible soil.

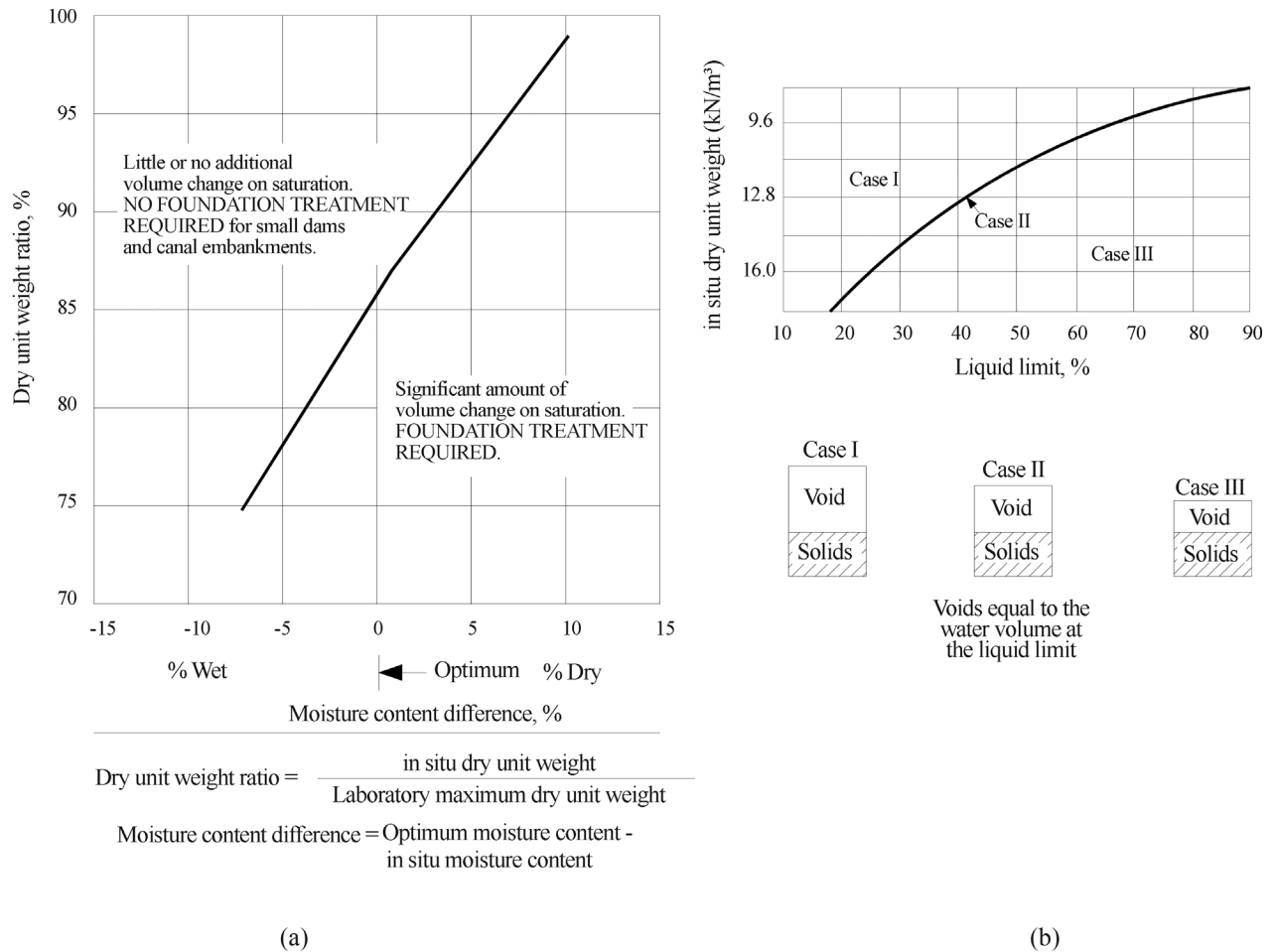


Figure 3 - Criteria for identifying collapsible soils. (a) based on relative compaction and moisture content difference; (b) based on dry unit weight and liquid limit (USBR, 1998).

### 3. Updating an Expedite Methods to Identify Potentially Collapsible Soils

In spite of the successful application of the Gibbs and Bara method, it is worth to recognize that it is not able to identify non-plastic soils and, in some instances, fail to identify some collapsible soils as can be confirmed checking some of the data of Table 1 presented in the Appendix, for instance soils 12, 14, 36, 63, and 67. Thus, based on the general concepts and physical characteristics of collapsible soils reported in the literature, it seems consistent to pursue a criterion to identify collapsible soils, considering in a direct way the usual looseness of collapsible soil, through compaction parameters. In this sense, the authors recover the proposals by Gibbs (1961) and de Mello (1973) that are updated with some data of collapsible soils from various parts of the world. Those proposals are reanalyzed and the possible range of values at which a soil should be considered as collapsible is enlarged. The proposed methods take into account the relative compaction of natural soil, relating the in situ dry unit weight ( $\rho_d$ ) with maximum dry density

( $\rho_{dmax}$ ) of soil as given by a Standard Proctor Test (ASTM D 698). Using these parameters it is possible to determine the natural relative compaction ( $RC_n$ ) of the soil.

$$RC_n = \frac{\rho_d}{\rho_{dmax}} \times 100(\%) \quad (1)$$

To define the critical condition for collapse, it was assumed that soil density was of highest importance because, for this type of deformation to occur, soils must be sufficiently loose so that they are capable of collapsing when their particle-to-particle bond is weakened by wetting or suction decrease.

However, the collapse also depends on the moisture content of the soil or on the degree of saturation. Although the soils must first be in a critically low-density condition for a collapse of structure to occur, the existing moisture content or the associated suction must be also considered an important part in the analysis. Soils which were already at an *in situ* high degree of saturation were expected to be minimally affected by additional wetting or suction decrease, as they will compress under load leaving small

room for collapse to takes place. Soils drier than optimum moisture content are capable to sustain appreciable loads with little compression due to the rigidity introduced by soil suction and were considered prone to collapse as indicated by the many results available (Escario and Saez 1973, Vilar and Gaioto 1994). To take into account the influence of moisture, the method by Gibbs (1961) also considers the moisture content deviation ( $\Delta w$ ), the difference between the actual soil moisture content ( $w$ ) and the Standard Proctor optimum moisture content ( $w_{opt}$ ).

$$\Delta w = w - w_{opt} \quad (2)$$

The value of  $\Delta w$  is negative when the soil is drier than optimum moisture content and positive when the soil is wetter than optimum moisture content.

As the original criteria analyzed do not consider load and the available information about load and collapse is limited, this variable was not considered in this paper.

To evaluate the boundary between collapsible and non collapsible soils different sets of test results on natural specimens of collapsible and non-collapsible soils were used. These data are gathered in Table 1 and as many of the original papers did not present all the soil characteristics data, some values were calculated or even assumed, when needed. In assuming data, especially for the Standard Compaction Tests, practical Tables based on Universal Classification System were used such as Table 2 in Appendix, adapted from USBR (1998). In the case of calculated or assumed values, the data are inserted in Table 1 in italic. In the same table, soils said as non-collapsible are identified by an asterisk.

Figure 4 shows the plot of natural relative compaction ( $RC_n$ ) and moisture content deficiency of the soil.

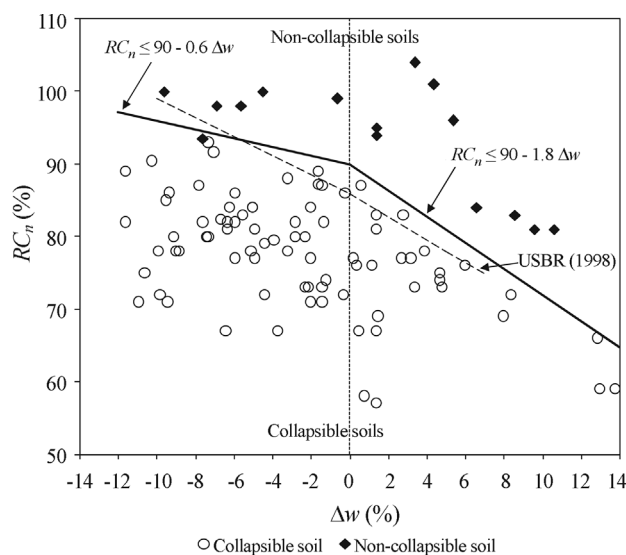


**Figure 4** - Relative compaction  $RC_n$  versus moisture content deviation of collapsible soils.

Inspection of Table 1 and Fig. 4 shows that the vast majority of collapsible soils are low dry density and dry soils, that is, they are poorly compacted materials showing dry density lower than  $1.50 \text{ g/cm}^3$  and moisture content deficiency. Collapsible behavior was also noticed for soils wetter than optimum moisture content, however always related to loose soils, with natural degree of compaction lower than approximately 85%. In general, collapsible soils showed  $RC_n$  lower than 90%, although at least one soil with  $RC_n = 95\%$  has suffered collapse. In this case the moisture content deviation was of about -8%, suggesting that even denser soils if dry can be subjected to collapse deformation if under large overburden stress. However, in many of these situations related to dense and fairly dry soils, the stress needed to induce collapse strains are very large, beyond the range of practical interest for the Geotechnical Engineer. Very few data of non-collapsible soil has been reported and they show usually  $RC_n$  larger than 90% as is the case of the soil from arid climate tested by Carvalho (1994) that has not shown wetting induced strains although they were dry and wetted at stresses as large as 400 kPa or present large moisture content when  $RC_n$  is lower than 90% as reported by Arman & Thornton (1973).

The trend shown by the data set in Fig. 4 confirms the original proposition by Gibbs, however also indicates that it should be slightly enlarged since some reported collapsible soils plotted above the boundary line. In this sense, the available information has lead to the proposition of the limit line drawn in Fig. 4 that separates collapsible and non-collapsible soils. If the natural relative compaction and moisture content deficiency plot below the limit line, significant wetting induced deformation should be expected and additional and more directed investigation may be performed to adequately characterize collapsing behavior, which necessarily includes the state of stress acting on the soil. As it is known, the magnitude of collapse strain depends on the stress and usually after reaching a maximum it then decreases to negligible values as the load is increased and the soil is compressed to a denser condition.

The limit lines of Fig. 4 also allows stating a relationship between dry density and moisture content deviation and the following condition should stand for a soil to be considered potentially collapsible:

a) for dry soils ( $w < w_{opt}$ )

$$100 \cdot \frac{\rho_d}{\rho_{d \max}} \leq 90 - 0.6 \Delta w \quad (3)$$

b) for wet soils ( $w > w_{opt}$ )

$$100 \cdot \frac{\rho_d}{\rho_{d \max}} \leq 90 - 1.8 \Delta w \quad (4)$$

In these equations,  $\Delta w$  is expressed as percentage. The relationships are valid up to -12% on the dry side and to

+14% on the wet side, since those were the limiting moisture content deviations found in the referenced papers.

As there are very few data above the limit line, caution should be exerted for soils that plot in the vicinity of this limit line. In this case, additional investigation should be performed to confirm collapse behavior, considering the key factors that influence collapse deformation.

Figure 4 allows also suggesting a tentative single index separating collapsing and non-collapsing soils. As can be seen the dry soils, that is, the soils with moisture content lower than optimum moisture content show  $RC_n$  lower than 90%, figure that tends to decrease for moisture content above the optimum water content. This index is larger than the value proposed by de Mello (1973) and therefore should replace it.

These expedite methods of collapsible soil identification were checked and updated to support the initial stages of investigation and to orientate, but not to substitute, the more elaborate investigation techniques, that will support the designer on choosing the solution for the problem under analysis. Thus, by performing very simple and conventional measurements, as the in situ unit weight and moisture content and the parameters of Standard Proctor test it is possible to define whether a given soil is potentially collapsible. In situ density can be measured by conventional methods, such as the sand replacement method, among others, while moisture content can be measured through speedy moisture tester or other applicable method, such as the oven method. In some instances, and considering that the proposed method was devised for preliminary investigation, an experienced engineer can use results from other sources and indirectly evaluate the soil characteristics of interest. For instance, soil identification following ASTM D2488 - Standard practice for description and identification of soils (visual-manual procedure) - allows classifying the soil according to the Universal Soil Classification System and obtain average Standard Proctor parameters from practical tables, such as Table 2 in the Appendix.

It must be recognized that the methods are difficult to apply to deeper soil horizons, unless some measurement of soil density and moisture content is available. In this case and indeed in a more comprehensive way, a natural strategy would be using some field test such as the common Standard Penetration Test, searching for low density sandy and clayey soils that are unsaturated. Some SPT profiles of collapsible soils are available, especially from the Center-West and Southeast Brazil (Cavalcante *et al.*, 2007 among others), which shows collapsible soils as being unsaturated loose to medium compact sandy soils and unsaturated soft clayey soils. However, the relationship between SPT and soil collapse must be seen with caution, since SPT is influenced by moisture content or suction. For instance, for collapsible soils developed under arid and semi arid climate, Ferreira (1995) and Souza Neto (2004) have shown that these highly desiccated soils can show high SPT values

during dry season, suggesting that their relative density is high. As an example, SPT performed in the dry season in a sandy soil of Petrolândia, Pernambuco, Brazil presents SPT higher than 10 blows. After three hours of flooding the SPT was reduced to about 70% of original value in the shallower portions of the soil profile (Ferreira, 1995) and after the rainy season, some measured values of SPT were reduced from 10 to about 5 blows, showing the influence of moisture content and suction on the number of blows and on the relative density (Souza Neto, 2004). The influence of moisture content or suction on the blow number of SPT has been addressed by other authors, such as Reginatto (1971) and Camapum de Carvalho *et al.* (2001) suggesting that SPT is of limited value in identifying collapsible soils. A possible alternative to overcome this point is to perform field tests with soil at natural moisture content and after flooding, analyzing the differences between both values; however the subject demands additional research in order to establish its efficiency.

Finally, it is worth to say that that both criteria updated in this paper indicate the collapsible nature of the sandy soil of Petrolândia, above referred to, since it shows natural relative compaction ( $RC_n$ ) lower than 80% and moisture content deviation of about -7% in the dry season (Ferreira, 1995).

#### 4. Conclusion

Collapsible soils are typically low density non-saturated soils that can be of different origins. These soils experience volume reduction or collapse strain when wetted at an almost constant stress, usually larger than the overburden stress. Collapse strains are known to depend on the dry density and moisture content of the soil and on the stress acting on it. An expedite method first proposed by Gibbs (1961) to identify collapsible soils, which considers that collapsible soils are naturally poorly compacted soils, with moisture content deficiency has been updated. The method takes into account both in situ density and moisture content and Standard Proctor compaction parameters of the soil, related through the natural relative compaction ( $RC_n$ ), relationship between in situ dry density ( $\rho_d$ ) and maximum dry density ( $\rho_{dmax}$ ) and moisture content deviation ( $\Delta w$ ), the difference between the in situ soil moisture content ( $w$ ) and optimum moisture content ( $w_{opt}$ ). Both parameters are related through Eq. 3 for dry soils and Eq. 4 for wet soils, that is soils that show moisture content larger than optimum moisture content.

The data gathered also allowed a simplified criterion that takes into account only dry density. In this option, soils that show negative moisture deviation and natural relative compaction ( $RC_n$ ) lower than 90% are classified as collapsible. This index tends to reduce as moisture content increases above optimum moisture content.

The updated methods were devised for preliminary studies and to optimize more complete investigation analy-

sis, not to substitute them, remembering that besides dry density and moisture content, the collapse strains are also function of stress whose influence is not addressed in this paper.

## References

- Alawaji, H.A. (2001). Shear induced collapse settlement of arid Soils. *Geotechnical and Geological Engineering*, 19(1):1-19.
- Alonso, E.E.; Gens, A. & Josa, A. (1990). A constitutive model for partially saturated soil. *Géotechnique*, 40(3):405-430.
- Arman, A. & Thornton, S.I. (1973). Identification of collapsible soils in Louisiana. *Highway Research Record*, 426: 14-22.
- ASTM D 698 (2007). Standard Test Methods for Laboratory Compaction Characteristics of Soil Using Standard Effort. *Annual Book of ASTM Standards*. ASTM International, West Conshohocken.
- ASTM D 2488 (2009). Standard Practice for Description and Identification of Soils (Visual-Manual Procedure). *Annual Book of ASTM Standards*. ASTM International, West Conshohocken.
- Beles, A.A.; Stanculescu, I.I. & Schally, V.R. (1969). Pre-wetting of loess soil foundation for hydraulic structures. In: *Proc 7<sup>th</sup> International Conference on Soil Mechanics and Foundation Engineering*, Mexico, v. 2, pp. 17-25.
- Benvenuto, C. (1983). Theoretical-Experimental Analysis of the Behavior of Some Collapsible Soils. M.Sc. Thesis, University of São Paulo (in Portuguese).
- Camapum de Carvalho, J.; Pereira, J.H.F.; Guimarães, R.C. & Abreu, P.S.B. (2001). Análise da influência da sucção nos resultados de SPT e SPT-T em solos porosos colapsáveis. In: *Anais 4<sup>o</sup> Simp. Bras. sobre Solos Não Saturados*, Porto Alegre, pp. 509-520.
- Cardoso, F.B.F.; Camapum de Carvalho, J. & Martins, E.S. (1998). Collapse phenomena in weathered soils with origins and depth different from Federal District. In: *Proceedings of the 11<sup>th</sup> Brazilian Congress of Soil Mechanics and Geotechnical Engineering*, Brasília, pp. 59-65 (In Portuguese).
- Carvalho, M.F. (1994). Study of Collapsible Soils from the Northeast of Minas Gerais State, Brazil. M.Sc. Thesis, University of São Paulo (in Portuguese).
- Cavalcante, E.H; Danziger, F.A.B.; Giacheti, H.L.; Coutinho, R.Q.; Souza, A.; Kormann, A.C.M.; Belicanta, A.; Pinto, C. S.; Costa Branco C.J.M.; Ferreira, C.V; Carvalho, D. de; Marinho, F.A.M.; Cintra, J.C.A.; Dourado, K.C. de A.; Moraes, L.S. de; Albuquerque Filho, L. H. A.; Almeida, M.S.S de; Gutierrez, N.H.M.; Albuquerque, P.J.R de; Chamecki, P.R.; Cunha, R.P. da; Teixeira, R.S.; Menezes, S.M. & Lacerda, W.A. (2007). Campos experimentais brasileiros. *Geotecnia*, 111:99-205.
- Clemence, S.P. & Finbarr, A.O. (1981). Design considerations for collapsible soils. *Journal Geotechnical Engineering Division, ASCE*, 107(3):305-317.
- Clevenger, W.A. (1956). Experiences with loess as foundation material. *Journal of the Mechanics and Foundation Division, ASCE*, 82(3):1-26.
- Cintra, J.C.A. (1998). *Foundations in Collapsible Soils*. Rima, São Carlos (in Portuguese).
- Collares, A.C.Z.B. & Vilar, O.M. (1998). Influence of saturation liquid pH on soil collapse. In: *Proc. 11<sup>th</sup> Brazilian Congress of Soil Mechanics and Geotechnical Engineering*, Brasília, pp. 123-129 (in Portuguese).
- Conciani, W. (1997). Study of Soil Collapse by Plate Load Tests with Tensiometers and Computed Tomography. Ph.D. Thesis, University of São Paulo (in Portuguese).
- Costa Jr., F.A. (2001). Infiltration Effects of Caustic Liqueur on Resistance Characteristics of a Lateritic Soil. Ph.D. Thesis, Pontifical Catholic University of Rio de Janeiro (in Portuguese).
- de Mello, V.F.B. (1973). *Class Notes of Soils Mechanics*. EP-USP, University of São Paulo.
- Delage, P.; Cui, Y.J. & Antoine, P. (2005). Geotechnical problems related with loess deposits in Northern France. In: *Proc. International Conference on Problematic Soils*, Eastern Mediterranean University, Famagusta, N. Cyprus, pp. 1-24.
- Denisov, N.Y. (1951). *Mechanical Properties of Loess and Loams*. Gosstroizdat, Moscou (in Russian).
- Derbyshire, E. & Mellors, T.W. (1988). Geological and geotechnical characteristics of some loess and loessic soils from China and Britain: A comparison. *Engineering Geology*, (25):135-175.
- Dudley, J.H. (1970). Review of collapsing soils. *Journal of the Soil Mechanics and Foundation Division*, 96(3):925-947.
- Escario, V. & Saez, J. (1973). Gradual collapse of soils originated by a suction decrease. In: *Proc. 8<sup>th</sup> International Conference on Soils Mechanics and Foundation Engineering*, Moscow, v. 4.2, pp. 123-124.
- Feda, J. (1966). Structural stability of subsident loess soil from Praha-Dejvice. *Engineering Geology*, 1(3):201-219.
- Ferreira, C.V.; Lobo, A.S.; Giacheti, H.L. & Conciani, W. (2004) Behavior of piles installed in collapsible soils. In: *Proc. 5<sup>th</sup> Brazilian Symposium on Unsaturated Soils*. São Carlos, v. 1, pp. 345-350 (In Portuguese).
- Ferreira, R.C.; Monteiro, L.B.; Peres, J.E.E. & Benvenuto, C. (1989). Some aspects on the behaviour of Brazilian collapsible soils. In: *Proc. 12<sup>th</sup> International Conference on Soil Mechanics and Foundation Engineering*, Rio de Janeiro, v. 1, pp. 117-120 (in Portuguese).
- Ferreira, S.R.M. (1993). Volume change in expansive and collapsible unsaturated soils. In: *Proc. 7<sup>th</sup> Brazilian Congress of Engineering Geology*, Poços de Caldas, v. 1, pp. 283-296 (in Portuguese).

- Ferreira, S.R.M. (1995). Colapso e Expansão de Solos Naturais Não Saturados devidos à Inundação. Tese de Doutorado, COPPE/UFRJ, 379 p.
- Ferreira, S.R.M.; Fucale, S.P. & Amorim, S.F. (1998). Behavior of volume change in collapsible soils studied through field tests. In: Proc. 11<sup>th</sup> Brazilian Congress of Soil Mechanics and Geotechnical Engineering, Brasília, pp. 171-178 (in Portuguese).
- Ferreira, S.R.M. (2015). Personal Communication, Federal University of Pernambuco.
- Foss, I. (1973). Red soil from Kenia as a foundation material. In: Proc. 8<sup>th</sup> International Conference on Soil Mechanics and Foundation Engineering, Moscow, v. 2.2, pp. 73-80.
- Fredlund, D.G. & Morgenstern, N.R. (1977). Stress State for Unsaturated Soils, Journal of Geotechnical Engineering Division, ASCE, 103(GT5):447-466.
- Gibbs, H.J. (1961). Properties Which Divide Loose and Dense Uncemented Soils. Bureau of Reclamation Report No, EM-608, Denver, CO (apud USBR, 1998).
- Gibbs, H.J. & Bara, J.P. (1967). Stability problems of collapsing soil. Journal of the Soil Mechanics and Foundation Division, ASCE, 93(4):577-594.
- Gutierrez, N.H.M.; Nóbrega, M.T. & Vilar, O.M. (2009). Influences of the microstructure in the collapse of a residual clayey tropical soil. Bulletin of Engineering Geology and the Environment, 68:107-116.
- Houston, S.L.; Houston, W.N. & Spadola, D.J. (1988). Prediction of field collapse of soils due to wetting. Journal of Geotechnical Engineering, ASCE, 114(1):40-58.
- Jennings, J.E. & Knight, K. (1957). The additional settlement of foundations due to a collapse of structure of sandy subsoils on wetting. In: Proc. 4<sup>th</sup> Conference on Soil Mechanics and Foundation Engineering, London, pp. 316-319.
- Klukanová, A. & Frankovská, J. (1998). Soil collapse. In: Proc. 8<sup>th</sup> International IAEG Congress, Association for Engineering Geology and Environment, Vancouver, pp. 3349-3355.
- Knodel, P.C. (1981). Construction of large canal on collapsing soils. Journal of the Geotechnical Engineering Division, ASCE, 107(GT1):79-94.
- Lutenegger, A.J. & Saber, R.T. (1998). Determination of collapse potential of soils. Geotechnical Testing Journal, ASTM, 11(3): 173-178.
- Mahler, C.F. & Mendonça, M.B. (1994). Micro-structural aspects of the collapsible soils from Bahia. In: Proc. 10<sup>th</sup> Brazilian Congress of Soil Mechanics and Geotechnical Engineering, Foz do Iguaçu, pp. 1149-1156 (in Portuguese).
- Monacci, M.D.; Carvalho, D. & Albuquerque, P.J.R. (1997). Collapsibility analysis of a residual soil from Campinas-SP, Brazil. In: Proc 3<sup>rd</sup> Brazilian Symposium on Unsaturated Soils, Rio de Janeiro, v. 1, pp. 113-119 (in Portuguese).
- Mustafaev, A.A.; Chigniev, G.D. & Nazirova, G.R. (1974). Rheological nature of the deformations caused by swelling in clays and by collapse in loess soils. Soil Mechanics and Foundation Engineering, 11(5):325-330.
- Phien-wej, N.; Pientong, T. & Balasubramaniam, A.S. (1992). Collapse and strength characteristics of loess in Thailand. Engineering Geology, 32:59-72.
- Reginatto, A.R. (1971). Standard penetration test in collapsible soils. In: Proc. IV Cong. Panam. de Mec. de Suelos e Ing.de Fundaciones, Puerto Rico, v. 2, p. 77-84.
- Reginatto, A.R. & Ferrero, J.C. (1973). Collapse potential of soils and soil-water chemistry. In: Proc. 8<sup>th</sup> International Conference on Soil Mechanics and Foundation Engineering, Moscow, v. 2.2, pp. 177-183.
- Reznik, Y.M. (1992). Determination of deformation properties of collapsible soils. Geotechnical Testing Journal, ASTM, 15(3):248-255.
- Rodrigues, R.A. & Lollo, J.A. (2004). Structural, physiographic and mechanical characteristics of two profiles of collapsible soils from Ilha Solteira-SP. Brazil. Solos e Rochas, 27:131-146 (in Portuguese).
- Rodrigues, R.A. & Vilar, O.M. (2006). Relationship between collapse and soil-water retention curve of a sandy soil. In: Proc. 4<sup>th</sup> International Conference on Unsaturated Soils, Carefree, Arizona, v. 1, pp. 1025-1036.
- Souza Neto, J.B. (2004). The Behavior of a Collapsible Soil Evaluate Through *in situ* and Laboratory Testing and Settlement Prediction Due to Wetting. Ph.D. Thesis, Federal University of Rio de Janeiro, COOPE (in Portuguese).
- Sultan, H.A. (1971). Some Engineering Aspects of Collapsing Soils. The University of Arizona, Tucson, 35 p.
- USBR (1998). Earth Manual, Part 1. 3<sup>rd</sup> ed. Bureau of Reclamation, Denver.
- Vilar, O.M.; Rodrigues, J.E. & Nogueira, J.B. (1981). Collapsible soils: A problem for tropical soil engineering. In: Proc. Brazilian Symposium of Tropical Soils, Rio de Janeiro, v. 1, pp. 209-224 (In Portuguese).
- Vilar, O.M. & Gaioto, N. (1994). Collapsible behavior of a compacted lateritic soil. In: Proc. 2<sup>nd</sup> Brazilian Symposium on Unsaturated Soils, Recife, pp. 185-190 (in Portuguese).
- Vilar, O.M. & Rodrigues, A.R. (2011). Collapse behavior of soil in a Brazilian region affected by a rising water table. Canadian Geotechnical Journal, 48:226-233.
- Zur, A. & Wiseman, G. (1973). A study of collapse phenomena of an undisturbed loess. In: Proc. 8<sup>th</sup> International Conference on Soils Mechanics and Foundation Engineering, Moscow, v. 2.2, pp. 265-269.

## Appendix

**Table 1** - Data from collapsible soil.

Soil	Clay (%)	Silt (%)	Sand (%)	$w_L$ (%)	$w_p$ (%)	Class. USCS	$n$ (%)	$S_r$ (%)	$\rho_d$ (g/cm <sup>3</sup> )	$w$ (%)	$\rho_{dmax}$ (g/cm <sup>3</sup> )	$w_{opt}$ (%)	$\Delta w$ (%)	$RC_n$ (%)	Reference
1	32	16	52	27	13	SC	42	37	1.551	10.1	2.125	12.4	-2.3	73	Benvenuto (1983)
2	27	7	66	23	16	SC	50	41	1.510	-	1.936	12.4	-	78	Ferreira <i>et al.</i> (1989)
3	2	8	89	NL	NP	SW	40	13	1.590	3.4	1.980	10.8	-7.4	80	Ferreira (1993)
4	3	19	76	18	13	SM	42	6	1.544	1.5	1.970	11.4	-9.9	78	Ferreira (1993)
5	50	30	20	50	25	CL	66	45	0.900	32.8	1.768	16.4	16.4	51	Ferreira <i>et al.</i> (1989)
6	50	37	13	80	46	MH	65	-	0.931	-	1.372	33.1	-	68	Ferreira <i>et al.</i> (1989)
7	61	6	33	54	27	CH	61	42	1.030	25.3	1.531	24.8	0.5	67	Ferreira <i>et al.</i> (1989)
8	42	15	43	41	19	CL	54	38	1.270	16.1	1.768	16.4	-0.3	72	Ferreira <i>et al.</i> (1989)
9	45	20	35	37	26	ML	63	39	1.130	21.6	1.645	20.1	1.5	69	Ferreira <i>et al.</i> (1989)
10	41	24	25	48	35	ML	65	55	1.080	33.0	1.645	20.1	12.9	66	Ferreira <i>et al.</i> (1989)
11	15	35	50	25	15	SC	46	40	1.440	12.8	1.906	12.4	0.4	76	Ferreira <i>et al.</i> (1989)
12	46	12	42	58	27	CH	54	60	1.240	26.2	1.531	24.8	1.4	81	Ferreira <i>et al.</i> (1989)
13	45	5	50	58	34	SM	59	50	1.120	26.2	1.906	12.4	13.8	59	Ferreira <i>et al.</i> (1989)
14	60	15	25	70	30	CH	61	56	1.050	32.8	1.531	24.8	8.0	69	Ferreira <i>et al.</i> (1989)
15	-	-	-	50	10	CL	54	33	1.250	14.4	1.768	16.4	-2.0	71	Ferreira <i>et al.</i> (1989)
16	32	23	44	28	18	SC	46	34	1.414	10.7	1.802	13.9	-3.2	78	Carvalho (1994)
17	27	14	59	NL	NP	SP	51	3	1.305	1.1	1.827	10.5	-9.4	71	Cardoso <i>et al.</i> (1998)
18	56	3	34	36	25	CL	46	41	1.388	13.2	1.620	19.1	-5.9	86	Carvalho (1994)
19(*)	58	6	33	38	25	CL	42	45	1.469	12.6	1.574	20.2	-7.6	93	Carvalho (1994)
20	39	27	33	32	20	CL	44	34	1.467	9.9	1.753	14.9	-5.0	84	Carvalho (1994)
21	17	51	32	28	18	CL	45	27	1.430	8.7	1.742	15.0	-6.3	82	Carvalho (1994)
22(*)	44	39	17	36	22	CL	34	57	1.740	10.8	1.768	16.4	-5.6	98	Carvalho (1994)
23(*)	5	24	71	NL	NP	SP	31	36	1.831	6.0	1.827	10.5	-4.5	100	Carvalho (1994)

Table 1 - Cont.

Soil	Clay (%)	Silt (%)	Sand (%)	$w_L$ (%)	$w_p$ (%)	Class. USCS	$n$ (%)	$S_r$ (%)	$\rho_d$ (g/cm <sup>3</sup> )	$w$ (%)	$\rho_{dmax}$ (g/cm <sup>3</sup> )	$w_{opt}$ (%)	$\Delta w$ (%)	$RC_n$ (%)	Reference
24	15	6	79	18	11	SC	46	22	1.440	7.2	2.040	8.6	-1.4	71	Rodrigues and Vilar (2006)
25	16	6	78	-	-	SC	36	4	1.684	0.8	2.100	8.1	-7.3	80	Mahler and Mendonça (1994)
26	43	12	45	37	25	ML	67	30	0.930	21.5	1.645	20.1	1.4	57	Conciani (1997)
27	39	51	10	45	32	ML	64	50	0.971	33.1	1.645	20.1	13.0	59	Conciani (1997)
28	67	19	13	52	35	MH	64	41	1.072	24.3	1.372	33.1	-8.8	78	Monacci <i>et al.</i> (1997)
29	39	48	13	66	42	MH	60	53	1.152	28.1	1.372	33.1	-5.0	84	Monacci <i>et al.</i> (1997)
30	24	35	41	28	18	SC	49	42	1.370	14.8	1.715	17.6	-2.8	80	Ferreira <i>et al.</i> (1998)
31	7	22	70	23	14	SC	41	19	1.620	5.2	1.965	11.1	-5.9	82	Ferreira <i>et al.</i> (1998)
32	48	39	13	51	38	MH	67	43	0.953	30.4	1.650	29.6	0.8	58	Collares and Vilar (1998)
33	13	22	65	23	14	SC	43	22	1.540	6.1	1.906	12.4	-6.3	81	Costa Jr. (2001)
34	74	16	10	57	42	MH	66	49	1.018	37.8	1.372	33.1	4.7	74	Gutierrez <i>et al.</i> (2009)
35	66	28	6	61	42	MH	62	65	1.133	35.9	1.372	33.1	2.8	83	Gutierrez <i>et al.</i> (2009)
36	27	8	65	25	15	SC	46	30	1.440	9.6	1.960	11.7	-2.1	73	Rodrigues and Lollo (2004)
37	clayey sand (0-6 m) clayey silt (6-12 m)			41	23	SC	51	56	1.374	20.8	1.906	12.4	8.4	72	Ferreira <i>et al.</i> (2004)
38a	7	2	91	NL	NP	SP-SM	39	4.6	1.628	1.08	1.800	11.3	-10.2	90.4	Souza Neto (2004)
38b	9	3	88	14	NP	SP-SM	39	6.9	1.618	1.68	1.880	11.0	-9.3	86.0	Souza Neto (2004)
38c	14	2	84	16	12	SM	39	8.7	1.615	2.11	1.970	9.7	-7.6	82.0	Souza Neto (2004)
38d	15	0	82	17	15	SM	37	9.8	1.673	2.15	2.030	8.8	-6.6	82.4	Souza Neto (2004)
38e	16	5	79	19	13	SM/SC	31	19.1	1.833	3.18	2.000	10.2	-7.0	91.7	Souza Neto (2004)
39	-	-	-	-	-	-	-	-	-	-	-	-	-11.6	89.0	Ferreira (2015)
40	-	-	-	-	-	-	-	-	-	-	-	-	-1.6	87.2	Ferreira (2015)
41	-	-	-	-	-	-	-	-	-	-	-	-	-3.9	79.5	Ferreira (2015)
42	10-15	82-87	3	NL	NP	SM	48	5	1.409	1.7	1.877	12.3	-10.6	75	Lutenegger and Saber (1988)

Table 1 - Cont.

Soil	Clay (%)	Silt (%)	Sand (%)	$w_L$ (%)	$w_p$ (%)	Class. USCS	$n$ (%)	$S_r$ (%)	$\rho_d$ (g/cm <sup>3</sup> )	$w$ (%)	$\rho_{dmax}$ (g/cm <sup>3</sup> )	$w_{opt}$ (%)	$\Delta w$ (%)	$RC_n$ (%)	Reference
43	10-15	82-87	3	33	NP	SM	51	4	1.329	1.4	1.877	12.3	-10.9	71	Lutenegger and Saber (1988)
44	10-15	82-87	3	33	NP	SM	50	7	1.358	2.5	1.877	12.3	-9.8	72	Lutenegger and Saber (1988)
45	11	68	-	31	24	ML	47	23	1.343	8.5	1.645	20.1	-11.6	82	Klukanová and Frankovská (1998)
46	7	38	-	24	21	SM	38	25	1.738	5.0	1.877	12.3	-7.3	93	Klukanová and Frankovská (1998)
47	6	26	-	25	20	SM-SC	40	39	1.656	9.1	1.877	12.3	-3.2	88	Klukanová and Frankovská (1998)
48(*)	29	50	-	43	25	CL	36	45	1.738	9.5	1.768	16.4	-6.9	98	Klukanová and Frankovská (1998)
49(*)	15	62	-	27	16	CL	31	37	1.775	6.8	1.768	16.4	-9.6	100	Klukanová and Frankovská (1998)
50	15	38	39	29	16	CL	44	60	1.535	17.0	1.768	16.4	0.6	87	Feda (1966)
51	17	42	41	26	16	CL	42	56	1.574	14.8	1.768	16.4	-1.6	89	Feda (1966)
52(*)	30	42	28	39	21	CL	39	76	1.664	17.8	1.768	16.4	1.4	94	Feda (1966)
53	20	30-40	40-50	18	13	SM-SC	46	27	1.430	8.5	1.940	9.7	-1.2	74	Phien-wej at al (1992)
54	16	21	63	21	17	SM-SC	-	-	1.254	8.3	1.874	12.0	-3.7	67	Alawaji (2001)
55	19	35	45	23	17	SM-SC	-	-	1.339	18.8	1.835	14.0	4.8	73	Alawaji (2001)
56	67% passing 200 sieve			-	-	-	46	-	1.433	9	1.868	11.0	-2.0	77	Houston <i>et al.</i> (1988)
57	18	72	10	28	22	CL - ML	48	53	1.390	18.1	1.645	20.1	-2.0	84	Delage <i>et al.</i> (2005)
58	-	-	-	39	16	CL	49	29	1.367	10.5	1.768	16.4	-5.9	77	Jennings and Knight (1957)
59	8	72	20	30	20	-	-	-	1.160	10.0	1.720	16.4	-6.4	67	Clevenger (1956)
60	12	60	28	-	-	SM	48	25	1.564	6.8	1.877	12.3	-5.5	83	Mustafaev <i>et al.</i> (1974)
61	18	-	-	-	-	SM	46	33	1.500	10.0	1.877	12.3	-2.3	80	Reznik (1992)
62	78	-	-	64	46	MH	60	44	1.100	24.0	1.372	33.1	-9.1	80	Foss (1973)

Table 1 - Cont.

Soil	Clay (%)	Silt (%)	Sand (%)	$w_L$ (%)	$w_p$ (%)	Class. USCS	$n$ (%)	$S_r$ (%)	$\rho_d$ (g/cm <sup>3</sup> )	$w$ (%)	$\rho_{dmax}$ (g/cm <sup>3</sup> )	$w_{opt}$ (%)	$\Delta w$ (%)	$RC_n$ (%)	Reference
63	< 30	> 60	10	31	16	CL	44	53	1.540	15.0	1.768	16.4	-1.4	87	Zur and Wiseman (1973)
64	-	-	-	-	-	CL	51	30	1.275	12.0	1.768	16.4	-4.4	72	Beles <i>et al.</i> (1969)
65	-	-	-	45	-	CL-SC	45	48	1.442	15.0	1.877	12.3	2.7	77	Gibbs and Bara (1967)
66	silt (0.06 - 0.01 mm)			32	22	CL	47		1.404	-	1.768	16.4	-	79	Derbyshire and Mellors (1988)
67	18	95% passing 200 sieve		37	19	CL	48	24	1.380	8.5	1.772	17.5	-9.0	78	Sultan (1971)
68	18	95% passing 200 sieve		43	20	CL	43	38	1.482	11.3	1.772	17.5	-6.2	84	Sultan (1971)
69	18	95% passing 200 sieve		67	28	CH	45	40	1.432	12.6	1.772	17.5	-4.9	81	Sultan (1971)
70	-	-	-	23	17	CL-M L	55	35	1.280	15.0	1.645	20.1	-5.1	78	Reginatto and Ferrero (1973)
71	20	17	43	25	14	SC	-	-	1.280	-	1.810	-	-	71	Dudley (1970)
72	12	16	72	21	12	SC	-	-	1.632	-	1.984	-	-	82	Dudley (1970)
73	10	19	38	20	16	GW-S W	37	34	1.708	7.4	2.226	12.3	-4.9	77	Dudley (1970)
74	5	85	10	NL	NP	SM	69	28	0.881	22.0	1.049	-	-	84	Dudley (1970)
75	2	68	30	NL	NP	SM	58	25	1.041	14.0	1.302	-	-	80	Dudley (1970)
76	7	84	9	33	25	ML	56	36	1.186	17.0	1.516	-	-	78	Dudley (1970)
77	10	70	20	-	-	ML	-	-	1.522	22.0	1.778	-	-	86	Arman and Thornton (1973)
78	18	70	12	-	-	ML	-	-	1.234	18.0	1.626	-	-	76	Arman and Thornton (1973)
79	10	70	20	-	-	ML	-	-	1.200	21.3	1.606	16.6	4.7	75	Arman and Thornton (1973)
80	10	70	20	-	-	ML	-	-	1.216	22.6	1.606	16.6	6.0	76	Arman and Thornton (1973)
81	10	70	20	-	-	ML	-	-	1.312	15.3	1.606	16.6	-1.3	82	Arman and Thornton (1973)
82	10	70	20	-	-	ML	-	-	1.264	12.2	1.606	16.6	-4.4	79	Arman and Thornton (1973)
83	10	70	20	-	-	ML	-	-	1.248	20.5	1.606	16.6	3.9	78	Arman and Thornton (1973)

**Table 1** - Cont.

Soil	Clay (%)	Silt (%)	Sand (%)	$w_L$ (%)	$w_p$ (%)	Class. USCS	$n$ (%)	$S_r$ (%)	$\rho_d$ (g/cm <sup>3</sup> )	$w$ (%)	$\rho_{dmax}$ (g/cm <sup>3</sup> )	$w_{opt}$ (%)	$\Delta w$ (%)	$RC_n$ (%)	Reference
84(*)	10	70	20	-	-	ML	-	-	1.520	18.0	1.606	16.6	1.4	95	Arman and Thornton (1973)
85(*)	10	70	20	-	-	ML	-	-	1.616	21.0	1.606	16.6	4.4	101	Arman and Thornton (1973)
86(*)	10	70	20	-	-	ML	-	-	1.664	20.0	1.606	16.6	3.4	104	Arman and Thornton (1973)
87(*)	10	70	20	-	-	ML	-	-	1.584	16.0	1.606	16.6	-0.6	99	Arman and Thornton (1973)
88	10	70	20	-	-	ML	-	-	1.168	20.0	1.606	16.6	3.4	73	Arman and Thornton (1973)
89	10	70	20	-	-	ML	-	-	1.328	18.0	1.606	16.6	1.4	83	Arman and Thornton (1973)
90(*)	10	70	20	-	-	ML	-	-	1.536	22.0	1.606	16.6	5.4	96	Arman and Thornton (1973)
91	10	70	20	-	-	ML	-	-	1.072	18.0	1.606	16.6	1.4	67	Arman and Thornton (1973)
92	18	70	12	-	-	ML	-	-	1.232	18.0	1.624	16.8	1.2	76	Arman and Thornton (1973)
93	18	70	12	-	-	ML	-	-	1.328	14.0	1.624	16.8	-2.8	82	Arman and Thornton (1973)
94	18	70	12	-	-	ML	-	-	1.248	17.0	1.624	16.8	0.2	77	Arman and Thornton (1973)
95	18	70	12	-	-	ML	-	-	1.248	20.0	1.624	16.8	3.2	77	Arman and Thornton (1973)
96(*)	12	68	20	-	-	ML	-	-	1.408	23.0	1.728	13.4	9.6	81	Arman and Thornton (1973)
97(*)	12	68	20	-	-	ML	-	-	1.456	20.0	1.728	13.4	6.6	84	Arman and Thornton (1973)
98(*)	12	68	20	-	-	ML	-	-	1.440	22.0	1.728	13.4	8.6	83	Arman and Thornton (1973)
99(*)	12	68	20	-	-	ML	-	-	1.392	24.0	1.728	13.4	10.6	81	Arman and Thornton (1973)

$\rho_s$  is solid density,  $n$  is porosity,  $\rho_d$  is dry density,  $w$  is moisture content,  $\rho_{dmax}$  is Standard Proctor maximum dry density,  $w_{opt}$  is Standard Proctor optimum moisture content,  $\Delta w$  is moisture deviation related to the Standard Proctor optimum moisture content and  $RC_n$  is relative compaction,  $w_L$  is liquid limit,  $w_p$  is plasticity limit. (\*) soils tested as non-collapsible.

**Table 2** - Average engineering properties of compacted soils (adapted from USBR 1998, Earth Manual).

Soil GROUP NAME	USCS soil type	Compaction	
		$\gamma_{d,max}$ (kN/m <sup>3</sup> )	$w_{opt}$ (%)
Well-graded gravel	GW	19.89	11.4
Poorly graded gravel	GP	19.07	12.2
Silty gravel	GM	18.19	15.7
Clayey gravel	GC	18.54	14.2
Well-graded sands	SW	20.19	9.1
Poorly graded sands	SP	18.27	10.5
Silty sands	SM	18.77	12.3
Clayey sands	SC	19.06	12.4
Silt	ML	16.45	20.1
Lean clay	CL	17.68	16.4
Elastic silt	MH	13.72	33.1
Fat clay	CH	15.31	24.8

# *SOILS and ROCKS*

An International Journal of Geotechnical and Geoenvironmental Engineering

## **Publication of**

**ABMS - Brazilian Association for Soil Mechanics and Geotechnical Engineering**

**SPG - Portuguese Geotechnical Society**

**Volume 38, N. 3, May-August 2015**

## **Author index**

Abbaszadeh, M.M.	49	Marinho, F.A.M.	81
Bandeira, A.P.N.	27	Martins, A.P.S.	9
Bicalho, K.V.	121, 149	Massad, F.	163, 349
Bu, W.	181	Mattos, R.C.	219
Candeias, M.	3	Mercadier, D.	149
Cardoso, A.S.	95	Musarra, M.	163
Costa Guerra, N.M. da	231	Pacheco, M.P.	67
Coutinho, R.Q.	27	Pretto, J.H.F.	81
Cui, Y.-J.	121, 149	Rivera-Sar, J.M.	59
Danziger, B.R.	67	Rodrigues, R.A.	265
De Leon Ferreira, L.	135	Romanel, C.	121
Delgado-Martin, J.	59	Sanchez-Tembleque, F.	59
Falcon-Suarez, I.	59	Santana, T.	3
Freitas, A.C.	67	Sestrem, L.P.	81
Froumentin, M.	149	Silva, F.T.	219
Futai, M.M.	9	Tang, A.M.	149
Gomes, R.C.	135	Viana, L. Andrade	231
Hemsi, P.S.	219	Vilar, O.M.	265
Houston, S.L.	49	Vivacqua, G.P.D.	121, 149
Juncosa-Rivera, R.	59	Xu, H.	181
Kawachi, E.Y.	219	Zapata, C.E.	49
Kormann, A.C.M.	81	Zhao, Y.	181
Lacerda, W.A.	9		



- > **Prospecção Geotécnica**  
*Site Investigation*
- > **Consultoria Geotécnica**  
*Geotechnical Consultancy*
- > **Obras Geotécnicas**  
*Ground Treatment-Construction Services*
- > **Controlo e Observação**  
*Field Instrumentation Services and Monitoring Services*
- > **Laboratório de Mecânica de Solos**  
*Soil and Rock Mechanics Laboratory*

Certificada ISO 9001 por



# Geocontrole



Parque Oriente, Bloco 4, EN10  
2699-501 Bobadela LRS  
Tel. 21 995 80 00  
Fax. 21 995 80 01  
e.mail: mail@geocontrole.pt  
www.geocontrole.pt





## Where engineering begins.

Behind a great work there's always a great company.

tgeotecnia enters in national and Spanish market with a wide range of solutions, with state of the art technology and qualified means necessities to engage geotechnical studies, projects and works.

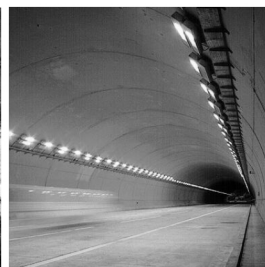
Currently, tgeotecnia is specialised in all kinds of work, from geologic-geotechnical studies and project development to slope stabilisation, reinforcement, soil treatment and special foundations.

The works carried out and client satisfaction, as well as the growing number of projects, are the proof that it is worth making innovation the lever of development.

tgeotecnia  
In the origin of construction

a dst group company

ph + 351 253 307 285 | geral@tgeotecnia.pt | www.dstsgps.com



**COBA**

**GEOLOGY AND GEOTECHNICS**

Hydrogeology • Engineering Geology • Rock Mechanics • Soil Mechanics • Foundations and Retaining Structures • Underground Works • Embankments and Slope Stability  
Environmental Geotechnics • Geotechnical Mapping



- Water Resources Planning and Management
- Hydraulic Undertakings
- Electrical Power Generation and Transmission
- Water Supply Systems and Pluvial and Wastewater Systems
- Agriculture and Rural Development
- Road, Railway and Airway Infrastructures
- Environment
- Geotechnical Structures
- Cartography and Cadastre
- Safety Control and Work Rehabilitation
- Project Management and Construction Supervision



**PORTUGAL**

CENTER AND SOUTH REGION  
Av. 5 de Outubro, 323  
1649-011 LISBOA  
Tel.: (351) 210125000, (351) 217925000  
Fax: (351) 217970348  
E-mail: coba@coba.pt  
www.coba.pt

Av. Marquês de Tomar, 9, 6º.  
1050-152 LISBOA  
Tel.: (351) 217925000  
Fax: (351) 213537492

**NORTH REGION**

Rua Mouzinho de Albuquerque, 744, 1º.  
4450-203 MATOSINHOS  
Tel.: (351) 229380421  
Fax: (351) 229373648  
E-mail: engico@engico.pt

**ANGOLA**

Praceta Farinha Leitão, edifício nº 27, 27-A - 2º Dto  
Bairro do Maculusso, LUANDA  
Tel./Fax: (244) 222338 513  
Cell: (244) 923317541  
E-mail: coba-angola@netcabo.co.ao

**MOZAMBIQUE**

Pestana Rovuma Hotel. Centro de Escritórios.  
Rua da Sé nº114. Piso 3, MAPUTO  
Tel./Fax: (258) 21 328 813  
Cell: (258) 82 409 9605  
E-mail: coba.mz@tdm.co.mz

**ALGERIA**

09, Rue des Frères Hocine  
El Biar - 16606, ARGEL  
Tel.: (213) 21 922802  
Fax: (213) 21 922802  
E-mail: coba.alger@gmail.com

**BRAZIL**

**Rio de Janeiro**  
COBA Ltd. - Rua Bela 1128  
São Cristóvão  
20930-380 Rio de Janeiro RJ  
Tel.: (55 21) 351 50 101  
Fax: (55 21) 258 01 026

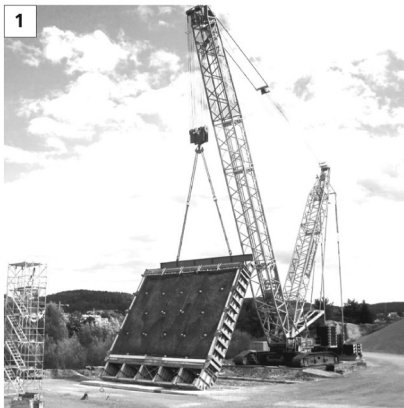
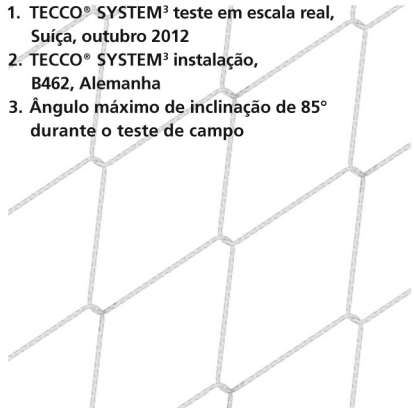
**Fortaleza**

Av. Senador Virgílio Távora 1701, Sala 403  
Aldeota - Fortaleza CEP 60170 - 251  
Tel.: (55 85) 3261 17 38  
Fax: (55 85) 3261 50 83  
E-mail: coba@esc-te.com.br

**UNITED ARAB EMIRATES**

Corniche Road - Corniche Tower - 5th Floor - 5B  
P. O. Box 38360 ABU DHABI  
Tel.: (971) 2 627 0088  
Fax: (971) 2 627 0087

1. TECCO® SYSTEM<sup>3</sup> teste em escala real, Suíça, outubro 2012
2. TECCO® SYSTEM<sup>3</sup> instalação, B462, Alemanha
3. Ângulo máximo de inclinação de 85° durante o teste de campo



## TECCO® SYSTEM<sup>3</sup> – Seu talude estabilizado

... validado por teste em escala real com inclinação do talude de até 85°.

A malha de aço de alta resistência TECCO®, as placas de ancoragem e garras de conexão TECCO®, juntas, estabilizaram com sucesso 230 toneladas de cascalho com 85° de inclinação em um ensaio em escala real.

- moldura de teste com dimensões 10 x 12 x 1.2m
- espaçamento dos grapmos 2.5m x 2.5m, utilizando Gewi 28mm

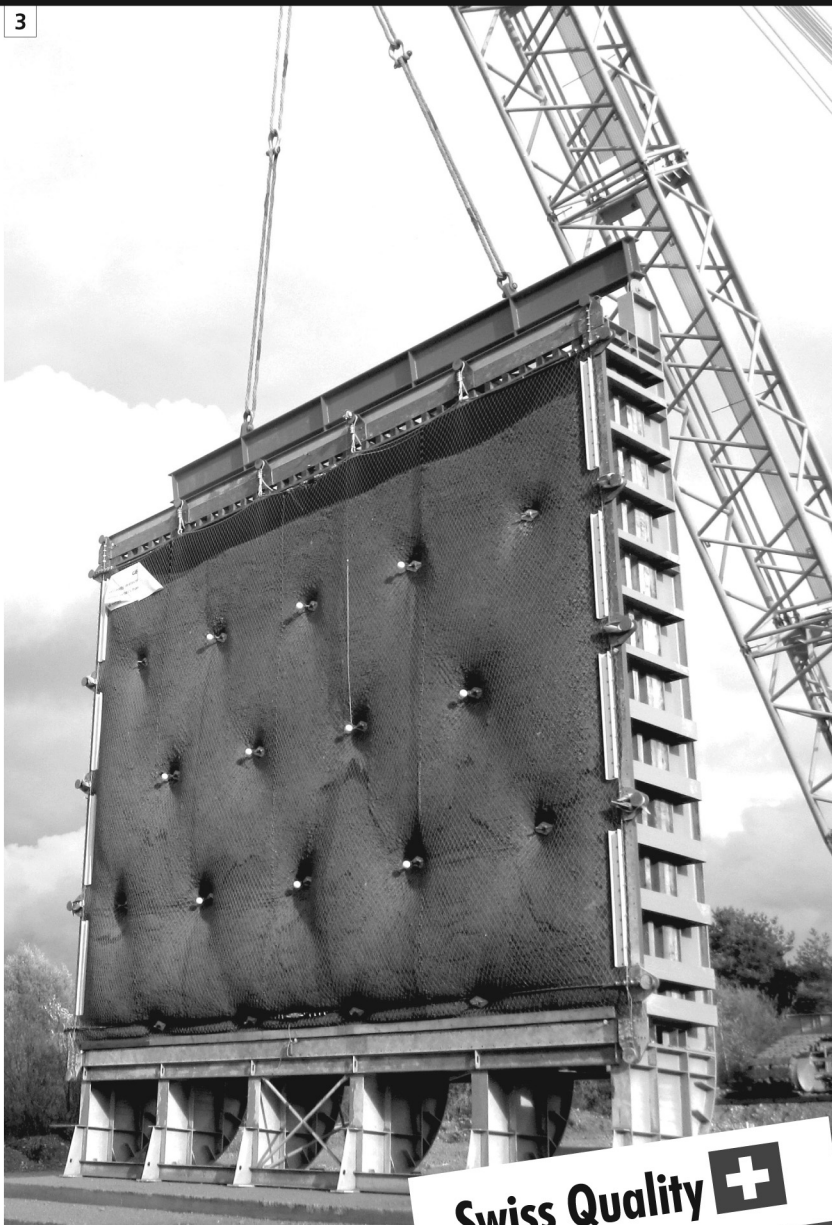
Para um estudo preliminar de solução de estabilização ou de riscos de desastres naturais nas obras em que você atua, entre em contato conosco através do e-mail [info@geobrugg.com](mailto:info@geobrugg.com)



Assista ou escaneie nosso filme com instalação TECCO® em [www.geobrugg.com/slopes](http://www.geobrugg.com/slopes)



**Geobrugg AG**, Geohazard Solutions  
 Rua Visconde de Pirajá, 82 sl.606  
 Ipanema - Rio de Janeiro • 22410-003  
 Fone: +55 21 3624.1449  
 Cel: +55 21 99979.1288  
[www.geobrugg.com](http://www.geobrugg.com)



Swiss Quality 

# SPECIALISTS IN GEOTECHNICAL IN-SITU TESTS AND INSTRUMENTATION

## GEOTECHNICAL SERVICES (onshore and offshore)

### ■ IN-SITU TESTS

Seismic CPT  
Cone Penetration Testing Undrained-CPTu (cordless system)  
Vane Shear Testing (electrical apparatus)  
Pressuremeter Testing (Menard)  
Flat Dilatometer Test-DMT (Machetti)  
Standard Penetration Test-SPT-T

### ■ INSTRUMENTATION

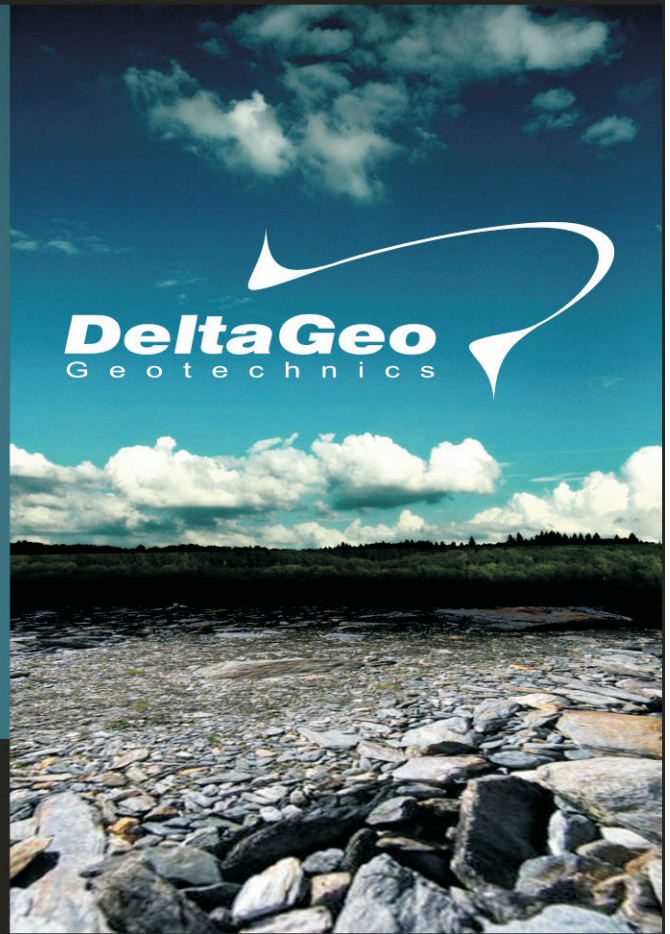
Instrumentation, installation and direct import  
Routine Monitoring  
Operation and Maintenance  
Engineering analyses  
Consultancy, design & geotechnical engineering services

### ■ SAMPLING

Soil sampling and monitoring  
Groundwater sampling and monitoring  
Field and laboratory testing

### ■ ENVIRONMENTAL

Environmental Services  
Soil and groundwater sampling and monitoring  
Field and laboratory testing

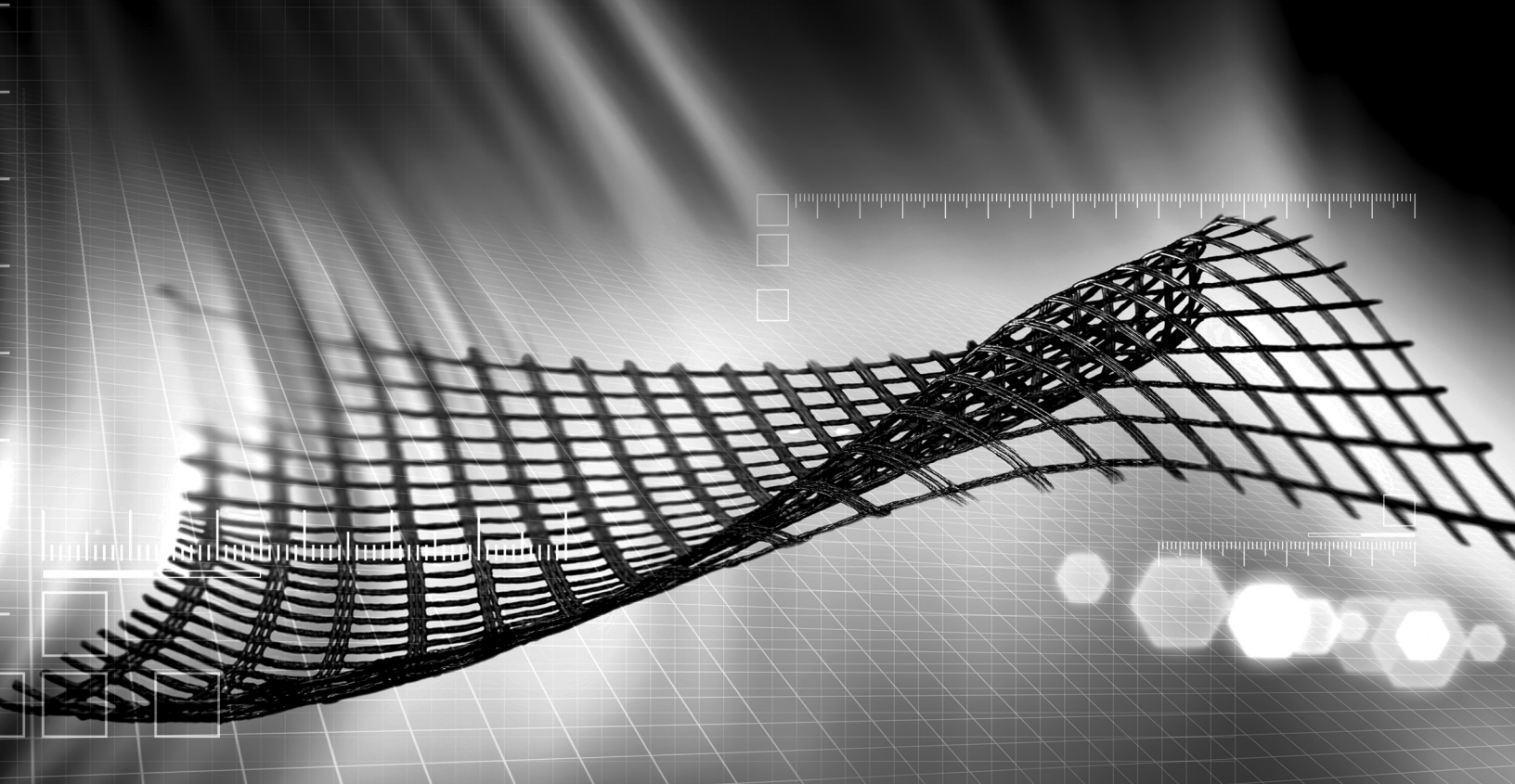


**0800 979 3436**

**São Paulo: +55 11 8133 6030**

**Minas Gerais: +55 31 8563 2520 / 8619 6469**

**[www.deltageo.com.br](http://www.deltageo.com.br) [deltageo@deltageo.com.br](mailto:deltageo@deltageo.com.br)**



# A strong, lasting connection.

With a history of over 150 years of pioneering in geosynthetics, we strive to create solutions for the most diverse engineering challenges.

Our business areas:



**Earthworks and  
Foundations**



**Environmental  
Engineering**



**Roads and Pavements**



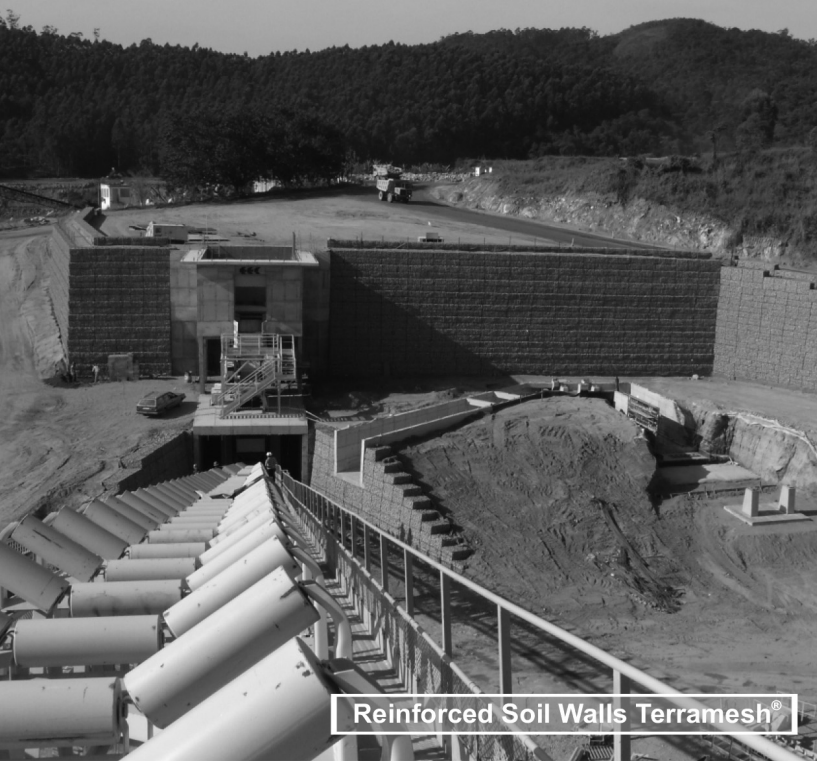
**Hydraulic Engineering**

Talk to HUESKER Brasil:  
[www.HUESKER.com.br](http://www.HUESKER.com.br)  
[HUESKER@HUESKER.com.br](mailto:HUESKER@HUESKER.com.br)  
+55 (12) 3903 9300

Follow HUESKER Brasil in social media:



**# HUESKER**  
Ideen. Ingenieure. Innovationen.



Reinforced Soil Walls Terramesh®



Gabions Retaining Walls

# GREAT GEOTECHNICAL WORKS REQUIRES GREAT SOLUTIONS



Waterproofing of Reservoirs, Lakes and Channels



Dynamic rockfall barriers

## BRASIL

Phone: 55 (11) 4525-5000  
Fax: 55 (11) 4599-4275  
info@br.maccaferri.com  
www.maccaferri.com/br

## PORTUGAL

Phone: (351) 218 968 282  
Fax: (351) 218 968 078  
info@es.maccaferri.com  
www.maccaferri.com/es



Engineering a better solution



Geotechnic and Rehabilitation

**TEIXEIRA DUARTE**  
ENGENHARIA E CONSTRUÇÕES, S.A.

- Head Office  
Lagoas Park – Edifício 2  
2740-265 Porto Salvo - Portugal  
Tel.: (+351) 217 912 300  
Fax: (+351) 217 941 120/21/26

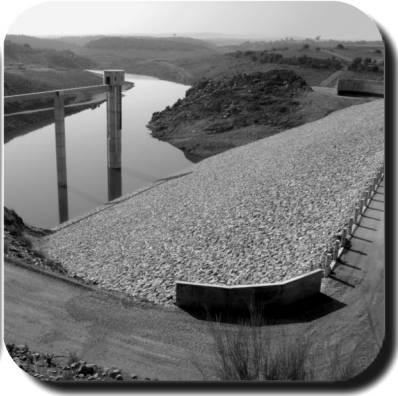
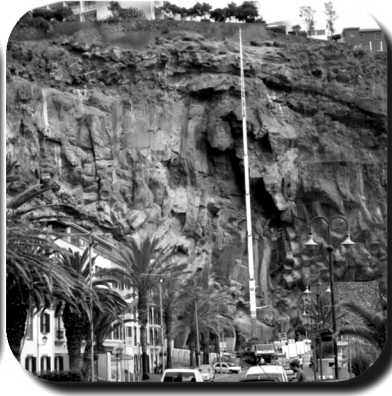
- Angola  
Alameda Manuel Van Dunen 316/320 - A  
Caixa Postal 2857 - Luanda  
Tel.: (+34) 915 550 903  
Fax: (+34) 915 972 834

- Algeria  
Parc Miremont – Rua A, Nº136 - Bouzareah  
16000 Alger  
Tel.: (+213) 219 362 83  
Fax: (+213) 219 365 66

- Brazil  
Rua Iguatemi, nº488 – 14º - Conj. 1401  
CEP 01451 - 010 - Itaim Bibi - São Paulo  
Tel.: (+55) 112 144 5700  
Fax: (+55) 112 144 5704

- Spain  
Avenida Alberto Alcocer, nº24 – 7º C  
28036 Madrid  
Tel.: (+34) 915 550 903  
Fax: (+34) 915 972 834

- Mozambique  
Avenida Julyus Nyerere, 130 – R/C  
Maputo  
Tel.: (+258) 214 914 01  
Fax: (+258) 214 914 00



**GEOLOGY - GEOTECHNICS - SUPERVISION OF GEOTECHNICAL WORKS**



**EMBANKMENT DAMS - UNDERGROUND WORKS - RETAINING STRUCTURES**



**SPECIAL FOUNDATIONS - SOIL IMPROVEMENT - GEOMATERIALS**

**CENOR** Consultores, S. A.

PORTUGAL | ANGOLA | ALGERIA | BRAZIL | CAPE VERDE | COLOMBIA  
MALAWI | MOROCCO | MOZAMBIQUE | EAST TIMOR | VENEZUELA

Rua das Vigias, 2. Piso 1 | Parque das Nações | 1990-506 LISBOA . PORTUGAL  
T. +351.218 437 300 | F. +351.218 437 301 | E. cenor@cenor.pt



MARCA  
DE QUALIDADE  
GESTOR GERAL DA QUALIDADE

ISO 9001  
ISO 14001  
OHSAS 18001  
BUREAU VERITAS  
Certificação



# Instructions for Submission of Manuscripts

## Category of the Papers

Soils and Rocks is the international scientific journal edited by the Brazilian Association for Soil Mechanics and Geotechnical Engineering (ABMS) and the Portuguese Geotechnical Society (SPG). The aim of the journal is to publish (in English) original research and technical works on all geotechnical branches.

According to its content the accepted paper is classified in one of the following categories: Article paper, Technical Note, Case Study or Discussion. An article paper is an extensive and conclusive dissertation about a geotechnical topic. A paper is considered as a technical note if it gives a short description of ongoing studies, comprising partial results and/or particular aspects of the investigation. A case study is a report of unusual problems found during the design, construction or the performance of geotechnical projects. A case study is also considered as the report of an unusual solution given to an ordinary problem. The discussions about published papers, case studies and technical notes are made in the Discussions Section.

When submitting a manuscript for review, the authors should indicate the category of the manuscript, and is also understood that they:

- assume full responsibility for the contents and accuracy of the information in the paper;
- assure that the paper has not been previously published, and is not being submitted to any other periodical for publication.

## Manuscript Instructions

Manuscripts must be written in English. The text is to be typed in a word processor (preferably MS Word), **single column**, using ISO A4 page size, left, right, top, and bottom margins of 25 mm, Times New Roman 12 font, and line spacing of 1.5. All lines and pages should be numbered. The text should be written in the third person.

The first page of the manuscript must include the title of the paper followed by the names of the authors with the abbreviation of the most relevant academic title. The affiliation, address and e-mail must appear below each author's name. An abstract of 200 words follows after the author's names. A list with up to six keywords at the end of the abstract is required.

Although variations on the sequence and title of each section are possible, it is suggested that the text contains the following sections: Introduction, Material and Methods, Results, Discussions, Conclusions, Acknowledgements, References and List of Symbols. A brief description of each section is given next.

**Introduction:** This section should indicate the state of the art of the problem under evaluation, a description of the problem and the methods undertaken. The objective of the work should be clearly presented at the end of the section.

**Materials and Methods:** This section should include all information needed to the reproduction of the presented work by other researchers.

**Results:** In this section the data of the investigation should be presented in a clear and concise way. Figures and tables should not repeat the same information.

**Discussion:** The analyses of the results should be described in this section.

**Conclusions:** The content of this section should be based on the data and on the discussions presented.

**Acknowledgements:** If necessary, concise acknowledgements should be presented in this section.

**References:** References to other published sources must be made in the text by the last name(s) of the author(s), followed by the year of publication, similarly to one of the two possibilities below:

...while Silva and Pereira (1987) observed that resistance depended on soil density... or It was observed that resistance depended on soil density (Silva and Pereira, 1987).

In the case of three or more authors, the reduced format must be used, e.g.: Silva *et al.* (1982) or (Silva *et al.*, 1982). Two or more citations belonging to the same author(s) and published in the same year are to be distinguished with small letters, e.g.: (Silva, 1975a, b, c.). Standards must be cited in the text by the initials of the entity and the year of publication, e.g.: ABNT (1996), ASTM (2003).

Full references shall be listed alphabetically at the end of the text by the first author's last name. Several references belonging to the same author shall be cited chronologically. Some examples are listed next:

Papers: Bishop, A.W. & Blight, G.E. (1963). Some aspects of effective stress in saturated and unsaturated soils. *Geotechnique*, 13(2):177-197.

Books: Lambe, T.W & Whitman, R.V. (1979). *Soil Mechanics*, SI Version. John Wiley & Sons, New York, 553 p.

Book with editors: Sharma, H.D.; Dukes, M.T. & Olsen, D.M. (1990). Field measurements of dynamic moduli and Poisson's ratios of refuse and underlying soils at a landfill site. Landva, A. & Knowles, G.D. (eds), *Geotechnics of Waste Fills - Theory and Practice*, American Society for Testing and Materials - STP 1070, Philadelphia, pp. 57-70.

Proceedings (printed matter or CD-ROM): Jamiolkowski, M.; Ladd, C.C.; Germaine, J.T. & Lancellotta, R. (1985). New developments in field and laboratory testing of soils. *Proc. 11th Int. Conf. on Soil Mech. and Found. Engn.*, ISSMFE, San Francisco, v. 1, pp. 57-153. (specify if CD ROM).

Thesis and dissertations: Lee, K.L. (1965). *Triaxial Compressive Strength of Saturated Sands Under Seismic Loading Conditions*. PhD Dissertation, Department of Civil Engineering, University of California, Berkeley, 521 p.

Standards: ASTM (2003). *Standard Test Method for Particle Size Analysis of Soils - D 422-63*. ASTM International, West Conshohocken, Pennsylvania, USA, 8 p.

Internet references: Soils and Rocks available at <http://www.abms.com.br> and downloaded on August 6th 2003.

On line first publications must also bring the digital object identifier (DOI) at the end.

Figures shall be either computer generated or drawn with India ink on tracing paper. Computer generated figures must be accompanied by the corresponding digital file (.tif, .jpg, .pcx, etc.). All figures (graphs, line drawings, photographs, etc.) shall be numbered consecutively and have a caption consisting of the figure number and a brief title or description of the figure. This number should be used when referring to the figure in text. Photographs should be black and white, sharp, high contrasted and printed on glossy paper.

Tables shall be numbered consecutively in Arabic and have a caption consisting of the table number and a brief title. This number should be used when referring to the table in the text. Units should be indicated in the first line of the table, below the title of each column. Acronyms should be avoided. When applicable, the units should come right below the corresponding column heading. Additional comments can be placed as footnotes.

Equations shall appear isolated in a single line of the text. Numbers identifying equations must be flushed with the right margin. International System (SI) units must be used. The definitions of the symbols used in the

equations must appear in the List of Symbols. It is recommended that the symbols used are in accordance with Lexicon in 8 Languages, ISSMFE (1981) and the ISRM List of Symbols.

The text of the submitted manuscript (including figures, tables and references) intended to be published as an article paper or a case history should not contain more than 30 pages, formatted according to the instructions mentioned above. Technical notes and discussions should have no more than 15 and 8 pages, respectively. Longer manuscripts may be exceptionally accepted if the authors provide proper explanation for the need of the required extra space in a cover letter.

### **Discussion**

Discussions must be written in English. The first page of a discussion should contain:

The title of the paper under discussion;

Name of the author(s) of the discussion, followed by their position, affiliation, address and e-mail. The author(s) of the discussion should refer to himself (herself/themselves) as the reader(s) and to the author(s) of the paper as the author(s).

Figures, tables and equations should be numbered following the same sequence of the original paper. All instructions previously mentioned for the preparation of article papers, case studies and technical notes also apply to the preparation of discussions.

### **Editorial Review**

Each paper will be evaluated by reviewers selected by the editors according to the subject of the paper. The authors will be informed about the results of the review process. If the paper is accepted, the authors will be required to submit a version of the revised manuscript with the suggested modifications. If the manuscript is rejected for publication, the authors will be informed about the reasons for rejection. In any situation comprising modification of the original text, classification of the manuscript in a category different from that proposed by the authors, or rejection, the authors can reply presenting their reasons for disagreeing with the reviewer comments.

### **Submission**

The author(s) must upload a digital file of the manuscript to the Soils and Rocks website.

### **Follow Up**

The online management system will provide a password to the corresponding author, which will enable him/her to follow the reviewing process of the submitted manuscript at the Soils and Rocks website.

**Volume 38, N. 3, September-December 2015****Table of Contents*****PACHECO SILVA LECTURE***

*New Developments in the Control and Prediction of the Movements  
Induced by Deep Excavations in Soft Soils*

M. Matos Fernandes 191

***ARTICLES***

*Use of Sugarcane Bagasse as Carbon Substrate in Permeable Reactive Barriers:  
Laboratory Batch Tests and Mathematical Modeling*

R.C. Mattos, P.S. Hemsí, E.Y. Kawachi, F.T. Silva 219

*Apparent Pressures on Multi-Propped Retaining Walls in Soils Under Drained Conditions  
with Shallow Water Table*

L. Andrade Viana, N.M. da Costa Guerra 231

*On the Interpretation of the Bidirectional Static Load Test*

F. Massad 249

***TECHNICAL NOTE***

*Revisiting Classical Methods to Identify Collapsible Soils*

O.M. Vilar, R.A. Rodrigues 265